The role of myocyte Extracellular Vesicles in inducing apoptosis of murine lung cancer CMT 64/61 cells

Presented by

Dona Mannaperuma

Submitted to the University of Hertfordshire in partial fulfilment of the requirements of the degree of

DOCTOR OF PHILOSOPHY (PhD)

June 2021

CONTENTS

Acknowledgement

First of all, I would like to express my sincere gratitude to my supervisor Prof. Jameel Inal for his invaluable advice, continuous support and guidance throughout my PhD studies. His unwavering enthusiasm for research, intelligence, style of supervision and importantly, his patience kept me constantly engaged with my research work. His demand for precision helped me to improve many skills including, verbal and written communication, research methods, observation, and meticulous attention to detail and made me a better person and potentially a skilful scientist. Put simply, I could not have imagined having a better supervisor for my PhD study. My gratitude extends to both University of Hertfordshire and London Metropolitan university for providing me the opportunity to undertake my research studies.

I would like to offer my special thanks to Dr. Sigrun Lange for her treasured support which was influential in shaping my entire study. Without your precious support it would have not been possible to complete my proteomics chapter. I take this opportunity to thank Dr. Brigitte Awamaria, who guided me from my undergraduate studies to take correct academic decisions at the correct times. I thank my fellow lab mates Dominik, William and Ramiya for all the support and stimulating discussions. My special thanks to all the technical staff who played a vital role in making my studies possible. Lee Rixon, you are the best lab manager I have ever seen; and Diana Francis (aka ‘Di’), thank you for providing me with all those reagents. You both made my lab work much easier and your help is much appreciated.

Finally, I would like to thank my family, my father, Mr. L Mannaperuma, my mother, Mrs. M. Perera, my partner, Hamed and my sister, Kalsani for your continuous support. I take this opportunity to thank my uncle Mr. Pathmesiri Perera for helping me to come to the UK for my studies. A special thanks to my working colleague Leonard, for covering for me whenever I

had to leave early from work to the research lab. You all have been there for me in both good and bad times, and it is greatly appreciated. THANKS TO YOU ALL!!!

Abstract

Extracellular vehicles (EVs) are a heterogeneous group of particles ranging from 15 nm to 1000 nm in diameter, released by almost every cell type, including tumours. These vesicles contain a complex cargo, including protein, lipid and nucleic acids, which reflect the status of the cell of origin. Increasing evidence suggests that EVs play an important role in intercellular communication, both locally and systemically, by transferring their cargo between cells and inducing phenotypical and functional changes in recipient cells. In cancer, the pro-tumourigenic role of EVs is well established; however, their capability as an anti-tumourigenic agent is still emerging. This study identified a novel anti-tumourigenic role of skeletal muscle (C2C12) derived EVs towards highly metastatic lung carcinoma cells (CMT 64/61).

Skeletal muscle is a rare site for malignant metastasis and the mechanism underling the rarity of this phenomenon has remained elusive. The data obtained in this study indicated that myocyte EVs at low concentration, up to 200 µg/ml, exert cytotoxic effects on lung carcinoma cells, whilst having no effect on normal fibroblast cells (NIH 3T3). Myocyte EVs induced morphological changes in carcinoma cell mitochondria, decreased mitochondrial membrane potential leading to increased caspase 3 and 9 activity and apoptosis. A significant % of apoptosis, 34.8%, was exerted by 200 µg/ml of myocyte EVs within 48 h. No significant apoptosis was seen in non-carcinoma cells. Cell cycle analysis revealed that myocyte EVs mediated carcinoma cell proliferation suppression via cell cycle arrest at S phase. Transwell migration assay indicated a dose dependent reduction in carcinoma cell migration towards the microenvironment containing myocyte EVs.

To further explore the possible protein cargo that exert above effects, proteomics analysis was conducted on myocyte EVs. Scaffold software identified 29 upregulated proteins in myocyte EVs and interestingly, STRING and KEGG analysis on these proteins identified 3 possible pathways that could exert cytotoxic, apoptotic and cytostatic effects on carcinoma cells.

Proteins including Cathepsin L1, Cathepsin B and Cathepsin D, involved in Lysosome and Apoptosis pathway whilst Decorin, Thrombospondin-1 and Cathepsin L1 in Proteoglycan in cancer pathway. While all of these proteins may contribute to the effects observed in carcinoma cells, Decorin (DCN) seemed a promising target due its already known anti-tumourigenic properties. Together these results indicate that skeletal muscle derived EVs function as an anti-tumourigenic agent; hence identifies as a potential therapeutic agent in the treatment of metastatic lung carcinoma.

Abbreviation

Abs	Apoptotic bodies
AD	Alzheimer’s disease
ADP	Adenosine diphosphate
ANOVA	Analysis of Variance
BCA	Bicinchoninic acid assay
BSA	Bovine serum albumin
Ca^{2+}	Calcium ion
CDE	Caveolin- Dependent Endocytosis
CME	Clathrin-mediated endocytosis
CME	Clathrin-mediated endocytosis
CO_2	Carbon dioxide
DCN	Decorin
ddH_2O	double deionized water
DISC	Death Inducing Signalling Complex
DLS	Dynamic Light Scattering
DMEM	Dulbecco's Modified Eagle Medium
DMSO	Dimethyl sulfoxide
DNA	Deoxyribonucleic acid
DPBS	Dulbecco’s Phosphate Buffered Saline
DTT	Dithiol threitol
ECL	Enhanced Chemiluminescence
EDTA	Ethylenediaminetetraacetic acid
EGFR	Epidermal Growth Factor Receptor
ERK	Extracellular signal-regulated kinase
ERK	Extracellular signal-Regulated Kinase
ESCRT	Endosomal Sorting Complexes Required for Transport
ESCRT	Endosome Sorting Complexes Required for Transport
EVs	Extracellular vesicles
FACS	Fluorescent activated cell sorter
FADD	Fas-associated death domain
FBS	Foetal Bovine Serum
FITC	Fluorescein isothiocyanate
FSC	Forward scatter
g	G-force
GTPases	Guanine triphosphatases
HCl	Hydrochloric acid
HRP	Horseradish peroxidase
IgG	Immunoglobulin G
IL	Interleukin
ILVs	Intraluminal vesicles
ISEV	International Society of Extracellular Vesicles
Kd	kilodalton

KEGG	Kyoto Encyclopedia of Genes and Genomes
LC	Liquid chromatography
LDH	Lactate dehydrogenase
m/z	mass / charge
MAPK	Mitogen-activated protein kinase
MHC	Major histocompatibility complex
miRNAs	Micro Ribonucleic acid
ml	milliliter
MISEV	Minimal Information for Studies of Extracellular Vesicles
MLCK	Myosin light chain kinase
mM	milli molar
MMPs	Matrix MetalloProteinases
MOMP	Mitochondrial Outer Membrane permeabilization
mRNA	Messenger Ribonucleic acid
MS	Mass spectrometer
MS	Multiple Sclerosis
MVBs	Multi Vesicular Bodies
MVs	Microvesicles
ncRNAs	Non-coding Ribonucleic acid
NSCLC	Non-small cell lung carcinoma
NTA	Nanoparticle Tracking Analysis
PBS	Phosphate-buffered saline
PLD	Phospholipase D
PPI	Protein-Protein Interactions
RA	Rheumatoid Arthritis
RNA	Ribonucleic acid
rRNA	Ribosomal ribonucleic acid
RTK	Receptor tyrosine kinase
SCLC	Small cell lung carcinoma
SDS	Sodium dodecyl sulphate
SMAC	Second Mitochondria-derived Activator of Caspase
STRING	Search Tool for the Retrieval of Interacting Genes/proteins
TEM	Transmission Electron Microscopy
TGF β	Transforming growth factor beta
TNF	Tumour necrosis factor
TRADD	TNF receptor-associated death domain
tRNA	Transfer ribonucleic acid
TSG	Tumour susceptibility gene
TSG101	Tumour Suppresor Gene 101
VAMP	Vesicle-associated membrane protein
w/v	weight/volume

1. Introduction

1.1 Extracellular Vesicles (EVs)

Extracellular vesicles (EVs) are attracting considerable interest in the scientific community due to their role in normal physiology as well as their involvement in every disease state possible in the human body, including cancer [1,2,3,4]. Almost every cell release EVs into the extracellular space and therefore, they can be detected in almost all body fluids including blood, urine, semen, bronchial fluid and saliva [5,6]. EVs are heterogenous, membrane bounded vesicles, which contain many lipids, proteins and nucleic acids that are derived from the parent cell. They are also enriched in certain molecules such as, adhesion molecules, cytoskeletal molecules, membrane trafficking molecules, signal transduction proteins, cytoplasmic enzymes, heat-shock proteins, chemokines, cytokines, proteinases and cell-specific antigens [7].

Over the years, diverse range of names has been given to EVs released by cells, including microparticles, microvesicles, ectosomes and exosomes. However, in recent years they were broadly classified into microvesicles and exosomes, based on their size, mechanism of generation and membrane surface markers [7,8,9]. Microvesicles (which have also been referred to as microparticles or ectosomes) [10] range from 100 nm to 1000 nm in size and are released from the plasma membrane by outward budding or pinching [11]. In contrast, exosomes typically range from 30-150 nm in diameter in size and are formed by inward budding of the limiting membrane of early endosomes, which mature into multi-vesicular bodies (MVBs) during the process [12]. However, certain exosomes, such as from Jurkat T cells, appear to retain the endosomal property of outward vesicle budding [13]. In recent years, The International Society of Extracellular Vesicles (ISEV) is discouraging the use of microvesicles and exosomes for EV classification and endorses the term “extracellular vesicles” as a generic term [14]. Furthermore, guideline set by ISEV recommends that EVs can be termed based on, “a) physical

characteristics of EVs, such as size ("small EVs" (sEVs) and "medium/large EVs" (m/lEVs), with ranges defined, for instance, respectively, < 100nm or < 200nm [small], or > 200nm [large and/or medium]) or density (low, middle, high, with each range defined); b) biochemical composition (CD63+/CD81+- EVs, Annexin A5-stained EVs, etc.); or c) descriptions of conditions or cell of origin (podocyte EVs, hypoxic EVs, large oncosomes, apoptotic bodies)"[14].

Emerging evidence suggests that EVs play pivotal roles in physiological processes such as cell differentiation, migration, angiogenesis [4,15] and immune response modulation [13], as well as pathological conditions such as cancer, neurological diseases and metabolic diseases [16,17]. EVs are known to modulate the above processes by mediating cell to cell communication via transfer of their cargo and to alter the status of recipient cells [18]. Furthermore, it was shown that EVs play essential roles in cell repair and homeostasis, for example EVs derived from platelets having the capability of repairing myocardial injury after an infarction [19]. With emerging functions of EVs in both physiological and pathological conditions, recent reviews have focused on clinical applications of EVs as a diagnostic and therapeutic agent.

1.2 Biogenesis, Isolation and Characterization

EVs are formed via multiple mechanisms (1) the formation of multi vesicular bodies (MVBs) through the endosomal systems [20] (employed by exosomes in the previous nomenclature) and (2) the outward budding and fission of the plasma membrane (employed by microvesicles in the previous nomenclature) (**Figure 1**).

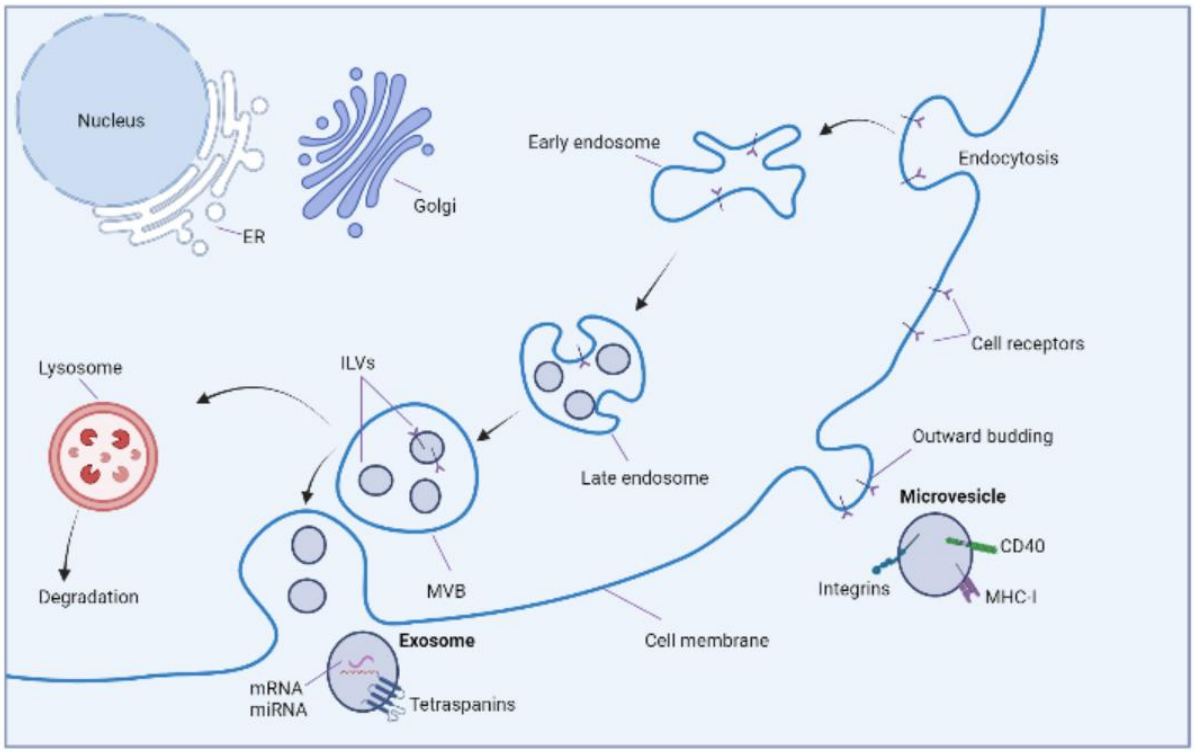

Figure 1: Biogenesis and secretion of EVs

Schematic representation of EV origin and release in eukaryotic cells. MVBs fuse with cell membrane to release ILVs as exosomes. Microvesicles are formed by outward budding and fission of the plasma membrane.

1.2.1 Exosome Biogenesis and Release

Exosomes originate from the endosomal system. Endosomes are formed by invagination of the plasma membrane, and they are separated into different compartments, such as late endosomes, early endosomes, and recycling endosomes [20]. The early endosomes mature into late endosomes, leading to form intraluminal vesicles (ILVs) by invagination of the endosomal membrane. This process leads to the formation of multivesicular endosomes or multivesicular bodies (MVBs). The MVBs either fuse with the cellular membrane to release ILVs as exosomes into the extracellular space or they fuse with the lysosome for degradation [20,21].

As described, the formation of exosomes is a multiple mechanism process. The endosome sorting complexes required for the transport (ESCRT) machinery plays an important role in the formation of ILVs and MVBs. The ESCRT is comprised of ESCRT 0, I, II, and III complexes, and they are recruited into the endosomal membrane in a stepwise manner [21]. ESCRT 0, identifies the ubiquitinated proteins on the outside of the endosomal membrane followed by ESCRT I which binds the ubiquitinated cargo on the endosomes [20]. Also, ESCRT I interact with ESCRT II and initiates endosomal membrane invagination. Furthermore, ESCRT III assembly is initiated by the activation of ESCRT II and finally ESCRT III completes the ILV scission into the MVB lumen [21]. This is the ESCRT dependent pathway; apart from ESCRT proteins it requires ESCRT associated proteins (ALIX, TSG101, Chmp4, and SKD1) to form MVBs containing MHC II, CD63, KFERQ-containing proteins and ubiquitinated proteins [22,23,24]. Alternatively, exosome biogenesis could occur through an ESCRT independent pathway, the syndecansyntenin-ALIX pathway, in which heparanase, syndecan heparan sulphate proteoglycans, ADP ribosylation factor 6 (ARF6), phospholipase D2 (PLD2), and syntenin are involved [24,25]. However, it is possible that other mechanisms of exosome biogenesis are regulated in parallel to the ESCRT pathway and vary depending on the vesicle content, cell origin and external stimuli. Furthermore, the release of exosomes to the extracellular space is regulated by many mechanisms including, RAB35 GTPases, cytoskeletal proteins, SNARE proteins, intracellular Ca^{2+} levels and intracellular pH gradients [26,27]. Exosomes released via these different mechanisms are enriched with different proteins; for example, the exosomes released via RAB27A/B are enriched with proteins such as, CD63, ALIX, and TSG101[28], whilst exosomes released via RAB GTPases, enriched with flotillin, Wnt, PLP, and the transferrin receptor (TfR) [29]. In conclusion, exosomes can be formed and released via different mechanisms containing different cargo content and vary depending on

the cell type and its physiological state. Moreover, aforementioned mechanisms could account for the heterogeneity observed in EV population secreted by different cells.

1.2.2 Microvesicle Biogenesis and Release

Biogenesis and release of MVs is less distinctive compared to the release of exosomes. In general, MVs are found to be formed by outward budding and fission of the plasma membrane. A combination of factors, such as, redistribution of phospholipids and contraction of the actin-myosin mechanism contribute to the formation of microvesicles [30]. Like for exosomes, the content of the MVs may depend on the mechanism underlying their release. For example, ADP-ribosylation factor 6 (ARF6) initiates a cascade that activates phospholipase D (PLD), then the extracellular signal-regulated kinase (ERK) phosphorylates and activates the myosin light chain kinase (MLCK), which in turn triggers the release of MVs [31]. MVs that are released through this pathway contained VAMP3, ARF6, β1-integrin, MHC-I and MT1MMP [32]. MVs formed by VPS4 ATPase with E3 ligase WWP2 interacting and ubiquitinating Arrestin 1 domain–containing protein 1 (ARRDC1) pathway contain TSG101, ARRDC1, and other cellular proteins [33]. Furthermore, MV release can be induced by increase of cytosolic Ca^{2+} levels as well as change in cellular physical state such as hypoxia and apoptosis [34,35,36].

1.2.3 Isolation and Characterisation of EVs

As discussed above, EVs represent a group of heterogeneous vesicles, mainly microvesicles and exosomes. Multiple different methods have been identified to isolate EVs from different biological samples. However, at present there is not an agreed research community 'Gold standard' method for EV isolation [37]. Different techniques are used to isolate EVs, based on their biophysical and biochemical properties, such as size, mass density, charge, and antigen exposure. Based on these properties most common methods currently in practice are,

differential centrifugation, density gradient centrifugation, size exclusion chromatography, immunoprecipitation, and ultrafiltration. Differential centrifugation is used in this current study as it is a conventional method, which uses centrifugal forces to separate cellular materials from a sample of EVs in a stepwise manner. In this study, $18{,}500 \times g$ was employed as the maximum speed as it was found to provide a reasonable yield of m/lEVs from cell culture medium.

Checking the purity, their size and count are essential steps in EVs based research as the isolated EV sample often contain contaminants including, lipids, small organelles and other undesired microparticles [38]. Similar to isolation methods, a gold standard for EVs analysis has not been defined in the science community yet. However, there are many techniques used in analysing EV samples including, Dynamic Light Scattering (DLS), Nanoparticle Tracking Analysis (NTA), flow cytometry and Transmission Electron Microscopy (TEM). The DLS and NTA measure the size of the particle based on their Brownian motion in solution. Compared to DLS, NTA uses the Brownian motion of the particles to measure the EVs size distribution as well as the concentration. However, both DLS and NTA are unable to detect and characterize isolated samples of apoptotic bodies (ABs) due to its particle size constraint [39]. The flow cytometry analysis involves using specific antibodies that recognise the EVs from its heterogenous sample. However, this method cannot evaluate the complex profiles of different types of EVs with multiple labels assessed for each EV. Therefore, Nanoscale flow cytometry is used to analyse and sort each EV individually [38]. Furthermore, TEM analysis is widely used in EV based research as it provides visual verification of EVs as well as an assessment of morphology and size, which can be indicative of the phenotype of EVs [40].

1.3 Extracellular Vesicles Content

It is well established that EVs are loaded with a plethora of biomolecules lipids, proteins, and nucleic acids, which can be transferred to recipient cells to exert cellular changes. Moreover, it has been shown that EV cargo loading is a selective process, as cargo composition differs across different EV populations and subtypes. However, various studies have shown that the contents of vesicles vary with the mode of biogenesis, cell type, and physiologic conditions [41]. Furthermore, recent studies found that specific proteins may mediate the loading of these biomolecules into EVs, which makes these cargos specific per vesicle and cell type [42,43,44].

1.3.1 Protein Content

Proteins that are associated with EV biogenesis are commonly found in all EVs [45,46]. For example, components of the ESCRTs biogenesis pathway such as, TSG101 and ALIX, HSC70 and HSP90β are found in all exosomes regardless of their cell origin. Therefore, these proteins are used as exosome marker proteins. Furthermore, exosomes generated from ESCRT independent pathway, are found to contain tetraspanin proteins such as, CD63, CD9 and CD81 [47,48,49,50]. Additionally, EVs contain proteins which are responsible for formation and release such as, RAB27A, RAB11B, and ARF6. Other proteins including signal transduction proteins (EGFR), antigen presentation (MHC I and MHC II) and transmembrane proteins (LAMP1, TfR) [20] were also found in EVs. Interestingly, proteins associated with organelles such as mitochondria and nucleus are mainly found in exosomal vesicles including, transcription factors such as, Notch and Wnt, which are associated with the nucleus [51]. However, it has been difficult to provide a definite protein composition of EVs as they can be varied due to different isolation techniques, cell type, culture sample and conditions.

Mass spectrometry-based proteomics has become the tool of current proteomics-based studies. Initially, EVs are lysed to extract the proteins and the remaining proteins are then digested into peptides, which are sent through liquid chromatography column for separation. These peptides are then ionised and introduced to mass spectrometry for analysis [52]. A mass spectrometer measures the mass-to-charge ratio (*m/z*) of ionized molecules. In tandem MS (MS/MS), multiple rounds of MS are carried out on the same sample, which gives detailed peaks for peptides. Resulted peaks are subjected to database searching [53], in which peptide fragments are compared to theoretical patterns in a data base using a software, such as Mascot [54] for protein identification. Proteins that are identified as MS were subjected to Search Tool for Retrieval of Interacting Genes/Proteins (STRING) analysis for functional protein interaction network analysis. It is a well-known data base which contain data on Protein-Protein Interactions (PPI). PPI plays an important role in cellular metabolism and through these protein interactions, protein functions can be identified. Use of gene ontology (GO) and biological pathways in STRING analysis can enhance the understanding of protein-protein functional association. To gain further mechanistic insight into these protein functions, the Kyoto Encyclopedia of Genes and Genomes (KEGG) pathway tool is widely used in proteomics analysis [55,56].

1.3.2 Lipid Content

Generally, lipid content of the EVs is known to be very similar to the lipid content of their cells of origin. Commonly found lipids in EVs are cholesterol, sphingomyelin, disaturated lipids, ganglioside GM3, phosphatidylserine, and ceramide [57]. However, the lipid content of the MVs is higher compared with that of the cells of origin and enriched with polyunsaturated glycerophosphoserine and phosphatidylserine [58]. Moreover, the membrane content of both

MVs and exosomes contains more phosphatidylserine and less phosphatidylcholine and diacyl-glycerol, compared to with the cellular plasma membrane of the cell of origin [29].

1.3.3 Nucleic Acid Content

Apart from proteins and lipids, EVs are enriched with a variety of nucleic acids, primarily RNAs such as, rRNAs and tRNAs. Commonly known RNAs present in EVs are, mRNAs, miRNAs, and rRNAs. Recent studies have found other RNAs such as, non-coding RNA (long and short,) tRNA fragments, vault RNA, piwi-interacting RNA, Y RNA and circular RNA in EVs [45,46,47,48]. Interestingly, RNA content in EVs have different profiles compared to the RNA content from the cell origin [20,49,50]. Furthermore, it was found that EVs protect RNAs from degradation and these RNAs contain biological state specific information which can be transferred to recipient cells and contribute to molecular and biological events occurring in the recipient cells [59]. Moreover, due to varied composition of these RNA cargo in EVs, their potential as biomarkers for pathological disorders have been discussed. Therefore, many EV RNA sequencing profiles are currently available on the extracellular RNA Atlas, compromising a variety of health conditions [60]. Apart from RNA, small number of genomic and mitochondrial DNA was also reported in some EVs [61].

1.4 Extracellular Vesicles Uptake by Recipient Cells

Various direct and indirect evidence suggests that EVs are internalized by many cell types through multiple ways. As mentioned earlier, EVs exert changes in recipient cells either by binding through surface receptor or by internalization and release of their cargo contents. Despite, overwhelming evidence suggesting that EVs can be internalised by cells and deliver their cargo, the exact mechanism responsible for EV internalisation has raised many debates in the research community. Many methods are utilised to visualise EV uptake by recipient cells,

including the use of fluorescent lipid membrane dyes, membrane permeable chemical compounds to stain EVs, whereafter the fluorescent intensities were measured using flow cytometry and confocal microscopy [62]. Currently, the most common method for detecting EV uptake is the use of fluorescent lipophilic dyes such as PKH67 [63,64], PKH26 [65] and rhodamine B [66] to stain the EV lipid membrane. Moreover, a range of other techniques have been used in conjunction with EV uptake assays, such as antibody tests to further investigate the molecular mechanisms of the EV uptake [62]. Various mechanisms of EV uptake by recipient cells have been proposed, including Clathrin-Mediated Endocytosis (CME), Caveolin- Dependent Endocytosis (CDE), phagocytosis, macrophinocytosis and plasma membrane fusion [62]. Additionally, specific protein-protein interactions and lipid raft protein interactions have also been investigated. Some of the proteins that have been implied in EV uptake are, tetraspanins, lectins, proteoglycans, integrins and immunoglobulins [41].

1.4.1 Endocytosis Uptake

Endocytosis is a broad term for a range of molecular internalisation pathways, and it is known to be the most favoured pathway of recipient cells for EVs uptake [67,68,69]. Several research groups have shown that, EVs are identified inside the recipient cells within 15 min of them been introduced, which suggests that endocytosis uptake can be an extremely rapid process [70,71]. Moreover, researchers have found that EV uptake via endocytosis is an active process which requires energy as well as a functioning cytoskeleton [68,72,73,74].

1.4.2 Clathrin-Mediated Endocytosis

Clathrin-mediated endocytosis (CME) is one of the key processes in which EVs transport from outside the cell to the interior. It is regulated by clathrin-coated vesicles that are endowed with the ability to cluster a range of transmembrane receptors and to locally bend the plasma

membrane, resulting in the formation of receptor-containing vesicles that bud into the cytoplasm. These vesicles then undergo uncoating of clathrin and fuse with endosomes to release their cargo [75]. Various studies have shown the involvement of CME on EV uptake. Chloropromazine known to prevent the formation of clathrin- coated cavities at the plasma membrane [75] has been shown to decrease the uptake of EVs by ovarian cancer recipient cells [68]. Dynamin2 is required for the formation of CME, and studies have shown that the inhibition of Dynamin2 prevented almost all EV uptake by the recipient cells [76]. Together, these studies suggest that CME play at least some part in EV uptake.

1.4.3 Caveolin- Dependent Endocytosis

Similar to clathrin- coated pits, caveolae form small invaginations in the plasma membrane, which can become internalised into the cell. They are formed by the assembly of integral membrane protein, caveolins, which bind directly to membrane cholesterol [77]. Caveolin-1 protein is known to play a crucial part in the formation of caveolae, as it was found that knockout of caveolin-1 gene in recipient cell, resulted in a significant decrease in EV uptake [78]. Furthermore, a recent study has shown that, upregulation of caveolin-1 expression enhanced the uptake of human umbilical vein endothelial cell derived EVs to neuronal cells in a mouse model [79]. Similar to CME, CDE plays a role in EV uptake, though the exact role of this pathway may depend on recipient cell and EV types.

1.4.4 Phagocytosis

Phagocytosis is a receptor mediated process that involves the formation of invaginations surrounding the material destined for internalisation. Phagocytosis is mostly performed by specialised cells such as macrophages and involves engulfing bacteria and fragments of dead

cells. Even though, phagocytosis is designed to internalise large particles, researchers have shown that particles as small as 85 nm in diameter have been internalised by phagocytosis [80]. PI3Ks play an important role in enabling membrane insertion into forming phagosomes [81]and inhibition of P13K has shown to reduce the EV uptake in dose dependent manner [70]. In another study, the EVs released by leukaemia cells were shown to be internalised by macrophages but were not internalised by other cell types [70]. Therefore, the results suggest that phagocytosis may play a role in EV uptake, and it is a cell specific process.

1.4.5 Cell Surface Membrane Fusion

While a majority of studies support the endocytosis EV uptake, few studies have investigated the possibility of direct fusion of EVs with the cell plasma membrane. When the EVs are in close proximity with the recipient cell, lipid bilayer of the EVs could fuse with the lipid bilayer of the recipient cell and form one consistent structure. This enables EVs to release their content into the cell cytoplasm. Several protein families participate in this process including SNAREs, Rab proteins, and SM-proteins [82]. A recent study has shown that some of the fluorescent labelled EVs were fused with melanoma cells and the uptake was enhanced by the acidic conditions [83]. Another study has shown the fusion of R18-labelled EVs with the plasma membrane of bone marrow-derived dendritic cells [62]. This evidence therefore suggests that cell surface membrane fusion is a possible route of EVs uptake and should not be ruled out.

1.5 EVs in Human Diseases

EVs can alter functions and phenotypes of the recipient cells by trafficking and releasing their bio cargo molecules into the recipient cells, which deregulates gene expressions and disrupts signalling pathways of the recipient cells [41]. Therefore, EVs and their involvement in diseases have been extensively studied in the context of cancer, inflammatory diseases,

neurodegenerative diseases, cardiovascular diseases and other pathologies. As cancer being the most prominent area of EV based research; a multitude of evidence has shown the ability of cancer derived EVs to modulate immune responses to promote cancer metastasis and tumour growth [84]. The implication of EVs in cancer will be separately discussed in this study.

EVs have been widely studied in the context of inflammation and autoimmune diseases including, multiple sclerosis (MS), rheumatoid arthritis (RA), Sjogren's syndrome and systemic lupus erythematosus. It has been found that EVs secreted by microglia containing IL1-β and MHC-II may trigger neuroinflammation and rapidly spread the antigens in MS [85]. In RA, T-cells or monocyte derived EVs are known to enhance the release of matrix metalloproteinases (MMPs) from fibroblast-like synoviocytes, which causes cartilage destructions and degradation [86,87].

Furthermore, implication of EVs in pathogenesis and protective aspects of neurodegenerative diseases has been also extensively researched. Neurodegenerative diseases such as Alzheimer's disease (AD) and Parkinson's disease are caused by accumulation of pathogenic misfolded proteins in the brain and CNS. A recent study has shown that proteins involved in AD, amyloid-β and hyperphosphorylated Tau are transmitted via EVs, which contributes to the accumulation of these misfolded proteins in brains [88]. Conversely, it was also shown that EVs may contribute to preventing accumulation of these pathogenic proteins in these neurodegenerative diseases [89].

Moreover, a recent study has suggested that EVs via their cargo might be involved in triggering, maintenance, and progression of reproductive- and obstetric-related pathologies such as endometriosis, polycystic ovarian syndrome, preeclampsia, gestational diabetes, and erectile

dysfunction [90]. Furthermore, there is evidence to suggest that viruses and other pathogens can use EVs to enter uninfected cells and spread the pathogen. For example, it was shown that HIV can use the EV uptake pathway to enter uninfected cells and exit infected cell by hijacking the EV secretory pathway for immune evasion [91].

1.6 Role of EVs in Cancer

1.6.1 Pro-Tumourigenic Effects

It is well established that the tumour microenvironment plays a pivotal role in cancer development and progression [84,92]. Cancer cells can adapt to the host environment, early in the neoplastic process, and ensure tumour survival and expansion [93]. Immunosuppression and complicated cellular crosstalk mechanisms orchestrate this process [94,95,96]. Direct cellular interactions or the secretion of soluble factors such as cytokines were known to mediate intercellular communication [97]. However, recent studies have shown that far-reaching pathways, namely EV-mediated cell-to-cell communication, play a pivotal role in cancer spread and progression. Indeed, EVs are proposed as a novel mode of intercellular communication for both long- and short-range cell signaling [98,99,100].

As noted earlier, EVs carry a rich cargo of biomolecules reflective of their cellular origin, including proteins, lipids, transcription factors as well as many nucleic acids, including DNA, mRNA and microRNAs [101] and transport them between cells [102]. An increasing number of research reports have shown the involvement of cancer derived EVs on cancer development, such as cell proliferation, [103,104,105] drug resistance,[106]angiogenesis,[107] immune modulations, [108] and pre-metastatic niche formation [109]. For example, cancer miRNA transported via EVs can be translated into functional proteins inside the recipient cells [110,111,112] and modulate surrounding cells such as endothelial, fibroblast and immune cells [107,108,113] to enhance cancer

growth and progression. Furthermore, miRNA containing EVs from breast cancer are able to modulate pre-metastatic lung cells by targeting cadherin and upregulating transcription factors [114]. Moreover, EVs have been revealed to transport membrane components including receptors, such as EGFRs,[115] cell adhesion proteins and enzymes which promote cancer metastasis and progression. Other reports have shown that, EVs from renal cancer stem cells stimulate angiogenesis and the formation of lung pre-metastatic niches [1] whilst, CD44v6 enriched EVs from pancreatic cancer cells promotes pre-metastatic niche formation in lymph nodes and lung tissues [116].

A multitude of studies have shown the involvement of EVs on cancer metastasis. Metastasis is a multi-step process in which, tumour cells infiltrate to adjacent tissue, migrate into blood vessels (intravasation), followed by extravasation, colonization and angiogenesis [117]. Several studies have reported that, EVs mediate the formation of pre-metastatic niches in various organs and transfer metastatic potential to organs [118]. For instance, melanoma cell derived EVs can promote lung metastasis by altering the extracellular matrix, by increasing vascular permeability and promoting other proangiogenic events [119,120]. Furthermore, it was found that cancer secreted EVs containing miR-105, destroy the tight junctions between endothelial cells and facilitate cancer cell migration to the brain [121]. It was also found that the EVs secreted by bone marrow mesenchymal stem cells promote cancer cell dormancy of metastatic breast cancer stem cells, through miRNA transfer [118]. In conclusion, cancer cell derived EVs can modify the tumour environment, promote pre-metastatic niches, enable metastatic process, and enhance cancer progression.

1.6.2 Anti-Tumourigenic Effects

Hitherto, many researchers have mainly focused on the pro-tumourigenic properties of EVs. However, the inexplicable nature of EVs has made scientists also focus on their anti-tumourigenic properties. The therapeutic efficacy of EVs may have bypassed some of the negative effects of EVs discussed earlier. For example, as a natural agent, EVs have become a potent therapeutic target for cancer treatment by interacting with the host immune system and reducing the unwanted side effects of anti- cancer treatments [122,123].

EVs secreted by murine dendritic cells containing α- fetoprotein have shown to elicit a strong immune response, resulting in decreased tumour growth in mice. Furthermore, recent clinical trials have employed dendritic cell derived EVs as an anti-cancer vaccine for lung cancer, melanoma, colorectal and hepatocellular carcinoma. These studies have shown that EVs induced an anti-tumour effect by inducing cytotoxic T- lymphocytes responses and increased T-cell activation [124,125,126,127]. Another study has discussed the effect of exosomes containing miR-375 on colon cancer, which inhibited cancer cell proliferation and invasion by blocking Bcl-2 [128]. Moreover, it was shown that exosomes containing circulating RNA -0051443 inhibited hepatocellular carcinoma progression by inducing apoptosis [129]. Mesenchymal stem cell derived exosomal miR-100 has been shown to inhibit breast cancer angiogenesis via modulating mTOR/HIF-1_/VEGF signalling [130]. Taken together, these findings suggest that uptake of EV cargo does not always result in pro-tumourigenic signaling. Therefore, this thesis will discuss the anti-tumourigenic effects of skeletal muscle derived EVs on lung carcinoma cell progression.

1.7 Diagnostic and Therapeutic Applications of EVs

EVs play an important role in many diseases, mainly promoting disease progression. EVs derived from these disease-state cells, encapsulate various biomarkers that are specific to them including, proteins, mRNAs, various non-coding RNAs and DNA fragments. Therefore, identifying, and unveiling of these biomarkers may provide a novel strategy for disease identification and treatments. EVs' prognostic impacts have been already demonstrated in many disease states, such as neurodegenerative, cardiac, reproductive, cancer and autoimmune disorders. A recent study reported that levels of EVs derived from platelet, endothelial cell and monocyte origin were significantly high in patients with metabolic diseases such as, type-2 diabetes, blood pressure, impaired glucose tolerance and obesity [83,131,132]. Elevated EV levels have also been noted in many cardiovascular diseases including atherosclerosis [133,134], deep vein thrombosis or pulmonary embolism [135,136] and in cerebrovascular disease [137]. Furthermore, it was found that cancer patients have elevated EV levels; sometimes ~ 40-fold high compared with healthy individuals [138]. Therefore, these varied levels of EV concentration in body fluids and their unique molecular signatures may enable the potential use of EVs as ideal diagnostic markers and as therapeutic targets.

EVs are well recognised as the mediators of intercellular cell communication through their cargo. Furthermore, due to their membrane composition they have the unique ability to cross tissue and cellular barriers [139]. Moreover, the capsulated cargos are protected against enzyme degradation during delivery and therefore, compared with synthetic drug carriers, EVs can be used as natural safe drug carries. Furthermore, EVs can be engineered to target specific organs which will enhance the drug delivery [140,141]. For example, a study conducted on a zebrafish brain cancer model has shown that exosomes loaded with anticancer drugs crossed the blood brain barrier to the brain tissue and exhibited enhanced therapeutic efficacy [142]. Furthermore,

a recent study in cardiovascular disease has shown that, EVs secreted by mesenchymal stem cells injected to injured heart resulted in healthy myocardium [143] therefore, EVs potentials in regenerative medicine field is also explored. Additionally, a recent finding in breast cancer, has shown that blocking the cancer promoting EV mediated signalling could be employed as a therapeutic strategy for breast cancer treatments [144]. Based on this evidence, further exploitation of EVs as a novel therapeutic strategy for many diseases seems promising.

1.8 Lung Cancer

With over 1.8 million new cases in 2020, lung cancer remains the most common cause of death from cancer and is estimated to be responsible for nearly 1 in 5 deaths [145]. In 2014, there were 35,895 lung cancer deaths in the UK, with a male: female ratio of around 12:10 [146]. The large majority of lung cancers (85%) are linked to tobacco smoking, including passive smoking [147]. Occupational exposure to carcinogens such as radon, asbestos, or silica accounts for a small number of cases per annum and the combination of these toxins and tobacco smoking increases the risk of cancer than with either factor alone [148]. Continuous exposure to cancer inducing agents, leads to the accumulation of multiple genetic mutations before respiratory epithelial cells becomes neoplastic. Mutations in cell growth genes (*K-RAS, MYC*), growth factor receptors (*EGFR, HER2/neu*), apoptosis gene (*BCL-2*) and tumour suppressor genes (*p53, APC*) accumulate resulting in lung carcinoma [148]. The factors contributing to the high mortality rate of lung cancer include late diagnosis, high rate of systemic recurrence and resistance to systemic therapy. Despite recent advances in lung cancer therapy, the overall prognosis remains very poor [149].

Lung cancer is generally classified as small cell lung carcinoma (SCLC) and non-small cell lung carcinoma (NSCLC). About 80% of lung cancers are NSCLS, which are further divided into squamous cell, large cell, adenocarcinomas and bronchioalveolar carcinomas [150]. SCLC

is a highly aggressive cancer, and it is strongly associated with tobacco smoking and accounts for ~15-20% of lung cancer cases [151]. SCLC is rapidly progressive and fatal due its rapid doubling time, high growth rate and widespread metastases. Unfortunately, most patients diagnosed having lung cancer eventually die due to widespread metastasis [147]. Lung cancer metastasises by lymphatic as well as blood vessels, however vascular invasion results in increased incidence of recurrence as well as shortened survival rates compared with the lymphatic route [152]. The most common sites of lung cancer metastases are liver, adrenal glands, bone, brain and bone marrow and they are known to occasionally present as a peripheral solitary pulmonary nodule [151,153]. However, haematogenous metastases to the limb skeletal muscles are extremely rare [154].

1.9 Apoptosis in Cancer

1.9.1 Overview of Apoptosis

Evasion of apoptosis is one of many hallmarks of all types of cancers. Apoptosis is the programmed cell death which is used to eliminate unwanted cells. Apoptosis occurs through two main pathways: the extrinsic or intrinsic pathway (**Figure 2**). These pathways are activated by both extracellular and intracellular signals, which activate the caspase proteins. Caspases are cysteine family proteins, which cleaves numerous proteins including cytoskeletal and nuclear proteins. As soon as the apoptosis signal occurs, the initiator caspases (caspase 2,8,9 and 10) cascade activates and leads to executioner caspase (caspase 3,6 and 7) activation. Other than caspases, there are many proteins that play a pivotal role in apoptosis such as, amyloid-B peptide, the Bcl-2 family of proteins, the p53 gene and the heat shock proteins (HSP).

1.9.1.1 Intrinsic Apoptotic Pathway

The intrinsic pathway is referred to as mitochondrial mediated apoptotic pathway and is activated by various extra and intracellular stress including, oxidative stress [155], stress caused by cytotoxic agents [155], surplus of Ca^{2+}, and growth factor deprivation [156] to name a few. The pathway activated by upregulation of BH3- only proteins, which induce BAX and BAK oligomerisation, leading to mitochondrial outer membrane permeabilisation (MOMP) [157]. Due to membrane permeabilisation, mitochondrial intermembrane proteins such as cytochrome c, second mitochondria-derived activator of caspase (SMAC) and Omi are released into the cytosol [156]. The cytochrome *c* combines with apoptotic protease-activating factor-1 (APAF-1), dATP and procaspase-9 to form the apoptosome [156,158]. Upon the formation of the apoptosome, caspase 9 activates followed by the activation of caspase 3 and 7 signalling cascade which leads to protein breakdown and cell death [156].

1.9.1.2 Extrinsic Apoptotic Pathway

Extracellular stimulus activates the extrinsic pathway and induces apoptosis. The pathway activates when extracellular ligands such as, TNF (tumour necrosis factor), Fas-L (Fas ligand), and TRAIL (TNF-related apoptosis-inducing ligand) bind to the extracellular domain of the DR (transmembrane death receptors) [158,159]. Stimulation of death receptors, result in the recruitment of adaptor molecules such as Fas-associated death domain (FADD), TNF receptor-associated death domain (TRADD) and procaspases -8 and 10 to the death receptors. Together they form DISC (death inducing signalling complex) [159,160]. Then the caspase 8 activates and dissociates from the DISC to start the cascade of caspase activation. Activated caspases including, caspases 3,6 and 7 start to cleave proteins and cytoskeleton leading to apoptosis [158,161].

As mentioned earlier, a main characteristic of cancer is to evade apoptosis, which then contributes to both tumourigenesis and treatment resistance. Cancer cells achieve this by suppressing the proapoptotic machinery and amplifying anti-apoptotic protein signals. For example, upregulation of antiapoptotic BCL-2 protein is present in most of the cancers and it inhibit apoptosis by inhibiting proapoptotic proteins such as, BAX and BAK in the intrinsic pathway.

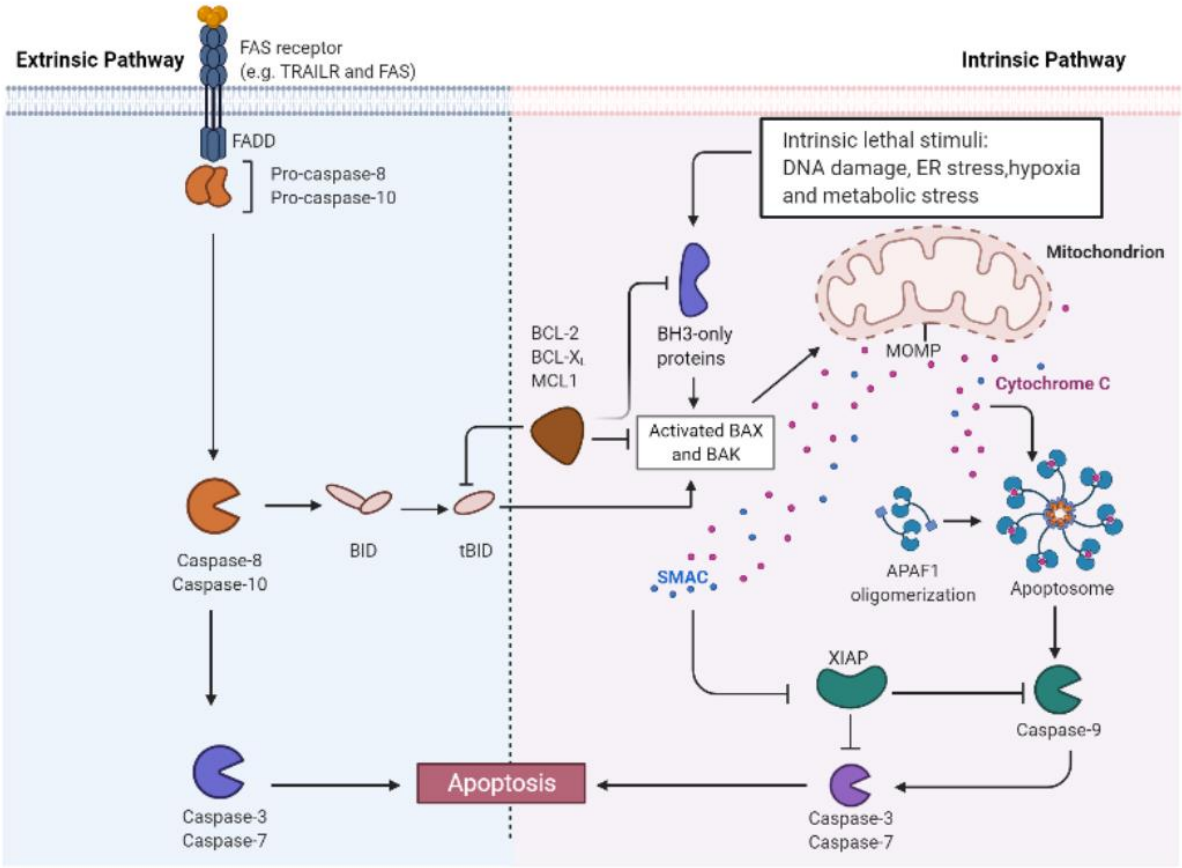

Figure 2: Schematic representation apoptosis signalling pathways

The extrinsic pathway is activated by binding of extracellular ligands to death receptors. Stimulation of death receptors form DISC complex which in turns activate caspase 8. The intrinsic pathway activates by upregulation of BH3 only proteins, which induce BAX and BAK leading to MOMP. Release of cytochrome c from mitochondria results in the formation of the apoptosome, which activates caspase 9. Caspase 8 from the extrinsic pathway and caspase 9 from the intrinsic pathway activate downstream caspase 3 resulting in cell death. The two pathways are linked through the cleavage of BH3 only protein Bid.

1.10 Apoptosis as a Cancer Therapy

Evasion of apoptosis is a hallmark of all types of cancer and therefore, targeting apoptosis has been the centre of attraction in recent cancer therapy research. This was further enhanced by the fact that apoptosis causes minimal damage to the healthy cells around the tumour but exerts maximum effect on cancer cells. As mentioned earlier, there are many proapoptotic and antiapoptotic proteins involved in both intrinsic and extrinsic pathways; therefore, enhancing proapoptotic proteins and inhibiting antiapoptotic proteins has been the main focus of apoptosis-based cancer therapy. For example, antiapoptotic proteins such as, BCL-2, BCL-XL proteins were inhibited by BH3 mimetics; ABT-737 in a small cell lung carcinoma cell line [162]. Some other targets that have been researched include, XIAP inhibition, through which downstream effector caspase 3 is enhanced in response to caspase 8 activation in extrinsic pathway [163]. Moreover, some anticancer therapy drugs targets death receptor ligands such as, TRAIL which, triggers the extrinsic apoptosis pathway and SMAC mimetics that enhance caspase activities [164]. Furthermore, other pathways and proteins involved in apoptosis such as p53, nuclear factor kappa B and the phosphatidylinositol 3 kinase pathways have been also targeted by rapamycin inhibitors [165]. Interestingly, some of the drugs such as arsenic trioxide are directly aimed at mitochondrial functions to cause intrinsic pathway apoptosis [166]. Even though, most of these drugs seems promising, sometimes cancer cells form intrinsic chemoresistance against these drugs. Therefore, there is a clear need for more apoptosis targeting using novel compounds with increased efficacy for cancer treatment.

1.11 Skeletal Muscle

1.11.1 Tumour Metastasis to Skeletal Muscle is Rare

Metastasis is the movement of cancer cells from a primary site to colonize distant organs and is the primary cause of cancer- related deaths [167]. Cancer metastasis mechanisms are extremely

complicated and involve many factors. Instead of being autonomous, tumour cells engage in bidirectional interactions with host organ microenvironments and alter genomic stability and immune responses, which facilitates their invasion survival and progression [167,168]. Therefore, the host microenvironment is a crucial factor in cancer metastasis. Most organs and tissues are subjected to cancer metastasis with the striking exception of skeletal muscle, in which cancer metastasis is very rare [169,17,171,172]. The prevalence of muscle metastasis varies from 0.03% to 5.6% in autopsy series[2] [173,174,175,176], and from 1.2% to 1.8% in radiological series [177,178] and most of these incidents are from primary lung carcinomas and malignant melanomas.

The rarity of cancer metastasis in skeletal muscle is surprising as the skeletal muscle compromises ~50% of the body mass. Moreover, skeletal muscle is a highly vascularized tissue. Over the years, researchers have postulated various reasons for this rarity, however a definitive mechanism has not yet been identified. Some researchers have linked this phenomenon to increased activity within the muscular system [179,180,181]. A recent study has confirmed that physical activity acts as a negative regulator for tumour cell growth in skeletal muscle tissue [182,183]. Skeletal muscles produce high levels of lactic acid and that has been linked to the rarity of cancer metastasis to skeletal system [183]. Several studies have also shown that muscle conditioned media exert a cytostatic effect upon tumour cells [184,185] and phenotypically convert and inhibit metastatic cells[234]. Low molecular weight factors, such as adenosine were suggested to be responsible for the inhibition of tumour growth [186]. Other mediators released by muscle cells may also account for the rarity of tumour metastases, including cytokines [186] with anticancer activity such as TNFα [187], TGFβ [188], lymphocyte infiltrating factor [189], interferon γ [190] and proteolytic enzymes such as plasminogen activator inhibitor [191,192].

Given the fact that EVs are cell origin specific, it is postulated that EVs may induce similar cellular effects to its parent cells. Therefore, this thesis aims to investigate the role of skeletal muscle derived EVs as contributing factor for the rarity of cancer progression observed in skeletal muscles.

1.11.2 Role of Skeletal Muscle Cell Derived EVs

It is well established that all cells in the body can secrete distinctive type of EVs to its microenvironment. EVs carry a cargo of various proteins, lipids, nucleic acids such as miRNAs and are themselves involved in intercellular communication. Recent studies found that skeletal muscles release EVs which play a key role in muscle physiology, homeostasis and in some metabolic diseases [193]. For example, miRNAs derived from skeletal myocytes play pivotal roles in skeletal muscle development, myogenesis and nutrient metabolism in physiological and pathological states [194,195]. Specific miRNAs in exosomes (miR-1, miR-21, miR-133, miR-182, and miR-206), are known to alter the gene expression in myocytes and therefore, modulating the physiology and pathology status of myocytes [195,196]. Furthermore, it is found that stress may promote the release of EVs from myotubes that are carrying a variety of cargoes, which can be transported via circulatory systems to other cells in the local environment [197].

Moreover, myocytes are known to release myokines, skeletal muscle cell specific cytokines, in response to stress, such as exercise. Over 600 [198] myokines were found in human myocyte culture medium including, Myostatin, Irisin, IL-6, IL-15, Myonectin, Decorin, SPARC and FSTL-1 to name few. Interestingly, some of these myokines have been found in myocyte EVs and they were known to be involved in cancer suppression. For example, a few mechanistic studies have shown the potential role of myokines such as, irisin, oncostatin and SPARC in the

suppression of colon and breast cancer growth [199]. Moreover, another study has shown the role of interleukin-6 (IL-6) and SPARC in the prevention of cancers by exercise [200].

Among all the myokines, decorin has been well researched as a cancer suppressor. A study using a decorin knock out mouse model has shown, that 30% of mice developed spontaneous intestinal tumour growth and invasion in the absence of decorin [201]. Furthermore, decorin has been shown to affect cancer progression by targeting key signalling molecules including, TGF-β and receptor tyrosine kinase which inhibit cancer cell growth, survival, metastasis and angiogenesis [202]. Moreover, over expression of decorin has induced apoptosis and cell cycle arrest in rat mesangial cell *in vitro* [203]. Taken together, it seems promising that some of these myokines and proteins in skeletal muscle EVs may act as a novel target in cancer suppression; therefore, this thesis will also investigate the protein cargos of myocyte derived EVs.

2. Aims of the Present Study

In recent years, extracellular vesicles (EVs) are attracting considerable interest in the scientific community due to their role in normal physiology as well as their involvement in in range of pathologies. In cancer, EVs have been known to act as carriers of various soluble proteins and shown to aid in tumour spread and survival. Most organs and tissues are subjected to cancer metastasis with the striking exception of skeletal muscle, in which cancer metastasis is very rare. Therefore, the aim of this study to elucidate whether skeletal muscle derived EVs carry certain bioactive proteins, which prevent cancer metastasis and progression in skeletal muscle system.

To understand the mechanism by which myocyte EVs inhibit cancer metastasis and progression to skeletal system, EVs from murine myocytes will be isolated and characterised by employing gold standard methods including, Nanoparticle Tracking Analysis, specific protein markers and Flow cytometry. Furthermore, various test will be carried out to investigate the effect of myocyte derived EVs on highly metastatic lung carcinoma cellular processes including, cell proliferation, cell cytotoxicity, cell migration, EV uptake by recipient cells and apoptosis. Finally, further test including proteomics and Western blot techniques will be considered to identify the certain bioactive proteins in myocyte derived EVs, which prevent cancer metastasis and progression in skeletal muscle system.

3. Materials and Methods

~~1.1~~3.1 Materials

~~1.1.1~~3.1.1 Reagents

Acrylamide/Bisacrylamide	Sigma-Aldrich
Annexin V Alexa Fluor 488	Invitrogen
Annexin V reagent	R&D Systems
BCA protein assay kit	Sigma-Aldrich
BSA (Bovine serum albumin)	Sigma-Aldrich
Bromophenol blue	Thermofisher Scientific
Caspase 3,8 and 9 Activity Assay	abcam
CytoTox 96® Cytotoxicity Assay	Promega
Coomassie brilliant blue	Thermofisher Scientific
Crystal violet stain	Thermofisher Scientific
DAPI-VECTASHIELD	Thermofisher Scientific
DMEM	Sigma-Aldrich
DMSO (Dimethyl sulfoxide)	Thermofisher Scientific
DTT (Dithiol threitol)	Thermofisher Scientific
ECL WB Detection Reagent	Thermofisher Scientific
Ethanol	Sigma-Aldrich
FBS (Foetal Bovine Serum)	Sigma-Aldrich
Glycine	Sigma-Aldrich
Guava Cell Cycle reagent	Guava Technologies, UK
Guava ViaCount reagent	Guava Technologies, UK
Guava Nexin reagent	Guava Technologies, UK
Halt Protease Cocktail	Thermofisher Scientific
HCl (Hydrochloric acid)	Thermofisher Scientific
Horse serum	Thermofisher Scientific
LysoTracker™ Green DND-26	Thermofisher Scientific
Milk powder	Thermofisher Scientific
MitoTracker™ Red CMXRos	Thermofisher Scientific
Na2HPO4	Thermofisher Scientific
Paraformaldehyde	Sigma-Aldrich
PBS (Phosphate Buffer Saline)	Sigma-Aldrich
Penicillin / Streptomycin	Sigma-Aldrich
PKH26	Sigma-Aldrich
PKH67	Sigma-Aldrich
Ponceau S	BioRad
Potassium chloride	Sigma-Aldrich
Propidium iodide	Sigma-Aldrich
Protein molecular weight marker	Sigma-Aldrich
SDS (Sodium dodecyl sulphate)	Thermofisher Scientific
Sodium chloride	Sigma-Aldrich
Tris base	Sigma-Aldrich
Trichloroacetic acid	Thermofisher Scientific
Trypan Blue	Thermofisher Scientific
Trypsin/ EDTA	Sigma-Aldrich
Tween 20	Sigma-Aldrich

~~1.1.2~~3.1.2 Technical Devices and Consumables

Cell culture flasks (25cm2)	Fisher Scientific
Cell culture flasks (75cm2)	Fisher Scientific
Centrifuge 5804 R	Eppendorf
Centrifuge 5810 R	Eppendorf
Chamber Slides	Thermofisher Scientific
Corning Transwell plate	Sigma Aldrich
Fluorescence microscope FL	Invetrogen EVOS
FLUOstar Omega plate reader	Olympus Corporation, Germany
Gel loading tips	Corning
Guava EasyCyte 8HT cytometer	Millipore
Heamocytometer	Fisher Scientific
Incubator Heraeus CO2- Auto- Zero	BMG Labtech, UK
Microcentrifuge 5417 R	Thermo Electron Corporation
Microplate (6- well)	Sigma Aldrich
Microplate (12- well)	Sigma Aldrich
Microplate (24- well)	Sigma Aldrich
Microplate (96- well)	Sigma Aldrich
NanoSight NS300 system	Malvern, UK
Nikon Inverted Microscope	Nikon Eclipse, Japan
PH- Meter 766 Calimatic	Jenway
Roto- Shake Genie	Denley
SE-12 rotor	Sorvall
Semi- dry transfer system	BioRad
Sorvall T-865 rotor	Sorvall
UVP Chemiluminescence	UVP Bioimaging Systems, UK

~~1.1.3~~3.1.3 Antibodies

Anti-Myogenin antibody (F5D)	Abcam
Mouse anti- IgG FITC	Abcam
Mouse anti CD63	Abcam
Anti TSG101	Abcam
HRP-labelled goat anti-rabbit IgG	BioRad

~~1.1.4~~3.1.4 Eukaryotic Cell lines

C2C12 Myoblast	ECACC catalogue no. 91031101
NIH 3T3 Fibroblast	ECACC catalogue no. 93061524
CMT 64/61 Lung Carcinoma	Ximbio catalogue no. 152751

~~1.1.5~~3.1.5 Eukaryotic cell culture media: Cellular Growth Medium

C2C12 Myoblast growth medium was DMEM containing 2mM Glutamine and Phenol red supplemented with 10% Foetal Bovine Serum (FBS) (v/v), 1% Penicillin / Streptomycin (v/v) , stored at 4°C.

C2C12 cell differentiated medium was DMEM containing 2mM Glutamine and Phenol red supplemented with 5% Horse Serum (HS) (v/v), 1% Penicillin / Streptomycin (v/v), stored at 4°C.

NIH 3T3 Fibroblast growth medium was DMEM containing 2mM Glutamine and Phenol red supplemented with 10% Foetal Bovine Serum (FBS), 1% Penicillin / Streptomycin (v/v), stored at 4°C.

CMT 64/61 Lung Carcinoma growth medium was Waymouth's MB 752/1 containing 2mM Glutamine and Phenol red supplemented with 10% Foetal Bovine Serum (FBS) (v/v), 1% Penicillin / Streptomycin (v/v), stored at 4°C.

~~1.1.6~~3.1.6 Experimental Buffers and Solutions

~~1.1.6.1~~3.1.6.1 Cell Freezing Medium (C2C12 and NIH 3T3 Cell lines)

20%	FBS (v/v)
10%	DMSO (v/v)
1%	Streptomycin (v/v)
69%	DMEM (v/v)

3.1.6.2 Cell Freezing Medium (CMT 64/61 Cell line)

20%	FBS (v/v)
10%	DMSO (v/v)
1%	Streptomycin (v/v)
69%	Waymouth's MB 752/1 (v/v)

3.1.6.3 SDS- PAGE solutions

3.1.6.3.1 (4×) SDS Sample buffer – pH 6.8

200 mM	Tris-HCl
25%	Glycine (w/v)
2%	SDS (w/v)
0.2%	Bromophenol blue (w/v)
20 mM	DTT (add fresh on the day)
	Millipore water

3.1.6.3.2 Electrophoresis running buffer (1L)

30 g	Tris-HCl, pH 8.3
144 g	Glycine
950 ml	20% SDS (w/v)
	ddH_2O

3.1.6.3.3 Coomassie Brilliant Blue G-250

0.025%	Coomassie blue (w/v)
10%	Acetic acid (v/v)
90%	ddH_2O

3.1.6.3.4 Transfer buffer (10×)

250 ml	Tris base
1925 ml	Glycine
	ddH_2O

3.1.6.3.5 Ponceau solutions

0.25%	Ponceau S (w/v)
3%	Trichloroacetic acid (v/v)
	ddH_2O

3.1.6.3.6 Phosphate Buffer Saline (PBS) Solution – 1L

140 mM	NaCl
2.7 mM	KCl
10 mM	Na_2HPO_4
1.8 mM	KH_2PO_4
	ddH_2O

3.1.6.3.7 Phosphate Buffer Saline – Tween 20 (PBS-T)

1L	PBS
1ml	Tween 20

3.1.6.3.8 Blocking buffer

5%	Milk powder (w/v)
	PBS-T

3.1.6.3.9 Antibody dilution buffer

3%	BSA (w/v)
	PBS

3.2 Methods

3.2.1 Maintaining Cell Lines

3.2.1.1 Adherent Cell Lines

Adherent cells, murine myoblast cells (C2C12) and murine fibroblast (NIH 3T3) were maintained in growth medium containing Dulbecco's modified Eagle's medium (DMEM) supplemented with 10% foetal bovine serum (FBS), 1% penicillin-streptomycin at 37 ^{o}C in 5% CO_2 atmospheric conditions. Murine lung carcinoma cell line (CMT 64/61) was maintained in growth medium containing Waymouth MB 752/1 medium supplemented with 10% foetal bovine serum (FBS), 1% penicillin-streptomycin. The cells were split, once the culture reached 70% confluence by washing twice with Phosphate – Buffered Saline (PBS) and adding 0.25%(v/v) trypsin/EDTA. After 10 min incubating at 37 ^{o}C with 5% CO_2 growth medium was added to inactivate the trypsin. The trypsinised cells were transferred into 50ml centrifuge tubes and spun at 200 × g for 5 min. The cell pellet was re-suspended in the appropriate

volume of growth medium and inoculated at the desired cell densities in new culture flasks. Growth medium was renewed every 2 to 3 days.

3.2.1.2 Cryopreservation of Eukaryotic Cells

To prepare frozen stocks for long term storage, adherent cells grown to almost 80% confluency and were trypsinised to attain a cell suspension. Then trypsinised cells were washed twice (200 × *g* , 5 min) with PBS and cell number was determined using Guava viacount assay. Cells were carefully resuspended in freeze mix, transferred into cryo-vials (Greiner) at 1×10^7 cells/ml in 1 ml volumes and immediately placed on ice. The cryo-vials were frozen at -80°C in special cryo boxes, which ensure a temperature decrease of 1°C per minute. For long-term storage the deep frozen cryo-vials were transferred to liquid nitrogen cell storage tanks.

3.2.1.3 Thawing Cells

To defrost cells, cryo-vials were removed from liquid nitrogen and immediately thawed in a waterbath at 37°C. After cleaning the lid with 70% ethanol, the content was transferred to a 15 ml centrifuge tube containing 9 ml of fresh growth medium, prewarmed to 37°C and cells were sedimented by centrifugation at the appropriate speed and time (200 × *g* , 5 min). To remove DMSO, the medium was discarded, and the pellet was resuspended in fresh growth medium. The cells were then placed into culture flasks of the same size as had been used prior to freezing and incubated at 37°C with 5% CO_2.

3.2.2 Extracellular Vesicles Collection and Analysis

3.2.2.1 Extracellular Vesicle Isolation from Cell Culture Medium

C2C12 myocytes and NIH 3T3 cells were grown in complete growth medium until 70% confluent. Then the cells were washed with pre- warmed PBS twice and cells were incubated

with 10 ml serum free medium for 16h at 37 ^{o}C in 5% CO_2 to avoid contamination with FBS EVs. After 16h, serum free medium was collected and centrifuged at 300 × g for 15 min to remove dead cells and debris, then 4,000 × g for 1h at 4 ^{o}C to remove apoptotic bodies. The resultant supernatant was ultracentrifuged at 18,500 × g for 1h at 4 ^{o}C. The isolated EV pellet was resuspended in filtered PBS and ultracentrifuge again at 18,500 × g for 1h at 4 ^{o}C to remove proteins and other low molecular weight factors bound to the EVs membrane surface. The MV pellet was resuspended in cold filtered DMEM.

3.2.2.2 Annexin Labelling of EVs

Isolated EVs (100 µl) was resuspended in Annexin binding buffer and Guava Nexin-FITC (100 µl). A control sample was performed by not adding Annexin binding buffer and Gauva Nexin –FITC to the EV sample. Sample was then incubated at RT for 30 min and was analysed immediately as directed by the manufacturer using the flow cytometer (Guava EasyCyte HT, Guava Technologies).

3.2.2.3 PKH26 Labelling of EVs

EVs from C2C12 myocytes were labelled with PKH dye according to the manufacturer instructions. 25 µl of EVs suspended in PBS was mixed with 250 µl of diluent C. Meanwhile, 2µl of the PKH26 dye was mixed with 250µl of diluent C and added to the EVs suspension prepared in earlier step. EVs/dye suspension was mixed thoroughly and left to incubate 5 min in ice. The staining was stopped by adding 500 µl of 1% BSA to the dye solution and incubated 1 minute on ice. The EV pellet was centrifuged at 18,500 × g for 1 hour at 4°C to remove excess dye. After centrifugation, the EV pellet was resuspended in PBS and washed by centrifuging 18,500 × g for 1 hour at 4°C for twice to remove unbounded dye. 10 µl (~20µg/ml) stained EVs were analysed by flow cytometry and fluorescent microscopy.

3.2.2.4 Nanoparticle Tracking Analysis of EVs

The concentration and the size of EVs isolated from C2C12 myocytes were analysed using the NanoSight NS300 system (Malvern Instruments, Malvern, UK) configured with sCMOS camera and blue488 laser type. For NTA analysis, EVs collected from 3.2×10^7 C2C12 cells and five different samples at different passages were collected. EVs were diluted in PBS to a final volume of 1 ml Following manufacturer's software manual, three 1-minute videos were captured at temperature between 17.8 – 19.2°C. The videos were analysed by the in-build NanoSight Software NTA 3.2.

3.2.3 Biochemical Methods

3.2.3.1 Promotion of C2C12 Cell Differentiation

Cells in the myoblast stage were differentiated into myocytes by replacing the growth medium into a serum free alternative. Once the myoblasts reached 90% confluence, cells were washed twice with PBS followed by addition of 10 ml of 5% horse serum containing skeletal muscle differentiation medium and maintained at 37 ^{o}C in 5% CO_2 for the time interval dictated by the experiment. Differentiation medium was then changed every other day. The time points used were 24h, 2 days, 3 days, and 4 days.

3.2.3.2 Preparation of Conditioned Media

Condition media were collected from both C2C12 myocytes and NIH-3T3 fibroblast cell lines. To collect the conditioned medium, both C2C12 and NIH-3T3 cells were seeded in flasks with 10% serum. Once they reached 80% confluency, cells were washed 3 times with PBS and serum- free DMEM was added. After 16h serum free medium was collected and centrifuged at 200 × *g* for 5 min to remove the dead cells and cell debris.

3.2.3.3 Determination of Protein Concentration

The concentration of proteins in EVs was determined by using the BCA Protein Assay Kit (Pierce, Thermo Scientific). The assay uses a combination of biuret reaction (reduction of Cu^{2+} ions to Cu^{+} ions by proteins in an alkaline medium) and the colorimetric detection of the Cu^{+} cations by a bicinchoninic acid containing colour agent. Following the manufacturer's instructions, a standard series of protein concentrations were prepared using PBS as the diluent. Standard concentrations were 0, 25, 125, 250, 500, 750, 1,000, 1500 and 2,000 µg/ml. The working reagent was prepared by mixing kit agent A and reagent B (ratio 50:1 respectively). A 10 µl of protein from each standard and unknown sample were mixed with 200 µl of working reagent in a 96 well plate followed by incubation at 37 ºC for 30 min. The plate was cooled at room temperature prior to measuring the absorbance at 562 nm on a FLUOstar Omega microplate reader. Protein concentrations of the unknown samples were determined by interpolation on a standard curve using GraphPad Software.

3.2.3.4 Preparation of Cell Lysates

Cell lysates were prepared for the C2C12 myoblast (24 hours after culturing) and C2C12 cells in differentiated media (24 hours and 4 days after). C2C12 cells grown in culture flasks were treated with trypsin and were sedimented by centrifugation (200 × g , 5 min at 15°C) and a haemocytometer was used to determine the cell number. Cells were resuspended in cold PBS, transferred to micro-centrifuge tubes and centrifuged to obtain a cell pellet. Carefully, PBS was aspirated, and cells were resuspended in ice cold RIPA lysis buffer (1ml per 10^7 cells). A constant agitation was created for 30 min at 4°C and the cells were then centrifuged at 12,000 × g for 20 min at 4°C. The tubes were gently removed from the centrifuge and place on ice, aspirate the supernatant and placed in a fresh tube kept on ice; the pellet was discarded. Protease

inhibitors were added to the sample and the total protein concentration was determined of the resultant supernatant.

3.2.3.5 Sample Preparation for SDS-Polyacrylamide Gel Electrophoresis

First, lysate samples collected from both cells and EVs protein concentration was determined by BCA assay. Desired protein volumes were taken and an equal volume of 2× Laemmli loading buffer containing 2-*β*-Mercaptoethanol was added, and the samples were boiled at 95°C for 4 min. Then the samples were then briefly centrifuged at 500 × *g*.

3.2.3.6 SDS-PAGE protein molecular weight standards

Prestained protein molecular weight marker (BioRad) was used as a standard loading, 10µl per gel. The standard represents bands of 10 to 250 kD prestained protein markers. The gel was later stained with Coomassie blue.

3.2.3.7 SDS- Polyacrylamide Gel Electrophoresis

Mini PROTEAN tetra vertical electrophoresis cell system (Bio-Rad), with Mini PROTEAN precast gels (4-20% TGX gels, Bio-Rad) were used to perform the gel electrophoresis. To perform electrophoresis, precast mini- gel was placed inside the Mini PROTEAN tetra vertical electrophoresis cell system. Electrophoresis running buffer was added to the inner and outer chambers of the tank and the plastic comb was carefully removed from the precast gel. Samples were loaded into the wells of precast gel using extra-long loading pipette tips. 5 µl of protein molecular weight standard was added to the first well on the gel. Electrophoretic separation was performed at 150 V (constant voltage) until the bromophenol blue front of the SDS sample buffer reached the end of the resolving gel. Gels were either stained with Coomassie Brilliant Blue R250 or transferred onto nitrocellulose membrane for Western blot analysis.

3.2.3.8 Western Blot Analysis

Proteins separated by gel electrophoresis were transferred to a nitrocellulose membrane for further analysis using a semidry transfer device, Bio-Rad Sartoblot system. A nitrocellulose membrane and two pieces of blotting paper (Whatman 3 MM, BioRad) were cut to the size of the separating gel. Blotting papers and the membrane were soaked in transfer buffer. One piece of blotting paper was placed on the cathode plate, and the nitrocellulose membrane was placed on top of the blotting paper. Electrophoresis gel was placed on top of the membrane, and a second blotting paper was also placed on top of the gel. Having removed air bubbles, the anode plate, also dampened with the transfer buffer was used to complete the sandwich. Electroblotting was carried at 15 V (constant voltage) for 1 h 10 min.

3.2.3.9 Reversible Ponceau Staining

To ensure successful protein transfer on to the hybond C nitrocellulose membrane, the membranes were incubated with Ponceau S solution for 1 min. Excessive Ponceau solution was removed by washing the membranes with deionized water until the protein bands were visible. Membranes were labelled and cut when needed for label with different primary antibodies.

3.2.3.10 Immunochemical Protein Detection using the ECL System

The nitrocellulose membrane was first incubated in blocking buffer (5% BSA, 3% or 6% milk in TBS-T) for 1 h at room temperature on a shaker. Following blocking, the membrane was rinsed with PBS-T and incubated with the primary antibody. The blot was probed with (1 µg/ml) primary antibody and incubated overnight at 4°C on a shaker. Three 5 min washing steps with PBS-T were performed and the membrane was incubated with secondary IgG

antibodies coupled to HRP in a 1:5000 dilution for 1 hour at room temperature. The unbound secondary antibody was removed by washing the membrane with TBS-T six times for 10 mins each. The last wash was performed using PBS without the Tween to avoid background noise. Visualisation was performed using the enhanced chemiluminescence reagent system (ECL, Amersham Pharmacia). The ECL solutions (reagent A and B) were mixed at equal volumes and the membranes were incubated with the mixture for 1 min at room temperature and chemiluminescence was detected using UVP ChemiDoc-It system (UVP systems, UK).

3.2.3.11 PKH67 Cell Labelling

CMT 64/61 cell were cultured in T75cm^3 flask until it reached 90% confluency. Cell were trypsinised and washed using serum free medium. 2×10^7 of cells were collected from the cell suspension and centrifuged at 400 × g for 5 min. After centrifugation, the supernatant was aspirated very carefully not to remove any cells. The cell pellet was mixed with 1 ml of diluent C to prepare a 2 × cell suspension. Meanwhile, 4 µl of PKH67 dye solution was mixed with 1 ml of diluent C and added to the cell suspension prepared earlier. Cell/dye suspension was incubated 5 min with periodic mixing. The staining was stopped by adding 2 ml of 1% BSA to the cell suspension and incubated for further 1 minute. Then the cell suspension was centrifuged at 400 × g for 10 min at 25 ^{0}C. Cell pellet was collected and resuspended in 10 ml complete growth medium and centrifuged at 400 × g for 5 min. Pellet was washed 2 more times with 10 ml of complete growth medium to ensure removal of unbound dye. After the final wash cell viability was assessed and 1×10^4 cells were cultured in glass bottom well plate. Cell plate was incubated at 37 ^{o}C in 5% CO_2 for 24 h and visualised under a fluorescent microscope.

3.2.3.12 Cell Viability Assay

In order to study the effect of C2C12 myocyte conditioned medium or EVs on murine lung carcinoma cell, CMT 64/61 cells were seeded in 24-well plates (at 1×10^4 cells per well) in triplicate and incubated for 24 h at 37 °C. On the day of the experiment, cells in the plate were first observed under a light microscope for cell attachment and then washed three times with pre-warmed PBS. Each well was treated with 5% FBS and appropriate conditioned medium and EVs protein concentration. Protein concentrations used to treat the CMT 64/61 cells were 100 µg/ml, 200 µg/ml, 300 µg/ml and 500 µg/ml. The volume of serum-free medium was adjusted to obtain a final volume of 500 µl per well and the plates incubated at 37°C for 48 h. Triplicate wells with untreated cells in 5% FBS was used as a control.

In co-culture experiment, each well was treated with 5% FBS and appropriate conditioned medium protein concentrations and EV concentrations. Triplicate wells with untreated cells in 5% FBS was used as a control. The volume of serum free medium was adjusted to obtain a final volume of 500 µl per well and the plate incubated at 37 °C for 48 h. After 48 h, plates were first observed under the microscope to check for contamination. The supernatant was then collected from each well and transferred to 1.5 ml micro- centrifuge tubes (one tube for each triplicate treatment). The wells were washed twice with Dulbecco's Phosphate Buffered Saline (DPBS) and the wells were treated with trypsin (25 µl of 0.25% Trypsin/EDTA) at 37°C for 5 min to detach the cells. Detached cells were resuspended in 175 µl of complete growth medium and collected into micro-centrifuge tubes. Cell viability was determined by flow cytometry using the Guava ViaCount Assay.

3.2.3.13 Cell Migration Assay

In order to investigate the effect of C2C12 derived EVs on Murine lung carcinoma cell (CMT 64/61), 1×10^5 cells were seeded in triplicate in Corning 8.0 µm Transwell® Inserts with serum free media. The appropriate C2C12 EV concentrations were added to the receiver wells in the transwell plates with 5% FBS. EVs-free receiver triplicates were performed as a background control. The plate was incubated at 37 °C for 24 h. After incubation, medium from both receiver and the insert were aspirated. The insert was washed twice with PBS. Cells that had adhered inside the insert were removed using a cotton swab and the insert was washed again with PBS. Crystal violet stain was used to stain the cells adhered to the insert membrane and the cells from 5 random areas were counted under the light microscope.

3.2.3.14 Cell Cytotoxicity Assay

To investigate the cell cytotoxicity effect of myocyte EVs on carcinoma cell line, Promega CytoTox 96 reagent was used. Carcinoma cell line, CMT 64/61 cells were seeded in 96-well plates (at 1×10^4 cells per well) in triplicate and wells were treated with 5% FBS containing growth medium with appropriate EV concentrations and incubated at 37 °C for 24 h. Triplicate wells without cells were served as a negative control to determine the culture medium background. A second, triplicate wells with untreated cells were served as control whilst, a final triplicate wells with untreated cells we set to determine the maximum Lactate dehydrogenase (LDH) release positive control. 50 µl aliquots from all the test and control wells were transferred to a fresh 96- well flat clear bottom well plate and, 50 µl of CytoTox 96 reagent was added to each sample aliquot. Plate was covered with a foil paper and incubated for 30 min at room temperature. To generate a maximum LDH release, 10 µl of 10X lysis solution was added to the positive cell wells 45 min before adding CytoTox 96 reagent. Finally, a 50 µl

of stop solution was added to each sample and absorbance recorded at 492 nm on a FLUOstar Omega microplate reader.

3.2.3.15 LysoTracker Analysis

Carcinoma cell line, CMT 64/61 cells were seeded at 1×10^4 cells per well in 24 well plate. Cells were seeded in triplicate and wells were treated with 5% FBS with and without appropriate EV concentrations and incubated at 37°C for 48 hours. After incubation, 5000 cells from each well were transferred to 96 well plate. A 75 nM of LysoTracker solution containing growth medium was added to each cell wells and incubated at 37°C for 45 min. Then the cells were washed, and lysosome fluorescent intensity was measured on a FLUOstar Omega microplate reader (Excitation: 504 nm and Emission: 511 nm, bottom reading).

An Additional set of carcinoma cells 1×10^4 were seeded in microscopic chamber slide and incubated at 37°C with appropriate EVs concentration as described in previously. After 48 h incubation, chamber slide was washed and 75 nM LysoTracker staining solution was added to each chamber and further incubated for 45 min. After staining, cells were washed with PBS and analysed by fluorescent microscope.

3.2.3.16 MitoTracker Analysis

Following manufacturer instruction, MitoTracker stock solution was prepared by dissolving MitoTraker in DMSO to a final concentration of 1 mM. Then a 100 nM staining solution was prepared by diluting the stock solution in appropriate volume of growth medium. Carcinoma cell line, CMT 64/61 cells were seeded at 1×10^4 cells per well in 24 well plate. Cells were seeded in triplicate and wells were treated with 5% FBS with and without appropriate EV concentrations and incubated at 37°C for 48 h. After incubation, 5000 cells from each well

were transferred to 96 well plate. Then the cells were resuspended in prewarmed growth medium containing MitoTracker staining solution for 30 min. After incubation, cells were washed and MitoTracker fluorescent intensity was measured on a FLUOstar Omega microplate reader (Excitation: 579 nm and Emission: 599 nm, bottom reading).

An Additional set of carcinoma cells at 1×10^4 were seeded in microscopic chamber slide and incubated at 37°C with appropriate EVs concentration as described previously. After 48 h incubation, chamber slide was washed, and 100 nM staining solution was added to each chamber and further incubated for 45 min. After staining, cells were washed with PBS and incubated 15 min with prewarmed PB containing 4% formaldehyde. After fixation cells were washed several times with PBS and analysed by fluorescent microscope.

3.2.3.17 Caspase Assay

In order to determine the apoptosis pathway, caspase 3,8, and 9 detection assays were performed. Carcinoma cell line, 1×10^4 cells/ 90 µl per well in triplicate were seeded into a 96 well plate. Cells were treated with 10 µl of growth medium containing desired concentrations of myocyte EVs. As control samples, cells were treated with 10 µl of growth medium (without testing compound) and well with 10 µl of growth medium but no cells were performed in triplicate. In addition, another set of control wells, cells without testing compound, were performed. Total volume was kept at 100 µl per well and plate was incubated at 37°C for 48 h.

On the day of the experiment, tri- caspase assay loading solution was prepared by diluting caspase substrate 1:200 in assay buffer. 100 µl of loading solution was added to each well and incubated the plate at room temperature, protected from light for 60 min. As a positive control, one cell set contained growth medium only were treated with 50 µM of H_2O_2 for 24 h prior

adding the caspase loading solution. After incubation, fluorescent intensity was measured on a FLUOstar Omega microplate reader (Caspase 3: Ex/Em = 535/620 nm (red), Caspase 8: Ex/Em = 490/525 nm (green), Caspase 9: Ex/Em = 370/450 nm (blue), bottom reading).

3.2.4 Light Microscopy and Cell Counting

Cells were observed by light microscope (Nikon Inverted Microscope, TS100) ×10 magnification to ascertain their morphological changes from the undifferentiated state (myoblast) to the differentiated state (myocytes). Number of cells in the resulting cell suspension was determined by using haemocytometer method. 100 µl of cell suspension was mixed with 100 µl of 0.4% trypan blue by gently pipetting, and then 100 µl of the mix were loaded into each chamber of the haemocytometer. Cell counts were performed in triplicate and analysed under a 10× objective. Standard method was performed when counting the cells using hand tally counter. Number of viable cells per ml was calculated using the standard method.

3.2.5 Fluorescent Microscopy Analysis

Carcinoma cells were cultured in 6 well microscopic chambers and treated with relevant myocyte EVs concentration for 48 h. After 48 h, supernatant was removed and washed with PBS and cells were incubated with relevant fluorescent dyes. Cells were washed with PBS three times to remove excessive fluorescent dye. Then the cells were fixed with 4% paraformaldehyde at 37°C for 15 min and washed with cold PBS. The cell culture chamber was separated from the microscopic slide and let air dry. Finally, coverslips were mounted on microscopic slide using DAPI-VECTASHIELD medium. Images were taken with inverted fluorescent microscope (Invetrogen EVOS FL).

3.2.6 Flow Cytometry

The Guava flow cytometer allows complex biological studies such as cell counting and viability testing, cytokine detection, cell activation marker analysis and other complex molecular analyses to be performed simultaneously. The Guava flow cytometer can be used to perform many different assays; however, for these studies only four assays were implemented. These were the ViaCount assay (for counting cells and determining viability), Cell cycle Analysis (for assessing cell cycle arrest), ExpressPlus assay (EVs marker Analysis) and Nexin assay (for reporting apoptosis).

3.2.6.1 Cell Viability Assay

Cell number and the viability was determined using Guava ViaCount assay. Carcinoma cell, 1×10^4 cells per well in triplicate were seeded into a 24 well plate with or without myocyte EVs. Guava ViaCount assay distinguishes between viable and non-viable cells based on the differential permeabilities of two DNA-binding dyes in the Guava ViaCount reagent. Cells were treated with 5% FBS and incubated for 48 h. On the day of the experiment, cells were trypsinised, washed, collected and replicates were combined to achieve the desired cell concentration per test. Stained cell sample was prepared by mixing 20 µl of cell suspension with 180 µl of Guava ViaCount reagent in 96 well plate. Cell viability assay was performed using Guava flow cytometer (Guava EasyCyte HT).

3.2.6.2 Apoptosis Assay

Carcinoma cell, 1×10^4 cells per well in triplicate were seeded into a 24 well plate with or without myocyte EVs. Cells were treated with 5% FBS and incubated for 48 h. On the day of the experiment, cells were trypsinised, washed, collected and replicates were combined to achieve the desired cell concentration per test. Cells were treated with 1% FBS and 100 µl of

Nexin reagent. The plate was incubated 20 min at room temperature and analysed by Guava flow cytometer (Guava EasyCyte HT).

3.2.6.3 Cell Cycle Analysis

To investigate the different cell cycle phase of the EVs treated carcinoma cells, Guava cell cycle assay was used. Based on the DNA content in the cell sample, assay helps to determine the percentage of cells in G0/G1, S, and G2/M phases. Carcinoma cell, 1×10^4 cells per well in triplicate were seeded into a 24 well plate with or without myocyte EVs. Cells were treated with 5% FBS and incubated for 48 h. On the day of the experiment, cells were trypsinised, washed 1 time with PBS, collected and replicates were combined to achieve the desired cell concentration per test. Cell pellet was transferred into 96 well plate and slowly resuspended in 200 µl of ice cold 70% ethanol. Plate was sealed and refrigerated for 12 hours. Cells were centrifuged at 300 × g for 5min and washed once with PBS. Samples were transferred into 96 well plate and incubated with 200 µl of Guava cell cycle reagent for 30 min at room temperature in dark. Following the incubation, samples were analysed using Guava flow cytometer (Guava EasyCyte HT). Data was analysed using ModFit software.

3.2.7 Proteomics

3.2.7.1 Sample Preparation

EVs from C2C12 myocytes and NIH 3T3 were collected for proteomics. Protein concentrations of EVs lysates were determined by using BCA assay and the samples were heated 95°C for 5 min. The samples were mixed with Laemmli sample buffer and loaded on to Mini-PROTEAN TGX gels (Bio-Rad). Electrophoretic separation was performed for approximately 5 min to concentrate the protein as bands, which then were cut and stored separately in Eppendorf tubes.

Sample were sent to the Cambridge Centre for Proteomics for LC-MS/MS analysis, using in gel digestion.

3.2.7.2 LC-MS/MS analysis

The protein samples gels were trypsin digested and analysed by Dionex Ultimate 3000 RSLC nanoUPLC and Q Exactive Orbitrap mass spectrometer (Thermo Fisher Scientific Inc, Waltham, MA, USA) systems. Peptides were separated by reverse-phase chromatography by using a Thermo Scientific reversephase nano Easy-Spray column (Thermo Scientific PepMap C18, 2µm particle size, 100A pore size, 75µm i.d. × 50 cm length).The isolated peptides were then loaded onto a pre-column (Thermo Scientific PepMap 100 C18, 5µm particle size, 100 Å pore size, 300 µm i.d. x 5mm length) from the Ultimate 3000 autosampler with 0.1% formic acid for 3 min at a flow rate of 10µL/min. Thereafter, the elution of peptides from pre-column was switched onto analytical column. It was facilitated by switching the column valve (solvent A = water + 0.1% formic acid; solvent B = 80% acetonitrile, 20% water + 0.1% formic acid). A linear gradient of 2–40% B was employed for 30min. The LC eluant was sprayed into the mass spectrometer using the Easy-Spray source (Thermo Fisher Scientific Inc.). All m/z values of eluting ions were measured in an Orbitrap mass analyser, set at a resolution of 70000 and was scanned between m/z 380 – 1500. Data dependant scans were employed to automatically isolate and generate fragment ions by higher energy collisional dissociation (HCD, NCE: 25%) in the HCD collision cell. The resulting fragment ions measurements were performed using the Orbitrap analyser, set at a resolution of 17500. Ions that were singly charged and ions with unassigned charge states were excluded from being selected for MS/MS and a dynamic exclusion window of 20 seconds was employed.

3.2.7.3 Database Searching

All the MS/MS data was converted to mgf files and data were analysed using Mascot (Matrix Science, London, UK; version" 2.6.0). The files were searched against the UniProt mus musculus database (55474 protein sequences) assuming the digestion enzyme trypsin. Mascot was searched with a fragment ion mass tolerance of 0.100 Da and a parent ion tolerance of 20 PPM. O+18 of pyrolysine and carbamidomethyl of cysteine were specified in Mascot as fixed modifications. Deamidated of asparagine and glutamine and oxidation of methionine were specified in Mascot as variable modifications.

3.2.7.4 Protein Identification

Scaffold (version Scaffold_4.11.1, Proteome Software Inc., Portland, OR) was used to validate MS/MS based peptide and protein identifications. Peptide identifications were accepted if they could be established at greater than 95.0% probability by the Peptide Prophet algorithm with Scaffold delta-mass correction. Protein identifications were accepted if they could be established at greater than 95.0% probability and contained at least 5 identified peptides. The significance threshold was set at $p < 0.05$. Protein probabilities were assigned by the Protein Prophet algorithm. Proteins that contained similar peptides and could not be differentiated based on MS/MS analysis alone were grouped to satisfy the principles of parsimony. Proteins were annotated with GO terms from NCBI (downloaded 24-Jan-2021). Pathway annotations were fetched fromreactome.org.

3.2.7.5 Protein Pathway Analysis

The STRING database aims to collect, score, and integrate all publicly available sources of protein–protein interaction information, and to complement these with computational predictions. To identify the protein- protein interactions network of the proteins derived from

both C2C12 myotubes and NIH 3T3 EVs, the proteins identified in Scaffold were submitted to STRING analysis (https://string-db.org/). Protein IDs were entered into the search box "multiple proteins" in STRING and "mus musculus" was chosen as the species database. Setting for the analysis was set as basic and the minimum required interaction score was set as medium confidence (0.400). These interactions are based on known and predicted interactions.

KEGG (Kyoto Encyclopaedia of Genes and Genomes) (KEGG PATHWAY Database (genome.jp)) is a collection of manually drawn pathway maps representing current knowledge of the molecular interactions, reaction, and reaction network for: Metabolism, Genetic information processing, Environmental information processing, Cellular processes, organismal systems, Human diseases and Drug development. The KEGG pathways were linked to STRING database and desired KEGG pathways were chosen from the list provided.

3.2.8 Statistical Analysis

Statistical analysis for all data presented was performed by the unpaired *t*-test for repeated measures using GraphPad Prism version 6.01 for Windows (GraphPad Software, San Diego, USA). Statistical correlations between data values were also determined using GraphPad Prism software. Differences giving a value of $p < 0.05$ with confidence interval of 95% were considered statistically significant.

~~2~~4 Skeletal Muscle (C2C12) Derived EVs Reduce Lung Carcinoma (CMT 64/61) Cell Viability and Migration

~~2.1~~4.1 Introduction

Skeletal muscle is rarely a site of cancer metastasis, even though skeletal muscle compromises ~50% of the total body mass. However, a definitive molecular or a cellular mechanism for this phenomenon has not yet been confirmed. The rarity of these metastases has been linked to many factors, including increased muscle activity [204], influence of β-adrenergic receptors on variability of blood flow between resting and exercise state [183] and increased level of lactic acid production [184]. Moreover, adenosine and other low molecular weight factors have been suggested to inhibit carcinoma growth via A3 adenosine receptor [186,187]. However, adenosine depleted condition media still exert a growth inhibitory effect on carcinoma cells which has led to the cytostatic effect of skeletal muscle conditioned media being speculated upon [205,206,207].

Extracellular Vesicles (EVs) are now in centre of attraction due to their role in normal physiology as well as their involvement in every disease state possible in the human body, including cancer [121,122]. Various studies have shown the role of EVs as an agent of cell repair and homeostasis. For instance, EVs derived from platelets have the capability of repairing myocardial injury after an infarction [208]. Others have reported the potential role of EVs as carriers of pharmacological and genetic therapeutic agents [209]. In cancer, EVs may aid in tumour survival and spread [12], influencing processes as diverse as differentiation, migration and angiogenesis [13] In contrast, a recent study has discussed the inhibitory effect of skeletal muscle progenitor cell-derived exosomes on prostate cancer cell proliferation, thus pointing to the potential of using EVs as a therapeutic agent in treating various solid cancers [210].

Based on these data, it is also possible to suggest that conditioned media containing skeletal muscle EVs may inhibit carcinoma cell growth and progression. Therefore, the purpose of this chapter was to isolate EVs from C2C12 myocytes effectively and to investigate their effects on

carcinoma cells. To achieve this, C2C12 myoblasts were differentiated into myocytes, followed by characterisation of myocyte derived EVs by flow cytometry, and Nanoparticle Tracking Analysis (NTA). Functions of these EVs on carcinoma cell viability, attachment, and migration, were analysed by using different experimental systems.

~~2.2~~4.2 Results

~~2.2.1~~4.2.1 C2C12 Cell Differentiation

Initial experiment was performed to differentiate the C2C12 myoblast to myocytes. This was pertinent, as the entire investigations would require extracellular vesicles (EVs) harvested from the differentiated state, myocytes. C2C12 is an immortalised murine myoblast cell line which readily proliferates in high serum conditions and differentiates to myocytes in low serum conditions. C2C12 myoblasts were grown in Dulbecco's modified Eagle's medium (DMEM) supplemented with 10% foetal bovine serum (FBS), 1% penicillin-streptomycin at 37^{o}C in 5% CO_2 atmospheric conditions. To induce myogenic differentiation, when about 90% cell confluency was attained, the serum containing medium was substituted with skeletal muscle differentiation medium, containing 5% horse serum. The cells were monitored after 24 h and after 2, 3 and 4 days of differentiation.

The cells depicted in **Figure 3A** represent the myoblast, which are flat, star shaped and mono-nucleated cells. Myogenic differentiation was recognised after 2 days by a change in cell shape and monolayer organization. By day 3, the cell shape changed progressively, the cells becoming elongated and packed closely together. By day 4, all cells had fused to form plurinucleate syncytia, the myotubes (**Figure 3B**).

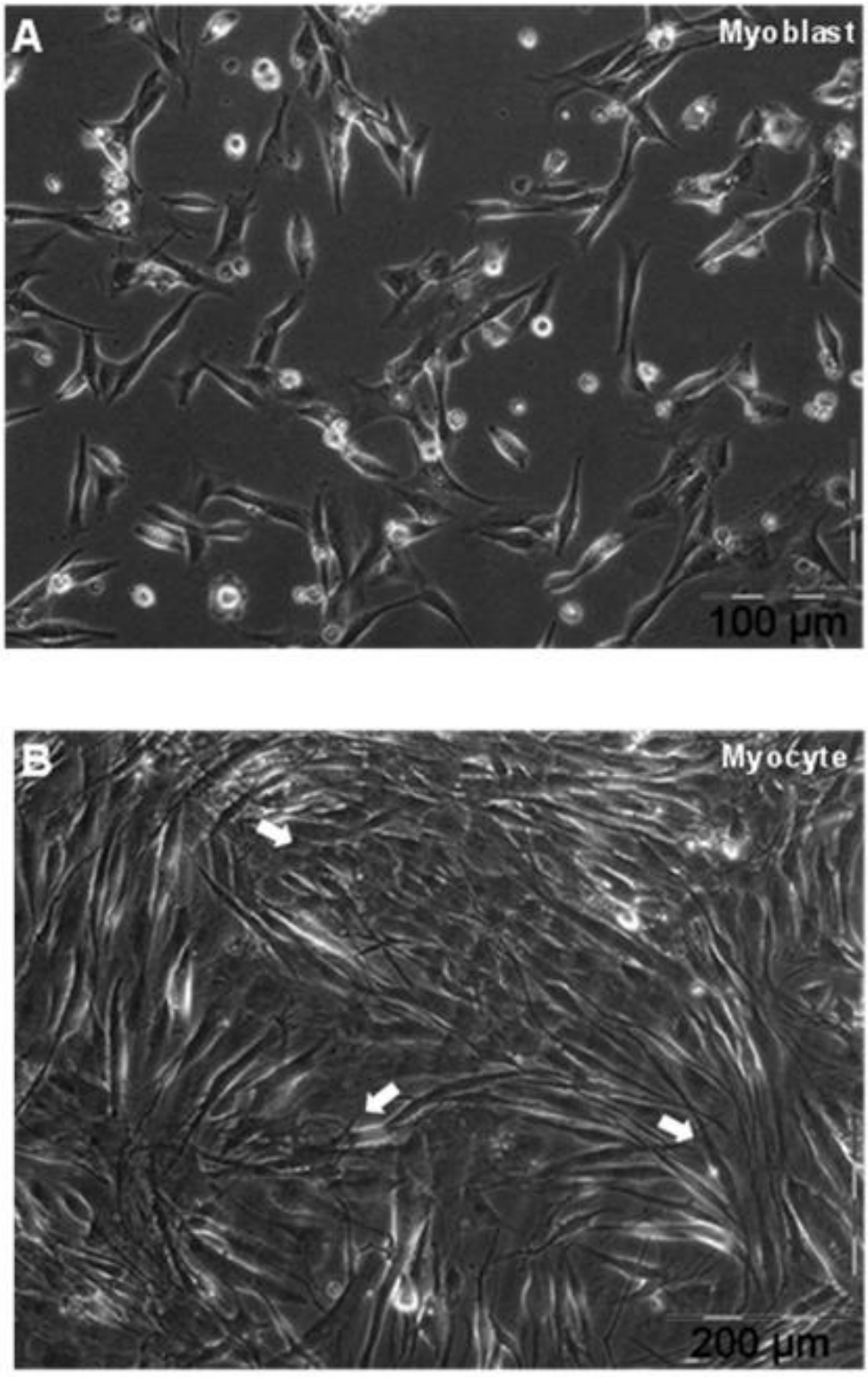

Figure 3: Differentiation of C2C12 myoblasts to myocytes

(A) Bright field image of C2C12 myoblast cells prior to differentiation. Scale bar: 100 µm. **(B)** Bright field image of differentiated C2C12 (myocytes) at day 4. White arrows show fusion and formation of syncytia. Scale bar: 100 and 200µm.

In addition to morphological changes, C2C12 cell differentiation was further confirmed by looking for expression of the myocyte-specific protein, myogenin, by western blotting. During differentiation of C2C12 cells, myoblasts undergo remodelling to form myocytes, which express myotube specific proteins, such as myogenin and myosin heavy chain (MHC)[211]. Western blot analysis was performed on cell lysates from C2C12 myotubes in growth medium (GM) on day 1 and cell lysates from C2C12 in differentiation medium (DM) on days 1 and 4.

For SDS-PAGE, 20 µg of proteins were used from each cell lysate. Electrophoretic separation was performed at 150 V (constant voltage) until samples reached the bottom of the gel. Resolved proteins were electroblotted using a semi-dry transfer device (Bio-Rad Sartoblot system) to a Hybond C nitrocellulose membrane for further analysis. The membrane was incubated with primary antibody, Myogenin Mab (F5D, 1 µg/ml) and then incubated with secondary goat anti-mouse HRP antibody (1:5,000). Actin was used as the loading control; its presence being identified by cutting the membrane close to 40 kDa and incubating with anti-actin primary antibody and secondary HRP-conjugated antibody. Protein standards were used as a guidance when separating the membrane.

As shown in (**Figure 4**), myogenin was not expressed in C2C12 cells in growth medium containing FBS. However, C2C12 cells incubated in 5% horse serum differentiation medium, have started to express myogenin after 24 h. Myogenin expression was found to increase by day 4 when mature myotubes were formed.

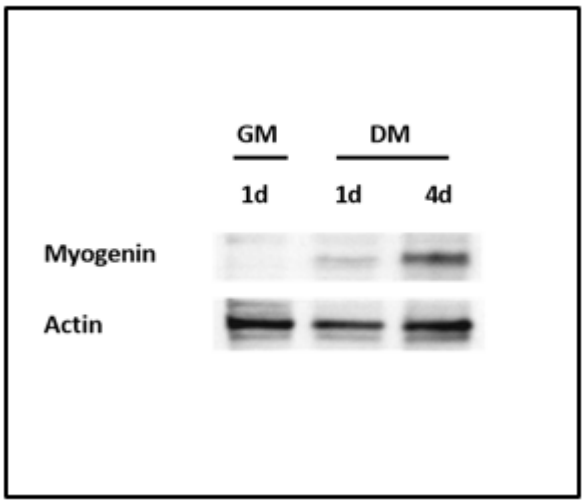

Figure 4: Myogenin expression of differentiated C2C12 myocytes

A 30 kDa band identified as Myogenin in western Blot analysis. **Lane 1:** C2C12 myoblasts treated with growth medium (GM) for 24 h. **Lane 2:** C2C12 cells treated with differentiation medium (DM) for 24 h. **Lane 3:** C2C12 cells treated with differentiation medium for 4 days. A 43 kDa band was identified as actin, which was used as a loading control to normalise the relative expression of myogenin.

~~2.2.2~~4.2.2 Characterisation of EVs derived from myocytes

The ISEV recommendation for characterisation of EVs suggest that each preparation of EVs be "1) defined by quantitative measures of the source of EVs (e.g. number of secreting cells, volume of biofluid, mass of tissue); 2) characterized to the extent possible to determine abundance of EVs (total particle number and/or protein or lipid content); 3) tested for presence of components associated with EV subtypes or EVs generically, depending on the specificity one wishes to achieve; and 4) tested for the presence of non-vesicular, co-isolated components"[14].

~~2.2.2.1~~4.2.2.1 Nanoparticle Tracking Analysis of C2C12 EVs

In accordance with ISEV guidelines, NTA was used to determine the number of particles secreted by given number of cells. NanoSight technology utilises the properties of Brownian motion and light scattering to obtain size distribution and particle concentration in liquid suspension. Depending on the instrument configuration and sample type, the NS300 allows rapid analysis of all types of nanoparticles ranging from 0.01 – 1 µm in diameter. For Nanoparticle Tracking Analysis (NTA), EVs from five different cell samples at different passages were collected. EVs were diluted in PBS to a final volume of 1 ml. Following the manufacturer's instructions, three 1-minute videos were captured at a temperature between 17.8 – 19.2 °C. The videos were analysed by the in-built NanoSight Software NTA 3.2.

The NTA results showed in **Figure 5** confirmed the heterogeneity of the EV population. The results were obtained from five different samples and three analyses showed that, C2C12 myocyte EVs consist of mainly 3 subpopulations: with peaks at 133.33 ±8.96 nm, 210.33 ±17.04 nm and 310.67 ±25.54 nm. As showed in **Table 1**, most of the C2C12 EVs had an average diameter between 118.0 ±1.9 nm and 265.5 ±12.2 nm and the mean size was 174.7 ±2.9, which suggested that these vesicles are medium/large EVs" (m/lEVs). Furthermore, NTA results show that approximately, 1×10^8 cells generate $1.79 \times 10^{10} \pm 2.74 \times 10^8$ EV particles per ml.

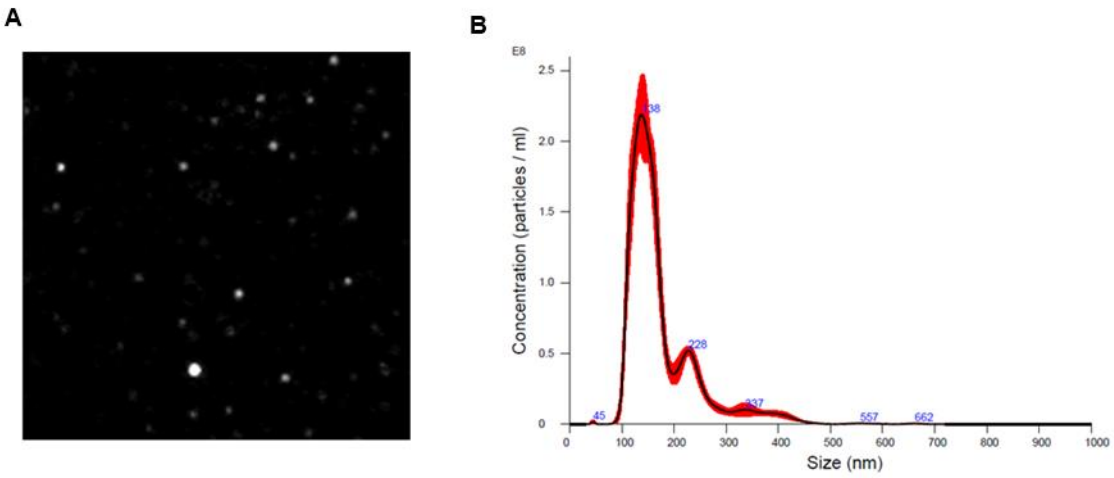

Figure 5: Characterisation of EVs by NTA

A) Screen shot of the video during EV analysis. **B)** Representative graph shows the results of particle concentration and their size measurement. NTA of this sample shows 3 populations of C2C12 EVs with modal peak diameters of 138 nm, 228 nm and 337 nm.

Table 1: Average data on C2C12 EV size detected by NTA. D10, D50 and D90 indicate the percentage of particles 10, 50 and 90% respectively. Data are mean ± SD, n = 3 independent biological samples.

Size of C2C12 EVs					
Mean (nm)	**Mode (nm)**	**SD (nm)**	**D10 (nm)**	**D50 (nm)**	**D90 (nm)**
174.7 +/- 2.9	137.7 +/- 5.6	69.4 +/- 3.0	118.0 +/- 1.9	152.3 +/- 1.6	265.5 +/- 12.2

~~2.2.2.2~~4.2.2.2 Characterisation of EVs by Protein Composition

According to ISEV, at least 3 different protein markers, one from transmembrane or GPI-anchored proteins associated to plasma membrane or endosomes, one Cytosolic protein and one protein from Major components of non-EV co-isolated structures must be analysed to demonstrate the nature of the EVs and the purity of the EV isolation method [14]. Therefore, western blot analysis was performed on the myocyte EV lysate, isolated from centrifugal method. CD63 was used as a transmembrane protein and TSG101 was used as a cytosolic protein. As the EVs were isolated from conditioned medium without bovine serum, the needed to test for non-EV component recommended by ISEV was regarded as unnecessary.

EV lysate at 20µg per lane was used and immunoblotted to detect EV marker CD63 and TSG101. The primary antibodies used were Anti-CD63 antibody - Late Endosome Marker (at 1/200) and Anti-TSG101 antibody (1/1000) and incubated for 1h at room temperature. As a secondary antibody HRP-labelled goat anti-rabbit at 1/2000 dilution was used. As shown in the (**Figure 6**), two strong bands were detected for both EV marker, CD63 (the band in the region of 25-30 kDa) and for TSG101 (region of 45 kDa), confirming the presence of EVs.

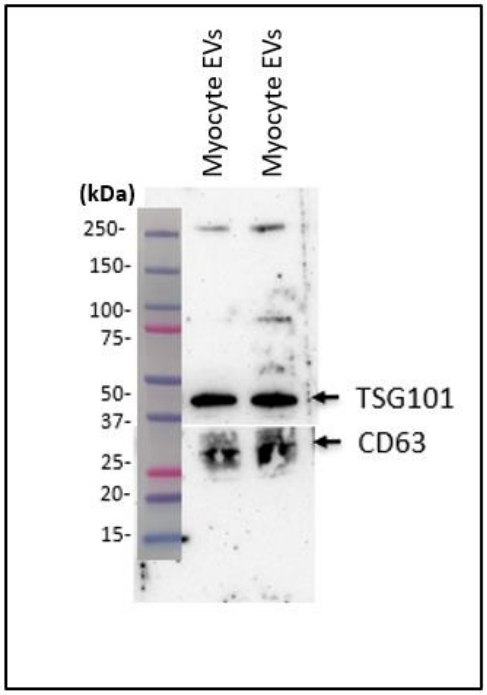

Figure 6: Characterisation of EVs by protein marker

To confirm the purity of myocyte EVs sample, CD-63 as a transmembrane protein and TSG-101 as a cytosolic protein were used. The band in the region of (25-30 kDa) was identified for CD-63 and the 45 kDa band for TSG-101.

~~2.2.2.3~~4.2.2.3 Flow Cytometry Analysis and Annexin V Labelling of Isolated EVs

To further confirm the purity of the myocyte EVs isolated by differential centrifugation, sample was stained with annexin V and analysed by flow cytometry. The vesicles were identified by their size and granularity, assessed by the logarithmic amplification of forward (FSC) and side scatter (SSC) signals, respectively (Figure 7A). Extracellular vesicles contain a lipid bilayer membrane, which contains rare lipids such as ceramide and amino phospholipids such as phosphatidylserine (PS). Unlike other lipids found in the plasma membrane, PS carries an uncommon net negative charge and, annexin V can recognize PS through coordinated Ca^{2+} ions.Therefore, fluorescently labeled annexin V-FITC has been used as a method to quantify exposed levels of PS in EVs.

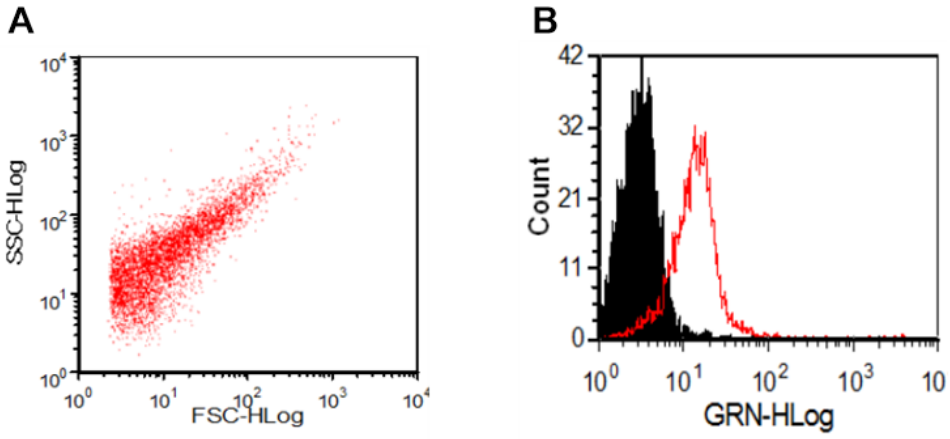

Figure 7: **Characterisation of MVs by Flow Cytometry**

A) Representative dot plot distribution of C2C12 myocyte EVs on a flow cytometer. Plot shows forward scatter (size) and side scatter (granularity). The vesicles were identified by their size and granularity, as assessed by the logarithmic amplification of forward (FSC) and side scatter (SSC) signals. **B)** Isolated EVs were analysed for PS expression by staining with annexin V-FITC. The resulting histogram shows approximately 70% of labelled EVs to be AnV-FITC positive. Unlabelled EVs, shown in black were used as a negative control.

~~2.2.3~~4.2.3 Murine Lung Carcinoma (CMT 64/61) Cell Line Grows Rapidly in Low Serum Conditions

Highly metastatic lung carcinoma cell line CMT 64/61, was used as the test cell line in this study. The CMT 64/61 cell line was originally derived from an alveologenic lung carcinoma from a C57BL/1CRF mouse [213]. In order to observe the growth rate of this cell line, 1×10^4 cells were grown in Waymouth′s MB 752/1 + 2 mM Glutamine + 10% Foetal Bovine Serum (FBS) in triplicate in 24-well plates with different serum concentrations. CMT 64/61 cells were directly put into serum-free medium instead of gradually reducing the serum concentration. Plates were incubated at 37 ºC in 5% CO_2 and cell medium was changed every 2 days. Cells were counted using a haemocytometer on day 2, 3, 4, and 5 to identify the growth rate of the cell line.

The growth curve of the cell culture with serum indicates a rapid cell proliferation within the first 2 days. Cell doubling time was calculated using GraphPad Prism v6.01 software for Windows (GraphPad Software Inc., San Diego, CA) by nonlinear regression (exponential growth equation) analysis. Cell doubling time with 10%, 5% and 1% serum are 0.6852, 0.9317 and 1.0169 days respectively. The doubling time without serum was 2.637 days. CMT 64/61 cells can therefore be maintained in a completely defined serum-free medium for up to 4 days; however, the growth rate is significantly lower than with supplemented serum. Furthermore, it was possible to directly introduce them to serum-free conditions, without the need to gradually reduce serum levels to allow cells to slowly adapt. It was thus shown that CMT 64/61 cells can survive and proliferate under stressed conditions such as serum depleted conditions.

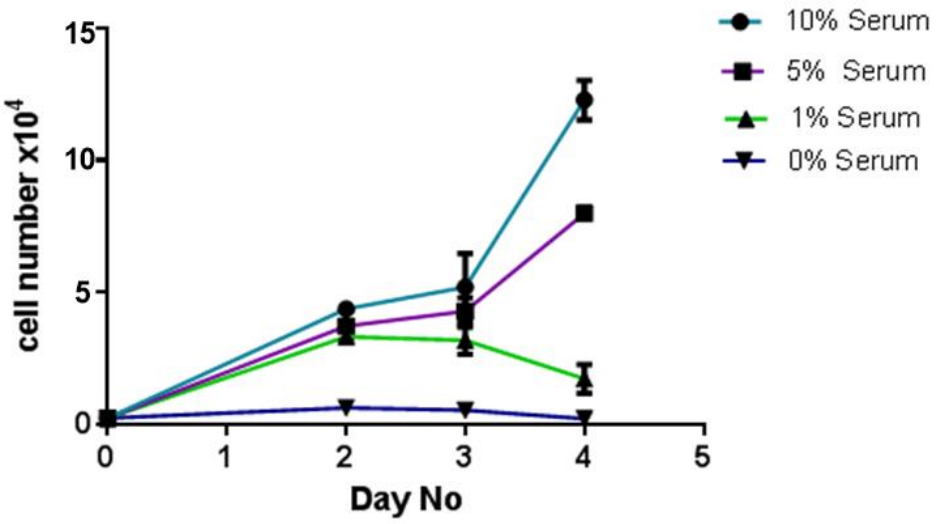

Figure 8: Increased growth rate of CMT 64/61 in 5 and 10% serum

CMT 64/61 cells were treated with or without serum and incubated at 37 ^{o}C in 5% CO_2. Cell numbers were calculated each day for 5 days. The growth rate of cells maintained in serum-free conditions was significantly lower in comparison to cells treated with 10% serum. The doubling time for cells in serum-free media were 2.637 compared to 0.6852 with 10% serum. Data are mean ± SD, n = 3 independent biological samples with 3 technical repeats per sample.

~~2.2.4~~4.2.4 Metastatic CMT 64/61 Carcinoma Cells Fail to Colonize Differentiated Skeletal Muscle *in vitro*

As mentioned earlier, most tissues are subject to cancer metastasis with the striking exception of skeletal muscle. In line with this view, a study conducted by Parlakian and group have demonstrated that after three weeks of tail vein injection of melanoma cells, organs such as lung, liver, heart, spleen, and intestine were colonized by melanoma cells but not the skeletal muscles [186]. Based on this observation, I have decided to investigate the fate of murine lung carcinoma cells, when directly introduced to differentiated skeletal muscle cells.

To monitor CMT 64/61 carcinoma cell growth in the presence of differentiated skeletal muscle cells, CMT 64/61 cells were directly introduced to C2C12 myocytes at a ratio of 1:4 and 1:40.

Due to the high proliferative rate of carcinoma cells, the optimal ratio of carcinoma to myocyte cells was determined to be 1:40, allowing for clear visualisation of the two cell types. Murine skeletal muscle cells (myocytes) were cultured to 80% confluency. On the day of the experiment, attached cells were washed with PBS and were co-cultured with CMT 64/61 carcinoma cells at the ratio of 1:4 and 1:40 (CMT 64/61: myocytes) respectively. The results obtained in **Figure 8** showed that carcinoma cell rapid proliferate by 48 h, therefore, cells were co-cultured for 48 h in 5% FBS. The various combinations of cell types were subjected to identical treatment to allow direct comparison of outcome. Murine fibroblast cell line (NIH-3T3) was used as a control cell line in this study, as it was known to facilitate and enhance cancer cell proliferation [212] and invasion [214].

When highly metastatic carcinoma cells (CMT 64/61) were co-cultured with skeletal myocytes (C2C12 cells) at different ratios, the carcinoma cells failed to colonize the skeletal cells at both ratios (CMT 64/61:C2C12; 1:40 and 1:4), and the morphology of the myocytes remained unchanged (**Figure 9b and c**). These observations were in an agreement with the observation made by Parlakian and group [186] *in vivo*. As expected, when the carcinoma cells were co-cultured with NIH 3T3 fibroblasts, it was found that carcinoma cells significantly invaded and colonized the fibroblast cells, even at a ratio of (CMT 64/61: NIH 3T3 of 1:40). The normal morphology of NIH 3T3 fibroblast cells were entirely affected by the carcinoma cells, as shown in (**Figure 9e and f**). Moreover, small lesion of new cell growth was seen on the culture CMT 64/61: NIH 3T3 of 1:4, and when compared those cells morphology with the CMT 64/61 cells grown in normal conditions **Figure 9g**, it was evident that carcinoma cell invaded and colonised fibroblasts within 48 h **Figure 9f**, indicated with yellow dotted line. Based on these observations, it was suggested that myocyte inhibit carcinoma cell invasion *in vitro.*

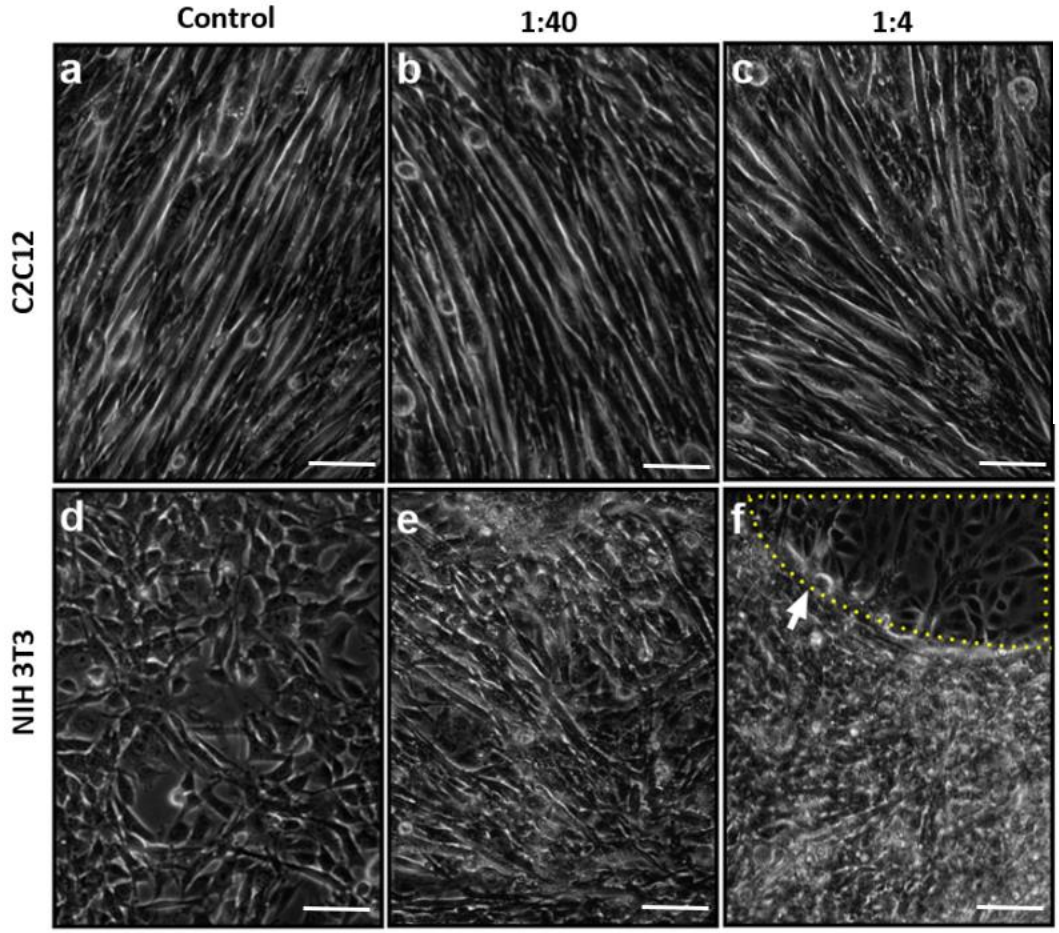

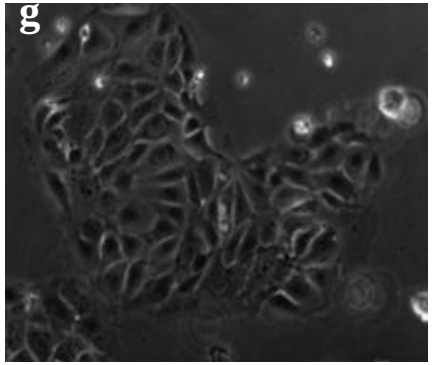

Figure 9: Co-cultures of highly metastatic murine lung carcinoma with differentiated murine skeletal muscle cells and murine fibroblast cells.

a) Normal morphology of differentiated skeletal muscle cells **b)** Skeletal muscle cells co-cultured with carcinoma cells at a high ratio (CMT 64/61:C2C12; 1:40) **c)** Skeletal muscle cells co-cultured with carcinoma cells at low ratio (CMT 64/61:C2C12; 1:4) **d)** Normal morphology of NIH 3T3 after 48 h **e)** Carcinoma cells were co- cultured with fibroblasts at a 1:40 ratio, showing cellular dysplasia on fibroblast cells **f)** Carcinoma cells at ratio of 1:4 invade and colonize fibroblast cells (area delineated by yellow dotted line showing invading carcinoma cells, confirmed by the cell morphology) **g)** Photomicrograph showing normal cell morphology of carcinoma cells CMT 64/61. Scale bar = 100 µm.

~~2.2.5~~4.2.5 Conditioned Medium from C2C12 Myocyte Cells Decrease Cell Viability of CMT 64/61 Murine Lung Carcinoma Cells

There is ever-increasing evidence for a multitude of ways in which the host microenvironment can promote cancer metastasis and progression [215]. For example, the bone marrow has been recognised to provide a highly supportive microenvironment for tumour growth and progression [216]. However, some host microenvironment known to exert anti-cancerous effects on carcinoma cells, including natural killer cells [217]. Based on that view, it was postulated myocyte microenvironment may exert inhibitory effects seen earlier on carcinoma cells.

To observe the effect of skeletal muscle (C2C12) myocyte microenvironment on murine lung carcinoma cell (CMT 64/61), carcinoma cells were seeded in 24-well plates at 1×10^4 cells per well in triplicate and incubated at 37 °C for 24 h. On the day of the experiment, attached cells were washed ×3 with PBS and treated with the appropriate concentrations of C2C12 conditioned medium in the presence of 5% FBS. Following a 48h incubation, the cells were processed and analysed for cell viability using Guava ViaCount reagent by flow cytometry. Carcinoma cell without CM treatment was used as a control. Conditioned medium (CM) from the murine fibroblast cell line (NIH-3T3) was used as a positive control.

The effect on cell viability of CMT 64/61 carcinoma cells treated either with increasing concentrations of C2C12 conditioned medium (CM) or NIH-3T3 CM, are presented in **Figure 10A and B** revealed a significant difference in cell viability. Essentially, increasing concentrations of C2C12 CM brought about a dose-dependent decrease in carcinoma cell viability and the increasing concentrations of NIH-3T3 CM brought about a dose-dependent increase in cell viability of carcinoma cells. As shown in the **Figure 10A**, morphology of the carcinoma cells treated with myocyte CM changed in a dose dependent manner. Carcinoma

cells treated with 100 µg/ml myocyte EVs morphology was similar to that on control culture. However, with the increasing concentration, few cell colonies were formed, and the number of cells present in the cell colonies also showed a reduction, indicated with white arrows. Furthermore, carcinoma cells treated with 500 µg/ml myocyte concentration, showed loss of cell membrane integrity and loss shape, indicated with yellow arrows. Conversely, in the presence of fibroblast (NIH-3T3) CM, carcinoma cells appeared to increase in numbers and decrease in size due to overgrowth in multilayers, indicated with red arrows (**Figure 10B**).

Cell viability assay data **Figure 11** revealed a significant decrease in cell viability of the carcinoma cells treated with myocyte CM in a dose dependent fashion. Whereas, NIH-3T3 CM, had no adverse effect on carcinoma cell proliferation, indeed conditioned medium from fibroblasts increased the carcinoma cell proliferation significantly. Together, these data in an agreement with other groups, which showed the cytostatic effect of skeletal muscle media on carcinoma cells [206,207] and another recognised the fibroblast as one of the vital components of the tumour microenvironment for tumour progression [215,218].

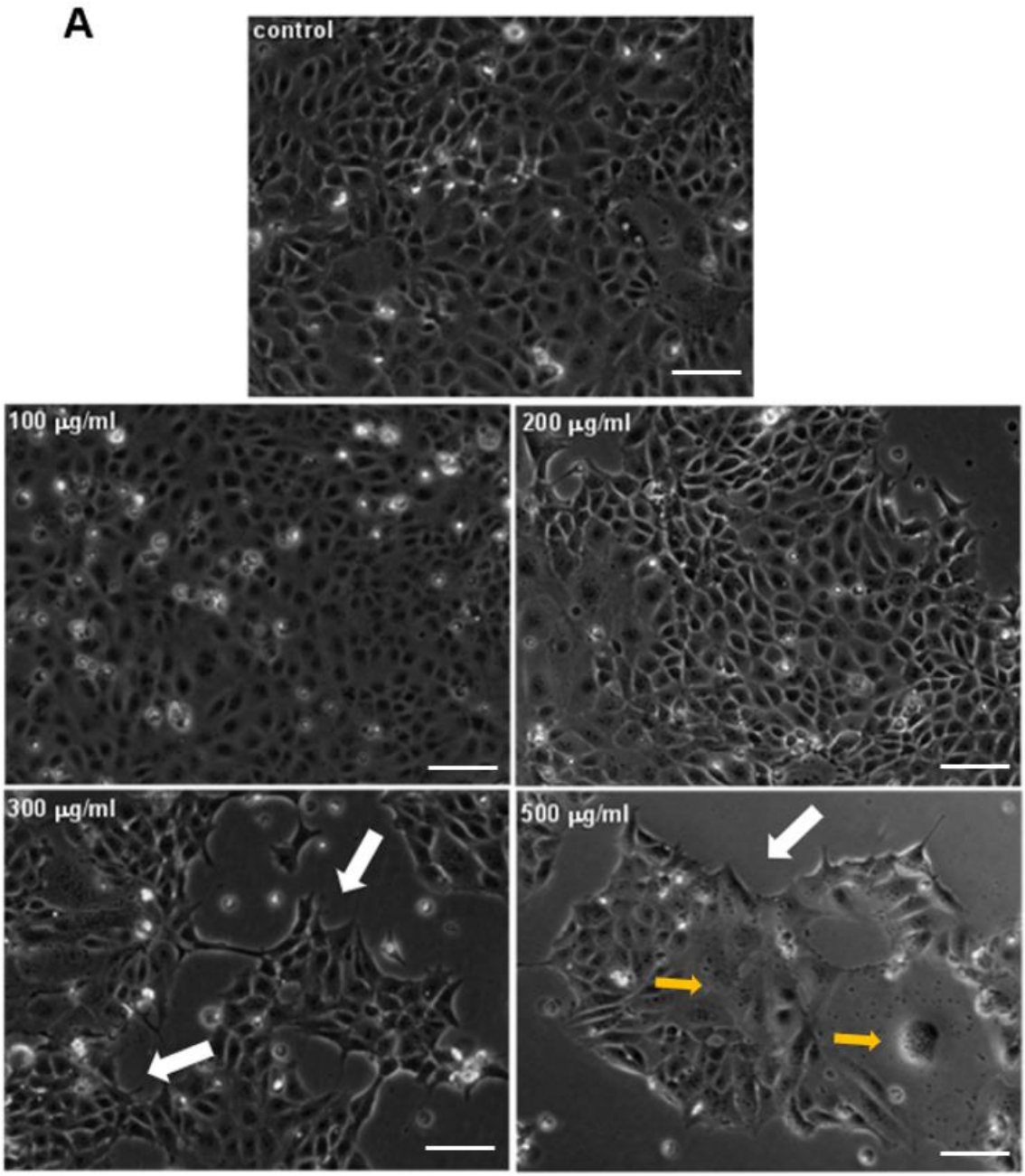

Figure 10A: Effect of myocyte CM on highly metastatic carcinoma cell morphology

A) Photomicrographs of CMT 64/61 murine lung carcinoma cells grown in 100, 200, 300 and 500 µg/ml of C2C12 conditioned medium (CM) or without (control). After 48 h in C2C12 CM, carcinoma cells showed dose-dependent decrease in numbers. Conditioned Medium concentrations of 300 µg/ml and 500 µg/ml showed cell colonies (white arrows) and cells in the colonies appeared less numerous. Carcinoma cells treated with 500 µg/ml of myocyte CM indicated loss of cell membrane integrity, indicate with yellow arrows. Scale bar = 100 µm.

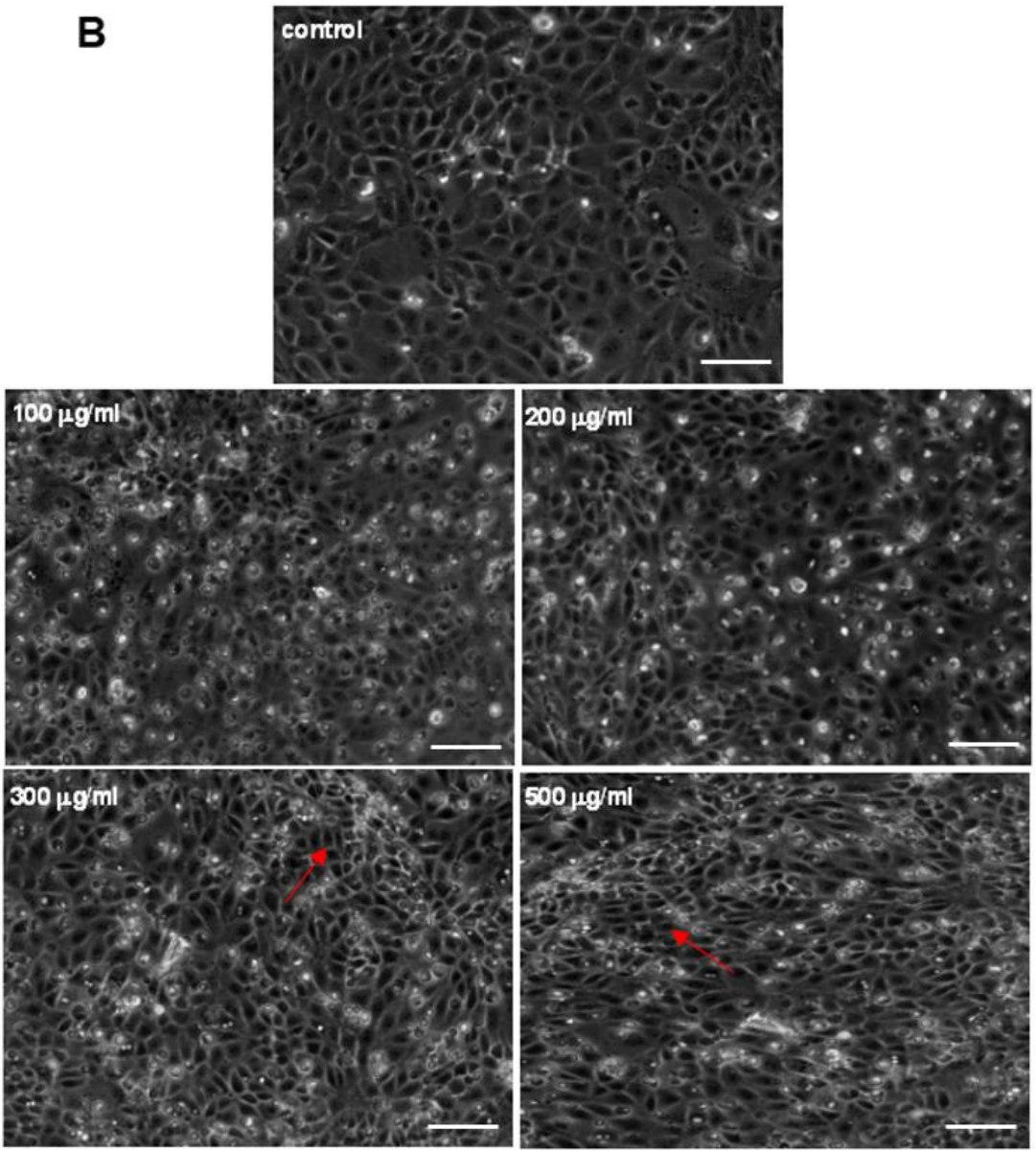

Figure 10B: Effect of fibroblast CM on highly metastatic carcinoma cell morphology

B) Photomicrographs of CMT 64/61 murine lung carcinoma cells grown in 100, 200, 300 and 500 µg/ml of NIH-3T3 CM and CMT 64/61 untreated control cells. After 48 h in NIH-3T3 CM, carcinoma cells increased in number and appeared reduced in size. Red arrows indicated the areas in which cells were grown in multilayers. Scale bar = 100 µm.

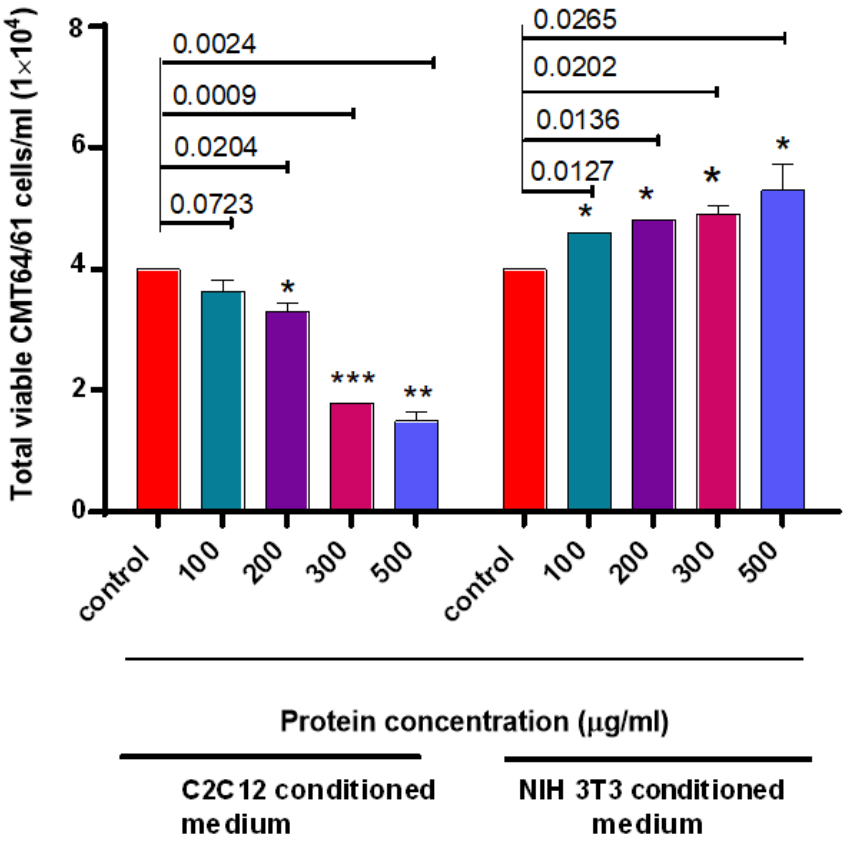

Figure 11: Conditioned media from C2C12 myocytes exert dose dependent reduction in cell viability on murine lung carcinoma cell line

Cell Viability analysis of carcinoma cells treated with C2C12 CM and NIH-3T3 CM. A range of protein concentrations of CM were added and incubated at 37 °C for 48 h. The cells were stained with Guava ViaCount reagent and analysed by flow cytometry. The data represents the mean ± standard deviation of one or two experiments performed in triplicate. *: $p < 0.05$ was considered statistically significant. Carcinoma cells treated with C2C12 conditioned medium exhibit significantly lower levels of cell viability in a dose-dependent manner. Data are mean ± SD, n = 3 independent biological samples with 3 technical repeats per sample.

~~2.2.6~~4.2.6 Skeletal Muscle Derived EVs Decrease Carcinoma Cell Viability

Extracellular vesicles in the tumour microenvironment are known to be involved in many cellular processes, mainly in cancer growth and migration. To elucidate the effect of C2C12 myocyte EVs, the likely key component of the CM used in the earlier experiments, on murine lung carcinoma viability, experimental conditions were maintained, similar concentrations of myocyte EVs (as for total protein in CM, before) being added to the carcinoma cells. EVs from NIH-3T3 cells were used as a positive control and cells with no treatment were used as negative control on CMT 64/61 carcinoma cells.

Cell viability for myocyte EV-treated carcinoma cells **Figure 12**, were as found previously (**Figure 11**). Due to the difference in sample sizes, it was not possible to compare the results from CM-treated samples with EV-treated samples. Nevertheless, it was apparent that myocyte EVs alone have a significant effect on carcinoma cell viability. This effect was dose-dependent and even at low myocyte EVs concentration, 100 µg/ml, carcinoma cells showed significant reduction in cell viability. Furthermore, the data presented suggests that the effect of myocyte EVs on carcinoma cells is greater compared to that which could be mediated by a similar protein concentration of myocyte CM. The role of EVs (mainly exosomes) promoting cancer cell proliferation has been reported in many studies [219,220]. However, a recent study on skeletal muscle progenitor cell-derived exosomes was found to inhibit prostate cancer cell proliferation [210]. Consistent with this view, one could postulate that decreased cell viability seen in here is due to inhibitory effect of myocyte EVs on carcinoma cell proliferation. However, cell viability assay used in here measure only living cells in the culture. Therefore, further investigations are needed to confirm the inhibitory effect of myocyte EVs on carcinoma cell proliferation.

In contrast, NIH 3T3 derived EVs had no significant effect on carcinoma cell viability, although a significant increase in cell viability was observed in the presence of NIH 3T3 CM. This implied that fibroblast EVs alone had no significant effect on carcinoma cell viability, but that together with other factors in the fibroblast microenvironment may cause a rapid increase in viable carcinoma cells.

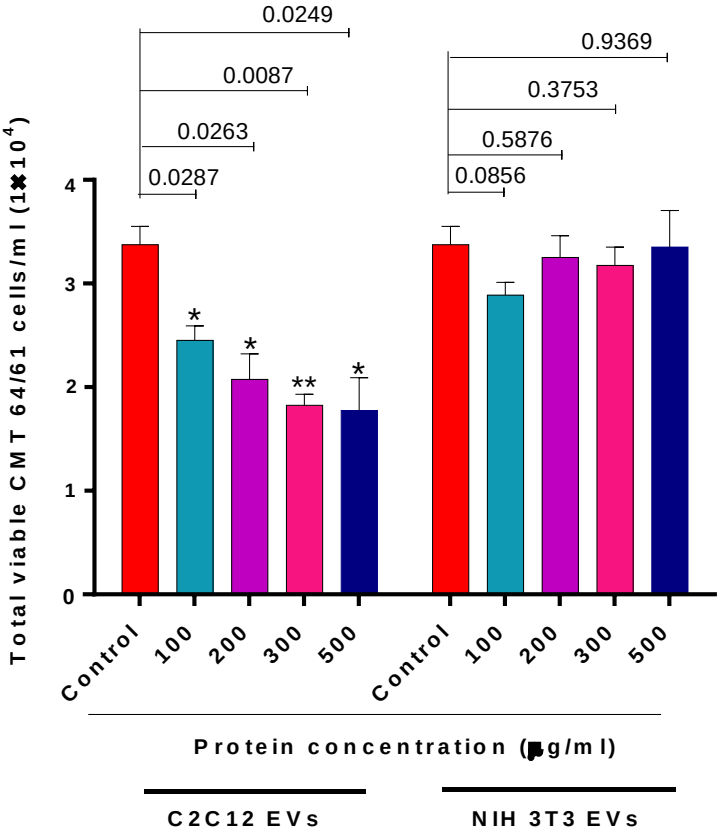

Figure 12: EVs derived from C2C12 myocytes exert an inhibitory effect on carcinoma cell viability

Cell Viability analysis of carcinoma cells treated with C2C12-derived EVs and NIH-3T3-derived EVs (control). A range of protein concentrations of EVs were added and incubated at 37°C for 48 hours. The cells were stained with Guava ViaCount reagent and analysed by flow cytometry. The data represents the mean ± standard deviation of one of two experiments performed in triplicate. *: $p < 0.05$ was considered statistically significant. Carcinoma cells treated with C2C12-derived EVs exhibit (in a dose-dependent manner) significantly lower levels of cell viability. A low concentration of C2C12 EVs (100 µg/ml) was shown to have a significant effect on carcinoma cell viability. Data are mean ± SD, n = 3 independent biological samples with 3 technical repeats per sample.

~~3.1.1~~4.2.7 Skeletal Muscle Derived EVs Express a Non-favourable Microenvironment on Metastatic Carcinoma Cell colony formation, possibly by reducing cell attachment

Cancer metastasis to skeletal muscle is very rare. The metastatic cells travelling through the circulatory system, needs to attach to the secondary site first before proliferating. Therefore, is it possible this non-favorable microenvironment exerts inhibitory effects on metastatic cell attachment?

To address this, it was decided to expose unattached CMT 64/61 carcinoma cells to myocyte EVs. In the experiment discussed in section **4.2.6**, myocyte EVs were introduced to already attached carcinoma cells. This time however, to make the experiment more physiological, non-attached carcinoma cells were introduced to the myocyte EVs. To do so, 1×10^4 unattached CMT 64/61 cells per well were co-cultured with or without C2C12 EVs for 48 h. Cell viability was then assessed using Guava ViaCount reagent by flow cytometry. Murine fibroblast (NIH-3T3) EVs and carcinoma cells without treatment were used as a control.

After 48 h incubation, EV-treated, and non-treated cells were observed by light microscopy (**Figure 13A and B**). Surprisingly, but not unexpectedly, carcinoma cells exposed to myocyte EVs showed low numbers of cell colonies. Furthermore, numbers of cells within such cell colonies were lower compared to those non-treated samples, as indicated by long arrows (**Figure 13A**). Significant changes in cell morphology were also observed, at higher concentrations of added EVs, indicated with short arrows (**Figure 13A**). Untreated CMT 64/61 carcinoma cells appeared polygonal in shape and formed colonies. However, some of the carcinoma cells treated with myocyte EVs (at concentrations of 300 and 500 µg/ml protein) for 48 h appeared elongated in shape. Furthermore, some of the carcinoma cell colonies looked

distorted in the middle **Figure 13A** and showed loss of cell membrane integrity, possibly cell lysis (indicated by orange arrow), unlike those treated with fibroblast EVs, showing no overt morphological change. The number of cell colonies and number of carcinoma cells within these colonies as observed by microscopy, showed a significant increase in a dose-dependent manner with increasing added NIH-3T3 fibroblast EVs (**Figure 13B**).

Cell viability assay was performed to obtain the number of viable cells. As expected, carcinoma cells treated with myocyte EVs showed a dose-dependent and significant (from >100 µg/m myocyte EV protein) decrease in cell viability compared to untreated control (**Figure 14**). NIH-3T3 EVs resulted in significantly increased cell viability of the treated lung carcinoma cells. In summary, EVs derived from C2C12 myocyte cells offer an unfavourable environment for migrating carcinoma cells; possibly lowering their attachment, manifest as a low number of cell colonies, with altered morphology and reduced cell viability.

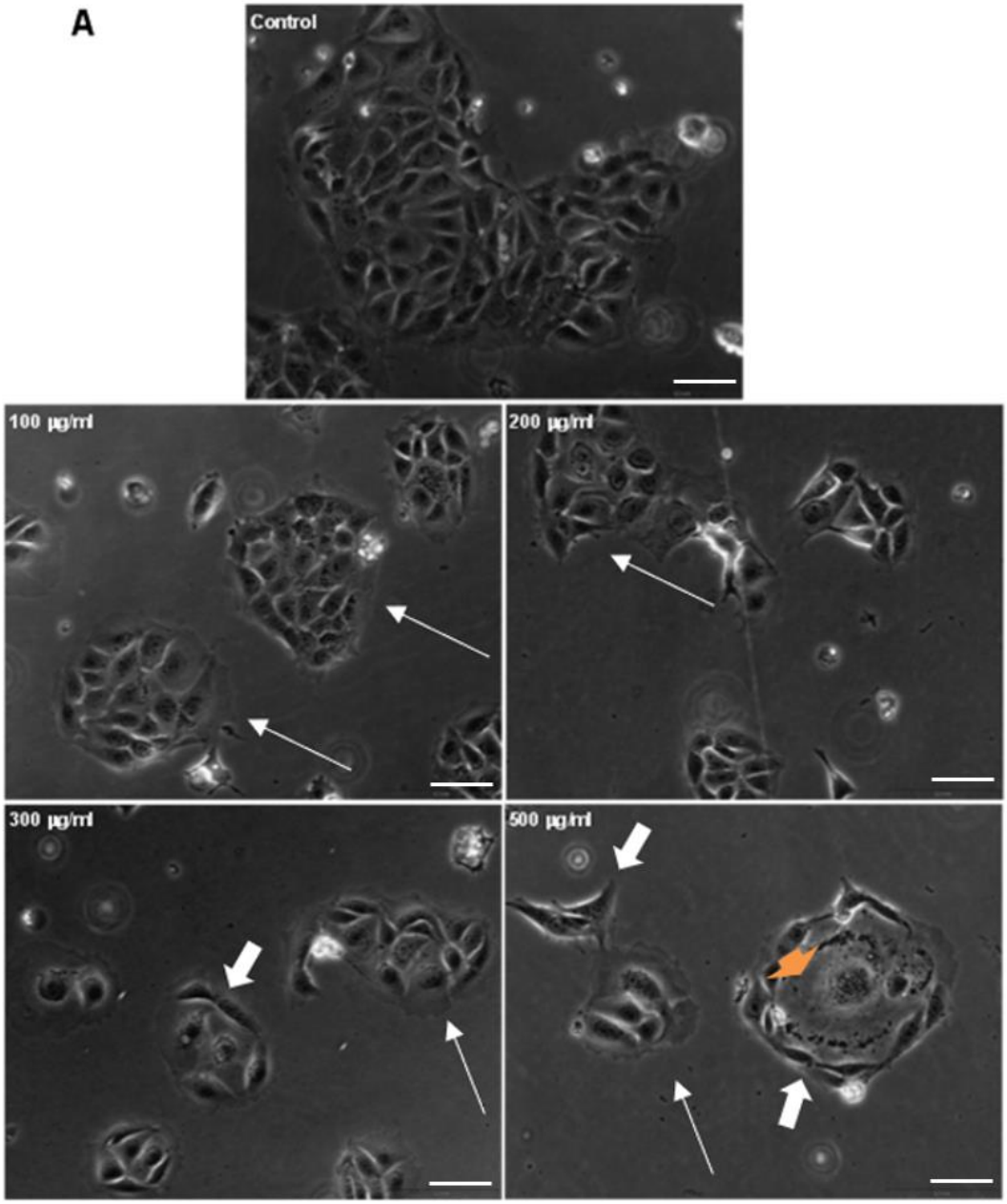

Figure 13A: Skeletal muscle derived EVs reduce cell colony formation and exert morphological changes on murine lung carcinoma cells

Photomicrographs of CMT 64/61 murine lung carcinoma cells grown in 100, 200, 300 and 500 µg/ml of C2C12 EVs or without (control). After 48 h, carcinoma cells showed morphological changes in a dose-dependent manner. At high EV concentration, some of the carcinoma cells appeared elongated shape (indicated with short arrows) compared to normal polygonal shape. Fewer cell clusters were formed and the number of cells within the cell clusters were low compared to non-treated sample. Long arrows indicate cell colonies. At high EV concentration carcinoma cell colonies were distorted, orange arrow indicating the area of possible cell lysis. Scale bar = 100 µm.

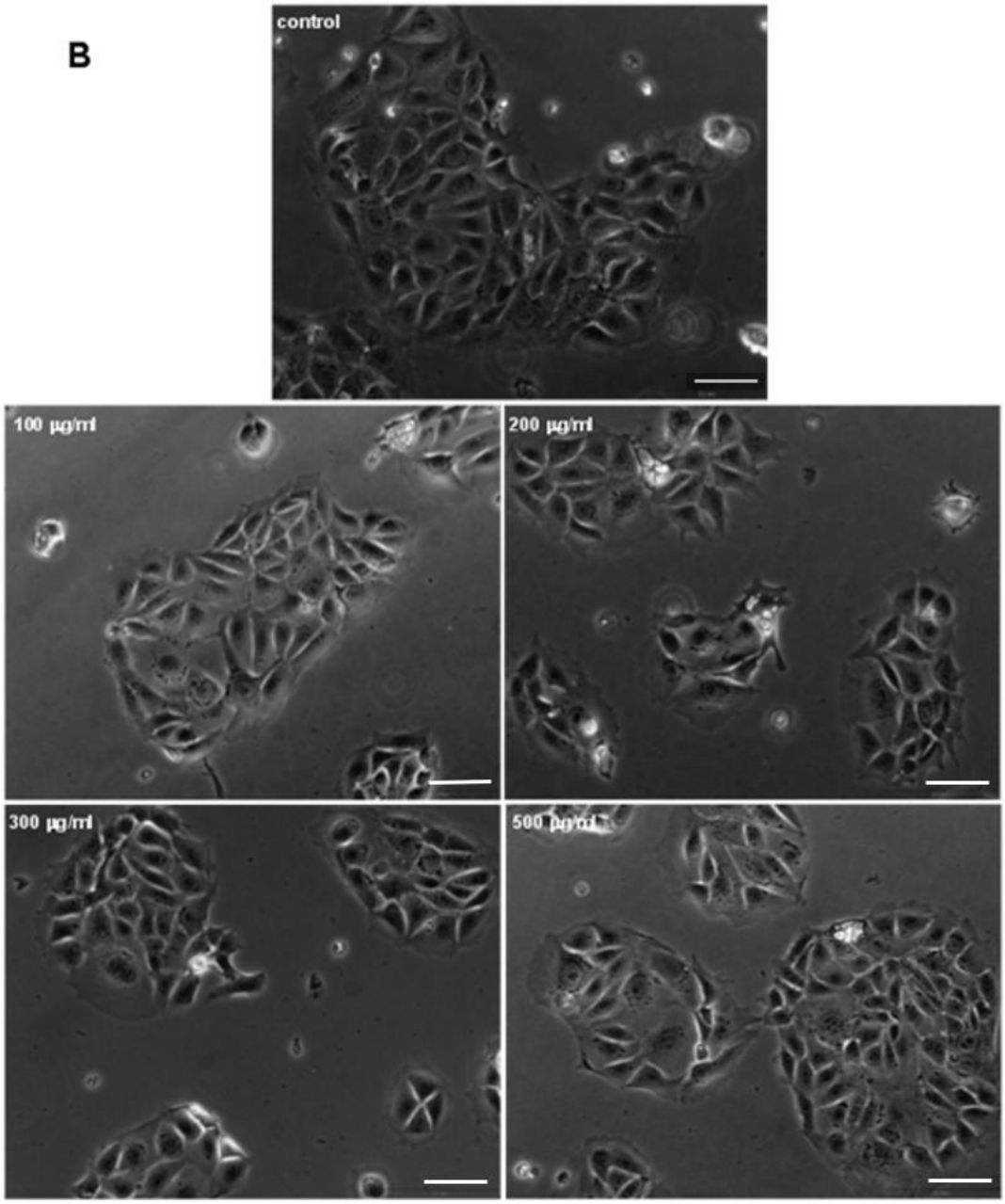

Figure 13B: Fibroblast derived EVs have no effect on carcinoma cell morphology or attachment

Photomicrographs of CMT 64/61 murine lung carcinoma cells grown in 100, 200, 300 and 500 µg/ml of NIH-3T3 EVs and CMT 64/61 untreated control cells. After 48 h in the presence of NIH-3T3 EVs, number of cell colonies and the cells within these colonies increased. Scale bar = 100 µm.

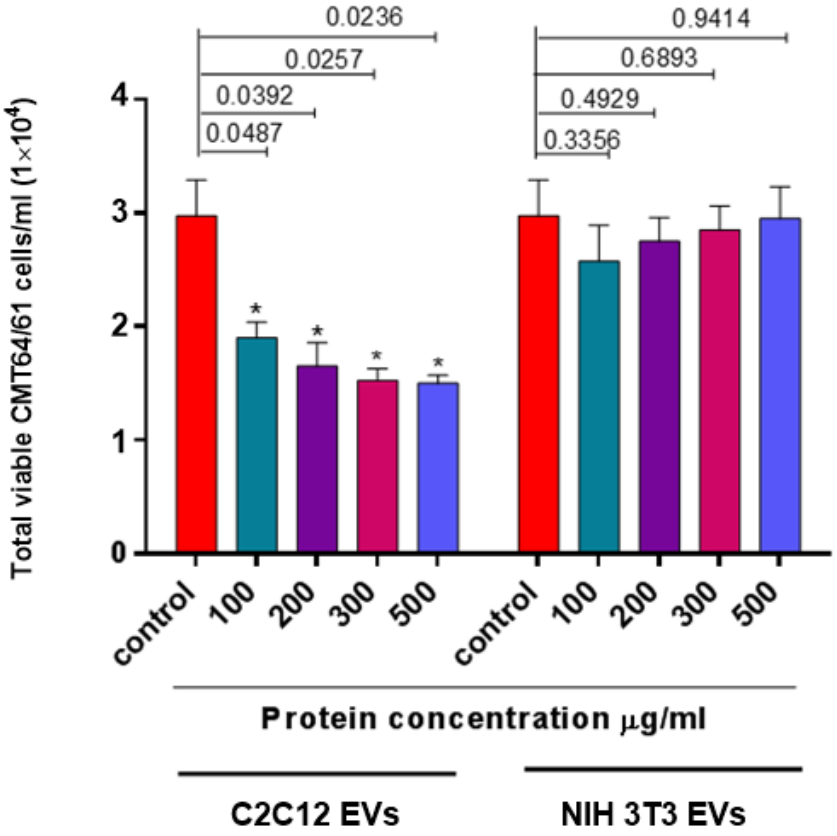

Figure 14: EVs from skeletal myocytes inhibit metastatic carcinoma cell colony formation and viability in a dose-dependent manner

Cell Viability analysis of CMT 64/61 carcinoma cells treated with C2C12 myocyte and NIH-3T3 fibroblast EVs. A range of protein concentrations of EVs was added and incubated at 37 °C for 48 h. The cells were stained with Guava ViaCount reagent and analysed by flow cytometry. The data represents the mean ± standard deviation of one or two experiments performed in triplicate. *: $p < 0.05$ was considered statistically significant. Carcinoma cells treated with C2C12 EVs exhibit significantly low levels of cell viability in a dose-dependent manner. Data are mean ± SD, n = 3 independent biological samples with 3 technical repeats per sample.

~~2.2.7~~4.2.8 Skeletal Muscle Derived EVs Inhibit Carcinoma Cell Migration

As mentioned earlier, most organs and tissues are subjected to cancer metastasis with the striking exception of skeletal muscle, in which cancer metastasis is very rare[141,142,143,144]. Over the years, researchers have postulated various reasons for this rarity, however a definitive mechanism has not yet been identified. In previous experiments, it was shown that skeletal muscle derived EVs reduce the carcinoma cell viability as well as the carcinoma cell adhesion. Based on these observations, it was postulated that skeletal muscle derived EVs may also play a role against cancer cell migration via chemotaxis.

In order to investigate the effect of C2C12 derived EVs on Murine lung carcinoma cell (CMT 64/61) migration, 1 x 10^5 CMT 64/61 cells were seeded in triplicate in Corning 8.0 µm Transwell® Inserts with serum free media. As shown in **Figure 15 A**, appropriate C2C12 EV concentrations were added to the receiver wells in the transwell plates with 5% FBS. In previous experiments, minimum EV concentrations,100 µg/ml and 200 µg/ml were shown to exert effects on carcinoma cells. Therefore, only those concentrations were used in this experiment. As a background control, serum-free media and 5% serum only receiver wells in triplicate were also performed. The 5% FBS was regarded as a chemoattractant (positive control) whilst serum free medium was used as the negative control. The plate was incubated at 37 °C for 24 hrs. After incubation, medium from both receiver and the insert were aspirated. The insert was washed twice with PBS. Cells that had adhered inside the insert were removed using a cotton swab and the insert was washed again with PBS. Crystal violet stain was used to stain the cells that had adhered to the insert membrane and the cells were counted from five randomly selected areas under the light microscope (**Figure 15B**). The percentage of cell migration was calculated using the formula:

$$\%\ \boldsymbol{Migration} = \frac{\boldsymbol{Number\ of\ cells\ (i.e, migrtaed\ cells) per\ insert}}{\boldsymbol{Total\ number\ of\ cells\ seeded}}\ \boldsymbol{x}\ \mathbf{100}\%$$

There was a significant increase in carcinoma cell migration towards the chemo-attractant (5% FBS) compared to that seen in serum free media (**Figure 15C**). This suggests that lung carcinoma cell migration was directed towards the chemoattractant. However, a significant reduction in carcinoma cell migration towards the wells containing 5% FBS with myocyte EVs was noted in a dose dependent manner (**Figure 15C**). As shown in the **Figure 15C**, 5% FBS with 100 µg/ml myocyte EVs promotes ~1.38-fold decrease in carcinoma cell migration when compared to positive control. Similarly, a ~2.58-fold decrease in carcinoma cell migration was observed in 5% FBS with 200 µg/ml myocyte EVs, compared to positive control. The results obtained here, agreed with the results obtained in earlier experiments, suggesting that myocyte EVs have an effect on carcinoma cellular processes in dose dependent manner. Furthermore, this provides some understanding into the rarity of cancer metastasis to the skeletal muscle system.

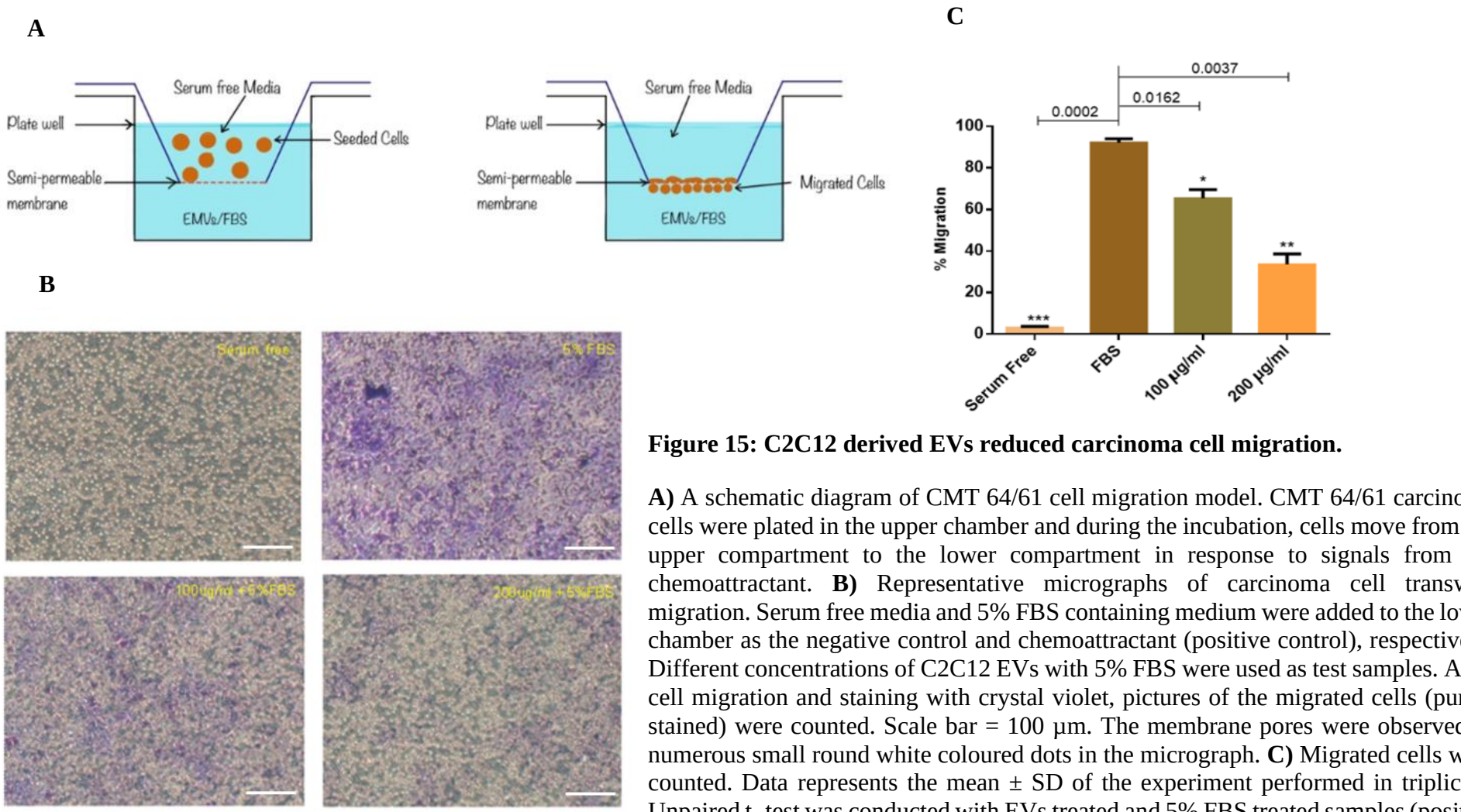

Figure 15: C2C12 derived EVs reduced carcinoma cell migration.

A) A schematic diagram of CMT 64/61 cell migration model. CMT 64/61 carcinoma cells were plated in the upper chamber and during the incubation, cells move from the upper compartment to the lower compartment in response to signals from the chemoattractant. **B)** Representative micrographs of carcinoma cell transwell migration. Serum free media and 5% FBS containing medium were added to the lower chamber as the negative control and chemoattractant (positive control), respectively. Different concentrations of C2C12 EVs with 5% FBS were used as test samples. After cell migration and staining with crystal violet, pictures of the migrated cells (purple stained) were counted. Scale bar = 100 µm. The membrane pores were observed as numerous small round white coloured dots in the micrograph. **C)** Migrated cells were counted. Data represents the mean ± SD of the experiment performed in triplicate. Unpaired t- test was conducted with EVs treated and 5% FBS treated samples (positive control). $P \leq 0.05$ was considered to be significant. The (*) indicates p value obtained from the unpaired t- test. A significant difference was noted between positive control and EV treated samples. Data are mean ± SD, n = 3 independent biological samples with 3 technical repeats per sample.

~~2.3~~4.3 Summary

This chapter was focused on correctly isolating EVs from myocytes and to observe their effects on highly metastatic murine lung carcinoma cells. Therefore, initial experiment conducted to differentiate C2C12 myoblasts to myocytes. Myoblast differentiation to myocytes was confirmed by the expression of myogenin protein, as myogenin and myosin heavy chain (MHC) expression is specific to myocytes [221]. By day 4, increased level of myogenin expression was observed on C2C12 cells incubated in differentiated medium, suggesting myoblast differentiation to mature myocytes.

The rarity of cancer metastasis to skeletal muscle has prompted many hypotheses over the years but a definitive mechanism has not yet been confirmed. In this chapter, this phenomenon was tested by introducing highly metastatic lung carcinoma cells (CMT 64/61) to myocytes (C2C12). As expected, carcinoma cells failed to colonize and grow when introduced to myocytes (C2C12), *in vitro*. However, at similar conditions, lung carcinoma cells invaded and colonized murine fibroblast cells (NIH 3T3) with in 48 h. Based on these observations, it was then postulated that the skeletal muscle microenvironment is unfavorable for highly metastatic carcinoma cell growth and metastasis. When myocyte CM was introduced to already established and proliferating murine lung carcinoma cells, a dose dependent inhibition of cell viability was observed. Furthermore, loss of cell membrane integrity in some carcinoma cells treated with high concentration of myocyte CM was observed. Loss of cell membrane integrity is a hallmark of cellular necrosis and apoptosis and therefore, decreased cell viability observed earlier is due to cytotoxic effect of myocyte CM or its anti-proliferative effect is questionable.

This study then investigated the effect of Extracellular vesicles on carcinoma cell progression as EVs are a key component of the cellular microenvironment. The present study, for the first

time demonstrated the effect of myocyte EVs on carcinoma cell viability, possibly cell attachment and migration. First, myocyte derived EVs were isolated by established methodology (differential centrifugation) as recently outlined in MISEV2018[14]. Characterisation of EVs was confirmed by detected exposed phosphatidylserine, sizing and abundance using Nanoparticle Tracking Analysis and by presence of EV specific proteins. When these EVs were incubated with already attached and established carcinoma cells, a dose dependent decrease in cell viability was noted. Interestingly, a significant decrease in cell viability was noted even at low EV concentration, 100 µg/ml. Then to make this experiment more physiological, lung carcinoma cells were introduced to the myocyte EVs containing microenvironment and investigated carcinoma cell attachment. A significant reduction in viable cells was noted compared to untreated culture. Number of cell colonies formed in the presence of myocyte EVs was reduced and a reduction in number of cells within the cell colonies were also noted. Furthermore, this effect was dose dependent. In addition, an altered cell morphology was noted in carcinoma cells treated with high concentration of myocyte EVs, above 300 µg/ml. Only few selected cells changed their cell morphology from polygonal to elongated in shape. Conversely, when NIH 3T3 EVs were introduced to lung carcinoma cells, increase in carcinoma cell numbers and colonies were noted.

Further investigations were carried out to observe the effect of myocyte EVs on carcinoma cell migration. Interestingly, Transwell migration assay indicated a reduction in percentage of carcinoma cell migration with the increasing myocyte EV concentration. Taken together, these results provide some insight into the involvement of myocyte EVs on rarity of cancer metastasis to skeletal muscles. However, to elucidate exact mechanism/mechanisms involved in this process needs further investigations.

35 Skeletal Muscle Derived EVs Induce Apoptosis of Lung Carcinoma Cells

~~3.1~~5.1 Introduction

The interest in Extracellular Vesicles (EVs) in recent years has increased exponentially [222], as many scientific groups continue to investigate their novel functions in normal physiology and in disease states, including cancer. EVs are involved in many physiological processes, including modulation of immune responses [13], cellular communication, cell growth and proliferation, maintenance of homeostasis [19] and reproductive activities [90]. They are also involved in pathological conditions including cardiovascular diseases [131,133], inflammatory diseases [87], pathogenic infections [91], and cancer [223,224].

Almost every review related to EVs in cancer, has discussed their pro-tumourigenic properties. It is now well established that cancer cell derived EVs, contain functional oncogenes that can create a favorable microenvironment for cancer development and progression [118]. Furthermore, their role in cancer invasion, metastasis, angiogenesis and immunosuppression have raised concerns [84,92]. However, recent reviews on EVs, have focused more on their clinical applications as a therapeutic agent, including their role as an effective diagnostic and prognostic biomarker [225], and as an organ specific drug carrier [140,141].

Currently, very little work has discussed the anti-tumourigenic properties of EVs. Furthermore, despite the wealth of studies associating EVs to the various pathophysiologies found in other organs, relatively few reports have investigated the properties of skeletal muscle-derived EVs. Earlier findings in this thesis discussed the isolation and analysis of skeletal muscle derived EVs and their inhibitory effect on carcinoma cell viability and migration. The data obtained suggested possible anticancer properties of skeletal muscle derived EVs. Therefore, the object of this chapter was to further analyse the effect of skeletal muscle EVs on the highly metastatic lung carcinoma cell line (CMT 64/61). This chapter goes on to look at the process of myocyte

EV uptake by carcinoma cells and their role in inducing cytotoxicity, changes in lysosomes, mitochondria, apoptosis, and inhibiting proliferation by cell cycle arrest.

~~3.2~~5.2 Results

~~3.2.1~~5.2.1 Temporal Myocyte EV Uptake by Carcinoma Cells CMT 64/61

EVs are taken up into recipient cells and release their content to induce changes in recipient cell molecular and biological processes [62]. Results presented thus far showed that myocyte derived EVs reduce carcinoma cell viability, migration and attachment in a dose dependent manner. Furthermore, it was shown that myocyte EVs induced morphological changes in random carcinoma cells during 48 h incubation period. Therefore, it was decided to set up an experiment to investigate the mechanism of myocyte EV uptake by carcinoma cells.

EV uptake by recipient cells can be visualised by use of fluorescent dyes that stain the EV membrane. Fluorescent PKH dyes such as, PKH67 and PKH26 are fluorescent dyes that are used to stain biological membranes. These dyes are extensively used in labelling cells and EVs in *in vitro* and *in vivo* cell tracking studies, as the regular cellular functions are not affected, including cell proliferation and cell viability [226,227]. To enhance the visualisation of EV uptake by carcinoma cells, both recipient cells and myocyte derived EVs were labelled with 2 different PKH dyes.

In this experiment cells from the lung carcinoma cell line CMT 64/61 were labelled with PKH67 (green) and EVs from the Murine skeletal muscle cell line C2C12 were labelled with PKH26 (red). EVs were labelled with PKH26 following the ultracentrifugation-based procedure and analysed by both flow cytometer and fluorescent microscope. Fluorescent microscopy analysis **Figure 16A** identified a heterogeneous population of labelled EVs. As expected, some vesicle aggregations were also noted, indicated with white arrows. The fluorescence histogram obtained by flow cytometer **Figure 16B** indicated fluorescent intensity and vesicle count. The red histogram shows the PKH26 labelled EVs whilst the black histogram

indicates the same concentrations of unlabelled EVs. When compared with the control sample, ~80% of the EVs in the population were PKH labelled.

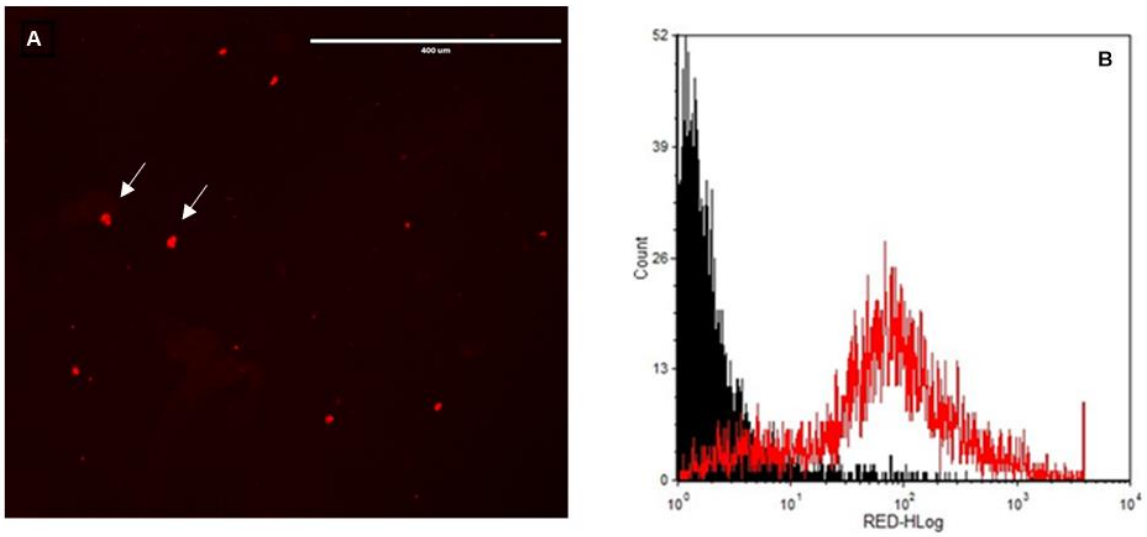

Figure 16: Analysis of PKH26 labelled myocyte EVs

C2C12 EVs were isolated by centrifugation and labelled with PKH26 dye according to the manufacturer's protocol. **A)** PKH26 labelled EVs within moving media under fluorescent microscope. Aggregated vesicles were indicated with white arrows. Scale bar= 400µm. **B)** Flow cytometry histogram showed the PKH26 labelled C2C12 EVs. 10 µl (approximately 20 µg/ml) EV samples were used; black histogram showed the unlabelled EVs used as a control. Red histogram showed the PKH26 labelled EVs. Approximately, 80% of the EVs expressed PKH fluorescence.

As yet, the exact mechanism of EV uptake by recipient cells has not been completely understood. However, there is growing evidence to suggest that EV uptake by recipient cells occurs in both a time- and dose-dependent manner [62,228]. In order to determine the myocyte-derived EV uptake by the recipient cells, 200 µg/ml of PKH26 (Red) labelled EVs were incubated with PKH67 labelled carcinoma cells and visualised over time. As shown in **Figure 17** the uptake of EVs by murine lung carcinoma cells (CMT 64/61) is time-dependent, more EVs being internalised with increasing time.

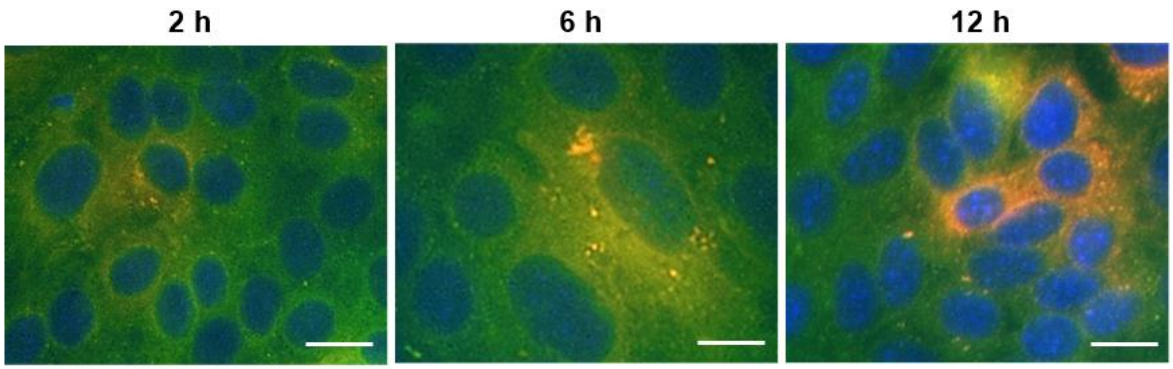

Figure 17: Time-dependent uptake of myocyte EVs by CMT 64/61 cells

Fluorescent micrographs showing overlay of PKH 67 (green) labelled carcinoma cells co-cultured with PKH 26 (red) labelled myocyte EVs for 2,6 and 12 h. DAPI staining (Blue) indicates cell nuclei. At 2 h post incubation a small amount of EVs internalisation was detectable by selected cells. By 12 h post incubation, an increased uptake of EVs was detected by selected carcinoma cells. Scale bar= 100 µm.

Results presented earlier in this thesis showed that maximal effects of myocyte EVs on carcinoma cell were exerted after 48 hours. Therefore, it was decided to observe the uptake of myocyte EVs by carcinoma cells after incubation for 48 h. As for the observations made in **Figure 17**, a specific and selective uptake of myocyte EVs by carcinoma cells was observed (**Figure 18**). Only few carcinoma cells in the same colony have shown myocyte EVs internalisation. However, the number of carcinoma cell with internalised EVs was increased compared to that observed after 12h, so possibly explaining the inhibition of cellular processes observed after 48 h. Moreover, fluorescent intensities were higher in some carcinoma cells than in others, which could be due to difference in EV uptake by different cells in the same colony (**Figure 18B**). Taken together, the results obtained here suggested that EV uptake by carcinoma cell is a selective process, not all carcinoma cells taking up myocyte EVs and that it is achieved in a time-dependent manner. Furthermore, these results support earlier observation, in which only selected carcinoma cells showed overt morphological changes (**Figure 12**).

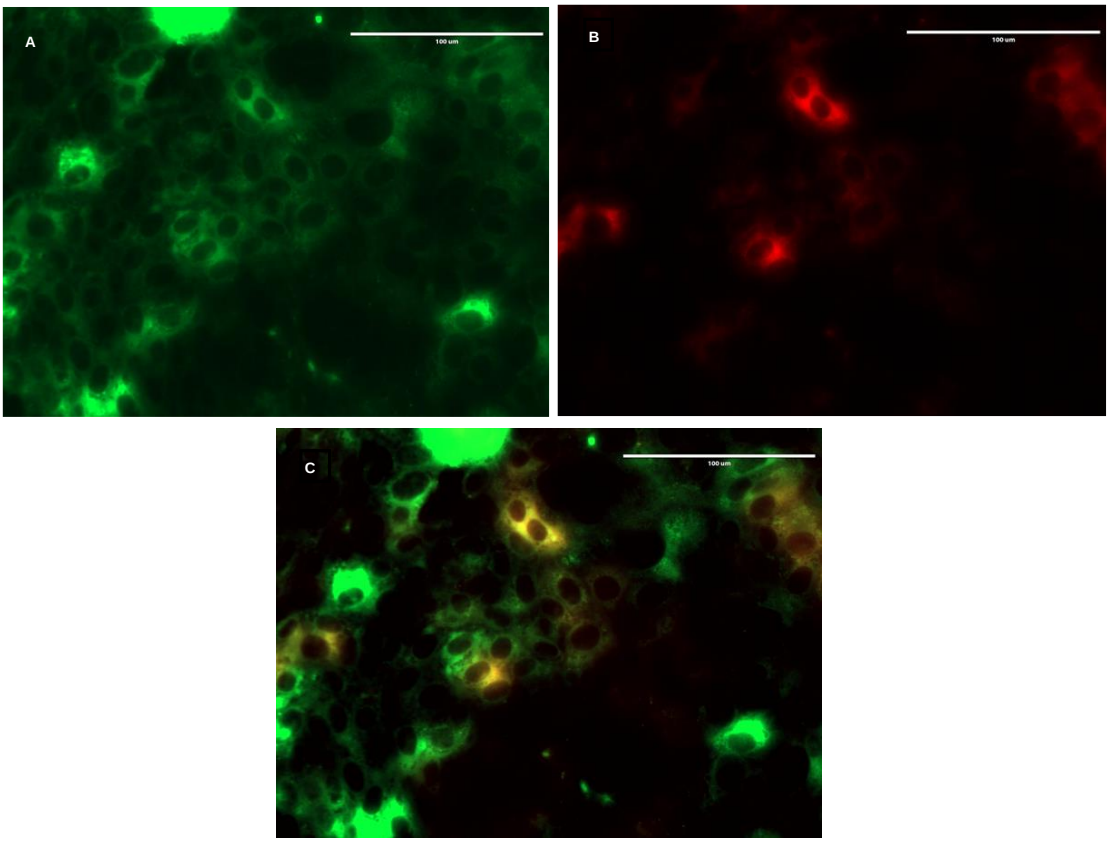

Figure 18: Uptake of PKH26 labelled C2C12 EVs by lung carcinoma cells.

A) The fluorescent microscopy image of PKH67 labelled lung carcinoma cells. **B)** Fluorescent microscopy image showing the internalised PKH26 labelled C2C12 EVs after 48 hours incubation with the lung carcinoma cell line CMT 64/61. **C)** Fluorescent microscopy image showing the overlap of PKH dyes. Scale bar= 100 µm.

~~3.2.2~~5.2.2 Skeletal Muscle Derived EVs Exert a Cytotoxic Effect on Highly Metastatic Carcinoma Cells

Since the myocyte EVs reduce carcinoma cell viability and migration in a dose dependent manner, it was decided to investigate whether myocyte EVs have a direct cytotoxic effect on carcinoma cells. Such cell-derived toxic agents can impact cells in various ways, including necrosis and apoptosis [229]. Damaged cells lose their cell membrane integrity, allowing non-permeable molecules, indicators of dead cells, to leak into the surrounding culture medium [230]. Cell cytotoxicity assays detect and measure these molecules and therefore, can be used to determine the toxic quality of such compounds on cells.

To investigate the cytotoxicity of C2C12 derived EVs on CMT 64/61 lung cancer cells, the Promega CytoTox 96 Non- Radioactive Cytotoxicity Assay, which measures the release and activity of lactate dehydrogenase (LDH) [230]. released LDH upon cell lysis in cell culture supernatants in a 30-minute coupled enzymatic assay (in which a tetrazolium salt is converted into a red formazan product) the amount of colour formed being proportional to the number of lysed cells [231] The CMT 64/61 carcinoma cells were seeded in 96-well plates (at 1 x 10^4 cells per well) in triplicate and wells were treated with 5% FBS and appropriate EV concentrations. After 24 h incubation, a cell cytotoxicity assay was performed as described in the Materials and Methods chapter. Instead of 48 h, a 24 h incubation period was chosen as the LDH has a half-life of approximately 9 hours when released into the cell culture media; therefore, it was essential to optimise the test exposure period. After the desired incubation period, samples were incubated in CytoTox 96 reagent and absorbance was recorded at 492 nm using a FLUOstar Omega microplate reader. The percentage of cytotoxicity was calculated using the formula below,

$$percent\ cytotoxicity\ \% = \frac{Experimental\ LDH\ release}{Maximum\ LDH\ release}\ X\ 100$$

When % cytotoxicity was calculated, it was evident that exposure to myocyte derived EVs resulted in a dose dependent cell cytotoxicity of carcinoma cells (Fig. 4A). A total of 50.82%, 66.98%, 88.85% and 106.9% cell cytotoxicity were measured in CMT 64/61 cells that were exposed to 100 µg/ml, 200 µg/ml, 300 µg/ml and 500 µg/ml myocyte EVs, respectively. Conversely, the control, non- EV treated sample showed 9.9% cytotoxicity. Compared to control cells, % cytotoxicity in EV treated cells was significant, as indicated in (**Figure 19A**). Furthermore, the results obtained support earlier observations made on cell viability, suggesting that myocyte EVs promote cell cytotoxicity in a dose-dependent manner, leading to a decrease in carcinoma cell viability.

Since myocyte EVs exert cytotoxicity in carcinoma cells even at low concentration (100 µg/ml of protein), it was decided to investigate their effect on non-carcinoma cells, using murine fibroblasts (NIH 3T3) as a control. Repeating the protocols on fibroblast cells, the % cytotoxicity data obtained is shown in (**Figure 19B**). Now, 15.72%, 18.74%, 50.60% and 104.5% cytotoxicity were measured in NIH 3T3 fibroblast cells exposed to 100 µg/ml, 200 µg/ml, 300 µg/ml and 500 µg/ml myocyte EVs respectively. Comparing treatment of CMT 64/61 lung carcinoma cells and normal fibroblast NIH 3T3 cells with C2C12 myocyte derived EVs, no significant increase in cell cytotoxicity was noted in cells treated with 100 µg/ml, 200 µg/ml myocyte EVs. However, a significant change was observed using 300 µg/ml of EVs and over 100% cell cytotoxicity was induced using 500 µg/ml of myocyte EVs.

Taken together, these data suggest that skeletal muscle derived EVs specifically induce cytotoxicity on highly metastatic carcinoma cells, with pronounced cell cytotoxicity being noted using low myocyte EV protein concentrations (100 and 200 µg/ml), whereas no significant effect was noted on non-carcinoma cells using these concentrations. Based on these findings, it was decided to use 100 µg/ml and 200 µg/ml of myocyte EV concentrations in future experiments, as these concentrations were non-cytotoxic to normal cells.

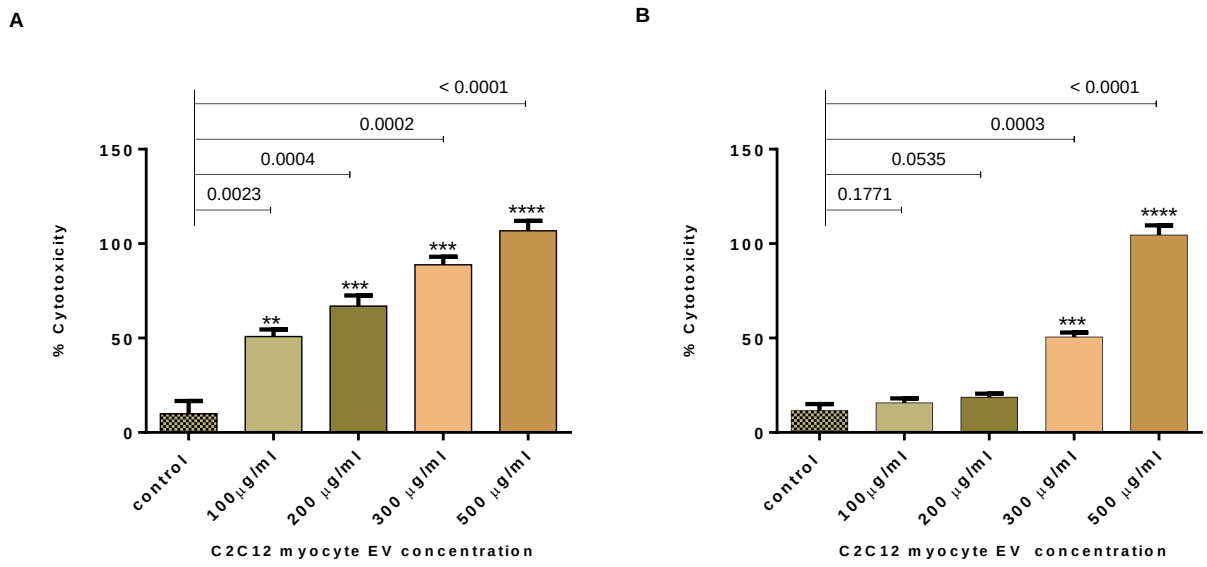

Figure 19: Myocyte derived EVs induced selective cytotoxicity on highly metastatic lung carcinoma cells but not on non-carcinoma cells

A) Murine lung carcinoma cells were seeded (1 x 10^4) in triplicate with or without murine myocyte, EVs. Cell supernatant was collected after 24 hours, and a cytotoxicity assay was performed. An unpaired t-test was used to compare EV treated versus non- treated samples. A dose-dependent significant cytotoxic effect was noted in cells treated with EVs at 100 µg/ml, 200 µg/ml, 300 µg/ml and 500 µg/ml. **B)** % cytotoxicity of murine fibroblast (NIH 3T3) cells treated with different concentrations of myocyte EVs. In contrast to carcinoma cells, no significant change in cytotoxicity was noted in fibroblast cells treated with 100 µg/ml, 200 µg/ml myocyte EVs. Data represents the mean ± SD of the experiment performed in triplicate. $P \leq 0.05$ were considered significant. The (∗) indicates *P* value obtained from the unpaired t-test. Data are mean ± SD, n = 3 independent biological samples with 3 technical repeats per sample.

~~3.2.3~~5.2.3 C2C12 Myocyte EVs Induce Lysosomal Changes in Lung Carcinoma Cells

Data presented earlier in **Figure 19** showed, that myocyte derived EVs induced dose dependent cell cytotoxicity on carcinoma cell line. As mentioned above, changes in cell membrane permeability are mostly associated with cell cytotoxicity. However, increased lysosomal membrane permeability is also known to cause cell cytotoxicity by releasing lysosomal proteases into cell cytosol [232]. Hence targeting lysosomes has been shown to be an effective cancer therapy. Lysosomes are known as the "suicidal bags" in the cell as they contain high content of hydrolytic enzymes. In the event of lysosomal membrane damage, these hydrolytic enzymes release into the cell cytosol and cause indiscriminate degradation of cellular components. Furthermore, research has shown that even only a partial lysosomal membrane permeability induces cell death by apoptosis [233,234,235,236].

Endocytosis is known to be the most favourable pathway of EVs uptake by recipient cells [222,237,238]. Most of the EVs taken up into cells via endocytosis, release their content into the recipient cell cytosol, which exerts changes in recipient cells. Therefore, one could postulate that myocyte derived EVs play a role in inducing lysosomal membrane permeability, leading to cellular cytotoxicity. To investigate the effect of myocyte derived EVs on the lysosomes of carcinoma cell, a LysoTracker Green DND-26 assay was performed.

LysoTracker dyes are fluorescent acidotropic dyes that are used in labelling and tracking acidic organelles such as lysosomes in live cells. In this experiment, LysoTracker Green DND-26 was used to label the lysosomes in murine lung carcinoma cells treated with or without murine skeletal myocyte EVs. A working concentration of 75 nM of LysoTracker solution was made by diluting 1 mM probe solution with cell growth medium. Carcinoma cell line, CMT 64/61 cells were seeded at 1 x 10^4 cells per well in a chamber slide, treated for adherent cell cultures.

Cells were seeded in triplicate and treated with appropriate EV concentrations for 48 h. After incubation cells were washed with PBS and incubated at 37 °C for 45 min with prewarmed LysoTracker containing growth medium. Cells were washed with PBS and loaded with fresh growth medium and cellular morphology was observed under the fluorescent microscope (**Figure 20A**).

Cancer cells are known to contain increased numbers of lysosomes in order to maintain homeostasis, to maintain cell proliferation and to survive under stress conditions [234,239,240]. The lung carcinoma cell line used in this study is highly metastatic and therefore expected to harbour an increased level of lysosomes. A clear visual localization of intracellular lysosomes in both EVs treated and non-treated cells was made initially (**Figure 20A**). Compared to control cell (non-EV treated), in myocyte-EV treated CMT 64/61 cells lysosomes appeared larger and more distinct, (indicated by white arrows in **Figure 20A**). Moreover, this effect was highly noticeable in carcinoma cells treated with 200 µg/ml of myocyte EVs. The implication of these results was that myocyte derived EVs cause changes in carcinoma cell lysosomes, possibly by altering the lysosomal membrane permeability. Increased lysosomal membrane permeability causing enlargement of lysosomes and enlarged lysosomes rupture easily to release hydrolytic enzymes to the cytosol,[241] enzymes that may cause cell cytotoxicity and induce cellular necrosis or apoptosis.

To investigate further, LysoTracker fluorescent intensity was measured. A separate batch of carcinoma cells were seeded at 1 x 10^4 cells per well in 24-well plates and subjected to myocyte EVs exactly as described above. After incubation, 5,000 cells from each well were transferred to a 96-well plate. 75 nM of LysoTracker solution containing growth medium was added to each cell well and incubated at 37 °C for 45 min. Then the lysosome fluorescent intensity was

measured on a FLUOstar Omega microplate reader (Excitation: 504 nm and Emission: 511 nm, bottom reading) (**Figure 20B**).

Fluorescence intensity of myocyte EV-treated cells was lower compared to untreated control cells **Figure 20B**, although a significant difference was not noted. As LysoTracker Green stains lysosomes, it was possible to make a quantitative estimate of the quantity of lysosomes by measuring fluorescent intensity. Accordingly, the number of lysosomes present in carcinoma cells treated with myocyte EVs **Figure 20B** was reduced, possibly due to their degradation; release of hydrolytic enzymes into the cytosol could then mediate cytoxicity resulting in necrosis/apoptosis.

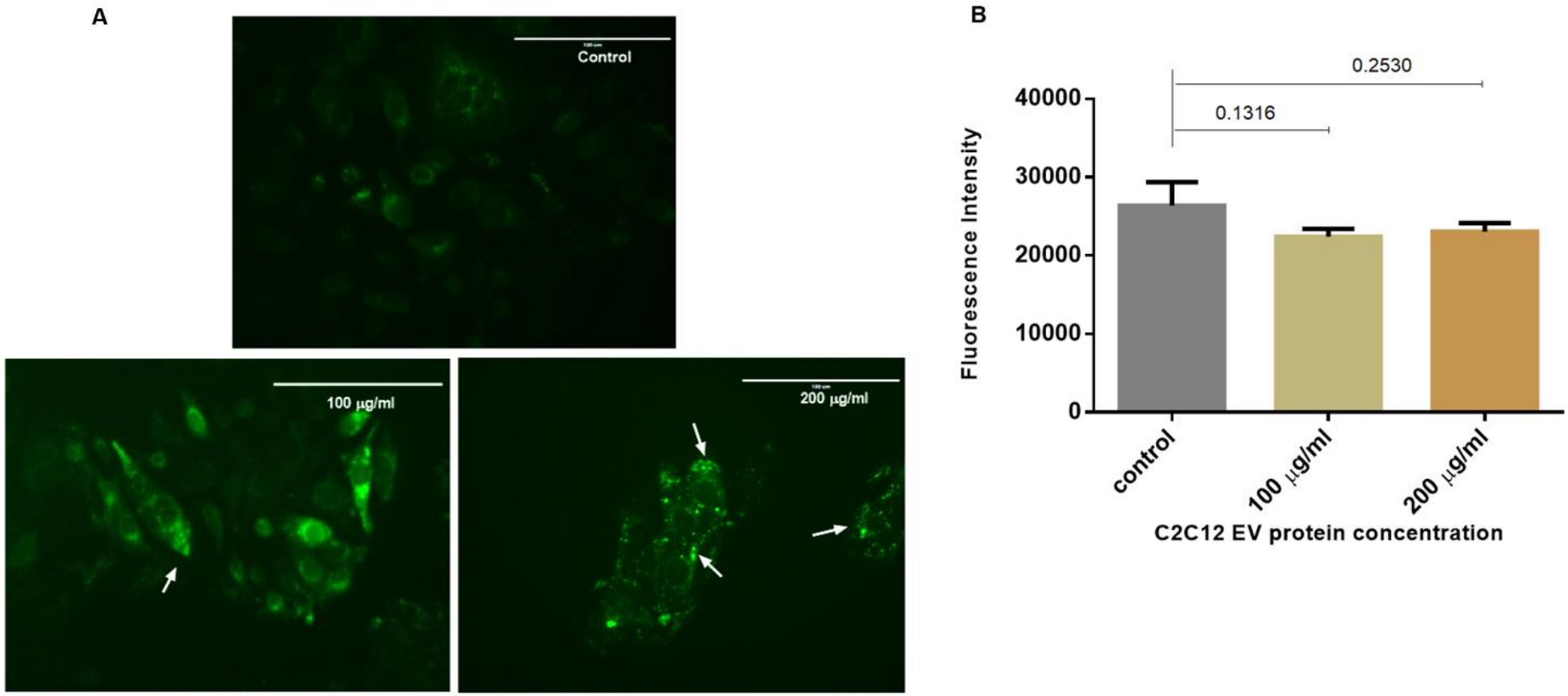

Figure 20: Myocyte derived EVs induce lysosomal dysfunction in lung carcinoma cells

A) Myocyte EVs induce lysosomal morphological changes. Carcinoma cells treated with myocyte EVs for 48 hours and stained with LysoTacker Green DND-26 for 30 min. Cells were observed by fluorescent microscope (Scale bar 100µm). Compared to control, untreated cells, lysosomes appeared bigger in cells treated with 100 and 200 µg/ml of EVs, indicated with white arrows. **B)** Lung carcinoma cells incubated with LysoTacker Green DND-26, the fluorescent intensity was measured by microplate reader (Excitation: 504 nm and Emission: 511 nm, bottom reading). $P \leq 0.05$ were considered significant. Data are mean ± SD, n = 3 independent biological samples with 3 technical repeats per sample.

~~3.2.4~~5.2.4 Myocyte Derived EVs Induce Mitochondrial Changes in CMT 64/61 Lung Cancer Cells

Lysosomal functions are critical in regulating mitochondrial activities [237,242]. Since myocyte EVs induced the described changes in lysosomes, it was decided to investigate the effect of myocyte EVs on mitochondria. Mitochondrial changes were therefore analysed using MitoTracker Red CMXRos fluorescent dye. This is a lipophilic cationic dye, which accumulates inside the mitochondria by means of their negative mitochondrial membrane potential [243,244]. As discussed in the methods section, MitoTracker assay was performed on myocyte EV-treated carcinoma cells. Cells of the muring lung carcinoma cell line, CMT 64/61, were seeded at 1×10^4 cells in triplicate and wells were treated with 5% FBS with and without appropriate EV concentrations for 48 h. After incubation, cells were stained with MitoTracker for 30 min, and observed by fluorescent microscope (**Figure 21A**).

Close examination of fluorescent micrographs showed mitochondrial changes in myocyte EV treated cells (**Figure 21A**). Selected areas were zoomed into for clear visualisation. Mitochondria in carcinoma cells treated with myocyte EVs showed fragmentation. As clearly indicated in the zoomed-in areas, mitochondrial fragmentation increased with increasing myocyte EV concentration. Furthermore, mitochondria in treated cells showed signs of swelling and again it was highly noticeable in carcinoma cells treated with 200 µg/ml of myocyte EVs. Taken together, these morphological changes indicated mitochondrial dysfunction.

The collapse of mitochondrial membrane potential (MMP) is a hallmark of mitochondrial dysfunction. To further analyse the effect of myocyte EVs on carcinoma cell MMP, a separate batch of carcinoma cells were seeded at 1 x 10^4 cells per well in 24 well plates and subjected

to identical experimental conditions as described above. After incubation, 5,000 cells from each well were transferred to a 96-well plate and were stained with MitoTracker for 30 min. MitoTracker fluorescent intensity was measured using the FLUOstar Omega microplate reader (Excitation: 579 nm and Emission: 599 nm, bottom reading) (**Figure 21B**). The MitoTracker Red CMXRos fluorescent dye accumulates inside mitochondria by their negative mitochondrial membrane potential [243,244]. A more polarised mitochondrial membrane potential will accumulate more dye, hence increased fluorescent intensity [245]. When compared to the control, untreated sample, the fluorescence intensities of myocyte EV-treated samples were significantly lower showing a dose-dependent decrease of mitochondrial membrane potential. Taken together, these results suggested that myocyte EVs cause morphological changes in carcinoma cell mitochondria, which leads to mitochondrial dysfunction and a decrease of mitochondrial membrane potential.

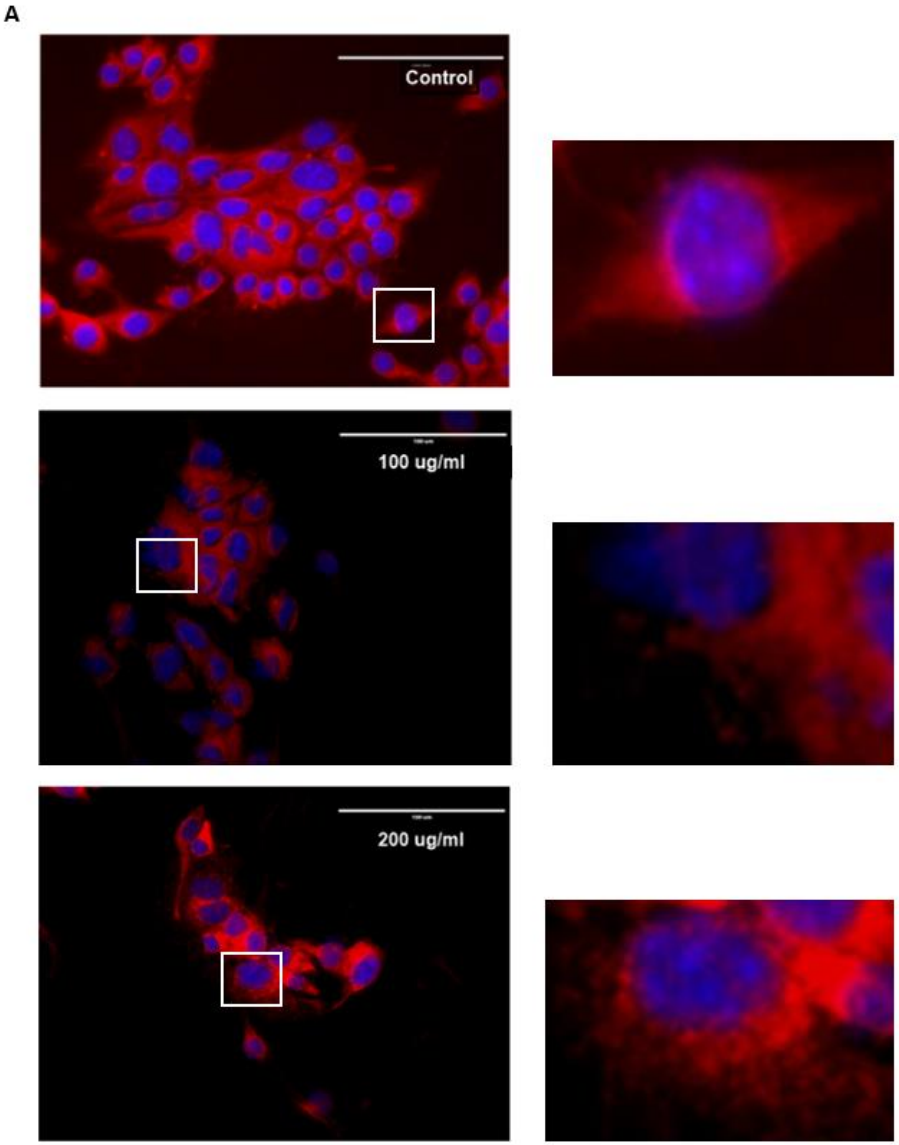

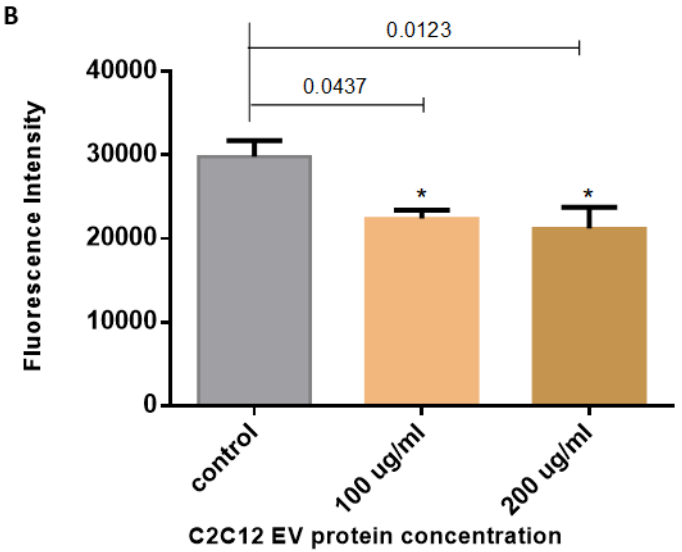

Figure 21: Myocyte derived EVs induce mitochondrial dysfunction in Carcinoma cells.

A) Myocyte derived EVs induced mitochondrial morphological changes. Carcinoma cell were treated with different concentrations of myocyte EVs for 48 hours and stained with MitoTracker Red CMXRos for 30 min, and cells were observed by fluorescent microscope (Scale bar 100µm). A selected area from each micrograph was zoomed in to, to analyse mitochondrial morphological changes. **B)** Myocyte EVs reduced mitochondrial membrane potential in carcinoma cells. Carcinoma cells incubated with MitoTracker Red CMXRos for 30 min, the fluorescent intensity was measured by microplate reader (Excitation: 579 nm and Emission: 599 nm, bottom reading). $P \leq 0.05$ were considered significant, as indicated by an asterisk. unpaired t- test. Data are mean ± SD, n = 3 independent biological samples with 3 technical repeats per sample.

~~3.2.5~~5.2.5 Myocyte Derived EVs Induce Apoptosis of Highly Metastatic Lung Carcinoma Cells

Having established that C2C12 myocyte derived EVs can induce mitochondrial dysfunction causing decreased MMP on highly metastatic murine lung carcinoma cells (CMT 64/61), further studies were conducted to investigate whether it leads to apoptosis of carcinoma cells. CMT 64/61 carcinoma cells, (1×10^4 cells per well) were seeded in triplicate into a 24-well plate with or without myocyte EVs. Cells were treated with 5% FBS and incubated for 24 h and 48 h. Non- treated cells were used as a control. On the day of the experiment, cells were detached with trypsin, washed, collected and replicates were combined to achieve the desired cell concentration per test. Cells were treated with 1% FBS and 100 µl of Nexin reagent. Plates were incubated for 20 min. at room temperature and analysed using a Guava flow cytometer (Guava EasyCyte 8HT).

The Nexin assay contains Annexin V-PE and 7-AAD dyes. Annexin V is a calcium dependent phospholipid binding protein and specifically binds phosphatidylserine (PS) [246]. PS is a membrane component which is typically localised in the inner leaflet of the plasma membrane, but which in early apoptosis is translocated from the inner leaflet to the outer leaflet of the plasma membrane, where Annexin V can readily bind [247,248]. In addition, the Nexin assay utilises 7-AAD (7-amino-actinomycin D) to detect dead or dying cells, as it is a fluorescent dye that binds to double stranded DNA. It is excluded from live, healthy cells as well as early apoptotic cells due to its ability to only penetrate through cells that have lost their membrane integrity [249]. Together, three populations of cells can be distinguished by the Nexin assay, non-apoptotic cells: Annexin V (-) and 7-AAD (-), Early apoptotic cells: Annexin V (+) and 7-AAD (-) and Late stage apoptotic and dead cells: Annexin V (+) and 7-AAD (+).

Interestingly, within 24 h a significant level of apoptosis was observed in the carcinoma cells treated with myocyte EVs (**Figure 22**). The d/ot-plot histogram in **Figure 22A** represents the percentage of live cells, early apoptotic cells, late apoptotic cells, and cell debris. By 24 h, the percentage live cells in 100 µg/ml and 200 µg/ml myocyte EVs treated samples had decreased in a dose-dependent manner, 85.8% and 81.2% respectively, whilst the % live cells in the untreated control sample remained 91.3%. Furthermore, the data obtained showed that the percentage of early apoptotic cells in 100 µg/ml and 200 µg/ml EV treated samples had increased to 8.9% and 11.1% respectively. A similar pattern was observed for the percentage of cells in late apoptosis.

By 48 h, a significant decrease in the live cell population was noted, 66.9% in 100 µg/ml EV treated and 63.1% in 200 µg/ml EV treated cell cultures. Moreover, a significant increase in late apoptosis was noted in EV treated cells from 4% for untreated control to 16.7% and 15.7% for 100 µg/ml and 200 µg/ml EV treated samples, respectively. Compared with the 24 h late apoptotic cell population, there was a ~5.56-fold increase in 100 µg/ml EV treated cells and ~3.27-fold increase in 200 µg/ml EV treated cells. Similarly, a ~1.70-fold increase in early apoptosis was noted in both EV treated samples by 48 h (compared to that at 24 h).

Statistical analysis of total apoptosis (sum of early and late apoptosis) was conducted between control and treated cell cultures (**Figure 22B**). As shown, a significant increase in percentage of apoptosis was noted within 24 h and was greater by 48 h. Moreover, the effect was dose dependent. Interestingly, these results are in an agreement with results obtained by cell viability assay, which showed a significant decrease in viable cells in myocyte EV treated cell cultures in a dose-dependent manner. Furthermore, results presented for % apoptosis at 24 h, correlates with the 24 h cytotoxicity % data, both showing dose-dependent effects on carcinoma cells.

Illustrating this, the % cytotoxicity fold-change between 100 µg/ml and 200 µg/ml EV-treated samples was ~1.32 and the fold-change for % apoptosis was ~1.33.

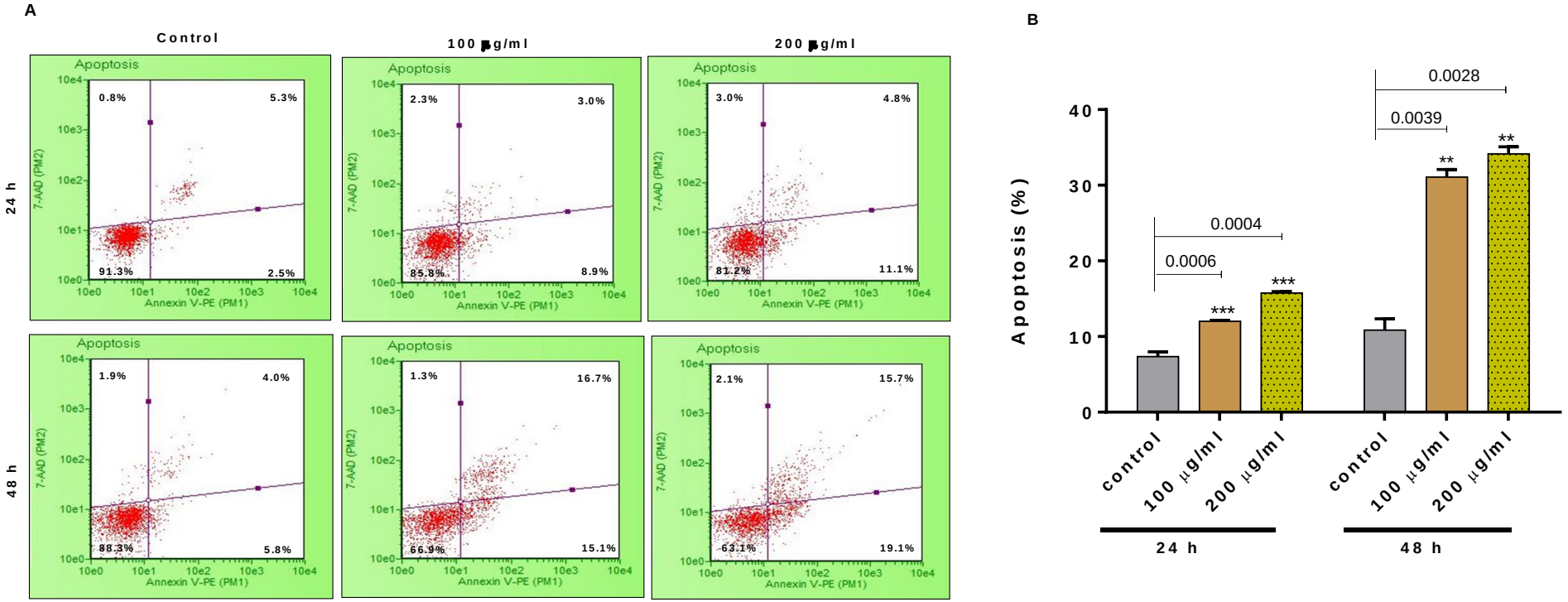

Figure 22: Skeletal muscle (C2C12) derived EVs induce apoptosis in highly metastatic lung carcinoma cells (CMT 64/61) in dose dependent manner.

A) Carcinoma cells were treated with different concentrations of myocyte EVs for 24 h and 48 h. Treated cells were analysed for apoptosis by flow cytometry using Guava Nexin Reagent. The histograms show 4 quadrants indicating different events, Lower-left quadrant: viable cells, [Annexin V-PE (-) and 7-AAD (-)], Lower- right quadrant: cells in the early stages of apoptosis [Annexin V-PE (+) and 7-AAD (-)], Upper-right quadrant: cells in the late stages of apoptosis or dead (by necrotic or apoptotic mechanisms) [Annexin V-PE (+) and 7-AAD (+)] and Upper-left quadrant: mostly nuclear debris [Annexin V-PE (-) and 7-AAD (+)]. **B)** Percentage of apoptosis analysed by the Guava Nexin software of myocyte EV treated carcinoma cells. $P \leq 0.05$ were considered significant. The (*) indicates P value obtained from the unpaired t-test. Compared to control cell cultures, a significant percentage of apoptosis was observed by 24 h in myocyte EV treated carcinoma cells. Percentage of apoptosis showed both dose and time dependent increases. Data are mean ± SD, n = 3 independent biological samples with 3 technical repeats per sample.

Having confirmed that myocyte EVs induce apoptosis on highly metastatic lung carcinoma cells, it was decided to investigate their effect on a normal cell line such as NIH 3T3 (murine fibroblasts). As shown earlier, with low concentrations of myocyte EVs, up to 200 µg/ml, not being cytotoxic to fibroblast cells, it was not expected to see apoptosis of fibroblasts were treated with 100 µg/ml and 200 µg/ml myocyte EVs. As before, NIH 3T3 cells, 1×10^4 cells per well in triplicate, were seeded into a 24 well plate with or without myocyte EVs. Cells were treated with 5% FBS and incubated for 24 h and 48 h. Non-treated cells were used as a control. On the day of the experiment, replicates were combined to achieve the desired cell concentration per test. Cells were treated with 1% FBS and 100 µl of Nexin reagent and analysed using the Guava flow cytometer (Guava EasyCyte 8HT).

Compared to control, untreated cells, insignificant decreases in live cells were noted for both 24 h and 48 h (**Figure 23A**). The data obtained here were very similar to data that presented in **Figure 23B**, %cytotoxicity of NIH 3T3 increasing (but not significantly) with the addition of 100 µg/ml and 200 µg/ml myocyte EVs. Similarly, % of total apoptosis was increased in both a time- and dose-dependent manner but not significantly so (**Figure 23B**). Taken together, these data suggest that myocyte EVs are more cytotoxic (inducing apoptosis) to carcinoma cells than normal cells.

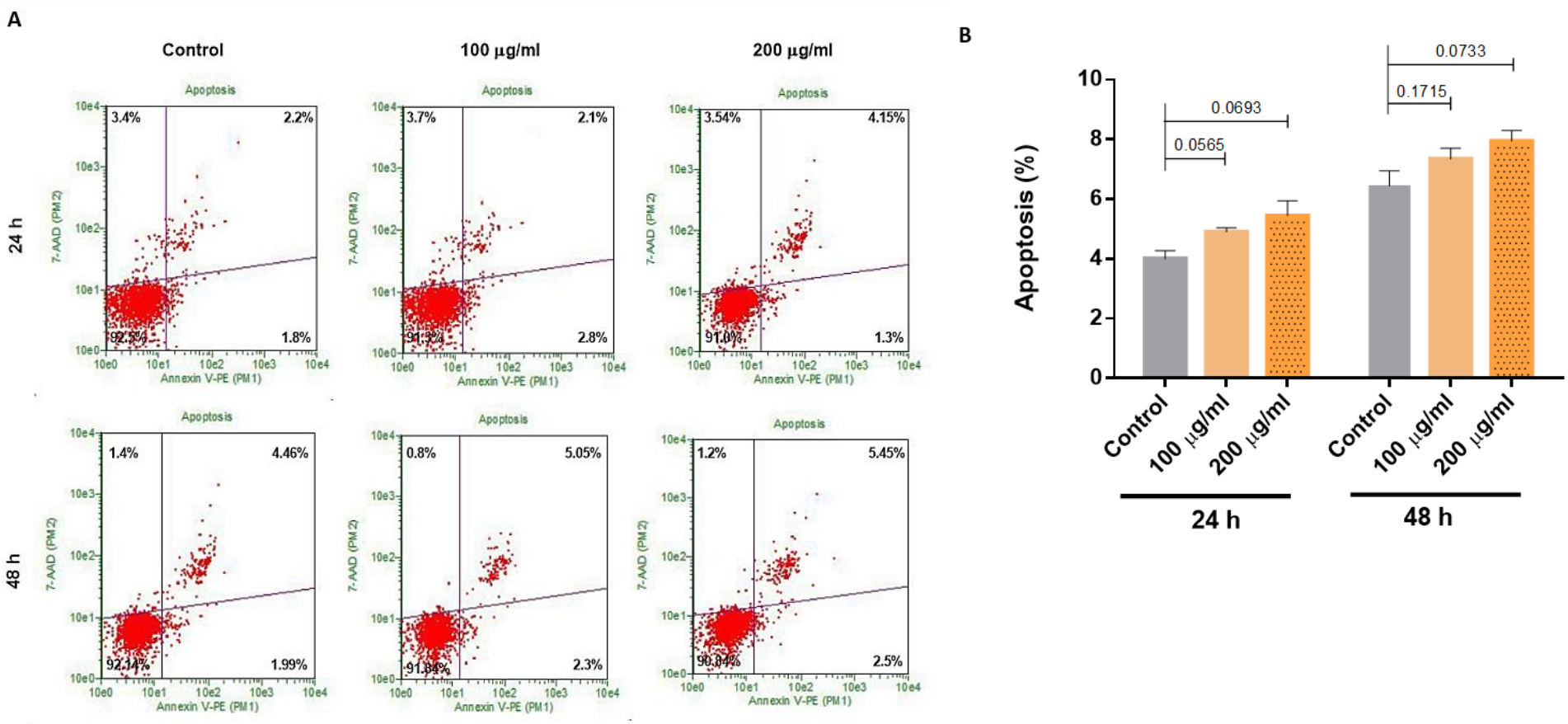

Figure 23: Apoptotic effect of skeletal muscle derived EVs on normal murine fibroblast NIH 3T3 cells

A) Murine fibroblast (NIH 3T3) cells were treated with different concentrations of myocyte EVs for 24 h and 48 h. The data obtained by the Guava Nexin assay was presented as a dot plot (Lower-left quadrant: viable cells, Lower- right quadrant: cells in the early stages of apoptosis, Upper-right quadrant: cells in the late stages of apoptosis or dead (by necrotic or apoptotic mechanisms) and Upper-left quadrant: mostly nuclear debris). **B)** Percentage of apoptosis analysed by the Guava Nexin software of fibroblast cells treated with myocyte EVs for 24 h and 48 h. $P \leq 0.05$ were considered significant (indicated by an asterisk). Compared to the untreated control cell, no significant difference was noted in the cultures treated with myocyte EVs. Data are mean ± SD, n = 3 independent biological samples with 3 technical repeats per sample.

~~3.2.6~~5.2.6 Skeletal Muscle Derived EVs Induce the Mitochondrial-Mediated Intrinsic Pathway of Apoptosis of Lung Carcinoma Cells

There are two core pathways by which apoptosis is mediated, the extrinsic or death receptor pathway and the intrinsic or mitochondrial pathway. Both pathways use caspases to carry out apoptosis. The extrinsic pathway is activated by binding of extracellular ligands to death receptors. For example, FasR forms the Death-Inducing Signalling Complex (DISC) as a result of trimerizing upon binding FasL. Together with caspase 8 a signal is transduced leading to apoptosis. The intrinsic pathway is activated by upregulation of BH3-only proteins, which induce BAX and BAK leading to mitochondrial outer membrane permeabilisation (MOMP). Release of cytochrome *c* from mitochondria result in the formation of apoptosome, which activates caspase 9. Caspase 8 from extrinsic pathway and caspase 9 from the intrinsic pathway then activate downstream caspase 3 resulting in cell death. The two pathways are linked through the cleavage of BH3-only protein Bid [250].

Based on the results presented thus far, it was evident that myocyte EVs induce apoptosis of highly metastatic lung carcinoma cells. Understanding the cascade of events that trigger apoptosis in response to myocyte EVs was thought to be a way to understand the mechanisms of action by identifying key molecules and their targets. Therefore, it was decided to identify the apoptotic pathway triggered by the myocyte EVs on highly metastatic lung carcinoma cells used previously. In order to determine the apoptosis pathway, caspase 3,8, and 9 detection assays were performed. CMT 64/61 murine lung carcinoma cells, (1×10^4 cells/ 90 µl per well) were seeded in triplicate into a 96 well plate. Cells were treated with growth medium containing myocyte EVs and incubated at 37 °C for 48 hours. On the day of the experiment, 100 µl of tri-caspase loading solution was added to each well and incubated at room temperature, whilst protecting from light, for 60 min. Hydrogen peroxide is widely used as an apoptosis inducer in

many cellular studies. A recent study found that, H_2O_2 induced apoptosis on HEK 293T cells (human embryonic kidney cell line), primary fibroblasts, and terminally differentiated myocardial cells. This was at concentrations of 0.1 to 1.6 mM [251]. Furthermore, a low concentration of H_2O_2 was found to induce the intrinsic apoptotic pathway on cell lines such PC12 [252] whilst higher concentrations were found to induce necrotis cell death [253]. Therefore, carcinoma cells were treated with 100 µM of H_2O_2 for 24 h and used as a positive control. After incubation, fluorescent intensity was measured on a FLUOstar Omega microplate reader (Caspase 3: Ex/Em = 535/620 nm (red), Caspase 8: Ex/Em = 490/525 nm (green), Caspase 9: Ex/Em = 370/450 nm (blue), bottom reading).

Supporting previous observations made using viability assays **Figure 12**, addition of myocyte EVs to lung carcinoma cells indicated a reduction in the number of cells in a dose-dependent manner (**Figure 24A**). Furthermore, some of the cells in the myocyte EV-treated sample showed loss of cell membrane asymmetry, (indicated by a white arrow (Fig. 10A)), a known hallmark of apoptosis [254]. Similarly, H_2O_2 treated carcinoma cells indicated similar morphological changes (indicated with white arrows) and reduction in cell numbers compared to control, untreated cells.

When caspase activities were measured, caspase 3 activity was significantly increased in carcinoma cells treated with myocyte EVs in a dose-dependent manner. Moreover, carcinoma cells treated with H_2O_2 also showed a significant increase in caspase 3 activity (**Figure 24B**). Although, no significant difference was observed in the caspase 8 activity, a slight increase was noted in carcinoma cells treated with both myocyte EVs and H_2O_2 (**Figure 24C**). Interestingly, caspase 9 activity was significantly increased in carcinoma cells treated with 200µg/ml myocyte EVs and H_2O_2. Surprisingly, caspase 9 activity in carcinoma cells treated

with 100µg/ml myocyte EVs, was not elevated compared to control (**Figure 24D**). Moreover, a highly significant increase in caspase 9 activity was measured in the carcinoma cells treated with 100 µM H_2O_2.

Caspase 3 is common to both the extrinsic and intrinsic apoptotic pathways, whereas caspase 8 and caspase 9 are specific to the extrinsic and intrinsic apoptotic pathways respectively. A significant elevation in caspase 3 and 9 was observed in the carcinoma cells treated with 200µg/ml myocyte EVs, suggesting that myocyte EVs induce mitochondrial-mediated intrinsic pathway apoptosis in highly metastatic carcinoma cells.

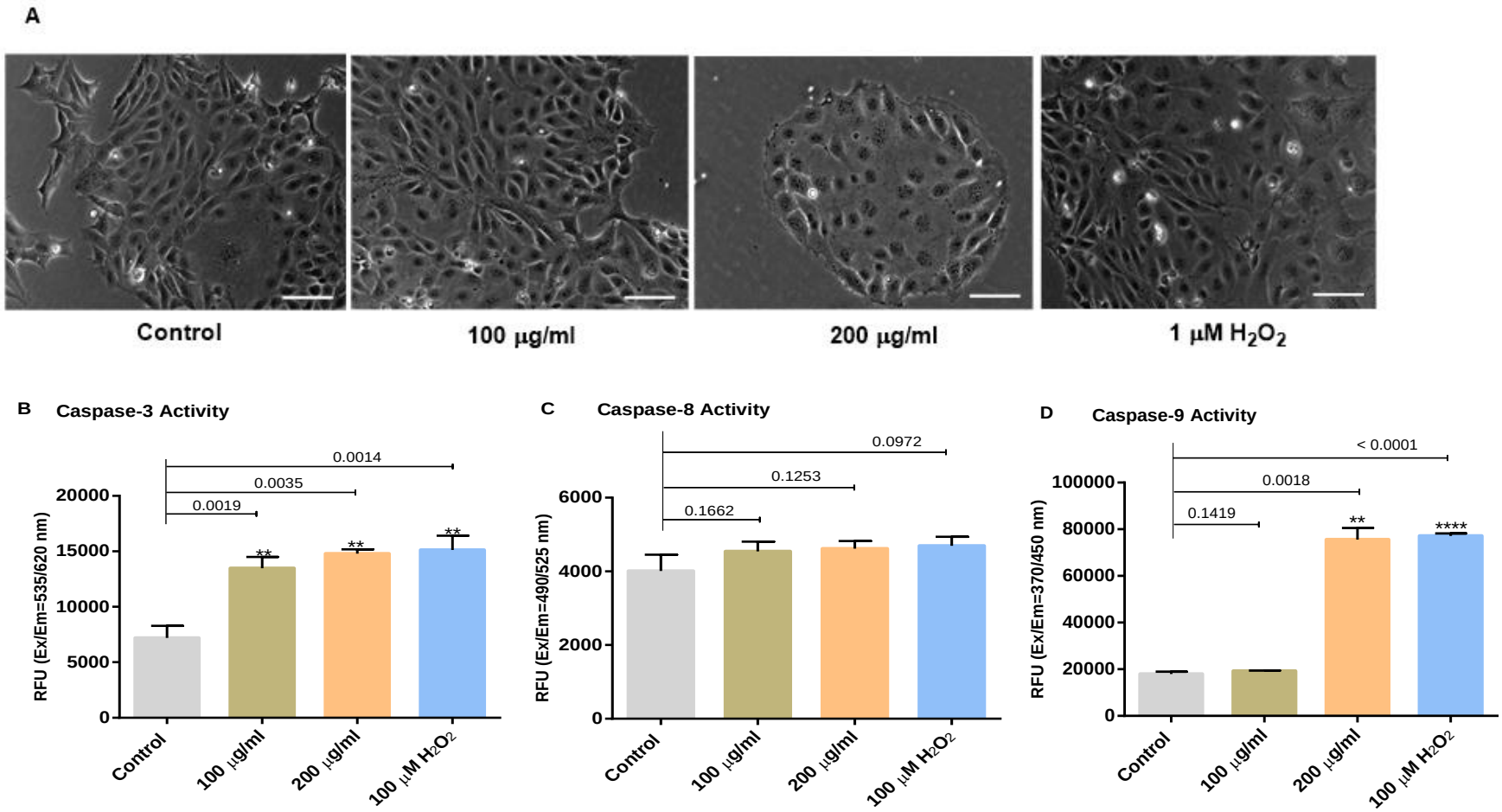

Figure 24: C2C12 myocyte EVs induce caspase 9 activity in murine lung carcinoma cells

A) Different concentrations of myocyte EVs induce morphological changes in carcinoma cells. Cells treated with myocyte EVs for 48 h, showed a dose dependent change in cell membrane asymmetry, indicated with white arrows. Apoptosis inducing H_2O_2 was used as a positive control. Carcinoma cells treated with H_2O_2 for 24 h showed a similar cell membrane asymmetry pattern. **B, C and D)** Caspase activity of 3,8 and 9 respectively in myocyte EV-treated carcinoma cells. The results were expressed as the mean ±S.D. ($P \leq 0.05$ vs control group, n=3). $P \leq 0.05$ were considered significant. Data are mean ± SD, n = 3 independent biological samples with 3 technical repeats per sample.

~~3.2.7~~5.2.7 C2C12 Myocyte Derived EVs Exert S Phase Cell Cycle Arrest on Murine Lung Carcinoma Cells (CMT 64/61 cell line)

The cell cycle is a series of event that takes place in a cell when cells grow and replicate. During DNA damage, cell cycle arrest occurs to facilitate DNA repair before cell replication. In an event of severe DNA damage, cell cycle arrest occurs and then induces apoptosis [255]. Since myocyte derived EVs induce apoptosis in carcinoma cells, it was decided to investigate the effect of myocyte EVs on carcinoma cell division by monitoring cell cycle events.

Flow cytometry was used to examine the changes in cell cycle, induced by myocyte EVs. Carcinoma cells, 1×10^4 cells per well in triplicate, were seeded into a 24-well plate with 100 µg/ml, 200 µg/ml myocyte EVs and without without EVs as control, for 48 h. Cells were then incubated in 70% ethanol for 12 h and on the day of the experiment cells were stained with Guava cell cycle reagent. Stained samples were examined by flow cytometry and the data obtained from was analysed by ModFit software.

Based on the DNA content in the cell sample, the Guava cell cycle assay helps to determine the percentage of cells in G_0/G_1, S, and G_2/M phases and, the fluorescent intensity is directly proportional to the amount of DNA content [256]. Therefore, the histogram profile presented in **Figure 25A** showed the cell distribution in each phase. The large peak in red (left) represents the cells in G_0/G_1 phase, the intermediate peak (hatched in blue) represents the cells in S phase and the final small peak in red (right) represents cells in G_2/M phases.

The results indicate that myocyte EVs induced S phase arrest in carcinoma cells (**Figure 25A and B**). Increasing the concentration of myocyte EVs indicated a significant increase in the S phase. Compared to control, untreated cells in S phase, 24.89%, there was a statistically

significant increase in 100 µg/ml and 200 µg/ml EV-treated samples of 37.41% and 39.90% respectively. DNA replication takes place during S phase of the cell cycle [257]; hence the increase of cells in S phase could suggest an accumulation of cells which were progressed from G_0/G_1 and got arrested in the S phase of the cell cycle. The S phase arrest prevents further DNA replication [257,258] and consistent with this, cells treated with myocyte EVs showed slower movement through G_2/M phase than their untreated counterparts. Concomitantly, there was a significant decrease in G_0/G_1 phase from 60.15% control cells to 37.4% and 39.90% in the carcinoma cells treated with 100 µg/ml and 200 µg/ml myocyte EVs respectively. Taken together, these data clearly indicated C2C12 myocyte EVs to impair cell cycle progression by inducing S phase arrest and preventing the cells from entering the proliferative phase and inducing apoptosis in a dose-dependent manner.

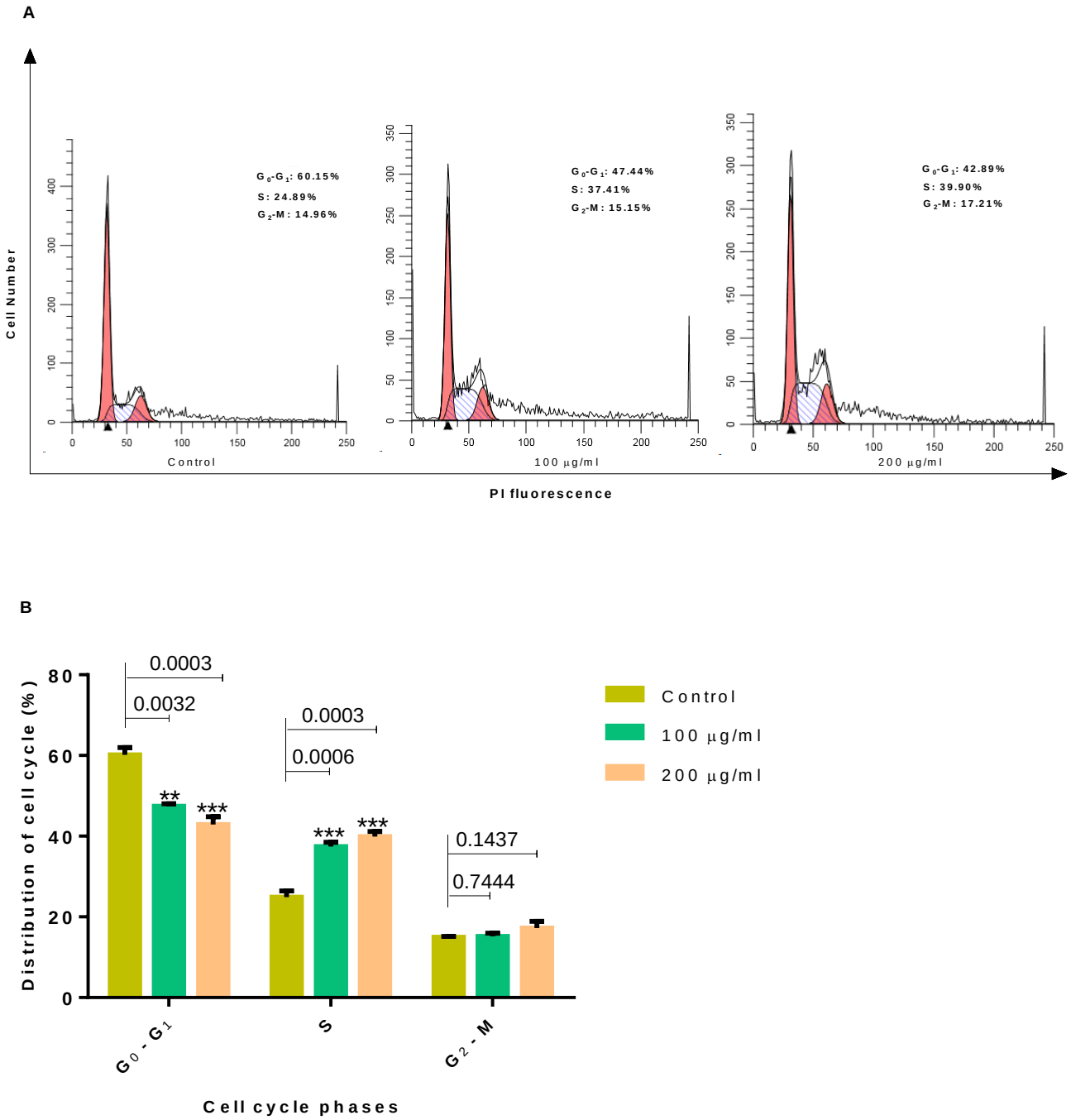

Figure 25: C2C12 myocyte EVs cause S phase cell cycle arrest in murine lung carcinoma cells (CMT 64/61)

A) Carcinoma cells treated with or without 100 µg/ml and 200 µg/ml myocyte EVs for 48 h. Cells were stained with Guava cell cycle reagent and flow cytometry was used to assess the cell cycle distribution. The histograms show the data analysed by ModFit software. **B)** The percentage distribution in the cell cycle is indicated in the histogram and was shown as mean ±S.D. ($P \leq 0.05$ vs control group). $P \leq 0.05$ were considered significant. Data are mean ± SD, n = 3 independent biological samples with 3 technical repeats per sample.

~~3.3~~5.3 Summary

Extensive research has been carried out on cancer derived EVs and their pro-tumourigenic properties. However, there is a paucity of research on the anti-tumourigenic properties of EVs. In this chapter, a novel anti-tumourigenic effect of skeletal muscle derived EVs have been described.

EVs are known to interact with recipient cells to induce intercellular signalling and cause changes to cell molecular and biological processes that, lead to changes in their physiological states, such as proliferation, attachment, and morphological changes. However, the exact mechanism of EV uptake by recipient cells has not yet been completely understood. Results obtained here showed that myocyte derived EV uptake by carcinoma cells was a time dependent process. Furthermore, results presented suggest that EV uptake by carcinoma cells is a selective process as only random cells within a colony show EV internalisation. Moreover, fluorescent intensities were higher in some carcinoma cells than others, suggesting that EV uptake by some carcinoma cells was more compared to other cells in the same colony. Interestingly, this selective uptake of EVs coincided with the results obtained earlier, which showed that only a few carcinoma cells exert morphological changes upon incubation with myocyte EVs.

Other data presented suggests that skeletal muscle derived EVs exert a dose-dependent cytotoxic effect on highly metastatic carcinoma cells. Therefore, this data is an agreement with the results presented in the previous chapter, which showed that carcinoma cell viability was reduced with increasing myocyte EV concentration. An effective anticancer agent should exert maximum cytotoxicity on carcinoma cells whilst exerting minimum damage to normal, healthy cells. Interestingly, low concentrations of myocyte EVs (100 µg/ml and 200 µg/ml) did not

have a significant cytotoxic effect on non-carcinoma cells, suggesting a specific cytotoxic effect of myocyte derived EVs. Only at, high concentrations of myocyte EVs (above 200 µg/ml) was a cytotoxic effect exerted on normal cells.

Further investigations revealed that myocyte EVs dose dependently induced carcinoma cell lysosomal enlargement and reduction in lysosome numbers. Strikingly, data obtained herein also showed that myocyte EVs induce dose dependent morphological changes in mitochondria including, mitochondrial fragmentation and swelling. Apart from morphological changes, a decrease in mitochondrial membrane potential was also observed.

The collapse of mitochondrial membrane potential (MMP) is a hallmark of mitochondrial dysfunction, which leads to mitochondrial mediated apoptosis [238]. Interestingly, these findings supported the results obtained in an apoptosis assay. A significant increase in apoptosis was noted in carcinoma cells treated with myocyte EVs and the effect was both dose and time dependent. However, myocyte EVs failed to induce significant % apoptosis in normal fibroblast cells (NIH 3T3). Interestingly, but not surprisingly, these data correlate with the cytotoxicity data which showed a specific cytotoxicity effect of myocyte derived EVs.

Further investigations have revealed more information about the apoptotic pathway induced by myocyte EVs on carcinoma cells. Caspases are key initiators and executioners of apoptosis and by their position in the apoptotic signalling cascade, the apoptotic pathway can be identified. Caspase 3 is common in both the extrinsic and intrinsic pathways, whereas caspase 9 is specific to the intrinsic pathway. Data obtained in caspase assays revealed increased activities of caspase 9 and 3 in carcinoma cells treated with myocyte EVs. Hence it was suggested that myocyte derived EVs induced mitochondrial mediated intrinsic apoptosis in carcinoma cells.

Finally, in this chapter evidence has been presented indicating the effect of myocyte EVs on carcinoma cell proliferation. Cell cycle assay results indicated that myocyte EVs induce S phase cell cycle arrest in carcinoma cells. Data indicated a dose dependent increase in cell cycle arrest at S phase alongside, a significant decrease of cells in G_0/G_1 phase. Unrepairable DNA damage induces cell cycle arrest preventing further DNA replication and cell proliferation [257,258]. Consistent with this view, cells treated with myocyte EVs showed a slower movement through the G_2/M phase (proliferative phase) than their untreated counterparts. Taken together, these data suggest that myocyte EVs can induce cytotoxicity, inhibit carcinoma cell proliferation, cause DNA damage, and induce apoptosis via activation of the intrinsic mitochondrial pathway.

46 Proteomics analysis of C2C12 myocyte extracellular vesicles

~~4.16~~4.16.1 Introduction

In general, all EVs released from cells are loaded with a range of macromolecules including various lipids, proteins, and nucleic acids. The contents of the EVs depends on their mode of biogenesis [48]. However, irrespective of cell type and biogenesis, proteins such as MHC II, tetraspanins, ESCRT proteins, Alix, TSG101, and heat-shock chaperones are commonly found in all EVs [48]. Intracellular organelles such as mitochondria, Golgi apparatus, lysosomes, and endoplasmic reticulum associated proteins are also found in EVs [259]. Furthermore, there is ample evidence to suggest that the protein content of EVs and their role mainly depends on the cell type from which they are derived. For example, carcinoma cell-derived EVs, play a pivotal role in cell proliferation, migration, angiogenesis, and apoptosis [260], whilst skeletal muscle-derived EVs play a role in muscle physiology and development of metabolic diseases [193].

Skeletal muscle is the largest organ in the human body [261] and highly adaptable to environmental and physiological changes. This is of particular importance as skeletal muscle is known to play a pivotal role in muscle mass, glucose, and energy homeostasis [262]. Furthermore, skeletal muscle contains the largest reservoir of proteins in the body [263]. In recent years, skeletal muscle is increasingly viewed as an endocrine organ. The secretome of skeletal muscle which includes cytokines and peptides, termed myokines [264,265] that it secretes is increasingly being shown to play important roles in body-wide metabolism, growth, and other functions [266]. Furthermore, myokines have been found to be packaged within skeletal muscle derived EVs have been regarded as a delivery vehicle for myokines [267].

Results presented in this study thus far, showed that myocyte derived EVs affect carcinoma cellular processes. It was shown that, myocyte derived EVs reduced the cell viability of highly metastatic lung carcinoma cells, attachment and reduce carcinoma cell migration. Furthermore,

results in chapter 4 showed that, myocyte derived EVs induced carcinoma cell cycle arrest at S phase, reducing cell proliferation and increased mitochondrial membrane permeability triggering intrinsic apoptosis. Based on these results, it was postulated that myokines and other proteins in myocyte EVs might play a role in these cellular changes.

Despite the wealth of studies associating EVs to the various pathophysiologies found in other organs, relatively few reports have investigated the protein content of skeletal muscle derived EV, themselves. Therefore, it was decided to perform a proteomics analysis on myocyte EVs in this chapter. Since by way of a control fibroblast derived EVs were found to have a positive effect on carcinoma cell growth and progression, proteomics analysis was also performed on fibroblast EVs as a positive control.

Mass spectrometry-based proteomics has become the tool of current proteomics-based studies. In this study, liquid chromatography-based Mass spectrometry (LC-MS/MS) was used to analyse the proteins in myocyte and fibroblast EVs. The results were then subjected to Mascot software for protein identification, these proteins then being further analysed and filtered using Scaffold software. Filtered proteins were then analysed by Search Tool for Retrieval of Interacting Genes/Proteins (STRING), a well-known data base which contains data on Protein-Protein Interactions (PPI). In order to analyse the functions and pathway of these proteins Kyoto Encyclopedia of Genes and Genomes (KEGG) was also used.

~~4.2~~6.2 Results

~~4.2.1~~6.2.1 Proteins Detected in C2C12 Myocyte EVs and NIH-3T3 EVs

The results discussed in previous chapters showed opposing effects of myocyte EVs and fibroblast EVs on murine lung carcinoma cell line, CMT 64/61, with myocyte EVs decreasing carcinoma cell proliferation and progression, with the same concentration of fibroblast EVs enhancing these processes. Proteins enhance and repress many cellular processes and their involvement in regulating cell proliferation, communication, division, apoptosis, and other such biological pathways and cellular processes are well documented. In terms of the effects skeletal muscle EVs, representing an important component of the skeletal muscle milieu and the type of environment it may present to metastasing carcinoma cells. It was therefore deemed important to assess differences in protein presence or absence in skeletal muscle EVs.

Here, protein presence or absence in both EVs from murine C2C12 myocytes and NIH-3T3 fibroblast cell lines were analysed. EV samples were analysed in duplicate, proteins presenting in both replicates being regarded as present. In accordance with the published convention, mean spectrum counts of less than five, were regarded as unreliable when working with small replicates. Therefore, protein mean spectrum counts of five or more were regarded as an indication of protein presence. A total of 1,001 proteins were detected between the myocyte and fibroblast EVs analysed. However, only 387 proteins contained 5 or more peptides as detected by mass spectrometry and so only the presence of those proteins was deemed reliable (**Table 2**).

A Venn diagram was constructed to represent the proteins identified in EV samples (**Figure 26**). As shown, 132 proteins common to both myocyte and fibroblast EVs were identified. From 387 proteins, 88 myotube specific proteins and 167 fibroblast specific proteins were also

identified. Strikingly, fibroblast EVs appeared to contain more cell specific proteins compared to myocyte EVs. As mentioned earlier, cell activities are controlled by proteins and some cellular activities are upregulated in the presence of specific protein/s whilst certain cellular activities are downregulated in the absence of specific protein/s. Therefore, identifying proteins present and absent in the EVs sample was essential.

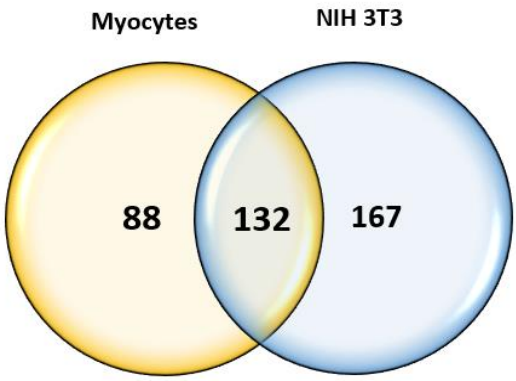

Figure 26: Proteins identified in both C2C12 myocyte EVs and NIH-3T3 EVs

387 species-specific proteins were identified from cellular EVs. Overall, 220 proteins were identified in myocyte EVs, and 299 proteins were detected in NIH-3T3 EVs. Of these, 132 proteins were overlapping while 88 proteins were specific to C2C12 myocyte EVs and 167 proteins were specific to NIH-3T3 EVs.

Table 2: Table of Proteins showing proteins present or absent in C2C12 myocytes and NIH-3T3 Extracellular Vesicles identified by liquid chromatography with tandem mass spectrometry (LC-MS/MS) analysis. Proteins present assigned (+), proteins absent assigned (-).

No.	Protein Name	Myocyte EVs	NIH-3T3 EVs
1	14-3-3 protein epsilon	+	+
2	14-3-3 protein gamma	+	+
3	14-3-3 protein theta (Fragment)	-	+
4	14-3-3 protein zeta/delta	+	+
5	26S proteasome non-ATPase regulatory subunit 2	-	+
6	26S proteasome non-ATPase regulatory subunit 6	-	+
7	40S ribosomal protein S11	-	+
8	40S ribosomal protein S16	-	+
9	40S ribosomal protein S3	-	+
10	40S ribosomal protein S3a	-	+
11	40S ribosomal protein S4, X isoform	-	+
12	40S ribosomal protein S7	-	+
13	40S ribosomal protein S9	-	+
14	40S ribosomal protein SA	-	+
15	60S acidic ribosomal protein P0	-	+
16	60S ribosomal protein L12	-	+
17	6-phosphogluconate dehydrogenase, decarboxylating	-	+
18	72 kDa type IV collagenase	+	+
19	Acetyl-CoA acetyltransferase, cytosolic	-	+
20	Actin, alpha skeletal muscle	+	+
21	Actin, cytoplasmic 1	+	+
22	Actin-related protein 2	-	+
23	Actin-related protein 2/3 complex subunit 4	-	+
24	Actin-related protein 3	-	+
25	Adenosylhomocysteinase	-	+
26	Adenylosuccinate synthetase isozyme 2	-	+
27	Adipocyte enhancer-binding protein 1	+	+
28	ADP-ribosylation factor 1	+	-
29	AHNAK nucleoprotein (desmoyokin)	+	-
30	Alanine--tRNA ligase, cytoplasmic	-	+
31	Alcohol dehydrogenase [NADP(+)]	-	+
32	Aldehyde dehydrogenase family 3 member B1	+	-
33	Aldose reductase	+	+
34	Alpha-actinin-1	+	+
35	Alpha-actinin-3	+	-
36	Alpha-actinin-4	+	+
37	Alpha-crystallin B chain	+	-
38	Alpha-enolase	+	+
39	Alpha-N-acetylglucosaminidase	+	-
40	Aminopeptidase N	+	-
41	Amyloid-beta A4 protein	+	-
42	Annexin A1	+	+
43	Annexin A2	+	+
44	Annexin A3	+	-
45	Annexin A5	+	+
46	Annexin A6	+	+
47	Annexin A7	+	-

48	Arginine--tRNA ligase, cytoplasmic	-	+
49	Asparagine synthetase [glutamine- hydrolyzing]	-	+
50	Asparagine--tRNA ligase, cytoplasmic	-	+
51	Aspartate aminotransferase, cytoplasmic	+	+
52	Aspartate aminotransferase, mitochondrial	+	-
53	Aspartate--tRNA ligase, cytoplasmic	-	+
54	ATP-citrate synthase	-	+
55	ATP-dependent RNA helicase A	-	+
56	Basement membrane-specific heparan sulphate proteoglycan core protein	+	+
57	Basigin	+	-
58	Beta-enolase	+	+
59	Beta-hexosaminidase subunit beta	+	-
60	Bifunctional glutamate/proline--tRNA ligase	-	+
61	Bifunctional purine biosynthesis protein PURH	-	+
62	Biglycan	+	+
63	Bin1 protein	+	-
64	Bone morphogenetic protein 1	+	+
65	Cadherin-15	+	-
66	Calpain-6	-	+
67	Calreticulin	+	+
68	Calsequestrin-2	+	+
69	Calsyntenin-1	+	+
70	Calumenin	+	-
71	Carboxypeptidase	+	-
72	Carboxypeptidase Q	+	-
73	Cartilage intermediate layer protein 1	+	-
74	Cathepsin B	+	+
75	Cathepsin D	+	+
76	Cathepsin L1	+	+
77	Cathepsin Z	+	-
78	CD151 antigen	+	-
79	CD81 antigen	+	-
80	CD82 antigen	+	+
81	Ceruloplasmin	-	+
82	Chloride intracellular channel protein 1	-	+
83	Clathrin heavy chain 1	+	+
84	Coatomer subunit alpha	-	+
85	Coatomer subunit beta	-	+
86	Coatomer subunit beta'	-	+
87	Cofilin-1	+	+
88	Cofilin-2	+	-
89	Coiled-coil domain-containing protein 80	+	-
90	Collagen alpha-1(I) chain	+	+
91	Collagen alpha-1(III) chain	+	+
92	Collagen alpha-1(V) chain	+	+
93	Collagen alpha-1(VI) chain	+	+
94	Collagen alpha-1(XII) chain	+	+
95	Collagen alpha-2(I) chain	+	+
96	Collagen alpha-2(IV) chain	-	+
97	Collagen alpha-2(V) chain	+	+
98	Collagen alpha-2(VI) chain	+	+
99	Collagen, type VI, alpha 3	+	+
100	Complement C1r-A subcomponent	+	-
101	Complement C1s-A subcomponent	+	-
102	Complement factor H	+	+
103	Copine-2	+	-

104	Creatine kinase B-type	+	-
105	Cullin-associated NEDD8-dissociated protein 1	-	+
106	Cystatin-C	+	+
107	Cytoplasmic dynein 1 heavy chain 1	-	+
108	Cytoplasmic dynein 1 intermediate chain 2	-	+
109	D-3-phosphoglycerate dehydrogenase	-	+
110	DEAD (Asp-Glu-Ala-Asp) box polypeptide 17, isoform CRA	-	+
111	Decorin	+	+
112	Desmin	+	-
113	Desmoplakin	+	+
114	Dihydropyrimidinase-related protein 2	-	+
115	DNA damage-binding protein 1	-	+
116	DNA replication licensing factor MCM2	-	+
117	DNA-(apurinic or apyrimidinic site) lyase	-	+
118	Dystroglycan	+	-
119	Ectonucleotide pyrophosphatase	+	-
120	EGF-containing fibulin-like extracellular matrix protein 2	-	+
121	EH domain-containing protein 1	+	+
122	EH domain-containing protein 4	+	+
123	Elongation factor 1-alpha 1	+	+
124	Elongation factor 1-delta	-	+
125	Elongation factor 1-gamma	-	+
126	Elongation factor 2	+	+
127	EMILIN-1	-	+
128	Endoplasmic reticulum chaperone BiP	+	+
129	Endoplasmin	+	+
130	Erythrocyte band 7 integral membrane protein	+	-
131	Eukaryotic initiation factor 4A-I	+	+
132	Eukaryotic peptide chain release factor subunit 1	-	+
133	Eukaryotic translation initiation factor 2 subunit 1	-	+
134	Eukaryotic translation initiation factor 2 subunit 3, X-linked	-	+
135	Eukaryotic translation initiation factor 3 subunit A	-	+
136	Eukaryotic translation initiation factor 3 subunit C	-	+
137	Eukaryotic translation initiation factor 3 subunit E	-	+
138	Eukaryotic translation initiation factor 3 subunit I	-	+
139	Eukaryotic translation initiation factor 3 subunit L	-	+
140	Eukaryotic translation initiation factor 5A (Fragment)	-	+
141	Exportin-1	-	+
142	Exportin-2	-	+
143	Extracellular matrix protein 1	+	-
144	Extracellular superoxide dismutase [Cu-Zn]	+	-
145	F-actin-capping protein subunit alpha-1	-	+
146	Farnesyl pyrophosphate synthase	-	+
147	Fascin	-	+
148	Fatty acid synthase	-	+
149	Fatty acid-binding protein, epidermal	-	+
150	Fibrillin-1	+	+
151	Fibronectin	+	+
152	Fibronectin type III domain-containing 1	+	-
153	Fibulin-1	+	-
154	Fibulin-7	+	-
155	Filamin, alpha	-	+
156	Follistatin-related protein 1	+	+
157	Fructose-bisphosphate aldolase A	+	+
158	Galectin-1	+	+
159	Galectin-3	+	-

160	Galectin-3-binding protein	+	+
161	Glucose-6-phosphate isomerase	+	+
162	Glutaredoxin-3	-	+
163	Glutathione S-transferase P 1	-	+
164	Glyceraldehyde-3-phosphate dehydrogenase	+	+
165	Glycine--tRNA ligase	-	+
166	Glypican-1	+	+
167	GMP synthase [glutamine-hydrolyzing]	-	+
168	Granulins	+	-
169	GTP-binding nuclear protein Ran	-	+
170	Guanine nucleotide-binding protein G(i) subunit alpha-2	+	+
171	Guanine nucleotide-binding protein G(I)/G(S)/G(T) subunit beta-2	+	+
172	Heat shock 70 kDa protein 4	+	+
173	Heat shock cognate 71 kDa protein	+	+
174	Heat shock protein HSP 90-alpha	+	+
175	Heat shock protein HSP 90-beta	+	+
176	Hepatoma-derived growth factor	-	+
177	Heterogeneous nuclear ribonucleoprotein A/B	-	+
178	Heterogeneous nuclear ribonucleoprotein A1	-	+
179	Heterogeneous nuclear ribonucleoprotein A3	-	+
180	Heterogeneous nuclear ribonucleoprotein K (Fragment)	-	+
181	Heterogeneous nuclear ribonucleoprotein L (Fragment)	-	+
182	Heterogeneous nuclear ribonucleoprotein R	-	+
183	Heterogeneous nuclear ribonucleoproteins A2/B1	+	+
184	High mobility group protein B1	-	+
185	Histone H1.2	-	+
186	Histone H2B type 1-B	-	+
187	Histone H4	+	+
188	Histone-binding protein RBBP7	-	+
189	Hsc70-interacting protein	+	+
190	Immunoglobulin superfamily member 8	+	+
191	Importin subunit beta-1	-	+
192	Importin-7	-	+
193	Insulin-like growth factor-binding protein 5	+	+
194	Insulin-like growth factor-binding protein 6	+	-
195	Integral membrane protein 2B	+	-
196	Integrin beta-1	+	-
197	Inter-alpha trypsin inhibitor, heavy chain 2	-	+
198	Isocitrate dehydrogenase [NADP] cytoplasmic	-	+
199	Isoform 2 of 4F2 cell-surface antigen heavy chain	+	-
200	Isoform 2 of Choline transporter-like protein 2	+	-
201	Isoform 2 of Fibulin-2	+	+
202	Isoform 2 of Filamin-C	+	+
203	Isoform 2 of Gelsolin	+	+
204	Isoform 2 of Heterogeneous nuclear ribonucleoprotein U	-	+
205	Isoform 2 of Lactadherin	+	+
206	Isoform 2 of Mannan-binding lectin serine protease 1	+	-
207	Isoform 2 of Nestin	+	-
208	Isoform 2 of Periostin	+	+
209	Isoform 2 of Spectrin alpha chain, non-erythrocytic 1	-	+
210	Isoform 2 of Sulfhydryl oxidase 1	+	+
211	Isoform 2 of Tenascin	+	+
212	Isoform 2 of Transcription intermediary factor 1-beta	-	+
213	Isoform 2 of Tripartite motif-containing protein 47	+	-
214	Isoform 2 of Tropomyosin alpha-3 chain	-	+
215	Isoform 2 of Unconventional myosin-Ic	+	-

216	Isoform 2 of V-type proton ATPase catalytic subunit A	-	+
217	Isoform 3 of Heterogeneous nuclear ribonucleoprotein D0	-	+
218	Isoform Alpha-7X2A of Integrin alpha-7	+	-
219	Isoform C1 of Heterogeneous nuclear ribonucleoproteins C1/C2	-	+
220	Isoform PLEC-1D of Plectin	+	+
221	Isoleucine--tRNA ligase, cytoplasmic	-	+
222	Junction plakoglobin	+	+
223	Kelch-like protein 41	+	-
224	Keratin, type I cytoskeletal 14	+	+
225	Keratin, type I cytoskeletal 16	+	+
226	Keratin, type I cytoskeletal 17	+	+
227	Keratin, type II cytoskeletal 5	+	+
228	Keratin, type II cytoskeletal 6A	+	+
229	Lactoylglutathione lyase	+	-
230	Laminin subunit beta-1	-	+
231	Laminin subunit gamma-1	-	+
232	Leucine--tRNA ligase, cytoplasmic	-	+
233	Leukocyte elastase inhibitor A	+	-
234	Leukotriene A-4 hydrolase	-	+
235	L-lactate dehydrogenase	+	+
236	Low density lipoprotein receptor-related protein 1	+	-
237	Lysine--tRNA ligase	-	+
238	Lysyl oxidase homolog 1	+	+
239	Major vault protein	+	+
240	Malate dehydrogenase, cytoplasmic	+	+
241	Malate dehydrogenase, mitochondrial	+	+
242	Matrilin-2	+	-
243	MCG116562, isoform CRA_a	+	+
244	MCG116671	-	+
245	MCG23377, isoform CRA_b	+	-
246	Mesothelin	+	+
247	Metalloproteinase inhibitor 1	+	-
248	Metalloproteinase inhibitor 2	+	-
249	Mimecan	+	-
250	Mitotic checkpoint protein BUB3	-	+
251	Moesin	+	+
252	Monocarboxylate transporter 1	+	-
253	Multifunctional protein ADE2	-	+
254	Myoferlin	+	-
255	Myosin-1	+	-
256	Myosin-3	+	+
257	Myosin-9	+	+
258	Neural cell adhesion molecule 1	+	+
259	Neutral alpha-glucosidase AB	-	+
260	Nidogen-1	-	+
261	Nidogen-2	+	-
262	Non-POU domain-containing octamer-binding protein	-	+
263	Nuclease-sensitive element-binding protein 1	-	+
264	Nucleobindin-1	+	+
265	Nucleolin	+	+
266	Nucleophosmin	-	+
267	Nucleoside diphosphate kinase	+	+
268	Olfactomedin-like protein 3	+	+
269	Peptidyl-glycine alpha-amidating monooxygenase	+	-
270	Peptidyl-prolyl cis-trans isomerase A	+	+

271	Peptidyl-prolyl cis-trans isomerase B	-	+
272	Peptidyl-prolyl cis-trans isomerase FKBP4	-	+
273	Peroxidasin homolog	+	+
274	Peroxiredoxin-1	+	+
275	Peroxiredoxin-2	-	+
276	Phenylalanine--tRNA ligase alpha subunit	-	+
277	Phenylalanine--tRNA ligase beta subunit	-	+
278	Phosphatidylethanolamine-binding protein 1	-	+
279	Phosphoglucomutase-1	+	-
280	Phosphoglycerate kinase 1	+	+
281	Phosphoglycerate mutase 1	+	+
282	Phospholipid transfer protein	+	-
283	Phosphoserine aminotransferase	+	+
284	Pigment epithelium-derived factor	+	+
285	Plasma membrane calcium-transporting ATPase 1	+	-
286	Plastin-3 (Fragment)	+	-
287	Platelet-activating factor acetylhydrolase IB subunit alpha	-	+
288	Platelet-activating factor acetylhydrolase	-	+
289	Plexin-B2	+	-
290	Poly(rC)-binding protein 1	-	+
291	Polyadenylate-binding protein 1	-	+
292	Predicted pseudogene 5580	-	+
293	Prelamin-A/C	+	+
294	Pre-mRNA-processing factor 19	-	+
295	Pre-mRNA-splicing factor ATP-dependent RNA helicase DHX15	-	+
296	Probable ATP-dependent RNA helicase DDX5	-	+
297	Probable ATP-dependent RNA helicase DDX6	-	+
298	Procollagen C-endopeptidase enhancer 1	+	+
299	Procollagen-lysine,2-oxoglutarate 5-dioxygenase 1	+	+
300	Procollagen-lysine,2-oxoglutarate 5-dioxygenase 3	-	+
301	Profilin-1	+	+
302	Programmed cell death 6-interacting protein	+	+
303	Proliferating cell nuclear antigen	-	+
304	Proliferation-associated 2G4	-	+
305	Prolyl endopeptidase	+	+
306	Prosaposin	+	+
307	Prostaglandin F2 receptor negative regulator	+	+
308	Proteasome subunit alpha type-3	-	+
309	Proteasome subunit alpha type-6	-	+
310	Proteasome subunit alpha type-7	+	+
311	Proteasome subunit beta type-5	+	+
312	Protein arginine N-methyltransferase 1	-	+
313	Protein disulfide-isomerase A3	+	+
314	Protein disulfide-isomerase	+	+
315	Protein kinase C and casein kinase II substrate protein 3	+	-
316	Protein kinase C and casein kinase substrate in neurons protein 2	+	-
317	Protein NOV homolog	+	-
318	Protein RCC2	-	+
319	Protein SET (Fragment)	-	+
320	Puromycin-sensitive aminopeptidase	-	+
321	Pyruvate kinase PKM	+	+
322	Rab GDP dissociation inhibitor beta	+	+
323	RAB1A, member RAS oncogene family	+	-
324	RAS-related C3 botulinum substrate 1, isoform CRA_a	-	+
325	Ras-related protein Rab-7a	+	+

326	Ras-related protein R-Ras2	+	-
327	Receptor of activated protein C kinase 1	-	+
328	Reticulon-4	+	-
329	Rho GDP-dissociation inhibitor 1	+	+
330	Ribonuclease 4	+	-
331	Ribonuclease inhibitor	-	+
332	Ribosomal protein	-	+
333	RuvB-like 1	-	+
334	Sarcoplasmic/endoplasmic reticulum calcium ATPase 1	+	-
335	Septin-11	-	+
336	Septin-2	-	+
337	Septin-7	-	+
338	Serine (or cysteine) peptidase inhibitor, clade B, member 6a	+	+
339	Serine protease HTRA1	+	-
340	Serine/threonine-protein phosphatase 2A 65 kDa regulatory subunit A alpha isoform	-	+
341	Serine/threonine-protein phosphatase 2A catalytic subunit alpha isoform	-	+
342	Serine/threonine-protein phosphatase PP1-alpha catalytic subunit	-	+
343	Serine-threonine kinase receptor-associated protein	-	+
344	Serine--tRNA ligase, cytoplasmic	-	+
345	Serpin H1	-	+
346	Sodium/potassium-transporting ATPase subunit alpha-1	+	-
347	Sodium/potassium-transporting ATPase subunit alpha-2	+	-
348	SPARC	+	+
349	Spectrin beta chain, non-erythrocytic 1	-	+
350	Spliceosome RNA helicase Ddx39b	-	+
351	Splicing factor 3B subunit 1	-	+
352	Spondin-2	+	-
353	Staphylococcal nuclease domain-containing protein 1	-	+
354	Stress-induced-phosphoprotein 1	-	+
355	SUMO-activating enzyme subunit 2	-	+
356	Synaptic vesicle membrane protein VAT-1 homolog	+	-
357	Talin-1	+	+
358	T-complex protein 1 subunit alpha	-	+
359	T-complex protein 1 subunit beta	-	+
360	T-complex protein 1 subunit delta	-	+
361	T-complex protein 1 subunit epsilon	-	+
362	T-complex protein 1 subunit eta	-	+
363	T-complex protein 1 subunit gamma	-	+
364	T-complex protein 1 subunit theta	-	+
365	T-complex protein 1 subunit zeta	-	+
366	Thrombospondin-1	+	+
367	Thrombospondin-2	+	-
368	Transaldolase	+	-
369	Transferrin receptor protein 1	+	-
370	Transgelin-2	-	+
371	Transitional endoplasmic reticulum ATPase	+	+
372	Transketolase	-	+
373	Translationally-controlled tumour protein	+	+
374	Triosephosphate isomerase	+	+
375	Tropomyosin beta chain	+	-
376	Tubulin alpha-1A chain	+	+
377	Tubulin beta-5 chain	+	+
378	Tubulin beta-6 chain	-	+
379	Tumour susceptibility gene 101 protein	+	-

380	Tyrosine-protein kinase Fyn	+	-
381	Ubiquitin-like modifier-activating enzyme 1	-	+
382	Vacuolar protein sorting-associated protein 35	-	+
383	Valine--tRNA ligase	-	+
384	Vimentin	+	+
385	Vinculin	+	+
386	Voltage-dependent calcium channel subunit alpha-2/delta-1	+	-
387	WD repeat-containing protein 1	-	+

~~4.2.2~~6.2.2 Protein-protein Interaction Network Identification of Proteins Detected in C2C12 Myotube and NIH-3T3 EVs

Proteins and their functional interactions are the key to many cellular processes. Therefore, identifying the protein network connectivity is pivotal in understanding many biological phenomena in cells. As mentioned above, the STRING database was used to analyse the protein-protein interactions in EVs. The STRING database aims to collect, score, and integrate all publicly available sources of protein–protein interaction information, and to complement these with computational predictions.

To identify the protein-protein interactions network of the proteins derived from both myocytes and fibroblast EVs, the data represented in **Table 2** was submitted to STRING analysis (https://string-db.org/). These interactions are based on known and predicted interactions. Proteins identified in C2C12 myocyte EV interactions are shown in **Figure 27 and 28** and protein interactions of NIH-3T3 EVs are presented in (**Figure 29**). Enrichment *p*-values for most of the protein-protein interaction (PPI) of C2C12 myocyte derived EVs, were found to be $p < 1.0 \times 10^{-16}$. However, some PPI enrichment values were found to be $p < 1.27 \times 10^{-5}$. This meant that proteins presented have more interactions among themselves than what would be expected for a random set of proteins of similar size, drawn from the genome. Such an enrichment indicates that the proteins are (at least partially) biologically connected, as a group.

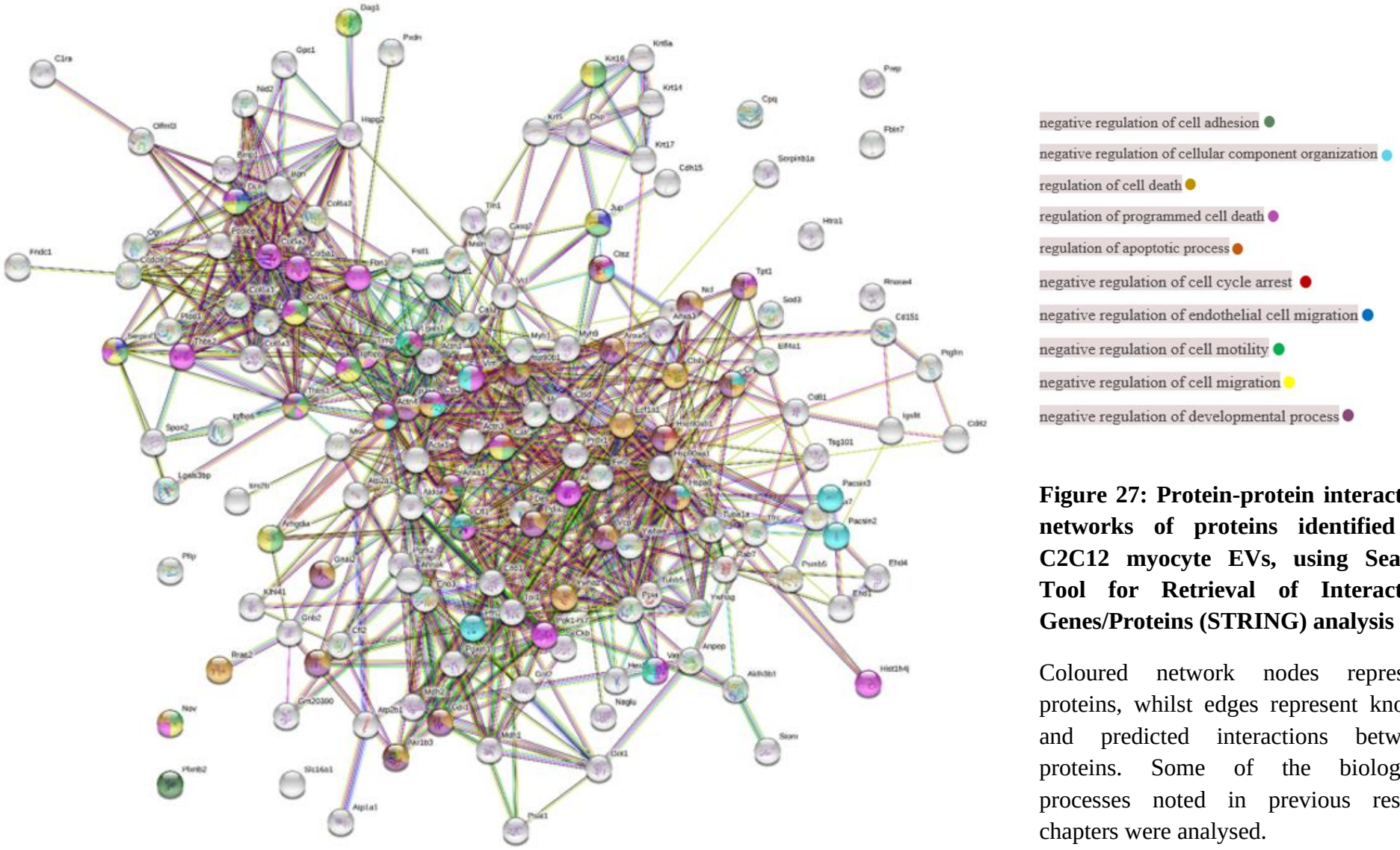

Figure 27: Protein-protein interaction networks of proteins identified in C2C12 myocyte EVs, using Search Tool for Retrieval of Interacting Genes/Proteins (STRING) analysis

Coloured network nodes represent proteins, whilst edges represent known and predicted interactions between proteins. Some of the biological processes noted in previous results chapters were analysed.

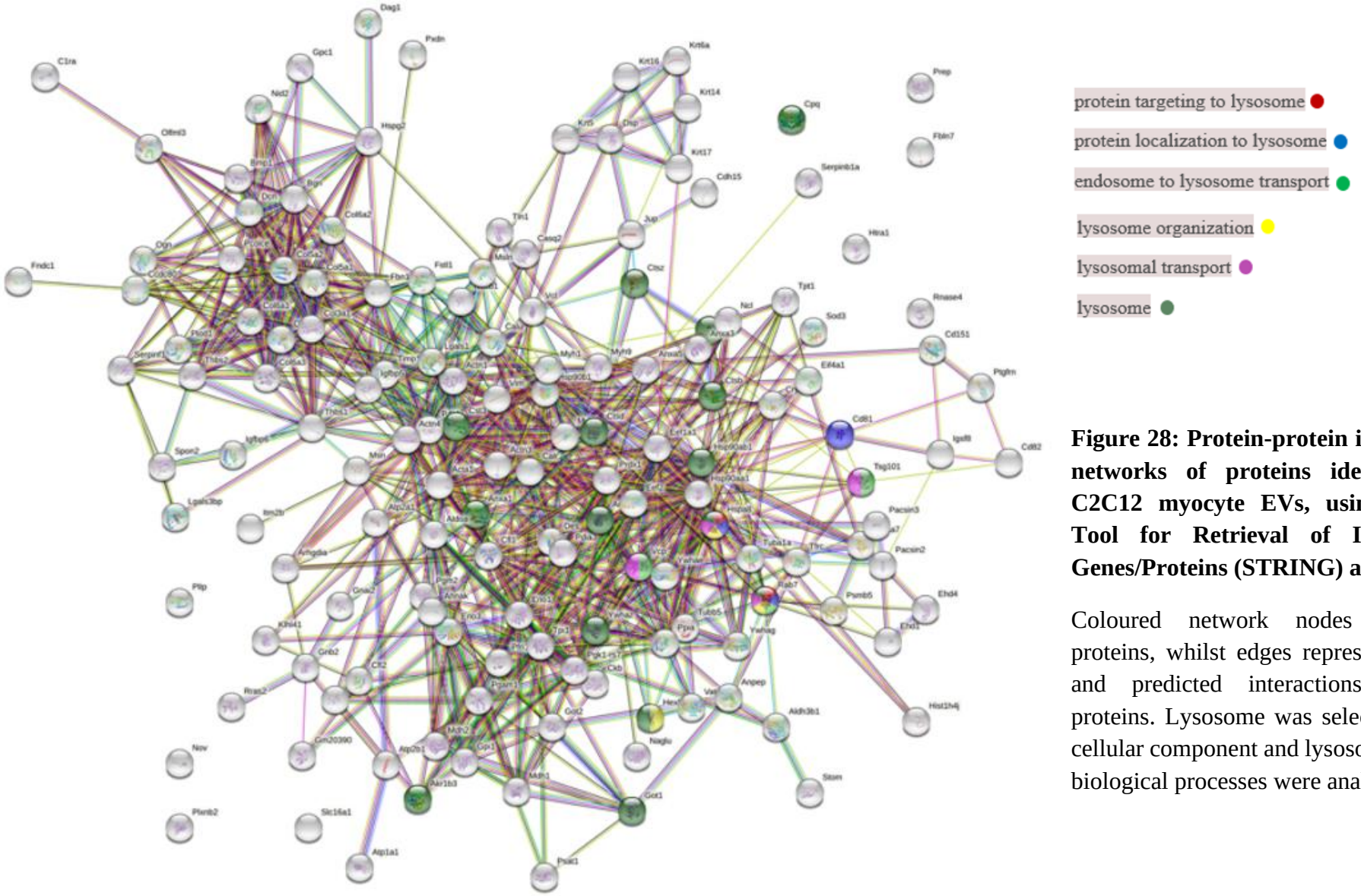

Figure 28: Protein-protein interaction networks of proteins identified in C2C12 myocyte EVs, using Search Tool for Retrieval of Interacting Genes/Proteins (STRING) analysis

Coloured network nodes represent proteins, whilst edges represent known and predicted interactions between proteins. Lysosome was selected as the cellular component and lysosome related biological processes were analysed.

A total of 220 myocyte proteins were submitted to the analysis, but only 149 proteins were identified by the database. Initially therefore, the biological processes of those proteins were determined. Gene Ontology (GO) analysis of the 149 proteins revealed many biological functional roles; processes such as glutamate catabolic processes, telomerase holoenzyme complex assembly, positive regulation of protein folding, and aspartate catabolic processes and their strength were all significant. Furthermore, many negative regulations of biological processes were also observed in the analysis. From these negatively regulated processes, 10 terms were selected for further analysis (**Figure 27**). The strength of some of the negative biological processes, such as cell cycle arrest, cell migration and cell adhesion were significantly high compared to a random protein network of similar size.

In order to identify the proteins related to particular cellular components, GO analysis of cellular components was selected. Many cellular component related proteins were observed and interestingly, lysosome related protein enrichment was significant, with a False Discovery Rate, FDR, *p* value of 2.3×10^{-6}. Therefore, GO analysis of lysosome related biological pathways were selected for further analysis (**Figure 28**). Among chosen biological pathways, lysosome organisation proteins and lysosomal transport protein strength were significant. A total of 15 different lysosome related proteins were detected and Beta-hexosaminidase subunit beta, Tumour susceptibility gene 101 protein (TSG101), caspase family proteins and Ras-related protein Rab-7a were to name but a few.

To confirm that myocyte EV protein interactions were different from fibroblast EV proteins, a total of 299 fibroblast EV proteins were submitted for GO analysis (**Figure 29**). Only 207 proteins were identified by the database. Few biological functional processes similar to myocyte proteins were identified including, negative regulation of cell adhesion, cell

migration, development process and endothelial cell migration. However, biological processes such as negative regulation of cell cycle arrest and negative regulation of cellular compartment organisation related protein interactions were not observed in fibroblast EVs. Moreover, lysosomal related proteins were also present in fibroblast EVs. However, only the lysosomal transport biological pathway was significant.

In summary, it was observed at this point that fibroblast EVs contain more proteins than myocyte EVs, but however, that myocyte EVs contained increased number of proteins that negatively regulate cellular processes including, processes suppressing carcinoma cell progression. Furthermore, myocyte EVs contained more lysosomal biological process protein interactions compared to fibroblast EVs.

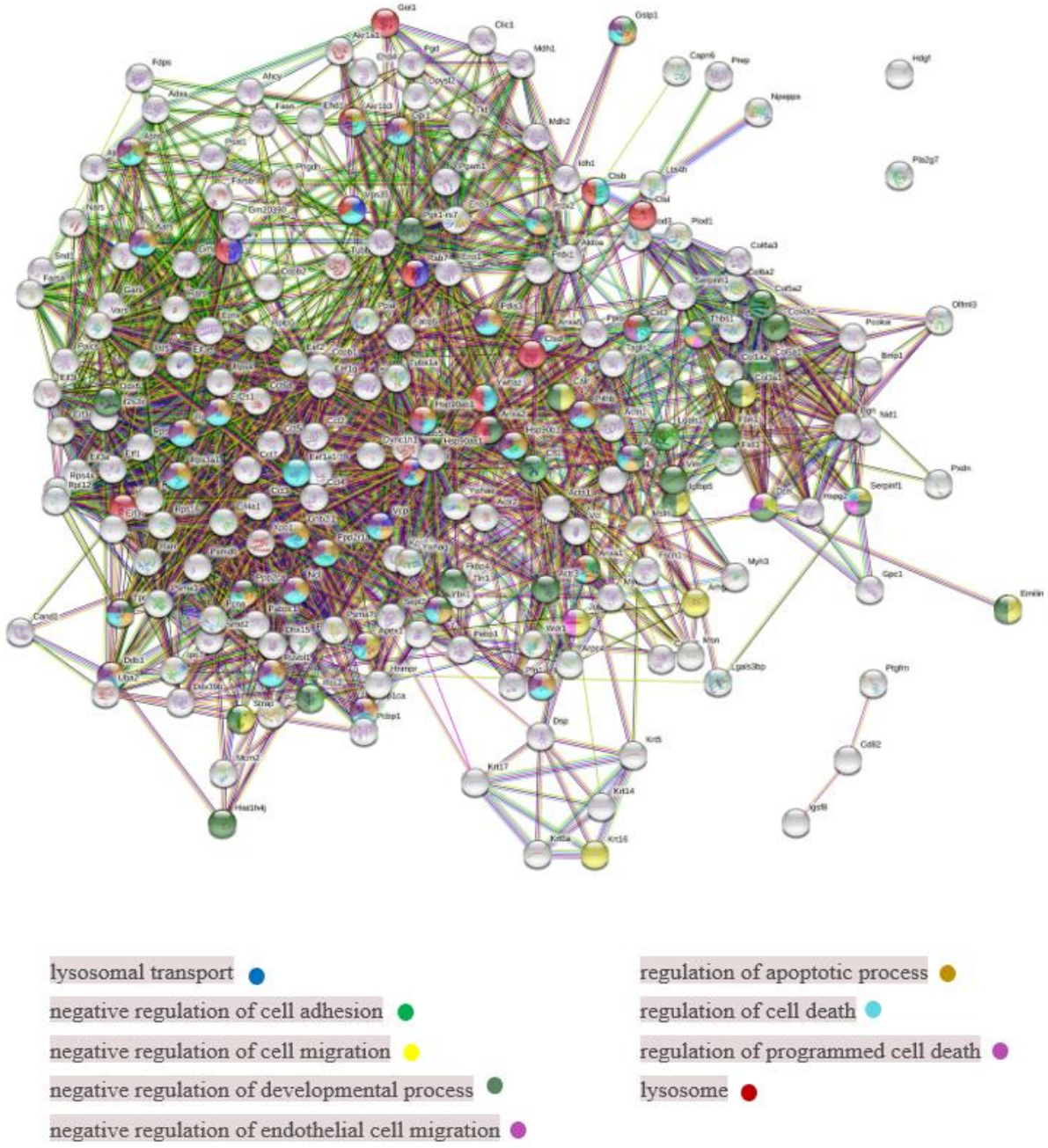

Figure 29: Protein-protein interaction networks of proteins identified in NIH-3T3 fibroblast EVs, using Search Tool for Retrieval of Interacting Genes/Proteins (STRING) analysis

Coloured network nodes represent proteins, whilst edges represent known and predicted interactions between proteins. Lysosome was selected as the cellular component and biological processes analysed in **Figure 27** were selected for comparison.

~~4.2.3~~6.2.3 Negative Regulations of Biological Processes Exerted by Myocyte Derived EV Proteins

The GO analysis on both myocyte and NIH-3T3 EVs helped to identify protein-protein interactions in biological processes. Moreover, it was helpful when identifying proteins related to cellular components, such as lysosomal proteins. It was noted that myocyte derived EVs had many negative biological processes related proteins compared to NIH-3T3 derived EVs. Interestingly, most of these negatively regulated biological processes coincided with the experimental data discussed in previous results chapters.

Having established that myocyte derived EV proteins induced apoptosis and growth suppression in carcinoma cells, further protein analysis was conducted on myocyte EV specific proteins. As showed in **Figure 26**, 88 myocyte EV specific proteins were identified. Those proteins were separately listed in (**Table 3**). Each identified protein was sequenced through UniProt (http://www.uniprot.org) to obtain UniProt name, correct protein accession number and Gene symbol. Furthermore, proteins that were common in both cell types but significantly high in myocyte EVs were also analysed. Built-in t-test statistical analysis was performed to identify those proteins and *p*-values ($p < 0.05$) were considered significant. From 132 common proteins, 19 proteins were identified as significantly high in myocyte derived EVs and listed in (**Table 4**).

Table 3: List of proteins specific to C2C12 myocyte EVs

UniProt Accession	UniProt Name	Status	Protein Name (88/387)	Gene Symbol
A0A0A6YW67	A0A0A6YW67_MOUSE	unreviewed	MCG23377, Predicted pseudogene 8797	Gm8797
Q61508	ECM1_MOUSE	reviewed	Extracellular matrix protein 1	Ecm1
P10852	4F2_MOUSE	reviewed	4F2 cell-surface antigen heavy chain	Slc3a2
Q61738	ITA7_MOUSE	reviewed	**Integrin alpha 7**	Itga7
Q62000	MIME_MOUSE	reviewed	Mimecan	Ogn
A0A0R4J0F8	A0A0R4J0F8_MOUSE	unreviewed	Cartilage intermediate layer protein 1	Cilp
P28798	GRN_MOUSE	reviewed	Progranulin	Grn
O88322	NID2_MOUSE	reviewed	Nidogen-2	Nid2
O35639	ANXA3_MOUSE	reviewed	Annexin A3	Anxa3 (Anx3)
Q08879	FBLN1_MOUSE	reviewed	Fibulin-1	Fbln1
P09055	ITB1_MOUSE	reviewed	**Integrin beta-1**	Itgb1
Q9R118	HTRA1_MOUSE	reviewed	Serine protease HTRA1	Htra1
P31001	DESM_MOUSE	reviewed	**Desmin**	Des
G3X8T3	G3X8T3_MOUSE	unreviewed	Carboxypeptidase	Ctsa
Q64299	CCN3_MOUSE	reviewed	CCN family member 3	Ccn3
P25785	TIMP2_MOUSE	reviewed	Metalloproteinase inhibitor 2	Timp2 (Timp-2)
Q8VDN2	AT1A1_MOUSE	reviewed	Sodium/potassium-transporting ATPase subunit alpha-1	Atp1a1

A0A286YDF5	A0A286YDF5_MOUSE	unreviewed	Myoferlin	Myof
Q3TWF3	Q3TWF3_MOUSE	unreviewed	Amyloid-beta A4 protein	App
Q03350	TSP2_MOUSE	reviewed	**Thrombospondin-2**	Thbs2 (Tsp2)
P84078	ARF1_MOUSE	reviewed	ADP-ribosylation factor 1	Arf1
A0A0R4J0I9	A0A0R4J0I9_MOUSE	unreviewed	Prolow-density lipoprotein receptor-related protein 1	Lrp1
P97449	AMPN_MOUSE	reviewed	Aminopeptidase N	Anpep
Q8CG14	CS1A_MOUSE	reviewed	Complement C1s-A subcomponent	C1sa (C1s)
E9Q616	E9Q616_MOUSE	reviewed	AHNAK nucleoprotein	Ahnak
Q9WTI7	MYO1C_MOUSE	reviewed	Unconventional myosin-Ic	Myo1c
A0A0A0MQM7	A0A0A0MQM7_MOUSE	unreviewed	Matrilin-2	Matn2
P53986	MOT1_MOUSE	reviewed	Monocarboxylate transporter 1	Slc16a1
Q9CPU0	LGUL_MOUSE	reviewed	Lactoylglutathione lyase	Glo1
Q501P1	FBLN7_MOUSE	reviewed	Fibulin-7	Fbln7
A2AUC9	KLH41_MOUSE	reviewed	Kelch-like protein 41	Klhl41
P62821	RAB1A_MOUSE	reviewed	Ras-related protein	Rab1A (Rab1)
Q8BMS2	SPON2_MOUSE	reviewed	Spondin-2	Spon2
A0A1B0GR11_MOUSE	A0A1B0GR11_MOUSE	unreviewed	Transaldolase	Taldo1
P55065	PLTP_MOUSE	reviewed	Phospholipid transfer protein	Pltp
Q99P72	RTN4_MOUSE	reviewed	Reticulon-4	Rtn4
P58774	TPM2_MOUSE	reviewed	Tropomyosin beta chain	Tpm2
P33146	CAD15_MOUSE	reviewed	Cadherin-15	Cdh15

Q8R2G6	CCD80_MOUSE	reviewed	Coiled-coil domain-containing protein 80	Ccdc80
A0A0R4J1D0	A0A0R4J1D0_MOUSE	unreviewed	Copine-2	Cpne2
O09164	SODE_MOUSE	reviewed	Extracellular superoxide dismutase	Sod3
P35762	CD81_MOUSE	reviewed	CD81 antigen	Cd81 **(**Tapa1)
G5E829	AT2B1_MOUSE	reviewed	Plasma membrane calcium-transporting ATPase 1	Atp2b1
Q62465	VAT1_MOUSE	reviewed	**Synaptic vesicle membrane protein VAT-1 homolog**	Vat1 (Vat-1)
G3UXY9	G3UXY9_MOUSE	unreviewed	Ectonucleotide pyrophosphatase	Enpp2
Q99K51	PLST_MOUSE	reviewed	Plastin-3	Pls3
Q9WUU7	CATZ_MOUSE	reviewed	**Cathepsin Z**	Ctsz
Q9D154	ILEUA_MOUSE	reviewed	Leukocyte elastase inhibitor A	Serpinb1a
P12032	TIMP1_MOUSE	reviewed	Metalloproteinase inhibitor 1	Timp1
P39688	FYN_MOUSE	reviewed	Tyrosine-protein kinase Fyn	Fyn
P16110	LEG3_MOUSE	reviewed	Galectin-3	Lgals3
Q6P1B9	Q6P1B9_MOUSE	unreviewed	Bin1 protein	Bin1
K3W4Q8	K3W4Q8_MOUSE	unreviewed	Basigin	Bsg
P84078/ P61205	ARF1_MOUSE/ ARF3_MOUSE	reviewed	**ADP-ribosylation factor 1**	Arf1/ Arf3
P97467	AMD_MOUSE	reviewed	Peptidyl-glycine alpha-amidating monooxygenase	Pam
Q9WVJ3	CBPQ_MOUSE	reviewed	Carboxypeptidase Q	Cpq
Q8CG16	C1RA_MOUSE	reviewed	Complement C1r-A subcomponent	C1ra (C1r)
Q62165	DAG1_MOUSE	reviewed	Dystroglycan	Dag1 (Dag-1)
P20060	HEXB_MOUSE	reviewed	Beta-hexosaminidase subunit beta	Hexb
E9Q043	E9Q043_MOUSE	unreviewed	Fibronectin type III domain-containing 1	Fndc1
O35887	CALU_MOUSE	reviewed	Calumenin	Calu
Q9D0F9	PGM1_MOUSE	reviewed	Phosphoglucomutase-1	Pgm1

O88325	O88325_MOUSE	unreviewed	Alpha-N-acetylglucosaminidase	Naglu
Q5SX40	MYH1_MOUSE	reviewed	Myosin-1	Myh1
P62071	RRAS2_MOUSE	reviewed	**Ras-related protein R-Ras2**	Rras2
Q07076	ANXA7_MOUSE	reviewed	Annexin A7	Anxa7 (Anx7)
P98064	MASP1_MOUSE	reviewed	Isoform 2 of Mannan-binding lectin serine protease 1	Masp1
P05202	AATM_MOUSE	reviewed	Aspartate aminotransferase	Got2 (Got-2)
O89051	ITM2B_MOUSE	reviewed	Integral membrane protein 2B	Itm2b
Q61187	TS101_MOUSE	reviewed	Tumour susceptibility gene 101 protein	Tsg101
Q6PIE5	AT1A2_MOUSE	reviewed	Sodium/potassium-transporting ATPase subunit alpha-2	Atp1a2
Q8R429	AT2A1_MOUSE	reviewed	Sarcoplasmic/endoplasmic reticulum calcium ATPase 1	Atp2a1
P54116	STOM_MOUSE	reviewed	Erythrocyte band 7 integral membrane protein	Stom
Q9JJH1	RNAS4_MOUSE	reviewed	Ribonuclease 4	Rnase4
O35566	CD151_MOUSE	reviewed	CD151 antigen	Cd151
Q04447	KCRB_MOUSE	reviewed	Creatine kinase B-type	Ckb
O88990	ACTN3_MOUSE	reviewed	Alpha-actinin-3	Actn3
E9Q1X8	E9Q1X8_MOUSE	unreviewed	Voltage-dependent calcium channel subunit alpha-2/delta-1	Cacna2d1
Q99JB8	PACN3_MOUSE	reviewed	**Protein kinase C and casein kinase II substrate protein 3**	Pacsin3
B2RXS4	PLXB2_MOUSE	reviewed	**Plexin-B2**	Plxnb2
Q8C0E3	TRI47_MOUSE	reviewed	E3 ubiquitin-protein ligase TRIM47	Trim47
Q62351	TFR1_MOUSE	reviewed	Transferrin receptor protein 1	Tfrc
P45591	COF2_MOUSE	reviewed	Cofilin-2	Cfl2
P47880	IBP6_MOUSE	reviewed	Insulin-like growth factor-binding protein 6	Igfbp6
P23927	CRYAB_MOUSE	reviewed	Alpha-crystallin B chain	Cryab
Q80VQ0	AL3B1_MOUSE	reviewed	**Aldehyde dehydrogenase family 3 member B1**	Aldh3b1

Table 4: List of proteins common in both C2C12 myocytes and CMT 64/61 carcinoma cells but significantly high in myocyte derived EVs

No.	Protein Name	Accession Number	*P* value	Protein Function
1	Collagen alpha-1(XII) chain	E9PX70_MOUSE	0.006	Type XII collagen interacts with type I collagen-containing fibrils and could be associated with the surface of the fibrils.
2	Filamin-C	FLNC_MOUSE	0.036	Muscle-specific filamin, which plays a central role in normal myogenesis and for maintaining the structural integrity of the muscle fibres.
3	Moesin	MOES_MOUSE	0.021	Connects the actin cytoskeleton to the plasma membrane and helps to regulate many cellular processes, including cell shape determination, membrane transport, and signal transduction. Plays an important role in immunity acting on both T and B-cells homeostasis and self-tolerance.
4	Fibrillin-1	FBN1_MOUSE	0.0032	Provide long-term force bearing structural support. Also plays a key role in tissue homeostasis through specific interactions with growth factors, such as the bone morphogenetic proteins (BMPs), growth and differentiation factors (GDFs) and latent transforming growth factor-beta-binding proteins (LTBPs), cell-surface integrins and other extracellular matrix protein and proteoglycan components
5	Adipocyte enhancer-binding protein 1	AEBP1_MOUSE	0.013	Regulates collagen fibrillogenesis and possibly involved in the organization and remodelling of the extracellular matrix.
6	Complement factor H	CFAH_MOUSE	0.0099	Modulates complement activation and thereby maintain a well-balanced immune response.
7	Prostaglandin F2 receptor negative regulator	FPRP_MOUSE	0.023	In myoblasts, associates with tetraspanins CD9 and CD81 to prevent myotube fusion during muscle regeneration.
8	Biglycan	PGS1_MOUSE	0.035	Possibly involved in collagen fibre assembly.
9	Cathepsin B	CATB_MOUSE	0.0092	A myokine which has been associated with many functions in cancer including, initiation, growth/tumour cell proliferation, angiogenesis, invasion, and metastasis. However, over expression of cathepsin B is known to induce apoptosis in cancer cells.
10	SPARC	A0A1L1SSH9_MOUSE	0.011	Regulate cell growth through interactions with the extracellular matrix and cytokines. Binds calcium and copper and prevent and suppress cancer growth.
11	Cathepsin L1	CATL1_MOUSE	0.041	Important for the overall degradation of proteins in lysosomes. Cathepsin L1 cleaves proteoglycan protein perlecan, which inhibits the growth and invasiveness of cancer cells and angiogenesis.

12	Prosaposin	E9PZ00_MOUSE	0.022	Participate in the lysosomal degradation of sphingolipids, which takes place by the sequential action of specific hydrolases.
13	Endoplasmic reticulum chaperone BiP	BIP_MOUSE	0.0096	Plays a key role in protein folding and quality control in the endoplasmic reticulum lumen.
14	Serine (or cysteine) peptidase inhibitor	F8WIV2_MOUSE	0.02	Binds to and stops, prevents, or reduces the activity of serine-type endopeptidases, enzymes that catalyze the hydrolysis of nonterminal peptide bonds in a polypeptide chain.
15	EH domain-containing protein 1	EHD1_MOUSE	0.044	Plays a role in myoblast fusion.
16	Sulfhydryl oxidase 1	QSOX1_MOUSE	0.015	Plays a role in disulfide bond formation in a variety of extracellular proteins.
17	Neural cell adhesion molecule 1	A0A0A6YY47_MOUSE	0.0068	Involves in cell adhesion molecule involved in neuron-neuron adhesion, neurite fasciculation, outgrowth of neurites.
18	EH domain-containing protein 4	EHD4_MOUSE	0.04	Plays a role in early endosomal transport.
19	Decorin	PGS2_MOUSE	0.028	Works as a cancer suppressor by targeting key signalling molecules including, TGF-β and receptor tyrosine kinase which inhibit cancer cell growth, survival, metastasis, and angiogenesis. Moreover, over expression of decorin has induced apoptosis and cell cycle arrest.

To identify the PPI network of the proteins listed in both **Table 3 and 4** data was submitted to STRING analysis (https://string-db.org/). From 107 proteins, only 84 proteins were detected by the database. Go analysis of these proteins revealed numerous biological processes related proteins (**Figure 30**). Average local clustering coefficient was noted as 0.433 and PPI enrichment -value of this protein cluster was $< 1.0 \times 10^{-16}$. These results indicated that the proteins in this cluster were at least partially biologically connected, and they had more interactions among themselves than expected in a similar size protein cluster [268].

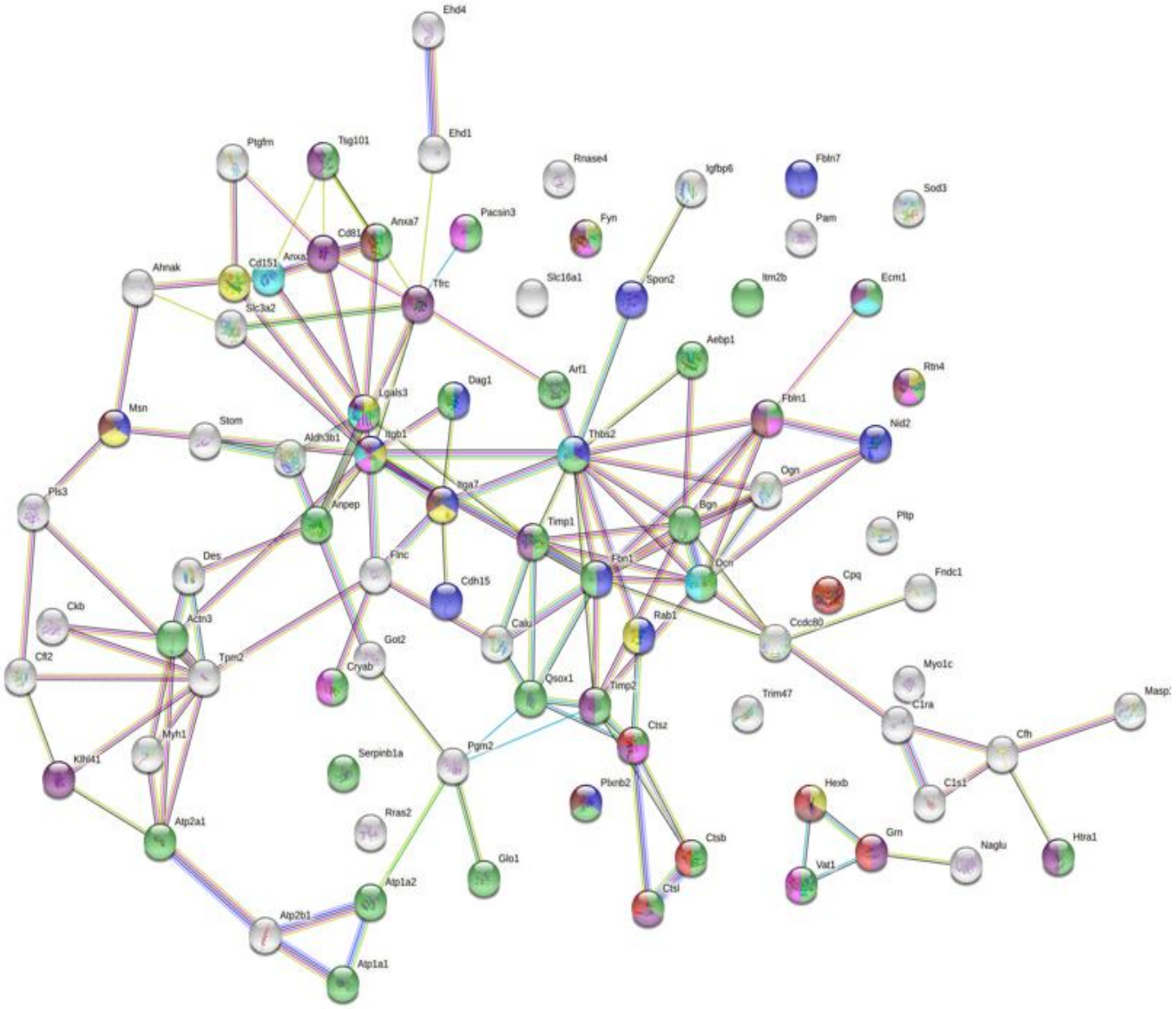

negative regulation of biological process
cell migration
negative regulation of cellular component organization
regulation of cell morphogenesis
regulation of angiogenesis
regulation of cell population proliferation
cell adhesion
lysosome

Figure 30: Protein-protein interaction networks of proteins specific to C2C12 myocyte EVs, using Search Tool for Retrieval of Interacting Genes/Proteins (STRING) analysis

Coloured network nodes represent proteins, whilst edges represent known and predicted interactions between proteins. Lysosome was selected as the cellular component and few other biological processes were analysed.

Indeed, most of the myocyte EVs proteins were cellular regulatory proteins. Interestingly, 34 out of 84 proteins (~40.47%) detected were responsible for negative regulations of biological processes. Those proteins were represented by a green node in (**Figure 30**). The few negatively regulated biological processes identified by the analysis were, cell communication, cellular component organisation, development processes and cell signalling. Furthermore, 6 myocyte specific lysosome related proteins were detected, including cathepsin L1, B, Z, Granulins, Beta-hexosaminidase subunit beta and Carboxypeptidase Q.

~~4.2.4~~6.2.4 KEGG Pathway analysis of upregulated myocyte EV proteins

Having confirmed that myocyte derived EVs contain proteins that negatively regulate cell migration, proliferation, adhesion, and morphogenesis, the biological pathways of upregulated proteins were analysed. Fold change by category for all myocyte EV proteins was calculated using the inbuilt Scaffold 4.11.1 statistical tool. As there were only two replicates, Fisher's Exact Test and multiple test correction (Benjamini-Hochberg correction) was selected. When calculating the fold change, fibroblast was used as the referenced category. Fold change *p*-values ≤ 0.05 were regarded as downregulated and fold changes *p*-values ≥ 2.0 were regarded as upregulated. The fold change cut-off points were automatically computed by the Scaffold software. From a total of 220 myocyte proteins, 29 proteins were upregulated and 13 were downregulated (**Figure 31**).

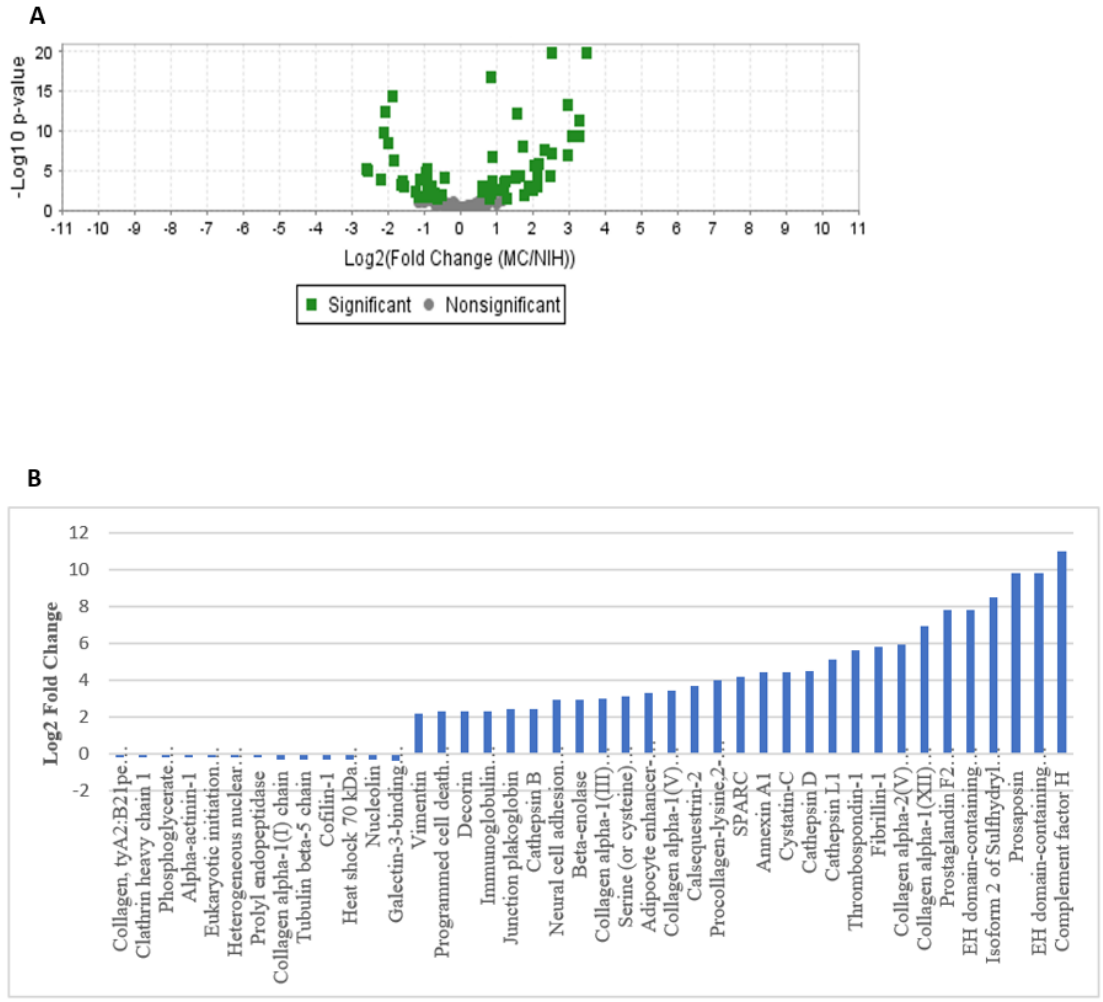

Figure 31: Differently expressed myocyte EVs proteins

A) Volcano plot representing myocyte EV proteins. Plotted significance versus fold change on the Y and X axes, respectively. Benjamini- Hochberg corrected *p*-value set as $p \leq 0.038$. Statistically significant proteins were represented by Green dots and nonsignificant proteins indicated by grey dots. Significant outliers were not represented. **B)** Upregulated and downregulated proteins in myocyte EVs were compared to fibroblast EVs. The fold change cut off points were automatically computed by the Scaffold software. Fold change *p*-values ≤ 0.05 were regarded as downregulated and fold changes with *p*-values ≥ 2.0 regarded as upregulated. Generally, proteins with positive fold change were regarded as upregulated and proteins with negative fold change considered to be down regulated.

To gain further insight into the whole chain of events caused by differently expressed proteins, upregulated proteins were selected for KEGG pathway analysis. KEGG (Kyoto Encyclopaedia of Genes and Genomes) (http://www.kegg.jp/) is a database resource for understanding high level roles and functions of the biological system such as cells, organisms, and the ecosystem at the molecular level[13]. KEGG pathway analysis through (https://string-db.org/) revealed 8 different pathways for selected proteins. These were the enriched pathways identified for upregulated proteins: (i) Antigen processing and presentation, (ii) Autophagy, (iii) Apoptosis, (iv) TGF beta signalling pathway, (v) phagosome, (vi) Protein digestion and absorption, (vii) Lysosomes and (viii) Proteoglycan in cancer. There were no pathways represented by more than 3 proteins; however, a significant enrichment was noted as the FDR values were $p \leq 0.05$. Furthermore, the average local clustering coefficient was 0.619 and the PPI enrichment $p< 1.0 \times 10^{-16}$ suggested that the proteins were at least partially biologically connected and had more interactions than expected.

Apoptosis, Lysosomes and Proteoglycan in cancer pathways were selected for further analysis (**Figure 32**). The strength value of Apoptosis pathway (mmu04210), Lysosome pathway (mmu04142) and Proteoglycan in cancer pathway (mmu05205) were 1.41, 1.45 and 1.24, respectively. The strength value determines how large the enrichment effect is and it is calculated by Log10 (observed proteins/expected proteins). Moreover, false discovery rate (FDR) for Apoptosis (mmu04210), Lysosome (mmu04142) and Proteoglycan in cancer (mmu05205) pathways *p*-values were found to be 0.0035, 0.0035 and 0.0055, respectively. FDR values below 0.05 suggested that selected pathways were significantly enriched. Furthermore, the line thickness between nodes indicated the confidence of the data between proteins (**Figure 32**). As showed in **Figure 32**, Cathepsin D, Cathepsin L1 and Cathepsin B proteins represented the Lysosome pathway. The same proteins were associated with the

Apoptosis pathway, whilst Decorin and Thrombospondin-1 included in Proteoglycans in cancer pathway.

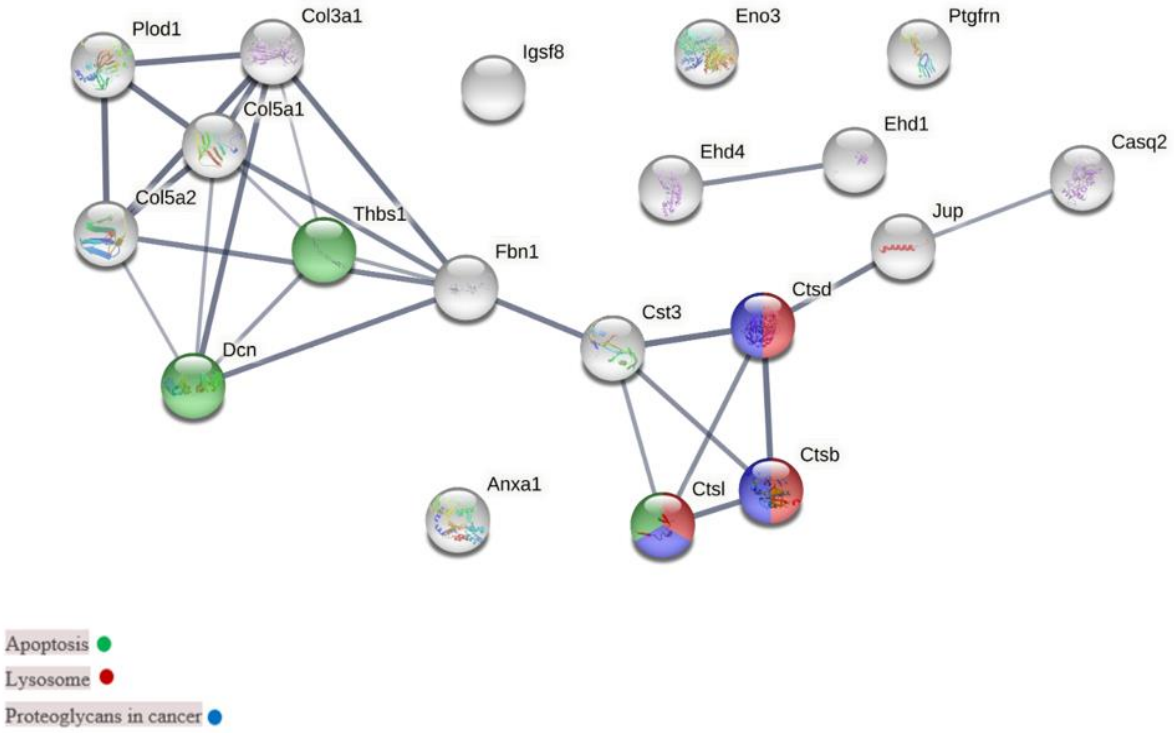

Figure 32: Kyoto Encyclopaedia of Genes and Genomes (KEGG) analysis of upregulated proteins

A few of the significantly enriched pathways were chosen. The colour coding for the pathway proteins represents their protein interactions within the network. Proteins with highest connection confidence were represented by thick lines.

~~4.2.4.1~~6.2.4.1 KEGG Analysis of Proteins Involved in Lysosomes Pathway

Lysosomes are membrane bounded organelles that function as the digestive system of cells. They contain an array of digestive proteins capable of degrading material taken up from outside of the cell and obsolete components of the cell itself. Substances requiring digestion are acquired by the lysosomes via many processes including, endocytosis, phagocytosis, and autophagy. Lysosomes contain nearly 50 different hydrolase proteins which are active at acidic pH (about 5).

Among the 8 different pathways obtained from KEGG analysis, the Lysosomes pathways was significantly enriched (FDR-0.0035). In order to visualise the protein interaction, it was mapped (**Figure 33**). Interestingly, lysosome acid hydrolase proteins including cathepsin L1, cathepsin B and cathepsin D were among the proteins that were significantly upregulated in myocyte EVs. Additionally, proteins that were specific to myocyte EVs such as alpha-N-acetylglucosaminidase (Naglu) and Beta-hexosaminidase subunit beta (Hexb) were also observed in the KEGG pathway.

Cathepsin B is a myokine which has been associated with many functions in cancer including, initiation, growth/tumour cell proliferation, angiogenesis, invasion, and metastasis [269]. However, over expression of cathepsin B is also known to induce apoptosis in cancer cells [270]. Furthermore, cytosolic cathepsin B, D and L are implicated in degradation of Bid, resulting in release of cytochrome c from mitochondria which induces intrinsic apoptosis [271]. Interestingly, a high confidence protein interaction between cathepsin B and cathepsin L were observed (**Figure 32**). Furthermore, data obtained earlier (**Figure 31B**) showed increased upregulation of cathepsin D and L in myocyte EVs. Based on these data, its suggests that

together these cathepsin proteins could induce carcinoma cell apoptosis via the intrinsic pathway.

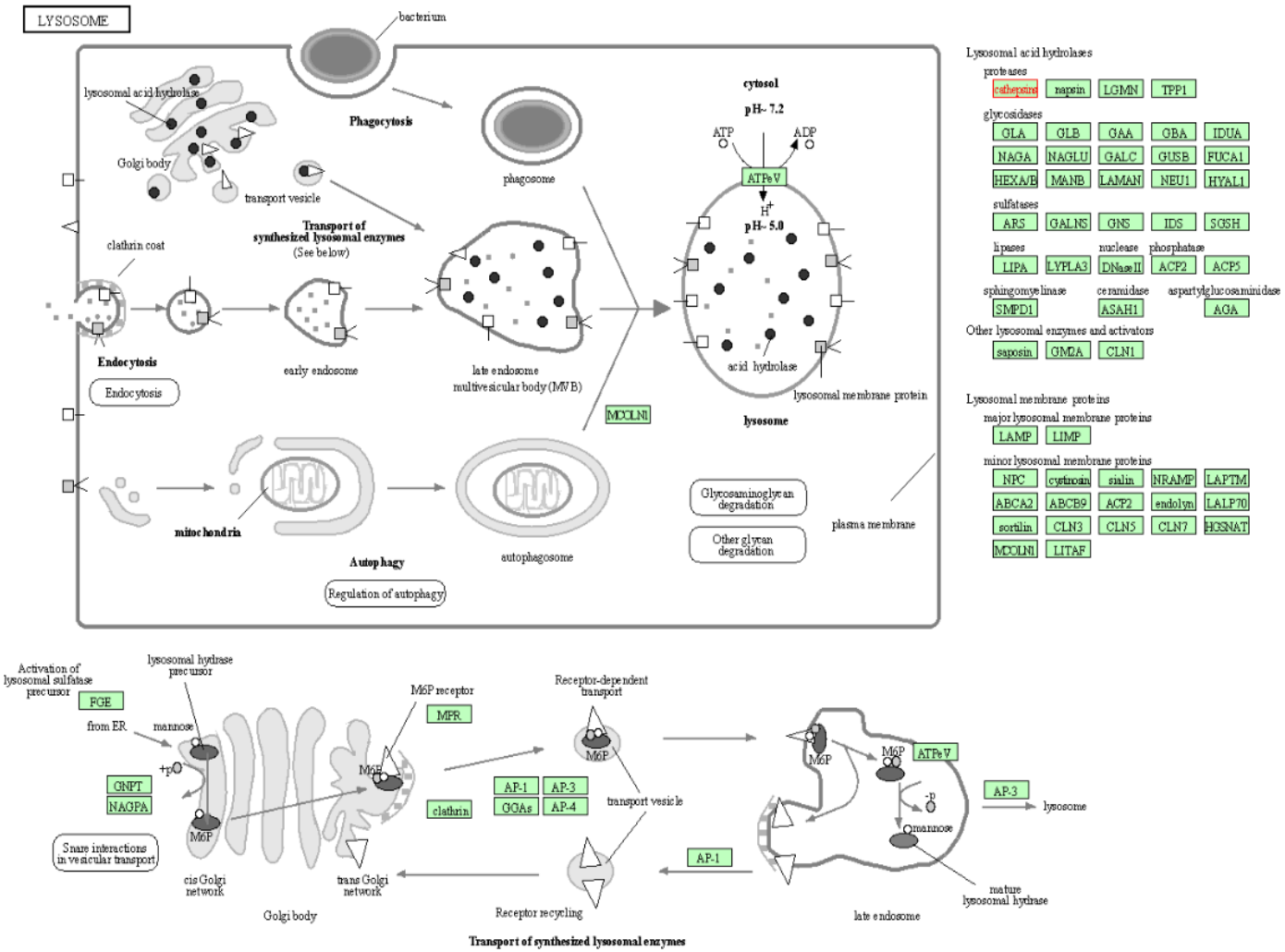

Figure 33: KEGG pathway map showed proteins involved in Lysosome pathway Proteins highlighted in red were expressed in enrichment analysis. Cathepsin proteins B, L and D were significantly increased in myocyte EVs, suggesting increased activities of these proteins in the lysosome pathway. Source: KEGG PATHWAY Database (genome.jp)

~~4.2.4.2~~6.2.4.2 KEGG Analysis of Proteins Involved in Apoptosis Pathway

Apoptosis described as a process that eliminates damaged or redundant cells by activation of caspases and externalisation of phosphatidylserine [272,273]. The mechanism consists of two pathways: the "extrinsic pathway," a transmembrane receptor mediated pathway and the "intrinsic pathway" a mitochondrial mediated pathway [274]. The extrinsic pathway is stimulated when extracellular ligands such as TNF (tumour necrosis factor), Fas-L (Fas ligand), and TRAIL (TNF-related apoptosis-inducing ligand) attach to extracellular transmembrane receptors such as type 1 TNF receptor (TNFR1), Fas (also called CD95/Apo-1) and TRAIL [275]. Stimulation of these extracellular transmembrane receptors activates caspase 8 and initiates the cascade of caspase activation [276]. On the other hand, the intrinsic pathway is mainly activated by various extra- and intra-cellular stress factors including, oxidative stress [277] and stress caused by cytotoxic agents [278]. The cellular stress leads to mitochondrial outer membrane permeabilization (MOMP) and the release of cytochrome c into the cytosol [279]. Initially caspase 9 is activated in the intrinsic pathway followed by caspase 3 which, ultimately leads to apoptosis [280].

As mentioned earlier, among the different pathways obtained by KEGG analysis, the apoptosis pathway showed significant enrichment. The false discovery rate (FDR) *p*-value for the pathway was 0.0035. The apoptosis pathway was mapped **Figure 34** to visualise protein interactions. Similar to lysosome pathway, cathepsin proteins were significantly enriched in apoptosis pathway too. Cathepsin L, B and D were significantly increased in myocyte EVs compared to fibroblast EVs. Cytosol cathepsin L, B and D have been reported in the literature to be associated with the term "Apoptosis". As discussed earlier, cytosol cathepsins increase MOMP which leads to the release of cytochrome c and triggers the intrinsic pathway of apoptosis.

Interestingly, the experimental data presented earlier suggested that myocyte EVs may have increased carcinoma cells' mitochondrial membrane permeability and caused apoptosis. Furthermore, it was shown that myocyte treated carcinoma cells had increased caspase 3 and 9 activities, which suggested that carcinoma cell apoptosis was here stimulated by the intrinsic pathway. Therefore, the empirically derived experimental data presented coincided with the results obtained by KEGG pathway analysis.

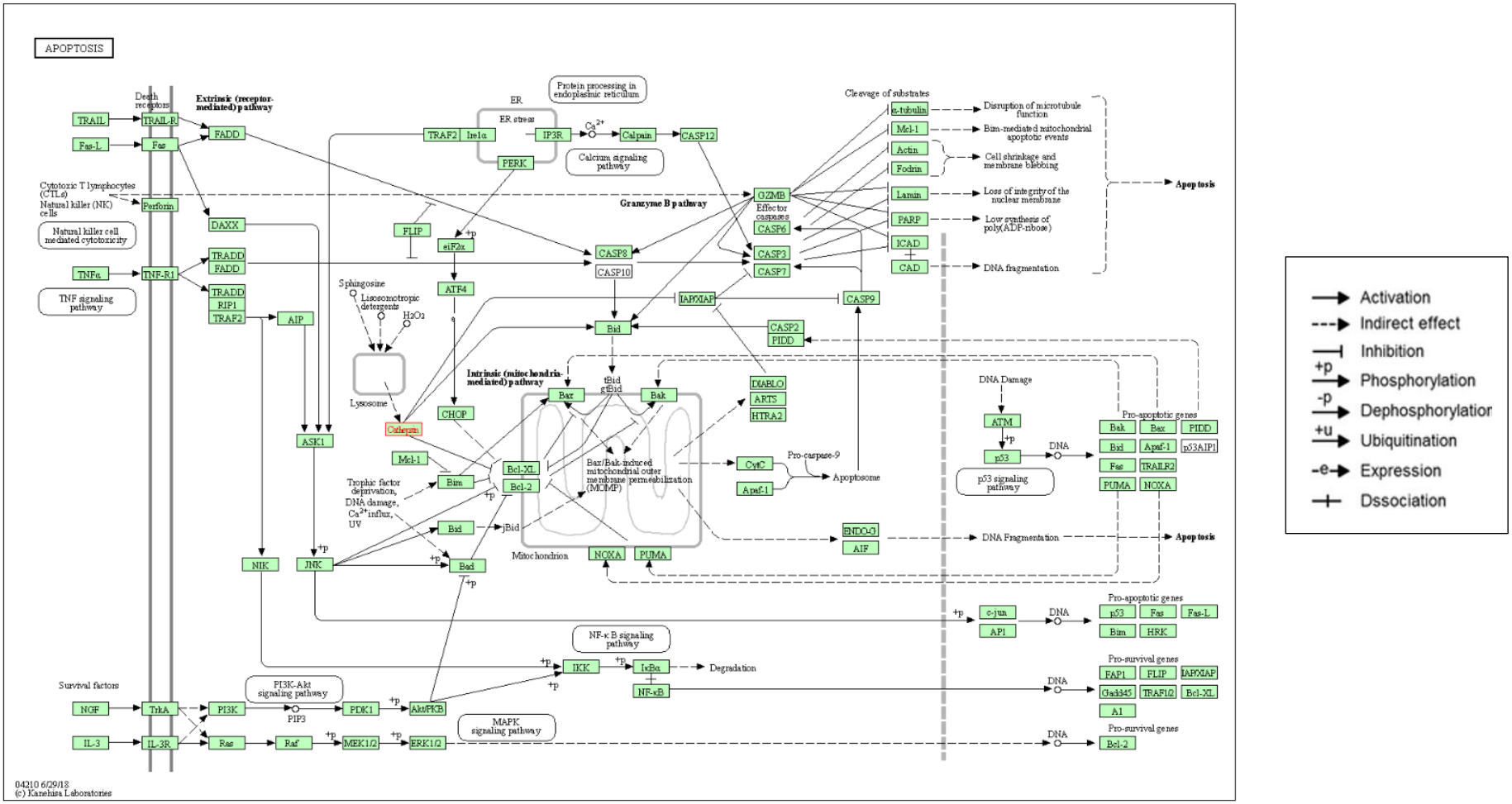

Figure 34: KEGG analysis showing proteins involved in Apoptosis pathway Significantly upregulated proteins were highlighted in red. Significantly increased cathepsin B, D and L1 in myocyte EVs showed their involvement in carcinoma cell apoptosis. Source: KEGG PATHWAY Database (genome.jp)

~~4.2.4.3~~6.2.4.3 KEGG Analysis of Proteins Involved in Proteoglycan Cancer Pathway

The Proteoglycan in cancer pathway was also enriched in KEGG analysis with an FDR of 0.0055. Proteoglycans are known to perform multiple functions in modulating cancer progression including proliferation, adhesion, angiogenesis, and metastasis. Hyaluronan (HA), heparan sulphate proteoglycans (HSPGs), chondroitin sulphate / dematan sulphate proteoglycans (CSPGs / DSPG) and keratan sulphate proteoglycans (KSPGs) were recognised as the main protein chains involved in the proteoglycan in cancer pathway. Proteoglycan hyaluronan (HA) binds with CD44 and promotes tumour cell growth, survival and migration [281], whereas membrane heparan sulphate proteoglycans (HSPGs) such as syndecan and glypicans (glycosylphosphatidylinositol-anchored proteoglycans) induce tumour cell survival, proliferation, migration and invasion by interacting with growth factors, chemokines and cytokines [282,283]. In contrast, some proteoglycans such as decorin in (CSPGs / DSPG) pathway and lumican in KSPGs pathway act as a tumour suppressor by initiating growth suppression and apoptosis [281].

KEGG analysis of upregulated proteins in **Figure 32**, identified decorin, thrombospondin-1 and cathepsin L1 as the enriched proteins in proteoglycans in cancer pathway. Interestingly, 2 of these proteins including, decorin and thrombospondin-1 were active in chondroitin sulphate / dematan sulphate proteoglycans (CSPGs / DSPG) chain. Therefore, only that pathway was selected and represented in here (**Figure 35**).

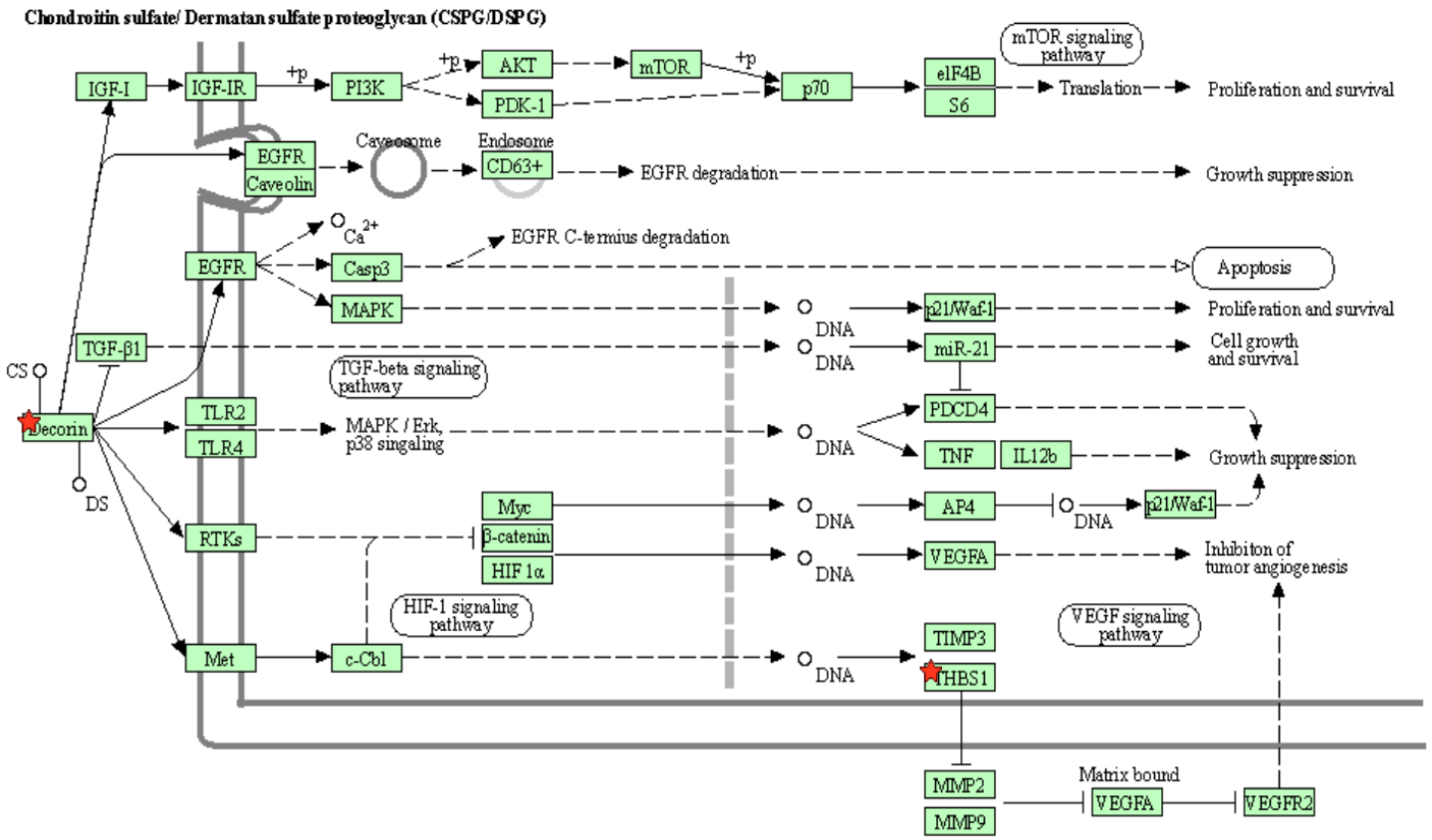

Figure 35: KEGG analysis showed Proteoglycan in Cancer pathway

Proteins highlighted in red were upregulated proteins in myocyte EVs. Decorin in chondroitin sulphate proteoglycans (CSPGs), dematan sulphate proteoglycans (DSPG) chain induces growth suppression and apoptosis, whereas thrombospondin-1 inhibits tumour angiogenesis. Source: KEGG PATHWAY Database (genome.jp)

Decorin is a key protein in proteoglycan in cancer pathway. Decorin core protein consists of 4 main domains and one of the domains contains GAG side chain, which is either chondroitin sulphate or dermatan sulphate [284]. Hence, all the possible protein interactions of both of these were shown in (**Figure 35**). As shown in (**Figure 35**), decorin interacts with many growth factors and their receptors leading to different signalling pathways. Interestingly, most of those pathway leads to growth suppression, apoptosis and inhibition of tumour angiogenesis.

The other proteoglycans that were upregulated in myocyte EVs was Thrombospondin-1. Thrombospondin-1 is an extracellular calcium binding glycoprotein which inhibits angiogenesis and tumourigenesis. A recent study has shown that upregulation of thrombospondin-1 significantly inhibited prostate cancer proliferation, migration and invasion in a dose-dependent manner [285]. Interestingly, decorin has been known to evoke thrombospondin -1 secretion and suppress angiogenesis [286]. Cathepsin family protein, cathepsin L1 is found in Heparan sulphate chain in the Proteoglycan in cancer pathway. Cathepsin L1 cleaves proteoglycan protein perlecan, which inhibits the growth and invasiveness of cancer cells [287] and angiogenesis [288]. Taken together, this information suggests another protein pathway that could lead the cancer cells to apoptosis.

~~4.2.5~~6.2.5 Decorin: A Myokine with Anti-Cancer Effects

The main focus of the proteomics analysis conducted in this chapter, was to identify myocyte EV protein/s that could inhibit lung carcinoma cell migration, cytotoxicity induced growth suppression, inhibit proliferation by cell cycle arrest and inducing apoptosis by enhancing MOMP. Interestingly, with the support of STRING and KEGG analysis, 5 possible proteins that could exert aforementioned effects including Cathepsin D, Cathepsin L1, Cathepsin B, decorin and thrombospondin-1 **Figure 32**, were selected. Among these proteins, decorin

interacts with many growth factors, receptors, and subsequent signalling pathways **Figure 35**, hence selected as a possible protein which exerted anti-tumourigenic effects.

Decorin (DCN) is a prototypical member of the small leucine-rich proteoglycan gene family[389] and it is composed of a protein core with a single glycosaminoglycan chain of chondroitin sulphate or dermatan sulphate. Decorin is mainly synthesised by fibroblast, smooth muscle cells and stressed vascular endothelial cells. Originally, DCN was known for its high affinity interactions with collagen fibres and the regulation of fibrillogenesis [289,290]. Recently, decorin was established as an exercise regulated myokine which is secreted in response to muscle contractions [291] and plays a major role in muscle cell differentiation, wound healing, muscular development, and regulation of inflammation [292].

Interestingly, in recent years EVs have been identified as delivery vehicles for myokines [267]. It is well established that skeletal muscle secretes myokines including, decorin into the extracellular milieu. However, the notion of skeletal muscle derived EVs carrying these myokines is in its infancy. For now, only one study have used mass spectrometry (LC-MS/MS) analysis to confirm the presence of decorin in skeletal muscle derived exosome like vesicles (ELVs) (www.exocarta.org and www.microvesicles.org). Another study has ascertained the presence of decorin in myocyte ELVs by mass spectrometry (LC-MS/MS) and western blot analysis [293]. However, to further confirm the presence of decorin in the murine myocyte (C2C12) mEVs used in this study, it was decided to perform western blot analysis (**Figure 36**).

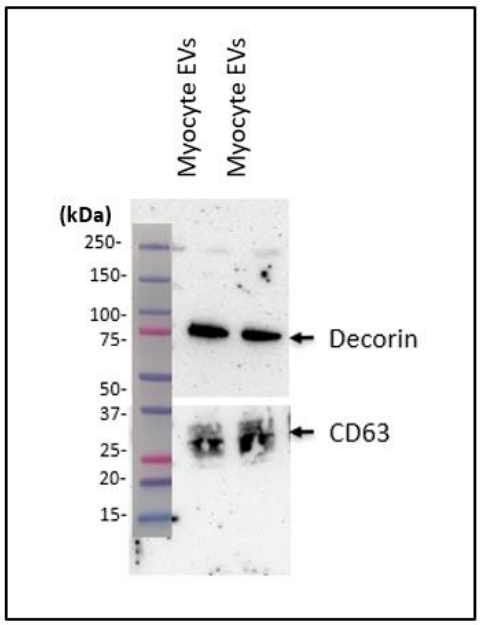

Figure 36: Western blot analysis to validate the presence of decorin in myocyte EVs.

A myocyte EV protein sample obtained for mass spectrometry analysis was used to validate the presence of decorin by western blotting. Duplicate protein samples were used. A clear specific band for decorin was detected at approximately 70-100 kDa (as indicated) using 0.5 µg/ml of Goat anti-mouse decorin antigen affinity purified polyclonal antibody, followed by HRP conjugated anti-goat IgG secondary antibody. In order to confirm that decorin was present in EVs, CD-63, an EV marker was used on the same blot. As indicated, a broad band between 25-30 kDa was detected for CD-63, validating the origin of the protein sample.

The clear thick band present for decorin in **Figure 36** validated and confirmed the presence of decorin in myocyte EVs. Interestingly, decorin's multiple interaction with growth factors, their receptors and following pathways has enabled it to act as an inhibitor of growth, metastasis and angiogenesis of tumours [202,295,296,297,298,299,300]. Moreover, the ability of decorin to induce cell cycle arrest and intrinsic apoptosis in lung cancer A549 cells via increased p21 and p53 was also demonstrated [301]. A recent study has also shown the role of decorin in mitophagy, mitochondrial autophagy and in causing apoptosis [293,302]. Interestingly, these effects correlate with the experimental data presented in this study, which showed growth inhibition, cell cycle arrest, and mitochondrial damage leading to apoptosis in lung carcinoma cells upon treatment with myocyte EVs. Furthermore, overexpression of decorin has been shown to induce

apoptosis and cell growth arrest in rat mesangial cells *in vitro* [294]. The statistical data obtained in **Figure 31B** indicates an overexpression of decorin in murine myocyte EVs compared to murine fibroblast cell line EVs. However, in the above Western blot experiment, decorin expression in fibroblast cell line EVs was not determined and compared with myocyte EVs. Therefore, **Figure 36** only validate only the presence of decorin in the myocyte EVs, but the overexpression of decorin in myocyte EVs remained unvalidated.

4.36.3 Summary

In this chapter, the protein content of skeletal muscle EVs and their biological pathways were analysed. Liquid chromatography-based Mass spectrometry was used to analyse the protein content of myocyte EVs. In addition, the protein content of fibroblasts was also analysed as unlike myocyte EVs, the fibroblast EVs enhanced carcinoma cell growth and progression. The comparison between these EV populations showed that ~34% of proteins identified were common to both EV populations, but that some proteins were differently expressed. Strikingly, ~43% of proteins were fibroblast EV specific and only ~23% proteins were myocyte EV specific.

Many proteins perform their function by binding to another molecule; therefore, proteins and their functional interactions are key to many biological processes. To better understand the protein interactions in myocyte and fibroblast EVs, STRING analysis was conducted. GO analysis of biological process showed that most of the proteins were regulatory proteins. However, compared to fibroblast EVs, myocyte EVs contained more proteins that negatively regulate biological processes. The strength of some of these negative biological processes such as cell cycle arrest, cell migration and cell adhesion were significantly higher compared to a random protein network of similar size. These findings coincided with the experimental data presented in earlier chapters, where it showed the negative effect of myocyte EVs on carcinoma cell migration and adhesion. Furthermore, myocyte EVs contained an increased number of lysosome related proteins compared to fibroblast EVs.

Having confirmed that myocyte derived EVs contain more proteins that negatively regulate cellular biological processes, fold change by category for all myocyte EV proteins was calculated. From total of 220 myocyte EV proteins, 29 were upregulated whilst 13 were

downregulated. To gain further insight into the whole chain of events caused by differently expressed proteins, upregulated proteins were selected for KEGG pathway analysis. Interestingly, myokines including decorin, cathepsin B and SPARC proteins were significantly upregulated in myocyte EVs compared to fibroblast EVs. KEGG pathway analysis revealed 8 different pathways for upregulated proteins. These significantly enriched pathways were: (i) Antigen processing and presentation, (ii) Autophagy, (iii) Apoptosis, (iv)TGFβ signalling pathway, (v) phagosome, (vi) Protein digestion and absorption, (vii) Lysosomes and (viii) Proteoglycan in cancer. Interestingly, 3 of these pathways, "apoptosis," "lysosomes" and "Proteoglycan in cancer" pathways coincided with the empirically derived data presented in this thesis. Cathepsin L1, B and D were mainly involved in apoptosis and lysosome pathways, whilst decorin, cathepsin L1 and thrombospondin-1 were involved in the Proteoglycan in cancer pathway. From above proteins, decorin was selected for further analysis as it has been already employed in cancer therapy. The thicker and darker band identified for decorin in western blot analysis confirmed the expression of decorin in myocyte EVs and it further validated the proteomics data obtained from the mass spectrometry.

~~5~~7 General Discussion

~~5.1~~7.1 Myocyte EV Isolation and Characterisation

Extracellular Vesicles (EVs) are nanometer sized membrane bounded particles released by all cell types into the extracellular milieu. They are detected in almost all body fluids including blood, urine, semen, bronchial fluid and saliva [5,6]. In recent years, they are attracting considerable interest in the scientific community due to their physiological role in infectious diseases, metabolic diseases, cancer and in the aging process [1,2,3,4]. EVs are known to modulate these processes by transferring their cargo of proteins, lipids and nucleic acids to recipient cells. With emerging functions of EVs in both physiological and pathological conditions, recent reviews have focused on clinical applications of EVs as both a diagnostic and therapeutic agent.

Despite the increasing interest and the advances in this field, at present there is no single optimal method to isolate EVs from non-vesicular entities of cellular origin [37]. Therefore, in 2018 the International Society for Extracellular Vesicles (ISEV) published a position statement, updating 2014 MISEV (Minimal Information for Studies of Extracellular Vesicles) guidelines, stating their recommendations for EV nomenclature, collection and processing, separation, characterisation, and functional studies. Based on this review, this thesis has used the separation and characterisation techniques recommended by ISEV. Here, EVs were isolated by differential ultracentrifugation. Having removed cells and cell debris, EVs were isolated using a maximum speed of 18,500 × g . Although isolation of EVs from other 'contaminating' macromolecules is an unrealistic goal, after washing the isolated EVs with EV-free buffer this yielded EVs that were largely free of proteins and other biomolecules.

In accordance with ISEV guidelines, Nanoparticle Tracking Analysis (NTA) was used to measure the concentration and size of the isolated EVs. It was found that approximately, 1×10^8 myocyte cells generate $1.79 \times 10^{10} \pm 2.74 \times 10^8$ EV particles per ml within 24 h. Furthermore,

based on NTA results, the EVs isolated in this thesis were identified as those of the medium/large EV (m/lEVs) subtype, as the mean value of the EVs was < 200 nm in size [14]. To further validate the presence of the EVs protein markers suggested by ISEV, the presence ofCD63 and TSG101, proteins associated with EV biogenesis [22,23,24], was assessed. As a non-protein EV marker, fluorescently labeled annexin V-FITC was used. EVs contain a lipid bilayer membrane, which contains rare lipids such as ceramide and amino phospholipids such as phosphatidylserine (PS),[13] which as in early apoptosis is flipped onto the outer leaflet. Unlike other lipids found in the plasma membrane, PS carries an uncommon net negative charge and, annexin V can recognize PS through coordinated Ca^{2+} ions [17]. The fluorescent intensity of annexin V binding to mEVs was measured using flow cytometer which confirmed that approximately 70% of the EVs isolated were annexin V positive.

~~5.2~~7.2 Lung Carcinoma Cells Selectively Govern Myocyte EV Uptake

EVs are known to alter physiological and pathological states of recipient cells by inducing intracellular signals and altering molecular pathways. This is achieved by either binding with recipient cell surface receptors or internalisation and release of the EV intravesicular cargo into the recipient cell cytosol [226]. Despite many recent advances and understanding in the EV field, the exact mechanism of EV uptake remains to be elucidated. Initially, many studies have reported the prevalence of EV uptake by any cell [303,304] but more recent studies indicate that it is a highly specific process as the recipient cells and the EVs require the correct surface receptors and ligands for interactions [304,305,306,307,308]. This study is an agreement with the latter process, as only few carcinoma cells in a colony were found to take up the myocyte EVs. This time dependent uptake resulted in higher fluorescent intensities in certain carcinoma cells, likely due to differing degrees of uptake by certain cells within the same colony. This observation could be explained from recent findings indicating that EV uptake can be affected

by the metabolic status of recipient cells, specifically that that neural stem cells which are metabolically active, exhibit a significantly higher capacity of internalizing EVs compared to mature neurons [228]. Cell cycle phase of recipient cells may also affect uptake. Working with prostate cancer cells, this work found increased uptake during G_2/M phase and less uptake in G_0/G_1 phase or S phase [309]. In other research using colorectal cancer cells it was found that the hypoxic status of the EVs released may influence uptake, EVs from hypoxic cells expressing proteins deemed to increase uptake [310]. It should also be pointed out that there are other possible mechanisms of EV uptake by cells, such as endocytosis. This includes receptor-mediated endocytosis, macropinocytosis and phagocytosis. Just as uptake mechanism used may be dependent on the cell type, EVs may be simultaneously taken up into cells by different mechanisms [311].

~~5.3~~7.3 Local Tumour Suppressive Effect of Skeletal Muscle Derived EVs

The next area of investigation focused on the hypothesis that skeletal muscle derived EVs play a significant role in suppressing cancer metastasis. Most organs and tissues are subjected to cancer metastasis with the striking exception of skeletal muscle, in which cancer metastasis is very rare [169,170,171,172]. The rarity of cancer metastasis in skeletal muscle is surprising as it is a highly vascularized tissue and compromises ~50% of the body mass. Although, several studies have linked high level of lactic acid [183], low molecular factors [186] and many cytokines [187] to the rarity of cancer progression in skeletal muscle, an exact mechanism(s) has not yet been elucidated. Here, it was shown that highly metastatic murine lung carcinoma cells (CMT 64/61) failed to colonise skeletal muscle cells (C2C12). This observation coincided with others reports *in vivo*, where it was found that no tumour appearance in skeletal muscle, but in neighbouring bone upon tail vein injection of carcinoma cells in mice [186,207].

Steven Paget's “Seed and Soil” hypothesis for metastasis, describes the need of a receptive microenvironment or niche for disseminating carcinoma cells to engraft distant sites [312,313]. Here, it was found that the skeletal muscle microenvironment exerts inhibitory effects on carcinoma cell viability when cultured with skeletal muscle conditioned media. Others have also seen similar effects exerted by skeletal muscle conditioned media including, carcinoma cell apoptosis [186] and growth inhibition [205]. Growing evidence identifies EVs as a pivotal constituent of the cellular microenvironment and recently, there has been increasing interest in the potential role of EVs as a positive and negative microenvironment modulator for cancer progression [314]. For example, cancer derived EVs were found to interact with immune cells to modulate the microenvironment and enhance immune evasion, cancer growth and progression [315]. By contrast, EVs are also known to exert inhibitory effects on cancer cells, including dendritic cell derived EVs able to modulate the tumour microenvironment and enhance immune responses to reduce lung metastasis [316]. Mesenchymal stem cell derived EVs also suppress human breast cancer angiogenesis [317]. These are just a few examples and further investigations to identify new functions are still ongoing.

The present study has shown for the first time, a novel function of skeletal muscle derived EVs as a local tumour suppressor. Carcinoma cells treated with myocyte EVs showed a dose dependent decrease in cell viability. Furthermore, the data presented suggests that the effect of myocyte EVs on carcinoma cells is greater compared to that which could be mediated by a similar protein concentration of myocyte conditioned media. In addition, when carcinoma cells were introduced to the myocyte EVs, a significant reduction in number of cell colonies formed and a reduction in number of cells in a cell colony was observed. This was explained by EVs derived from skeletal muscle cells offering an unfavourable environment for migrating carcinoma cells, lowering their capacity for attachment, and which was manifest as a resulting

low number of cell colonies being established. Furthermore, overt changes in cell morphology were noted in some carcinoma cells treated with myocyte EVs the cells becoming irregular in shape and showed loss of cell membrane integrity.

~~5.3.1~~7.3.1 Role of Myocyte EVs in Inducing Apoptosis of Carcinoma Cells

An ideal anticancer therapeutic agent should destroy or incapacitate cancer cells causing minimal damage to surrounding healthy bystander cells [318]. Here, for the first time the results presented in this thesis show the cytotoxic effect of myocyte EVs on lung carcinoma cells. The myocyte EVs, even at very low concentration (100 µg/ml), exerted specific and significant cytotoxicity on carcinoma cells but not on normal fibroblast cells. However, myocyte EV concentrations over 200 µg/ml showed significant cytotoxicity on normal cells.

Cytotoxic agents can impact cells in various ways, including necrosis and apoptosis [229], which reduce the number of viable cells in culture. Furthermore, the observed loss of cell membrane integrity and shape indicated possible induction of necrosis or apoptosis. Growing evidence suggests that lysosomes are involved in shaping cell death by modulating external and internal stimuli [232]. Results obtained in this study indicated a dose dependent decrease in numbers of lysosomes but increase in lysosome size, upon incubation with myocyte EVs. Increased lysosomal membrane permeability causes enlargement of lysosomes and enlarged lysosomes rupture easily to release hydrolytic enzymes to the cytosol [241], which would explain the observed reduction in lysosome numbers. Lysosomes are known as the “suicidal bags” in the cell as they contain high levels of hydrolytic enzymes. In the event of lysosomal membrane damage, these hydrolytic enzymes are released into the cell cytosol and cause indiscriminate degradation of cellular components, inducing cell death by necrosis [232]. Other research has

shown that partial lysosomal membrane permeability induces cell death by apoptosis [233,234,235,236]. Hence targeting lysosomes has been shown to be an effective cancer therapy.

From previous studies it is known that changes in lysosomal function induce changes in mitochondrial membrane composition, which impairs mitochondrial functions and induces apoptosis by release of cytochrome c to the cytosol[456]. In recent years, targeting apoptosis has been identified as the most successful non-surgical method in cancer therapy [161]. Therefore, a primary objective of cancer therapy beside cancer gene therapy and immunotherapy is the induction of apoptosis of cancer cells whilst limiting death of normal cells [319]. Recently, clinical application of natural killer cell derived EVs has been discussed as it was found that they could induce targeted apoptosis on a variety of carcinoma cells via activation of the intrinsic pathway [320]. Similarly, the present study for the first time finds that EVs from skeletal muscle cells exerts a specific apoptotic effect on lung carcinoma cells with pronounced cell death after 48h, whereas no effect was observed upon normal fibroblasts. Further investigations revealed impaired mitochondrial functions through reduced mitochondrial membrane potential and increased caspase 3 and caspase 9 in carcinoma cells treated with myocyte EVs, suggesting mitochondrial dependent (intrinsic pathway) apoptosis.

The intrinsic apoptotic pathway can be activated by a variety of both intracellular and extracellular factors [155,156]. In the case of skeletal muscle myocyte cell derived EV induction of carcinoma cells, one factor responsible could have been a change in the permeability of the lysosomal membrane. This would induce cathepsin B and D release into the cytosol and cleave Bid protein [321], which could induce apoptosis by mediating release of cytochrome c from mitochondria into cytosol [322,323]. Moreover, Bid induces homo-oligomerization of BAX and BAK, which leads to mitochondrial outer membrane permeabilization (MOMP) [324], leading

to intrinsic pathway apoptosis. Another factor is the direct cytotoxicity of myocyte EVs on carcinoma cells, which could have upregulated the BH3-only proteins. This would alter mitochondrial membrane potential and induce BAX and BAK oligomerisation, leading to mitochondrial outer membrane permeabilization (MOMP) [157], a route independent of Bid. In summary the results presented here here indicate multiple potential cell death mechanisms mediated by skeletal muscle derived EVs resulting in cytotoxicity of lung carcinoma cells.

~~5.3.2~~7.3.2 Role of Myocyte EVs on Carcinoma Cell Proliferation

In the past decade, studies on EVs and their pro-tumourigenic functions have increased exponentially. Conversely, more recently work has started to identify anti-tumourigenic properties of EVs, mainly in terms of growth inhibition. For example, gastric epithelial cell derived exosomal protein gastrokine-1 was found to inhibit gastric carcinogenesis by downregulating HRas/Raf/MEK/ERK signalling pathways [325]. In colon cancer, exosomes carrying microRNA-375 inhibit cancer cell progression and dissemination via Bcl-2 blocking [326]. Furthermore, normal fibroblast derived exosomes containing microRNA 520-b has been shown to impede the progression of pancreatic cancer [327].

A recent study has shown that skeletal muscle progenitor cell-derived exosomes inhibit prostate cancer cell proliferation [210]. Furthermore, a previous investigation had identified the effect of skeletal muscle conditioned media on tumour growth, in which a G_0/G_1 growth was exerted on tumour cells [205]. The present study for the first time identifies the anti-proliferative effects of myocyte EVs, specifically medium sized EVs, also known as microvesicles (mEVs). Lung carcinoma cells treated with myocyte EVs exited the cell cycle at S phase, in which cells replicate their DNA. S phase arrest prevented cell progression to G2/M phase, thereby inhibiting cell proliferation.

~~5.3.3~~7.3.3 Role of Myocyte EVs on Carcinoma Cell Migration

To successfully metastasise, carcinoma cells must infiltrate adjacent tissue, intravasate, extravasate and proliferate at a distance site [117]. Chemotaxis and chemokinesis are together known to play a crucial role in cancer metastasis. In many cancer metastases, organ specific stromal cells induce chemotaxis by releasing signalling proteins that attracts cancer cells, causing organ specific metastasis [328,329] and EVs are known to modulate and enhance this process. However, EVs derived from some cells known to inhibit organ specific metastasis, including dendritic cells derived EVs modulate the tumour microenvironment and enhance immune responses to reduce lung metastasis [316]. Results obtained herein, are in an agreement with the latter, as the cell migration assay showed a significant reduction in carcinoma cell migration in the presence of myocyte EVs. Furthermore, upon migration to skeletal muscle, carcinoma cells will undergo apoptosis, which provides a further explanation for the rarity of metastatic tumours in skeletal muscles.

~~5.4~~7.4 Myocyte EV Protein Content and Detection of Upregulated Protein Candidates that may Induce Apoptosis of Carcinoma Cells

It is well established that EVs are loaded with a plethora of biomolecules lipids, proteins, and nucleic acids, which can be transferred to recipient cells to exert cellular changes. In this study, liquid chromatography-based Mass spectrometry analysis was used to identify the proteins in myocyte EVs. When proteins in myocyte EVs were compared to normal fibroblast cell EV proteins, 29 upregulated proteins were identified. The STRING analysis identified total of 8 significantly enriched biological pathways for these upregulated proteins in myocyte EVs and interestingly, these pathways, “apoptosis,” “lysosomes” and “Proteoglycan in cancer”

pathways coincided with the empirically derived data presented in this study. Upregulated proteins for these pathways were, cathepsin L1, cathepsin D and cathepsin B in both apoptosis and lysosome pathways, decorin, cathepsin L1 and thrombospondin-1 in the Proteoglycan in cancer pathway.

In recent years, lysosome related proteins have been reported in publications on cell death. Many lysosomes related proteins have been identified as key regulators of apoptotic cell death. The lysosomal protease family consisting of cysteine cathepsins B, C, F, H, K, L, O, S, V, W and X and the aspartic cathepsin D have been identified as key regulators of cell death [330]. Among those proteins, cathepsin D, L1 and B have been identified as apoptosis inducing proteins. In the proteomics study presented in this thesis, cathepsin L1, cathepsin B and cathepsin D were identified as upregulated proteins in myocyte EVs. Overexpression of cathepsin B, D and L in the cytosol has been implicated in degradation of Bid. Cleavage of Bid by cathepsin D induces Bax-mediated release of cytochrome c from mitochondria into the cytosol. In turn, cytochrome c initiates caspase 9 activity followed by stimulation of the caspase 3 cascade which leads to intrinsic apoptosis [280]. This explanation concurs with the experimental data presented in this thesis, which suggests that myocyte EVs unload their cargo containing cathepsins into the carcinoma cell cytosol and induce mitochondrial membrane permeability leading to intrinsic apoptosis.

This study also confirmed the presence of decorin, a key player in the proteoglycan in cancer pathway, in myocyte EVs. Decorin has been studied extensively in its purified form as a tumour suppressor. However, the respective role of this protein in isolated myocyte EVs has not been previously investigated. Decorin is a myokine which belongs to the leucine-rich proteoglycan family. Interestingly, decorin expression in tumours is significantly reduced from the levels

expressed in normal tissues [301,331]. It is reported that overexpression of decorin could block the cell cycle arrest at G1 phase and inhibit the invasiveness of lung cancer A549 cells causing cell apoptosis and inhibition of metastasis via increased p53 and p21 expression [301]. Moreover, recent studies have shown the role of decorin in mitophagy and mitochondrial autophagy causing intrinsic apoptosis [293,302]. In addition, decorin negatively regulates insulin-like growth factor receptor I (IGF-IR) [297,298] and hepatocyte growth factor receptor (Met) [332]and inhibits tumour cell growth and migration [300].

The above functions strongly support the observations made in this study and therefore, propose an additional pathway of carcinoma cell suppression mediated by skeletal muscle derived EVs. Murine lung carcinoma cell uptake of myocyte EVs and subsequent release of their cargo containing decorin into the carcinoma cell cytosol, by increasing the levels of decorin likely induces carcinoma cell apoptosis, growth suppression by cell cycle arrest and inhibition of carcinoma cell migration.

~~5.5~~7.5 Conclusion and Future Perspectives

Cancer progression in skeletal muscle is very rare. The data in this thesis provides further evidence to support this notion and demonstrates the effect of skeletal muscle derived EVs on lung carcinoma cells. Growing evidence highlights the importance of EVs in modulating many diseases by transporting their cargo between cells. In cancer, EVs are widely discussed as a pro-tumourigenic agent; however, their role as an anti-tumourigenic agent started to emerge recently. In this thesis a novel anti-tumourigenic mechanism of skeletal muscle derived EVs has been discussed.

In conclusion, the efficacy of skeletal muscle derived EVs as an anti-tumourigenic agent that selectively exerts apoptosis on highly metastatic lung carcinoma cells was unexpected and novel. The myocyte EVs exert their specific cytotoxic effect on carcinoma cells which induces changes in mitochondrial membrane. Cell death was significantly controlled by both initiator caspase 9 and executioner caspase 3 leading to the intrinsic pathway of apoptosis. In addition, myocyte EVs inhibits lung carcinoma cell proliferation by cell cycle arrest at S phase and inhibit carcinoma cell migration. Finally, protein levels of decorin inside myocyte EVs may be related to the ability of myocyte EVs to induce the anti-tumourigenic effects observed. Consequently, further investigation on decorin as a protein cargo of myocyte EVs is warranted for the elucidation of the mechanism underlying the rarity of cancer metastasis in skeletal muscle. Furthermore, the positive outcomes of this research provide a strong basis for myocyte EVs as a novel therapeutic agent for highly metastatic lung carcinoma.

~~6~~8 References

References

1. Grange C, Tapparo M, Collino F et al. Microvesicles Released from Human Renal Cancer Stem Cells Stimulate Angiogenesis and Formation of Lung Premetastatic Niche. *Cancer Res*. 2011;71(15):5346-5356. doi:10.1158/0008-5472.can-11-0241

2. Camussi G, Deregibus M, Bruno S, Cantaluppi V, Biancone L. Exosomes/microvesicles as a mechanism of cell-to-cell communication. *Kidney Int*. 2010;78(9):838-848. doi:10.1038/ki.2010.278

3. Bruno S, Grange C, Deregibus M et al. Mesenchymal Stem Cell-Derived Microvesicles Protect Against Acute Tubular Injury. *Journal of the American Society of Nephrology*. 2009;20(5):1053-1067. doi:10.1681/asn.2008070798

4. Muralidharan-Chari V, Clancy J, Sedgwick A, D'Souza-Schorey C. Microvesicles: mediators of extracellular communication during cancer progression. *J Cell Sci*. 2010;123(10):1603-1611. doi:10.1242/jcs.064386

5. Zaborowski M, Balaj L, Breakefield X, Lai C. Extracellular Vesicles: Composition, Biological Relevance, and Methods of Study. *Bioscience*. 2015;65(8):783-797. doi:10.1093/biosci/biv084

6. Baffour S, Kyeremeh R, Odoom A, Seidu M. Biological Functions of Plasma Membrane-Derived Extracellular Vesicles and Their Role in Diseases. *Journal of Cells*. 2015;1(2):33-42. doi:10.18488/journal.97/2015.1.2/97.2.33.42

7. Théry C, Zitvogel L, Amigorena S. Exosomes: composition, biogenesis and function. *Nature Reviews Immunology*. 2002;2(8):569-579. doi:10.1038/nri855

8. EL Andaloussi S, Mäger I, Breakefield X, Wood M. Extracellular vesicles: biology and emerging therapeutic opportunities. *Nature Reviews Drug Discovery*. 2013;12(5):347-357. doi:10.1038/nrd3978

9. Théry C, Ostrowski M, Segura E. Membrane vesicles as conveyors of immune responses. *Nature Reviews Immunology*. 2009;9(8):581-593. doi:10.1038/nri2567

10. Yang C, Robbins P. Immunosuppressive Exosomes: A New Approach for Treating Arthritis. *Int J Rheumatol*. 2012;2012:1-8. doi:10.1155/2012/573528

11. Borges F, Reis L, Schor N. Extracellular vesicles: structure, function, and potential clinical uses in renal diseases. *Brazilian Journal of Medical and Biological Research*. 2013;46(10):824-830. doi:10.1590/1414-431x20132964

12. Jabalee J, Towle R, Garnis C. The Role of Extracellular Vesicles in Cancer: Cargo, Function, and Therapeutic Implications. *Cells*. 2018;7(8):93. doi:10.3390/cells7080093

13. Robbins P, Morelli A. Regulation of immune responses by extracellular vesicles. *Nature Reviews Immunology*. 2014;14(3):195-208. doi:10.1038/nri3622

14. Lötvall J, Hill A, Hochberg F et al. Minimal experimental requirements for definition of extracellular vesicles and their functions: a position statement from the International Society for Extracellular Vesicles. *J Extracell Vesicles*. 2014;3(1):26913. doi:10.3402/jev.v3.26913

15. Roos M, Gennero L, Denysenko T et al. Microparticles in physiological and in pathological conditions. *Cell Biochem Funct*. 2010;28(7):539-548. doi:10.1002/cbf.1695

16. Thompson A, Gray E, Heman-Ackah S et al. Extracellular vesicles in neurodegenerative disease — pathogenesis to biomarkers. *Nature Reviews Neurology*. 2016;12(6):346-357. doi:10.1038/nrneurol.2016.68

17. Xu R, Rai A, Chen M, Suwakulsiri W, Greening D, Simpson R. Extracellular vesicles in cancer — implications for future improvements in cancer care. *Nature Reviews Clinical Oncology*. 2018;15(10):617-638. doi:10.1038/s41571-018-0036-9

18. Balaj L, Lessard R, Dai L et al. Tumour microvesicles contain retrotransposon elements and amplified oncogene sequences. *Nat Commun*. 2011;2(1). doi:10.1038/ncomms1180

19. Benameur T, Andriantsitohaina R, Carmen Martínez M. Therapeutic potential of plasma membrane-derived microparticles. *Pharmacological Reports*. 2009;61(1):49-57. doi:10.1016/s1734-1140(09)70006-4

20. Abels E, Breakefield X. Introduction to Extracellular Vesicles: Biogenesis, RNA Cargo Selection, Content, Release, and Uptake. *Cell Mol Neurobiol*. 2016;36(3):301-312. doi:10.1007/s10571-016-0366-z

21. Teng F, Fussenegger M. Shedding Light on Extracellular Vesicle Biogenesis and Bioengineering. *Advanced Science*. 2020;8(1):2003505. doi:10.1002/advs.202003505

22. Pols M, Klumperman J. Trafficking and function of the tetraspanin CD63. *Exp Cell Res*. 2009;315(9):1584-1592. doi:10.1016/j.yexcr.2008.09.020

23. Wollert T, Hurley J. Molecular mechanism of multivesicular body biogenesis by ESCRT complexes. *Nature*. 2010;464(7290):864-869. doi:10.1038/nature08849

24. Baietti M, Zhang Z, Mortier E et al. Syndecan–syntenin–ALIX regulates the biogenesis of exosomes. *Nat Cell Biol*. 2012;14(7):677-685. doi:10.1038/ncb2502

25. Ghossoub R, Lembo F, Rubio A et al. Syntenin-ALIX exosome biogenesis and budding into multivesicular bodies are controlled by ARF6 and PLD2. *Nat Commun*. 2014;5(1). doi:10.1038/ncomms4477

26. Milane L, Singh A, Mattheolabakis G, Suresh M, Amiji M. Exosome mediated communication within the tumour microenvironment. *Journal of Controlled Release*. 2015;219:278-294. doi:10.1016/j.jconrel.2015.06.029

27. Foley J. Heparanase Promotes Exosome Release. *Sci Signal*. 2013;6(271):ec84-ec84. doi:10.1126/scisignal.2004245

28. Stenmark H. Rab GTPases as coordinators of vesicle traffic. *Nature Reviews Molecular Cell Biology*. 2009;10(8):513-525. doi:10.1038/nrm2728

29. Laulagnier K, Grand D, Dujardin A et al. PLD2 is enriched on exosomes and its activity is correlated to the release of exosomes. *FEBS Lett*. 2004;572(1-3):11-14. doi:10.1016/j.febslet.2004.06.082

30. Akers J, Gonda D, Kim R, Carter B, Chen C. Biogenesis of extracellular vesicles (EV): exosomes, microvesicles, retrovirus-like vesicles, and apoptotic bodies. *J Neurooncol*. 2013;113(1):1-11. doi:10.1007/s11060-013-1084-8

31. Hugel B, Martínez M, Kunzelmann C, Freyssinet J. Membrane Microparticles: Two Sides of the Coin. *Physiology*. 2005;20(1):22-27. doi:10.1152/physiol.00029.2004

32. Muralidharan-Chari V, Clancy J, Plou C et al. ARF6-Regulated Shedding of Tumour Cell-Derived Plasma Membrane Microvesicles. *Current Biology*. 2009;19(22):1875-1885. doi:10.1016/j.cub.2009.09.059

33. Nabhan J, Hu R, Oh R, Cohen S, Lu Q. Formation and release of arrestin domain-containing protein 1-mediated microvesicles (ARMMs) at plasma membrane by recruitment of TSG101 protein. *Proceedings of the National Academy of Sciences*. 2012;109(11):4146-4151. doi:10.1073/pnas.1200448109

34. Sedgwick A, D'Souza-Schorey C. The biology of extracellular microvesicles. *Traffic*. 2018;19(5):319-327. doi:10.1111/tra.12558

35. Li B, Antonyak M, Zhang J, Cerione R. RhoA triggers a specific signaling pathway that generates transforming microvesicles in cancer cells. *Oncogene*. 2012;31(45):4740-4749. doi:10.1038/onc.2011.636

36. Wang T, Gilkes D, Takano N et al. Hypoxia-inducible factors and RAB22A mediate formation of microvesicles that stimulate breast cancer invasion and metastasis. *Proceedings of the National Academy of Sciences*. 2014;111(31):E3234-E3242. doi:10.1073/pnas.1410041111

37. Davis C, Phillips H, Tomes J et al. The importance of extracellular vesicle purification for downstream analysis: A comparison of differential centrifugation and size exclusion chromatography for helminth pathogens. *PLoS Negl Trop Dis*. 2019;13(2):e0007191. doi:10.1371/journal.pntd.0007191

38. Spittler A, Görgens A. Analysis of extracellular vesicles by flow cytometry – basics, limitations and prospects. *How cells communicate - an introduction to extracellular vesicles*. 2019;1(1):40-45. doi:10.47184/tev.2019.01.06

39. Soo C, Song Y, Zheng Y et al. Nanoparticle tracking analysis monitors microvesicle and exosome secretion from immune cells. *Immunology*. 2012;136(2):192-197. doi:10.1111/j.1365-2567.2012.03569.x

40. Brisson A. Comment on "Quality of extracellular vesicle images by transmission electron microscopy is operator and protocol dependent". *J Extracell Vesicles*. 2019;8(1):1648996. doi:10.1080/20013078.2019.1648996

41. Kwok Z, Wang C, Jin Y. Extracellular Vesicle Transportation and Uptake by Recipient Cells: A Critical Process to Regulate Human Diseases. *Processes*. 2021;9(2):273. doi:10.3390/pr9020273

42. Jenjaroenpun P, Kremenska Y, Nair V, Kremenskoy M, Joseph B, Kurochkin I. Characterization of RNA in exosomes secreted by human breast cancer cell lines using next-generation sequencing. *PeerJ*. 2013;1:e201. doi:10.7717/peerj.201

43. Li S, Lin Z, Jiang X, Yu X. Exosomal cargo-loading and synthetic exosome-mimics as potential therapeutic tools. *Acta Pharmacol Sin*. 2018;39(4):542-551. doi:10.1038/aps.2017.178

44. Zhang Y, Liu Y, Liu H, Tang W. Exosomes: biogenesis, biologic function and clinical potential. *Cell Biosci*. 2019;9(1). doi:10.1186/s13578-019-0282-2

45. Kim S, Kim H, Park M et al. Caspase-8 controls the secretion of inflammatory lysyl-tRNA synthetase in exosomes from cancer cells. *Journal of Cell Biology*. 2017;216(7):2201-2216. doi:10.1083/jcb.201605118

46. Guix F, Sannerud R, Berditchevski F et al. Tetraspanin 6: a pivotal protein of the multiple vesicular body determining exosome release and lysosomal degradation of amyloid precursor protein fragments. *Mol Neurodegener*. 2017;12(1). doi:10.1186/s13024-017-0165-0

47. Morita E, Sandrin V, Chung H et al. Human ESCRT and ALIX proteins interact with proteins of the midbody and function in cytokinesis. *EMBO J*. 2007;26(19):4215-4227. doi:10.1038/sj.emboj.7601850

48. Théry C, Boussac M, Véron P et al. Proteomic Analysis of Dendritic Cell-Derived Exosomes: A Secreted Subcellular Compartment Distinct from Apoptotic Vesicles. *The Journal of Immunology*. 2001;166(12):7309-7318. doi:10.4049/jimmunol.166.12.7309

49. van Niel G, Porto-Carreiro I, Simoes S, Raposo G. Exosomes: A Common Pathway for a Specialized Function. *The Journal of Biochemistry*. 2006;140(1):13-21. doi:10.1093/jb/mvj128

50. Géminard C, de Gassart A, Blanc L, Vidal M. Degradation of AP2 During Reticulocyte Maturation Enhances Binding of Hsc70 and Alix to a Common Site on TfR for Sorting into Exosomes. *Traffic*. 2004;5(3):181-193. doi:10.1111/j.1600-0854.2004.0167.x

51. Kalra H, Simpson R, Ji H et al. Vesiclepedia: A Compendium for Extracellular Vesicles with Continuous Community Annotation. *PLoS Biol*. 2012;10(12):e1001450. doi:10.1371/journal.pbio.1001450

52. Karpievitch Y, Polpitiya A, Anderson G, Smith R, Dabney A. Liquid chromatography mass spectrometry-based proteomics: Biological and technological aspects. *Ann Appl Stat*. 2010;4(4). doi:10.1214/10-aoas341

53. Nesvizhskii A, Vitek O, Aebersold R. Analysis and validation of proteomic data generated by tandem mass spectrometry. *Nat Methods*. 2007;4(10):787-797. doi:10.1038/nmeth1088

54. Perkins D, Pappin D, Creasy D, Cottrell J. Probability-based protein identification by searching sequence databases using mass spectrometry data. *Electrophoresis*. 1999;20(18):3551-3567. doi:10.1002/(sici)1522-2683(19991201)20:18<3551::aid-elps3551>3.0.co;2-2

55. Khatri P, Sirota M, Butte A. Ten Years of Pathway Analysis: Current Approaches and Outstanding Challenges. *PLoS Comput Biol*. 2012;8(2):e1002375. doi:10.1371/journal.pcbi.1002375

56. Du J, Li M, Yuan Z et al. A decision analysis model for KEGG pathway analysis. *BMC Bioinformatics*. 2016;17(1). doi:10.1186/s12859-016-1285-1

57. Llorente A, Skotland T, Sylvänne T et al. Molecular lipidomics of exosomes released by PC-3 prostate cancer cells. *Biochimica et Biophysica Acta (BBA) - Molecular and Cell Biology of Lipids*. 2013;1831(7):1302-1309. doi:10.1016/j.bbalip.2013.04.011

58. Bucki R, Bachelot-Loza C, Zachowski A, Giraud F, Sulpice J. Calcium Induces Phospholipid Redistribution and Microvesicle Release in Human Erythrocyte Membranes

by Independent Pathways. *Biochemistry*. 1998;37(44):15383-15391. doi:10.1021/bi9805238

59. Pua H, Happ H, Gray C et al. Increased Hematopoietic Extracellular RNAs and Vesicles in the Lung during Allergic Airway Responses. *Cell Rep*. 2019;26(4):933-944.e4. doi:10.1016/j.celrep.2019.01.002

60. Murillo O, Thistlethwaite W, Rozowsky J et al. exRNA Atlas Analysis Reveals Distinct Extracellular RNA Cargo Types and Their Carriers Present across Human Biofluids. *Cell*. 2019;177(2):463-477.e15. doi:10.1016/j.cell.2019.02.018

61. Waldenström A, Gennebäck N, Hellman U, Ronquist G. Cardiomyocyte Microvesicles Contain DNA/RNA and Convey Biological Messages to Target Cells. *PLoS One*. 2012;7(4):e34653. doi:10.1371/journal.pone.0034653

62. Mulcahy L, Pink R, Carter D. Routes and mechanisms of extracellular vesicle uptake. *J Extracell Vesicles*. 2014;3(1):24641. doi:10.3402/jev.v3.24641

63. Svensson K, Christianson H, Wittrup A et al. Exosome Uptake Depends on ERK1/2-Heat Shock Protein 27 Signaling and Lipid Raft-mediated Endocytosis Negatively Regulated by Caveolin-1. *Journal of Biological Chemistry*. 2013;288(24):17713-17724. doi:10.1074/jbc.m112.445403

64. Fitzner D, Schnaars M, van Rossum D et al. Selective transfer of exosomes from oligodendrocytes to microglia by macropinocytosis. *J Cell Sci*. 2011;124(3):447-458. doi:10.1242/jcs.074088

65. Yuyama K, Sun H, Mitsutake S, Igarashi Y. Sphingolipid-modulated Exosome Secretion Promotes Clearance of Amyloid-β by Microglia. *Journal of Biological Chemistry*. 2012;287(14):10977-10989. doi:10.1074/jbc.m111.324616

66. Tian T, Zhu Y, Hu F, Wang Y, Huang N, Xiao Z. Dynamics of exosome internalization and trafficking. *J Cell Physiol*. 2013;228(7):1487-1495. doi:10.1002/jcp.24304

67. Montecalvo A, Larregina A, Shufesky W et al. Mechanism of transfer of functional microRNAs between mouse dendritic cells via exosomes. *Blood*. 2012;119(3):756-766. doi:10.1182/blood-2011-02-338004

68. Morelli A, Larregina A, Shufesky W et al. Endocytosis, intracellular sorting, and processing of exosomes by dendritic cells. *Blood*. 2004;104(10):3257-3266. doi:10.1182/blood-2004-03-0824

69. Escrevente C, Keller S, Altevogt P, Costa J. Interaction and uptake of exosomes by ovarian cancer cells. *BMC Cancer*. 2011;11(1). doi:10.1186/1471-2407-11-108

70. Feng D, Zhao W, Ye Y et al. Cellular Internalization of Exosomes Occurs Through Phagocytosis. *Traffic*. 2010;11(5):675-687. doi:10.1111/j.1600-0854.2010.01041.x

71. Fabbri M, Paone A, Calore F et al. MicroRNAs bind to Toll-like receptors to induce prometastatic inflammatory response. *Proceedings of the National Academy of Sciences*. 2012;109(31):E2110-E2116. doi:10.1073/pnas.1209414109

72. Christianson H, Svensson K, van Kuppevelt T, Li J, Belting M. Cancer cell exosomes depend on cell-surface heparan sulfate proteoglycans for their internalization and

functional activity. *Proceedings of the National Academy of Sciences*. 2013;110(43):17380-17385. doi:10.1073/pnas.1304266110

73. Flanagan M, Lin S. Cytochalasins block actin filament elongation by binding to high affinity sites associated with F-actin. *Journal of Biological Chemistry*. 1980;255(3):835-838. doi:10.1016/s0021-9258(19)86105-7

74. Lamaze C, Fujimoto L, Yin H, Schmid S. The Actin Cytoskeleton Is Required for Receptor-mediated Endocytosis in Mammalian Cells. *Journal of Biological Chemistry*. 1997;272(33):20332-20335. doi:10.1074/jbc.272.33.20332

75. Wang L, Rothberg K, Anderson R. Mis-assembly of clathrin lattices on endosomes reveals a regulatory switch for coated pit formation. *Journal of Cell Biology*. 1993;123(5):1107-1117. doi:10.1083/jcb.123.5.1107

76. Barrès C, Blanc L, Bette-Bobillo P et al. Galectin-5 is bound onto the surface of rat reticulocyte exosomes and modulates vesicle uptake by macrophages. *Blood*. 2010;115(3):696-705. doi:10.1182/blood-2009-07-231449

77. Kumari S, MG S, Mayor S. Endocytosis unplugged: multiple ways to enter the cell. *Cell Res*. 2010;20(3):256-275. doi:10.1038/cr.2010.19

78. Costa Verdera H, Gitz-Francois J, Schiffelers R, Vader P. Cellular uptake of extracellular vesicles is mediated by clathrin-independent endocytosis and macropinocytosis. *Journal of Controlled Release*. 2017;266:100-108. doi:10.1016/j.jconrel.2017.09.019

79. Yue K, Zhang P, Zheng M et al. Neurons can upregulate Cav-1 to increase intake of endothelial cells-derived extracellular vesicles that attenuate apoptosis via miR-1290. *Cell Death Dis*. 2019;10(12). doi:10.1038/s41419-019-2100-5

80. Rudt S, Müller R. In vitro phagocytosis assay of nano- and microparticles by chemiluminescence. III. Uptake of differently sized surface-modified particles, and its correlation to particle properties and in vivo distribution. *European Journal of Pharmaceutical Sciences*. 1993;1(1):31-39. doi:10.1016/0928-0987(93)90015-3

81. Stephens L, Ellson C, Hawkins P. Roles of PI3Ks in leukocyte chemotaxis and phagocytosis. *Curr Opin Cell Biol*. 2002;14(2):203-213. doi:10.1016/s0955-0674(02)00311-3

82. Rothman J. Control of Membrane Fusion in Exocytosis. *Biophys J*. 2013;104(2):11a. doi:10.1016/j.bpj.2012.11.089

83. Li S, Wei J, Zhang C et al. Cell-Derived Microparticles in Patients with Type 2 Diabetes Mellitus: a Systematic Review and Meta-Analysis. *Cellular Physiology and Biochemistry*. 2016;39(6):2439-2450. doi:10.1159/000452512

84. Lin W, Karin M. A cytokine-mediated link between innate immunity, inflammation, and cancer. *Journal of Clinical Investigation*. 2007;117(5):1175-1183. doi:10.1172/jci31537

85. Miyagawa T, Hasegawa K, Aoki Y et al. MT1-MMP recruits the ER-Golgi SNARE Bet1 for efficient MT1-MMP transport to the plasma membrane. *Journal of Cell Biology*. 2019;218(10):3355-3371. doi:10.1083/jcb.201808149

86. Skriner K, Adolph K, Jungblut P, Burmester G. Association of citrullinated proteins with synovial exosomes. *Arthritis & Rheumatism*. 2006;54(12):3809-3814. doi:10.1002/art.22276

87. Cloutier N, Tan S, Boudreau L et al. The exposure of autoantigens by microparticles underlies the formation of potent inflammatory components: the microparticle-associated immune complexes. *EMBO Mol Med*. 2012;5(2):235-249. doi:10.1002/emmm.201201846

88. Dinkins M, Dasgupta S, Wang G, Zhu G, Bieberich E. Exosome reduction in vivo is associated with lower amyloid plaque load in the 5XFAD mouse model of Alzheimer's disease. *Neurobiol Aging*. 2014;35(8):1792-1800. doi:10.1016/j.neurobiolaging.2014.02.012

89. Fuller O, Whitham M, Mathivanan S, Febbraio M. The Protective Effect of Exercise in Neurodegenerative Diseases: The Potential Role of Extracellular Vesicles. *Cells*. 2020;9(10):2182. doi:10.3390/cells9102182

90. Chan J, Morgan C, Adrian Leu N et al. Reproductive tract extracellular vesicles are sufficient to transmit intergenerational stress and program neurodevelopment. *Nat Commun*. 2020;11(1). doi:10.1038/s41467-020-15305-w

91. Urbanelli L, Buratta S, Tancini B et al. The Role of Extracellular Vesicles in Viral Infection and Transmission. *Vaccines (Basel)*. 2019;7(3):102. doi:10.3390/vaccines7030102

92. Balkwill F, Charles K, Mantovani A. Smoldering and polarized inflammation in the initiation and promotion of malignant disease. *Cancer Cell*. 2005;7(3):211-217. doi:10.1016/j.ccr.2005.02.013

93. Parmiani G, Maccalli C. The early antitumour immune response is necessary for tumour growth. *Oncoimmunology*. 2012;1(6):930-934. doi:10.4161/onci.21455

94. Rivoltini L, Canese P, Huber V et al. Escape strategies and reasons for failure in the interaction between tumour cells and the immune system: how can we tilt the balance towards immune-mediated cancer control?. *Expert Opin Biol Ther*. 2005;5(4):463-476. doi:10.1517/14712598.5.4.463

95. Zou W. Immunosuppressive networks in the tumour environment and their therapeutic relevance. *Nature Reviews Cancer*. 2005;5(4):263-274. doi:10.1038/nrc1586

96. Motz G, Coukos G. Deciphering and Reversing Tumour Immune Suppression. *Immunity*. 2013;39(1):61-73. doi:10.1016/j.immuni.2013.07.005

97. Raposo G, Stoorvogel W. Extracellular vesicles: Exosomes, microvesicles, and friends. *Journal of Cell Biology*. 2013;200(4):373-383. doi:10.1083/jcb.201211138

98. Simons M, Raposo G. Exosomes – vesicular carriers for intercellular communication. *Curr Opin Cell Biol*. 2009;21(4):575-581. doi:10.1016/j.ceb.2009.03.007

99. Balaj L, Lessard R, Dai L et al. Tumour microvesicles contain retrotransposon elements and amplified oncogene sequences. *Nat Commun*. 2011;2(1). doi:10.1038/ncomms1180

100. Cossetti C, Iraci N, Mercer T et al. Extracellular Vesicles from Neural Stem Cells Transfer IFN-γ via Ifngr1 to Activate Stat1 Signaling in Target Cells. *Mol Cell*. 2014;56(4):609. doi:10.1016/j.molcel.2014.11.009

101. Kalra H, Drummen G, Mathivanan S. Focus on Extracellular Vesicles: Introducing the Next Small Big Thing. *Int J Mol Sci*. 2016;17(2):170. doi:10.3390/ijms17020170

102. Valadi H, Ekström K, Bossios A, Sjöstrand M, Lee J, Lötvall J. Exosome-mediated transfer of mRNAs and microRNAs is a novel mechanism of genetic exchange between cells. *Nat Cell Biol*. 2007;9(6):654-659. doi:10.1038/ncb1596

103. Hong B, Cho J, Kim H et al. Colorectal cancer cell-derived microvesicles are enriched in cell cycle-related mRNAs that promote proliferation of endothelial cells. *BMC Genomics*. 2009;10(1):556. doi:10.1186/1471-2164-10-556

104. Kogure T, Lin W, Yan I, Braconi C, Patel T. Intercellular nanovesicle-mediated microRNA transfer: A mechanism of environmental modulation of hepatocellular cancer cell growth. *Hepatology*. 2011;54(4):1237-1248. doi:10.1002/hep.24504

105. Zhang L, Zhang S, Yao J et al. Microenvironment-induced PTEN loss by exosomal microRNA primes brain metastasis outgrowth. *Nature*. 2015;527(7576):100-104. doi:10.1038/nature15376

106. Challagundla K, Wise P, Neviani P et al. Exosome-Mediated Transfer of microRNAs Within the Tumour Microenvironment and Neuroblastoma Resistance to Chemotherapy. *JNCI: Journal of the National Cancer Institute*. 2015;107(7). doi:10.1093/jnci/djv135

107. Kosaka N, Iguchi H, Hagiwara K, Yoshioka Y, Takeshita F, Ochiya T. Neutral Sphingomyelinase 2 (nSMase2)-dependent Exosomal Transfer of Angiogenic MicroRNAs Regulate Cancer Cell Metastasis*. *Journal of Biological Chemistry*. 2013;288(15):10849-10859. doi:10.1074/jbc.m112.446831

108. Fabbri M, Paone A, Calore F et al. MicroRNAs bind to Toll-like receptors to induce prometastatic inflammatory response. *Proceedings of the National Academy of Sciences*. 2012;109(31):E2110-E2116. doi:10.1073/pnas.1209414109

109. Fong M, Zhou W, Liu L et al. Breast-cancer-secreted miR-122 reprograms glucose metabolism in premetastatic niche to promote metastasis. *Nat Cell Biol*. 2015;17(2):183-194. doi:10.1038/ncb3094

110. Katsuda T, Kosaka N, Ochiya T. The roles of extracellular vesicles in cancer biology: Toward the development of novel cancer biomarkers. *Proteomics*. 2014;14(4-5):412-425. doi:10.1002/pmic.201300389

111. Pegtel D, Cosmopoulos K, Thorley-Lawson D et al. Functional delivery of viral miRNAs via exosomes. *Proceedings of the National Academy of Sciences*. 2010;107(14):6328-6333. doi:10.1073/pnas.0914843107

112. Zhang Y, Liu D, Chen X et al. Secreted Monocytic miR-150 Enhances Targeted Endothelial Cell Migration. *Mol Cell*. 2010;39(1):133-144. doi:10.1016/j.molcel.2010.06.010

113. Webber J, Spary L, Sanders A et al. Differentiation of tumour-promoting stromal myofibroblasts by cancer exosomes. *Oncogene*. 2014;34(3):290-302. doi:10.1038/onc.2013.560

114. Rana S, Malinowska K, Zöller M. Exosomal Tumour MicroRNA Modulates Premetastatic Organ Cells. *Neoplasia*. 2013;15(3):281-IN31. doi:10.1593/neo.122010

115. Kosaka N, Iguchi H, Yoshioka Y, Takeshita F, Matsuki Y, Ochiya T. Secretory Mechanisms and Intercellular Transfer of MicroRNAs in Living Cells. *Journal of Biological Chemistry*. 2010;285(23):17442-17452. doi:10.1074/jbc.m110.107821

116. Jung T, Castellana D, Klingbeil P et al. CD44v6 Dependence of Premetastatic Niche Preparation by Exosomes. *Neoplasia*. 2009;11(10):1093-IN17. doi:10.1593/neo.09822

117. Al-Mehdi A, Tozawa K, Fisher A, Shientag L, Lee A, Muschel R. Intravascular origin of metastasis from the proliferation of endothelium-attached tumour cells: a new model for metastasis. *Nat Med*. 2000;6(1):100-102. doi:10.1038/71429

118. Fujita Y, Yoshioka Y, Ochiya T. Extracellular vesicle transfer of cancer pathogenic components. *Cancer Sci*. 2016;107(4):385-390. doi:10.1111/cas.12896

119. Peinado H, Alečković M, Lavotshkin S et al. Melanoma exosomes educate bone marrow progenitor cells toward a pro-metastatic phenotype through MET. *Nat Med*. 2012;18(6):883-891. doi:10.1038/nm.2753

120. Somasundaram R, Herlyn M. Melanoma exosomes: messengers of metastasis. *Nat Med*. 2012;18(6):853-854. doi:10.1038/nm.2775

121. Zhou W, Fong M, Min Y et al. Cancer-Secreted miR-105 Destroys Vascular Endothelial Barriers to Promote Metastasis. *Cancer Cell*. 2014;25(4):501-515. doi:10.1016/j.ccr.2014.03.007

122. Gilligan K, Dwyer R. Extracellular Vesicles for Cancer Therapy: Impact of Host Immune Response. *Cells*. 2020;9(1):224. doi:10.3390/cells9010224

123. Pirisinu M, Pham T, Zhang D, Hong T, Nguyen L, Le M. Extracellular vesicles as natural therapeutic agents and innate drug delivery systems for cancer treatment: Recent advances, current obstacles, and challenges for clinical translation. *Semin Cancer Biol*. 2020. doi:10.1016/j.semcancer.2020.08.007

124. Dai S, Wei D, Wu Z et al. Phase I Clinical Trial of Autologous Ascites-derived Exosomes Combined With GM-CSF for Colorectal Cancer. *Molecular Therapy*. 2008. doi:10.1038/sj.mt.6300407

125. Schadendorf D, Nestle F, Broecker E et al. Dacarbacine (DTIC) versus vaccination with autologous peptide-pulsed dendritic cells (DC) as first-line treatment of patients with metastatic melanoma: Results of a prospective-randomized phase III study. *Journal of Clinical Oncology*. 2004;22(14_suppl):7508-7508. doi:10.1200/jco.2004.22.90140.7508

126. Butts C. O-083 A multicenter phase IIB randomized study of the liposomal MUC1 vaccine L-BLP25 for immunotherapy of advanced non-small cell lung cancer (NSCLC). *Lung Cancer*. 2005;49:S30. doi:10.1016/s0169-5002(05)80216-8

127. Lu Z, Zuo B, Jing R et al. Dendritic cell-derived exosomes elicit tumour regression in autochthonous hepatocellular carcinoma mouse models. *J Hepatol*. 2017;67(4):739-748. doi:10.1016/j.jhep.2017.05.019

128. Zaharie F, Muresan M, Petrushev B et al. Exosome-Carried microRNA-375 Inhibits Cell Progression and Dissemination via Bcl-2 Blocking in Colon Cancer. *Journal of Gastrointestinal and Liver Diseases*. 2015;24(4):435-443. doi:10.15403/jgld.2014.1121.244.375

129. Chen W, Quan Y, Fan S et al. Exosome-transmitted circular RNA hsa_circ_0051443 suppresses hepatocellular carcinoma progression. *Cancer Lett*. 2020;475:119-128. doi:10.1016/j.canlet.2020.01.022

130. Pakravan K, Babashah S, Sadeghizadeh M et al. MicroRNA-100 shuttled by mesenchymal stem cell-derived exosomes suppresses in vitro angiogenesis through modulating the mTOR/HIF-1α/VEGF signaling axis in breast cancer cells. *Cellular Oncology*. 2017;40(5):457-470. doi:10.1007/s13402-017-0335-7

131. Eichner N, Gilbertson N, Gaitan J et al. Low cardiorespiratory fitness is associated with higher extracellular vesicle counts in obese adults. *Physiol Rep*. 2018;6(10):e13701. doi:10.14814/phy2.13701

132. Loh Y. Welcome to the journal of Extracellular Vesicles and Circulating Nucleic Acids: a new open-access scientific journal. *Extracell Vesicles Circ Nucl Acids*. 2020. doi:10.20517/evcna.2020.03

133. Chironi G, Simon A, Hugel B et al. Circulating Leukocyte-Derived Microparticles Predict Subclinical Atherosclerosis Burden in Asymptomatic Subjects. *Arterioscler Thromb Vasc Biol*. 2006;26(12):2775-2780. doi:10.1161/01.atv.0000249639.36915.04

134. Heiss C, Amabile N, Lee A et al. Brief Secondhand Smoke Exposure Depresses Endothelial Progenitor Cells Activity and Endothelial Function. *J Am Coll Cardiol*. 2008;51(18):1760-1771. doi:10.1016/j.jacc.2008.01.040

135. Diehl K, Hull R, Morton D et al. A good practice guide to the administration of substances and removal of blood, including routes and volumes. *Journal of Applied Toxicology*. 2001;21(1):15-23. doi:10.1002/jat.727

136. Myers D, Hawley A, Longo C et al. D-dimer, P-selectin, and microparticles: Novel markers to predict deep venous thrombosis. *Thromb Haemost*. 2005;94(12):1312-1317. doi:10.1160/th05-06-0426

137. Li P, Qin C. Elevated Circulating VE-Cadherin+CD144+Endothelial Microparticles in Ischemic Cerebrovascular Disease. *Thromb Res*. 2015;135(2):375-381. doi:10.1016/j.thromres.2014.12.006

138. König L, Kasimir-Bauer S, Bittner A et al. Elevated levels of extracellular vesicles are associated with therapy failure and disease progression in breast cancer patients undergoing neoadjuvant chemotherapy. *Oncoimmunology*. 2017;7(1):e1376153. doi:10.1080/2162402x.2017.1376153

139. Ha D, Yang N, Nadithe V. Exosomes as therapeutic drug carriers and delivery vehicles across biological membranes: current perspectives and future challenges. *Acta Pharmaceutica Sinica B*. 2016;6(4):287-296. doi:10.1016/j.apsb.2016.02.001

140. Correction: Pancreatic Cancer-Derived Exosomes Causes Paraneoplastic β-cell Dysfunction. *Clinical Cancer Research*. 2015;21(19):4495-4495. doi:10.1158/1078-0432.ccr-15-1524

141. Mentkowski K, Lang J. Exosomes Engineered to Express a Cardiomyocyte Binding Peptide Demonstrate Improved Cardiac Retention in Vivo. *Sci Rep*. 2019;9(1). doi:10.1038/s41598-019-46407-1

142. Yang T, Martin P, Fogarty B et al. Exosome Delivered Anticancer Drugs Across the Blood-Brain Barrier for Brain Cancer Therapy in Danio Rerio. *Pharm Res*. 2015;32(6):2003-2014. doi:10.1007/s11095-014-1593-y

143. Wang C, Chen C, Lin W et al. Direct intramyocardial injection of mesenchymal stem cell sheet fragments improves cardiac functions after infarction. *Cardiovasc Res*. 2007;77(3):515-524. doi:10.1093/cvr/cvm046

144. Sun H, Burrola S, Wu J, Ding W. Extracellular Vesicles in the Development of Cancer Therapeutics. *Int J Mol Sci*. 2020;21(17):6097. doi:10.3390/ijms21176097

145. Sung H, Ferlay J, Siegel R et al. Global Cancer Statistics 2020: GLOBOCAN Estimates of Incidence and Mortality Worldwide for 36 Cancers in 185 Countries. *CA Cancer J Clin*. 2021;71(3):209-249. doi:10.3322/caac.21660

146. Deaths registered in England and Wales in 2010, by cause. *Monthly Digest of Statistics*. 2011;790(1):159-174. doi:10.1057/mds.2011.82

147. Nutting C. Cancer. Principles & practice of oncology (6th edn). Ed. by V T DeVita Jr, S Hellman and S A Rosenburg, pp. lxxii+3235, 2001 (Lippincott Williams & Wilkins, Philadelphia, PA), $235.00 ISBN 0-781-72229-2. *Br J Radiol*. 2002;75(894):567-567. doi:10.1259/bjr.75.894.750567a

148. Shepherd F. Maintenance Therapy Comes of Age for Non–Small-Cell Lung Cancer, but at What Cost?. *Journal of Clinical Oncology*. 2011;29(31):4068-4070. doi:10.1200/jco.2011.37.8349

149. Ferlay J, Autier P, Boniol M, Heanue M, Colombet M, Boyle P. Estimates of the cancer incidence and mortality in Europe in 2006. *Annals of Oncology*. 2007;18(3):581-592. doi:10.1093/annonc/mdl498

150. Lung cancer pathology in smokers, ex-smokers and never smokers. *Lung Cancer*. 1995;12(3):277. doi:10.1016/0169-5002(95)98756-z

151. Chang B, Park C, Choy H. Current Update on the Management of Locally Advanced Non-small Cell Lung Cancer. *J Lung Cancer*. 2006;5(1):1. doi:10.6058/jlc.2006.5.1.1

152. Gabor S. Invasion of blood vessels as significant prognostic factor in radically resected T1-3N0M0 non-small-cell lung cancer. *European Journal of Cardio-Thoracic Surgery*. 2004;25(3):439-442. doi:10.1016/j.ejcts.2003.11.033

153. Ettinger D, Aisner J. Changing Face of Small-Cell Lung Cancer: Real and Artifact. *Journal of Clinical Oncology*. 2006;24(28):4526-4527. doi:10.1200/jco.2006.07.3841

154. Skeletal muscle metastases from lung cancer. *Lung Cancer*. 1987;3(3-4):142. doi:10.1016/s0169-5002(87)80199-x

155. Lomonosova E, Chinnadurai G. BH3-only proteins in apoptosis and beyond: an overview. *Oncogene*. 2008;27(S1):S2-S19. doi:10.1038/onc.2009.39

156. Jan R, Chaudhry G. Understanding Apoptosis and Apoptotic Pathways Targeted Cancer Therapeutics. *Adv Pharm Bull*. 2019;9(2):205-218. doi:10.15171/apb.2019.024

157. Fulda S, Debatin K. Extrinsic versus intrinsic apoptosis pathways in anticancer chemotherapy. *Oncogene*. 2006;25(34):4798-4811. doi:10.1038/sj.onc.1209608

158. Igney F, Krammer P. Death and anti-death: tumour resistance to apoptosis. *Nature Reviews Cancer*. 2002;2(4):277-288. doi:10.1038/nrc776

159. Zaman S, Wang R, Gandhi V. Targeting the apoptosis pathway in hematologic malignancies. *Leuk Lymphoma*. 2014;55(9):1980-1992. doi:10.3109/10428194.2013.855307

160. Goldar S, Khaniani M, Derakhshan S, Baradaran B. Molecular Mechanisms of Apoptosis and Roles in Cancer Development and Treatment. *Asian Pacific Journal of Cancer Prevention*. 2015;16(6):2129-2144. doi:10.7314/apjcp.2015.16.6.2129

161. Apoptosis: A Target for Anticancer Therapy. *Int J Mol Sci*. 2018;19(2):448. doi:10.3390/ijms19020448

162. Oltersdorf T, Elmore S, Shoemaker A et al. An inhibitor of Bcl-2 family proteins induces regression of solid tumours. *Nature*. 2005;435(7042):677-681. doi:10.1038/nature03579

163. Deveraux Q. IAPs block apoptotic events induced by caspase-8 and cytochrome c by direct inhibition of distinct caspases. *EMBO J*. 1998;17(8):2215-2223. doi:10.1093/emboj/17.8.2215

164. Lopez J, Tait S. Mitochondrial apoptosis: killing cancer using the enemy within. *Br J Cancer*. 2015;112(6):957-962. doi:10.1038/bjc.2015.85

165. Perotti A, Maur M, Viganò L et al. Phase Ib pharmacokinetic (PK) and pharmacodynamic (PD) study to define the optimal dose for combining the mTOR inhibitor AP23573 with capecitabine (CAPE). *Journal of Clinical Oncology*. 2006;24(18_suppl):3065-3065. doi:10.1200/jco.2006.24.18_suppl.3065

166. Chou W, Dang C. Acute promyelocytic leukemia: recent advances in therapy and molecular basis of response to arsenic therapies. *Curr Opin Hematol*. 2005;12(1):1-6. doi:10.1097/01.moh.0000148552.93303.45

167. Saint-Pol J, Gosselet F, Duban-Deweer S, Pottiez G, Karamanos Y. Targeting and Crossing the Blood-Brain Barrier with Extracellular Vesicles. *Cells*. 2020;9(4):851. doi:10.3390/cells9040851

168. Fidler I, Kripke M. The challenge of targeting metastasis. *Cancer and Metastasis Reviews*. 2015;34(4):635-641. doi:10.1007/s10555-015-9586-9

169. Dai J, Lu Y, Roca H et al. Immune mediators in the tumour microenvironment of prostate cancer. *Chin J Cancer*. 2017;36(1). doi:10.1186/s40880-017-0198-3

170. SARMA D, KOVAC A, SOCORRO N. Metastatic Carcinoma of the Skeletal Muscle. *South Med J*. 1981;74(4):484-485. doi:10.1097/00007611-198104000-00028

171. Plaza J, Perez-Montiel D, Mayerson J, Morrison C, Suster S. Metastases to soft tissue. *Cancer*. 2007;112(1):193-203. doi:10.1002/cncr.23151

172. Ali S. Skeletal Muscle Metastasis from Non Small Cell Lung Cancer (NSCLC) a Rare Case Report. *Open Access Journal of Surgery*. 2016;1(5). doi:10.19080/oajs.2016.01.555573

173. SUDO A, OGIHARA Y, SHIOKAWA Y, FUJINAMI S, SEKIGUCHI S. Intramuscular Metastasis of Carcinoma. *Clin Orthop Relat Res*. 1993;&NA;(296):213???217. doi:10.1097/00003086-199311000-00036

174. Freeman C. Skin Metastasis From Malignant Neoplasms-Reply. *Arch Dermatol*. 1983;119(2):98. doi:10.1001/archderm.1983.01650260006006

175. Hasegawa S, Sakurai Y, Imazu H et al. Metastasis to the Forearm Skeletal Muscle from an Adenocarcinoma of the Colon: Report of a Case. *Surg Today*. 2000;30(12):1118-1123. doi:10.1007/s005950070013

176. Hur J, Yoon C, Jung W. Multiple skeletal muscle metastases from renal cell carcinoma 19 years after radical nephrectomy. *Acta radiol*. 2007;48(2):238-241. doi:10.1080/02841850601089128

177. Carter R. The Spread of Tumours in the Human Body. *J Clin Pathol*. 1974;27(5):432-433. doi:10.1136/jcp.27.5.432-c

178. McNally O, Hughes S, Clarke J, Lynch T. A5 Unsuspected soft tissue and skeletal metastases detected by PET/CT when compared to conventional imaging. *Nucl Med Commun*. 2006;27(12):1014. doi:10.1097/00006231-200612000-00019

179. Surov A, Köhler J, Wienke A et al. Muscle metastases: comparison of features in different primary tumours. *Cancer Imaging*. 2014;14(1). doi:10.1186/1470-7330-14-21

180. Weiss L. Biomechanical interactions of cancer cells with the microvasculature during hematogenous metastasis. *Cancer and Metastasis Reviews*. 1992;11(3-4):227-235. doi:10.1007/bf01307179

181. Giovannucci E. Physical Activity, Obesity, and Risk for Colon Cancer and Adenoma in Men. *Ann Intern Med*. 1995;122(5):327. doi:10.7326/0003-4819-122-5-199503010-00002

182. McTiernan A. Physical Activity, Weight, Diet, and Breast Cancer Risk Reduction. *Arch Intern Med*. 2010;170(20). doi:10.1001/archinternmed.2010.416

183. Hiroux C, Vandoorne T, Koppo K, De Smet S, Hespel P, Berardi E. Physical activity counteracts tumour cell growth in colon carcinoma C26-injected muscles: an interim report. *Eur J Transl Myol*. 2016;26(2). doi:10.4081/ejtm.2016.5958

184. Seely S. Possible reasons for the high resistance of muscle to cancer. *Med Hypotheses*. 1980;6(2):133-137. doi:10.1016/0306-9877(80)90079-1

185. Bar-Yehuda S, Barer F, Volisson L, Fishman P. Resistance of Muscle to Tumour Metastases: A Role for A3 Adenosine Receptor Agonists. *Neoplasia*. 2001;3(2):125-131. doi:10.1038/sj.neo.7900138

186. Parlakian A, Gomaa I, Solly S et al. Skeletal Muscle Phenotypically Converts and Selectively Inhibits Metastatic Cells in Mice. *PLoS One*. 2010;5(2):e9299. doi:10.1371/journal.pone.0009299

187. Fishman P, Bar-Yehuda S, Barer F, Madi L, Multani A, Pathak S. The A3 Adenosine Receptor as a New Target for Cancer Therapy and Chemoprotection. *Exp Cell Res*. 2001;269(2):230-236. doi:10.1006/excr.2001.5327

188. Husmann I, Soulet L, Gautron J, Martelly I, Barritault D. Growth factors in skeletal muscle regeneration. *Cytokine Growth Factor Rev*. 1996;7(3):249-258. doi:10.1016/s1359-6101(96)00029-9

189. Birnbaum M, Trink B, Shainberg A, Salzberg S. Activation of the interferon system during myogenesis in vitro. *Differentiation*. 1990;45(2):138-145. doi:10.1111/j.1432-0436.1990.tb00467.x

190. ROSZTÓCZY I, MEGYERI K, PAPÓS M. Interferon Production by Normal Mouse Tissues in Organ Cultures. *J Interferon Res*. 1989;9(5):509-515. doi:10.1089/jir.1989.9.509

191. Lafyatis R, Lechleider R, Roberts A, Sporn M. Secretion and transcriptional regulation of transforming growth factor-beta 3 during myogenesis. *Mol Cell Biol*. 1991;11(7):3795-3803. doi:10.1128/mcb.11.7.3795

192. Takada S, Nagato Y, Yamamura M. Effect of cyclic polylactates on tumour cells and tumour bearing mice. *IUBMB Life*. 1997;43(1):9-17. doi:10.1080/15216549700203761

193. Rome S, Forterre A, Mizgier M, Bouzakri K. Skeletal Muscle-Released Extracellular Vesicles: State of the Art. *Front Physiol*. 2019;10. doi:10.3389/fphys.2019.00929

194. Güller I, Russell A. MicroRNAs in skeletal muscle: their role and regulation in development, disease and function. *J Physiol*. 2010;588(21):4075-4087. doi:10.1113/jphysiol.2010.194175

195. Drummond M, Glynn E, Fry C, Dhanani S, Volpi E, Rasmussen B. Essential Amino Acids Increase MicroRNA-499, -208b, and -23a and Downregulate Myostatin and Myocyte Enhancer Factor 2C mRNA Expression in Human Skeletal Muscle. *J Nutr*. 2009;139(12):2279-2284. doi:10.3945/jn.109.112797

196. He W, Calore F, Londhe P, Canella A, Guttridge D, Croce C. Microvesicles containing miRNAs promote muscle cell death in cancer cachexia via TLR7. *Proceedings of the National Academy of Sciences*. 2014;111(12):4525-4529. doi:10.1073/pnas.1402714111

197. Zablocki D, Sadoshima J. Inside-Out Signaling. *Circulation*. 2015;131(24):2097-2100. doi:10.1161/circulationaha.115.016978

198. Loprinzi P. Memory may be Enhanced from Exercise-Induced Myokine Production of Cathepsin B. *J Behav Health*. 2019;(0):1. doi:10.5455/jbh.20180827014702

199. Severinsen M, Pedersen B. Muscle–Organ Crosstalk: The Emerging Roles of Myokines. *Endocr Rev*. 2020;41(4):594-609. doi:10.1210/endrev/bnaa016

200. Whitham M, Febbraio M. The ever-expanding myokinome: discovery challenges and therapeutic implications. *Nature Reviews Drug Discovery*. 2016;15(10):719-729. doi:10.1038/nrd.2016.153

201. Bi X, Tong C, Dockendorff A et al. Genetic deficiency of decorin causes intestinal tumour formation through disruption of intestinal cell maturation. *Carcinogenesis*. 2008;29(7):1435-1440. doi:10.1093/carcin/bgn141

202. Yamaguchi Y, Mann D, Ruoslahti E. Negative regulation of transforming growth factor-β by the proteoglycan decorin. *Nature*. 1990;346(6281):281-284. doi:10.1038/346281a0

203. WU H, WANG S, XUE A et al. Overexpression of decorin induces apoptosis and cell growth arrest in cultured rat mesangial cellsin vitro. *Nephrology*. 2008;13(7):607-615. doi:10.1111/j.1440-1797.2008.00961.x

204. Wolin K, Yan Y, Colditz G. Physical activity and risk of colon adenoma: a meta-analysis. *Br J Cancer*. 2011;104(5):882-885. doi:10.1038/sj.bjc.6606045

205. Bar-Yehuda S, Barer F, Volisson L, Fishman P. Resistance of Muscle to Tumour Metastases: A Role for A3 Adenosine Receptor Agonists. *Neoplasia*. 2001;3(2):125-131. doi:10.1038/sj.neo.7900138

206. Weiss L. Biomechanical destruction of cancer cells in skeletal muscle: a rate-regulator for hematogenous metastasis. *Clin Exp Metastasis*. 1989;7(5):483-491. doi:10.1007/bf01753809

207. Herbowski L. Missing Skeletal Muscle Metastases of Papillary Thyroid Carcinoma. *Diagnostics*. 2020;10(7):457. doi:10.3390/diagnostics10070457

208. Walsh T, Poole A. Do platelets promote cardiac recovery after myocardial infarction: roles beyond occlusive ischemic damage. *American Journal of Physiology-Heart and Circulatory Physiology*. 2018;314(5):H1043-H1048. doi:10.1152/ajpheart.00134.2018

209. György B, Hung M, Breakefield X, Leonard J. Therapeutic Applications of Extracellular Vesicles: Clinical Promise and Open Questions. *Annu Rev Pharmacol Toxicol*. 2015;55(1):439-464. doi:10.1146/annurev-pharmtox-010814-124630

210. Sinha K, Yarmand R, Kahraman N et al. Abstract 1156: Skeletal muscle progenitor cell-derived exosomes have therapeutic potential in inhibition of prostate cancer cell proliferation. *Tumour Biology*. 2019. doi:10.1158/1538-7445.am2019-1156

211. Maglara A, Vasilaki A, Jackson M, McArdle A. Damage to developing mouse skeletal muscle myotubes in culture: protective effect of heat shock proteins. *J Physiol*. 2003;548(3):837-846. doi:10.1113/jphysiol.2002.034520

212. Hu T, Hu J. Melanoma-derived exosomes induce reprogramming fibroblasts into cancer-associated fibroblasts via Gm26809 delivery. *Cell Cycle*. 2019;18(22):3085-3094. doi:10.1080/15384101.2019.1669380

213. Peck A, Bach F. A miniaturized mouse mixed leukocyte culture in serum-free and mouse serum supplemented media. *J Immunol Methods*. 1973;3(2):147-163. doi:10.1016/0022-1759(73)90030-6

214. Rajah T, Rajah T, Rambo D et al. Influence of Antiestrogens on NIH-3T3-Fibroblast-Induced Motility of Breast Cancer Cells. *Chemotherapy*. 2000;47(1):56-69. doi:10.1159/000048502

215. Imaging the Role of the Tumour Microenvironment in Tumour Progression and Metastasis. *Cancer Cell Microenviron*. 2016. doi:10.14800/ccm.1206

216. Olechnowicz S, Edwards C. Contributions of the Host Microenvironment to Cancer-Induced Bone Disease. *Cancer Res*. 2014;74(6):1625-1631. doi:10.1158/0008-5472.can-13-2645

217. Melaiu O, Lucarini V, Cifaldi L, Fruci D. Influence of the Tumour Microenvironment on NK Cell Function in Solid Tumours. *Front Immunol*. 2020;10. doi:10.3389/fimmu.2019.03038

218. The Role of Microenvironment in Tumourigenesis: Focus on Dendritic Cells in Human Papillomavirus E6, E7-transformed keratinocytes. *Cancer Cell Microenviron*. 2015. doi:10.14800/ccm.874

219. Ren R, Sun H, Ma C, Liu J, Wang H. Colon cancer cells secrete exosomes to promote self-proliferation by shortening mitosis duration and activation of STAT3 in a hypoxic environment. *Cell Biosci*. 2019;9(1). doi:10.1186/s13578-019-0325-8

220. Soldevilla B, Rodríguez M, San Millán C et al. Tumour-derived exosomes are enriched in ΔNp73, which promotes oncogenic potential in acceptor cells and correlates with patient survival. *Hum Mol Genet*. 2013;23(2):467-478. doi:10.1093/hmg/ddt437

221. Jackson M, Maglara A, McArdle. Heat shock proteins and skeletal muscle reponse to exercise-induced oxidative stress. *Pathophysiology*. 1998;5:112. doi:10.1016/s0928-4680(98)80720-7

222. Sabanovic B, Piva F, Cecati M, Giulietti M. Promising Extracellular Vesicle-Based Vaccines against Viruses, Including SARS-CoV-2. *Biology (Basel)*. 2021;10(2):94. doi:10.3390/biology10020094

223. Bernardi S, Zanaglio C, Farina M, Polverelli N, Malagola M, Russo D. dsDNA from extracellular vesicles (EVs) in adult AML. *Ann Hematol*. 2020;100(5):1355-1356. doi:10.1007/s00277-020-04109-z

224. Sheehan C, D'Souza-Schorey C. Tumour-derived extracellular vesicles: molecular parcels that enable regulation of the immune response in cancer. *J Cell Sci*. 2019;132(20). doi:10.1242/jcs.235085

225. Holdenrieder S. Extracellular vesicles as gold mine for new diagnostic and therapeutic approaches in medicine. *How cells communicate - an introduction to extracellular vesicles*. 2019;1(1):10-17. doi:10.47184/tev.2019.01.01

226. Joshi B, de Beer M, Giepmans B, Zuhorn I. Endocytosis of Extracellular Vesicles and Release of Their Cargo from Endosomes. *ACS Nano*. 2020;14(4):4444-4455. doi:10.1021/acsnano.9b10033

227. Progatzky F, Dallman M, Lo Celso C. From seeing to believing: labelling strategies for in vivo cell-tracking experiments. *Interface Focus*. 2013;3(3):20130001. doi:10.1098/rsfs.2013.0001

228. Jurgielewicz B, Yao Y, Stice S. Kinetics and Specificity of HEK293T Extracellular Vesicle Uptake using Imaging Flow Cytometry. *Nanoscale Res Lett*. 2020;15(1). doi:10.1186/s11671-020-03399-6

229. McGuigan C, Li X. Cytotoxicity and genotoxicity of phenazine in two human cell lines. *Toxicology in Vitro*. 2014;28(4):607-615. doi:10.1016/j.tiv.2013.12.007

230. T R, A N, R M, N K, J V. Cytotoxicity Assays: In Vitro Methods to Measure Dead Cells. PubMed. https://pubmed.ncbi.nlm.nih.gov/31070879/. Published 2021. Accessed June 8, 2021.

231. Kumar P, Nagarajan A, Uchil P. Analysis of Cell Viability by the Lactate Dehydrogenase Assay. *Cold Spring Harb Protoc*. 2018;2018(6):pdb.prot095497. doi:10.1101/pdb.prot095497

232. Boya P, Kroemer G. Lysosomal membrane permeabilization in cell death. *Oncogene*. 2008;27(50):6434-6451. doi:10.1038/onc.2008.310

233. Guicciardi M, Leist M, Gores G. Lysosomes in cell death. *Oncogene*. 2004;23(16):2881-2890. doi:10.1038/sj.onc.1207512

234. Kroemer G, Jäättelä M. Lysosomes and autophagy in cell death control. *Nature Reviews Cancer*. 2005;5(11):886-897. doi:10.1038/nrc1738

235. Tardy C, Codogno P, Autefage H, Levade T, Andrieu-Abadie N. Lysosomes and lysosomal proteins in cancer cell death (new players of an old struggle). *Biochimica et Biophysica Acta (BBA) - Reviews on Cancer*. 2006;1765(2):101-125. doi:10.1016/j.bbcan.2005.11.003

236. Terman A, Kurz T, Gustafsson B, Brunk U. Lysosomal labilization. *IUBMB Life (International Union of Biochemistry and Molecular Biology: Life)*. 2006;58(9):531-539. doi:10.1080/15216540600904885

237. Wong Y, Ysselstein D, Krainc D. Mitochondria–lysosome contacts regulate mitochondrial fission via RAB7 GTP hydrolysis. *Nature*. 2018;554(7692):382-386. doi:10.1038/nature25486

238. Li N, Zhan X. Mitochondrial Dysfunction Pathway Networks and Mitochondrial Dynamics in the Pathogenesis of Pituitary Adenomas. *Front Endocrinol (Lausanne)*. 2019;10. doi:10.3389/fendo.2019.00690

239. Sukhai M, Prabha S, Hurren R et al. Lysosomal disruption preferentially targets acute myeloid leukemia cells and progenitors.

240. Zhitomirsky B, Assaraf Y. Lysosomes as mediators of drug resistance in cancer. *Drug Resistance Updates*. 2016;24:23-33. doi:10.1016/j.drup.2015.11.004

241. Ono K, Kim S, Han J. Susceptibility of Lysosomes to Rupture Is a Determinant for Plasma Membrane Disruption in Tumour Necrosis Factor Alpha-Induced Cell Death. *Mol Cell Biol*. 2003;23(2):665-676. doi:10.1128/mcb.23.2.665-676.2003

242. Zhang X, Cheng X, Yu L et al. MCOLN1 is a ROS sensor in lysosomes that regulates autophagy. *Nat Commun*. 2016;7(1). doi:10.1038/ncomms12109

243. Poot M, Zhang Y, Krämer J et al. Analysis of mitochondrial morphology and function with novel fixable fluorescent stains. *Journal of Histochemistry & Cytochemistry*. 1996;44(12):1363-1372. doi:10.1177/44.12.8985128

244. Pendergrass W, Wolf N, Poot M. Efficacy of MitoTracker Green? and CMXrosamine to measure changes in mitochondrial membrane potentials in living cells and tissues. *Cytometry*. 2004;61A(2):162-169. doi:10.1002/cyto.a.20033

245. Perry S, Norman J, Barbieri J, Brown E, Gelbard H. Mitochondrial membrane potential probes and the proton gradient: a practical usage guide. *Biotechniques*. 2011;50(2):98-115. doi:10.2144/000113610

246. Meers P, Mealy T. Phospholipid Determinants for Annexin V Binding Sites and the Role of Tryptophan 187. *Biochemistry*. 1994;33(19):5829-5837. doi:10.1021/bi00185a022

247. Martin S, Reutelingsperger C, McGahon A et al. Early redistribution of plasma membrane phosphatidylserine is a general feature of apoptosis regardless of the initiating stimulus: inhibition by overexpression of Bcl-2 and Abl. *Journal of Experimental Medicine*. 1995;182(5):1545-1556. doi:10.1084/jem.182.5.1545

248. Logue S, Elgendy M, Martin S. Expression, purification and use of recombinant annexin V for the detection of apoptotic cells. *Nat Protoc*. 2009;4(9):1383-1395. doi:10.1038/nprot.2009.143

249. Schmid I, Uittenbogaart C, Jamieson B. Live-cell assay for detection of apoptosis by dual-laser flow cytometry using Hoechst 33342 and 7-amino-actinomycin D. *Nat Protoc*. 2007;2(1):187-190. doi:10.1038/nprot.2006.458

250. Retracted: Apoptosis and Molecular Targeting Therapy in Cancer. *Biomed Res Int*. 2020;2020:1-1. doi:10.1155/2020/2451249

251. Xiang J, Wan C, Guo R, Guo D. Is Hydrogen Peroxide a Suitable Apoptosis Inducer for All Cell Types?. *Biomed Res Int*. 2016;2016:1-6. doi:10.1155/2016/7343965

252. Yamakawa H, Ito Y, Naganawa T et al. Activation of caspase-9 and -3 during H2O2-induced apoptosis of PC12 cells independent of ceramide formation. *Neurol Res*. 2000;22(6):556-564. doi:10.1080/01616412.2000.11740718

253. Furukawa M, K-Kaneyama J, Yamada M, Senda A, Manabe A, Miyazaki A. Cytotoxic Effects of Hydrogen Peroxide on Human Gingival Fibroblasts In Vitro. *Oper Dent*. 2015;40(4):430-439. doi:10.2341/14-059-l

254. Fink S, Cookson B. Apoptosis, Pyroptosis, and Necrosis: Mechanistic Description of Dead and Dying Eukaryotic Cells. *Infect Immun*. 2005;73(4):1907-1916. doi:10.1128/iai.73.4.1907-1916.2005

255. Chen J. The Cell-Cycle Arrest and Apoptotic Functions of p53 in Tumour Initiation and Progression. *Cold Spring Harb Perspect Med*. 2016;6(3):a026104. doi:10.1101/cshperspect.a026104

256. Olivero O, Tejera A, Fernandez J et al. Zidovudine induces S-phase arrest and cell cycle gene expression changes in human cells. *Mutagenesis*. 2005;20(2):139-146. doi:10.1093/mutage/gei019

257. Errico A, Costanzo V. Mechanisms of replication fork protection: a safeguard for genome stability. *Crit Rev Biochem Mol Biol*. 2012;47(3):222-235. doi:10.3109/10409238.2012.655374

258. Cimprich K. Probing ATR Activation with Model DNA Templates. *Cell Cycle*. 2007;6(19):2348-2354. doi:10.4161/cc.6.19.4755

259. Zaborowski M, Balaj L, Breakefield X, Lai C. Extracellular Vesicles: Composition, Biological Relevance, and Methods of Study. *Bioscience*. 2015;65(8):783-797. doi:10.1093/biosci/biv084

260. Sheehan C, D'Souza-Schorey C. Tumour-derived extracellular vesicles: molecular parcels that enable regulation of the immune response in cancer. *J Cell Sci*. 2019;132(20). doi:10.1242/jcs.235085

261. Aoi W, Sakuma K. Skeletal muscle: a novel and intriguing characteristics as a secretory organ. *Biodiscovery*. 2013;(7). doi:10.7750/biodiscovery.2013.7.2

262. Jaiswal N, Gavin M, Quinn W et al. The role of skeletal muscle Akt in the regulation of muscle mass and glucose homeostasis. *Mol Metab*. 2019;28:1-13. doi:10.1016/j.molmet.2019.08.001

263. Mann W. Report of the task group on reference man. *Int J Appl Radiat Isot*. 1977;28(4):448-449. doi:10.1016/0020-708x(77)90145-4

264. Pratesi A. Skeletal muscle: an endocrine organ. *CLINICAL CASES IN MINERAL AND BONE METABOLISM*. 2013. doi:10.11138/ccmbm/2013.10.1.011

265. Cantley J. The control of insulin secretion by adipokines: current evidence for adipocyte-beta cell endocrine signalling in metabolic homeostasis. *Mammalian Genome*. 2014;25(9-10):442-454. doi:10.1007/s00335-014-9538-7

266. Le Gall L, Ouandaogo Z, Anakor E et al. Optimized method for extraction of exosomes from human primary muscle cells. *Skelet Muscle*. 2020;10(1). doi:10.1186/s13395-020-00238-1

267. Trovato E, Di Felice V, Barone R. Extracellular Vesicles: Delivery Vehicles of Myokines. *Front Physiol*. 2019;10. doi:10.3389/fphys.2019.00522

268. Millan-Cubillo A, Martin-Perez M, Ibarz A, Fernandez-Borras J, Gutiérrez J, Blasco J. Proteomic characterization of primary cultured myocytes in a fish model at different myogenesis stages. *Sci Rep*. 2019;9(1). doi:10.1038/s41598-019-50651-w

269. Mohamed M, Sloane B. multifunctional enzymes in cancer. *Nature Reviews Cancer*. 2006;6(10):764-775. doi:10.1038/nrc1949

270. Aggarwal N, Sloane B. Cathepsin B: Multiple roles in cancer. *PROTEOMICS - Clinical Applications*. 2014;8(5-6):427-437. doi:10.1002/prca.201300105

271. Chwieralski C, Welte T, Bühling F. Cathepsin-regulated apoptosis. *Apoptosis*. 2006;11(2):143-149. doi:10.1007/s10495-006-3486-y

272. Mukhopadhyay S, Panda P, Sinha N, Das D, Bhutia S. Autophagy and apoptosis: where do they meet?. *Apoptosis*. 2014;19(4):555-566. doi:10.1007/s10495-014-0967-2

273. Mustafa D, Mohammed H. Cytotoxicity Effect of Laserpitium Carduchorum Extract in Mcf-7 Human Breast Cancer Cells Via Cell Cycle Arrest and Induction if Apoptosis. *International Journal of Psychosocial Rehabilitation*. 2020;24(03):1620-1628. doi:10.37200/ijpr/v24i3/pr200910

274. Elmore S. Apoptosis: A Review of Programmed Cell Death. *Toxicol Pathol*. 2007;35(4):495-516. doi:10.1080/01926230701320337

275. Jin Z, El-Deiry W. Overview of cell death signaling pathways. *Cancer Biol Ther*. 2005;4(2):147-171. doi:10.4161/cbt.4.2.1508

276. Medema J. FLICE is activated by association with the CD95 death-inducing signaling complex (DISC). *EMBO J*. 1997;16(10):2794-2804. doi:10.1093/emboj/16.10.2794

277. Ghavami S, Kerkhoff C, Los M, Hashemi M, Sorg C, Karami-Tehrani F. Mechanism of apoptosis induced by S100A8/A9 in colon cancer cell lines: the role of ROS and the effect of metal ions. *J Leukoc Biol*. 2004;76(1):169-175. doi:10.1189/jlb.0903435

278. Mustafa D, Mohammed H. Cytotoxicity Effect of Laserpitium Carduchorum Extract in Mcf-7 Human Breast Cancer Cells Via Cell Cycle Arrest and Induction if Apoptosis. *International Journal of Psychosocial Rehabilitation*. 2020;24(03):1620-1628. doi:10.37200/ijpr/v24i3/pr200910

279. Fulda S, Debatin K. Targeting Apoptosis Pathways in Cancer Therapy. *Curr Cancer Drug Targets*. 2004;4(7):569-576. doi:10.2174/1568009043332763

280. Yuan S, Akey C. Apoptosome Structure, Assembly, and Procaspase Activation. *Structure*. 2013;21(4):501-515. doi:10.1016/j.str.2013.02.024

281. Iozzo R, Sanderson R. Proteoglycans in cancer biology, tumour microenvironment and angiogenesis. *J Cell Mol Med*. 2011;15(5):1013-1031. doi:10.1111/j.1582-4934.2010.01236.x

282. Tkachenko E, Rhodes J, Simons M. Syndecans. *Circ Res*. 2005;96(5):488-500. doi:10.1161/01.res.0000159708.71142.c8

283. Mundhenke C, Meyer K, Drew S, Friedl A. Heparan Sulfate Proteoglycans as Regulators of Fibroblast Growth Factor-2 Receptor Binding in Breast Carcinomas. *Am J Pathol*. 2002;160(1):185-194. doi:10.1016/s0002-9440(10)64362-3

284. Seidler D, Dreier R. Decorin and its galactosaminoglycan chain: Extracellular regulator of cellular function?. *IUBMB Life*. 2008;60(11):729-733. doi:10.1002/iub.115

285. YANG F, JIANG X, SONG L et al. Quercetin inhibits angiogenesis through thrombospondin-1 upregulation to antagonize human prostate cancer PC-3 cell growth in vitro and in vivo. *Oncol Rep*. 2015;35(3):1602-1610. doi:10.3892/or.2015.4481

286. Neill T, Jones H, Crane-Smith Z, Owens R, Schaefer L, Iozzo R. Decorin induces rapid secretion of thrombospondin-1 in basal breast carcinoma cells via inhibition of Ras homolog gene family, member A/Rho-associated coiled-coil containing protein kinase 1. *FEBS Journal*. 2013;280(10):2353-2368. doi:10.1111/febs.12148

287. Trout A, Rutkai I, Biose I, Bix G. Review of Alterations in Perlecan-Associated Vascular Risk Factors in Dementia. *Int J Mol Sci*. 2020;21(2):679. doi:10.3390/ijms21020679

288. Mathiak M, Yenisey C, Grant D, Sharma B, Iozzo R. A Role for Perlecan in the Suppression of Growth and Invasion in Fibrosarcoma Cells. Cancer Research. https://cancerres.aacrjournals.org/content/57/11/2130. Published 2021.

289. Danielson K, Baribault H, Holmes D, Graham H, Kadler K, Iozzo R. Targeted Disruption of Decorin Leads to Abnormal Collagen Fibril Morphology and Skin Fragility. *Journal of Cell Biology*. 1997;136(3):729-743. doi:10.1083/jcb.136.3.729

290. Keene D, San Antonio J, Mayne R et al. Decorin Binds Near the C Terminus of Type I Collagen. *Journal of Biological Chemistry*. 2000;275(29):21801-21804. doi:10.1074/jbc.c000278200

291. Kanzleiter T, Rath M, Görgens S et al. The myokine decorin is regulated by contraction and involved in muscle hypertrophy. *Biochem Biophys Res Commun*. 2014;450(2):1089-1094. doi:10.1016/j.bbrc.2014.06.123

292. Reszegi A, Horváth Z, Fehér H et al. Protective Role of Decorin in Primary Hepatocellular Carcinoma. *Front Oncol*. 2020;10. doi:10.3389/fonc.2020.00645

293. Neill T, Schaefer L, Iozzo R. Oncosuppressive functions of decorin. *Mol Cell Oncol*. 2015;2(3):e975645. doi:10.4161/23723556.2014.975645

294. WU H, WANG S, XUE A et al. Overexpression of decorin induces apoptosis and cell growth arrest in cultured rat mesangial cellsin vitro. *Nephrology*. 2008;13(7):607-615. doi:10.1111/j.1440-1797.2008.00961.x

295. Järvinen T, Prince S. Decorin: A Growth Factor Antagonist for Tumour Growth Inhibition. *Biomed Res Int*. 2015;2015:1-11. doi:10.1155/2015/654765

296. Iozzo R, Moscatello D, McQuillan D, Eichstetter I. Decorin Is a Biological Ligand for the Epidermal Growth Factor Receptor. *Journal of Biological Chemistry*. 1999;274(8):4489-4492. doi:10.1074/jbc.274.8.4489

297. Schönherr E, Sunderkötter C, Iozzo R, Schaefer L. Decorin, a Novel Player in the Insulin-like Growth Factor System. *Journal of Biological Chemistry*. 2005;280(16):15767-15772. doi:10.1074/jbc.m500451200

298. Morrione A, Neill T, Iozzo R. Dichotomy of decorin activity on the insulin-like growth factor-I system. *FEBS Journal*. 2013;280(10):2138-2149. doi:10.1111/febs.12149

299. Goldoni S, Humphries A, Nyström A et al. Decorin is a novel antagonistic ligand of the Met receptor. *Journal of Cell Biology*. 2009;185(4):743-754. doi:10.1083/jcb.200901129

300. Sofeu Feugaing D, Götte M, Viola M. More than matrix: The multifaceted role of decorin in cancer. *Eur J Cell Biol*. 2013;92(1):1-11. doi:10.1016/j.ejcb.2012.08.004

301. S L, JF X, WJ C, HP L, CP H. Human decorin regulates proliferation and migration of human lung cancer A549 cells. PubMed. https://www.ncbi.nlm.nih.gov/pubmed/24342321. Published 2021.

302. Schaefer L, Tredup C, Gubbiotti M, Iozzo R. Proteoglycan neofunctions: regulation of inflammation and autophagy in cancer biology. *FEBS J*. 2016;284(1):10-26. doi:10.1111/febs.13963

303. Svensson K, Christianson H, Wittrup A et al. Exosome Uptake Depends on ERK1/2-Heat Shock Protein 27 Signaling and Lipid Raft-mediated Endocytosis Negatively Regulated by Caveolin-1. *Journal of Biological Chemistry*. 2013;288(24):17713-17724. doi:10.1074/jbc.m112.445403

304. Zech D, Rana S, Büchler M, Zöller M. Tumour-exosomes and leukocyte activation: an ambivalent crosstalk. *Cell Communication and Signaling*. 2012;10(1):37. doi:10.1186/1478-811x-10-37

305. Kooijmans S, Aleza C, Roffler S, van Solinge W, Vader P, Schiffelers R. Display of GPI-anchored anti-EGFR nanobodies on extracellular vesicles promotes tumour cell targeting. *J Extracell Vesicles*. 2016;5(1):31053. doi:10.3402/jev.v5.31053

306. Laulagnier K, Javalet C, Hemming F et al. Amyloid precursor protein products concentrate in a subset of exosomes specifically endocytosed by neurons. *Cellular and Molecular Life Sciences*. 2017;75(4):757-773. doi:10.1007/s00018-017-2664-0

307. Sancho-Albero M, Navascués N, Mendoza G et al. Exosome origin determines cell targeting and the transfer of therapeutic nanoparticles towards target cells. *J Nanobiotechnology*. 2019;17(1). doi:10.1186/s12951-018-0437-z

308. Jurgielewicz B, Yao Y, Stice S. Kinetics and Specificity of HEK293T Extracellular Vesicle Uptake using Imaging Flow Cytometry. *Nanoscale Res Lett*. 2020;15(1). doi:10.1186/s11671-020-03399-6

309. Lázaro-Ibáñez E, Neuvonen M, Takatalo M et al. Metastatic state of parent cells influences the uptake and functionality of prostate cancer cell-derived extracellular vesicles. *J Extracell Vesicles*. 2017;6(1):1354645. doi:10.1080/20013078.2017.1354645

310. ENDZELIŅŠ E, ĀBOLS A, BUŠS A et al. Extracellular Vesicles Derived from Hypoxic Colorectal Cancer Cells Confer Metastatic Phenotype to Non-metastatic Cancer Cells. *Anticancer Res*. 2018;38(9):5139-5147. doi:10.21873/anticanres.12836

311. Bonsergent E, Grisard E, Buchrieser J, Schwartz O, Théry C, Lavieu G. Quantitative characterization of extracellular vesicle uptake and content delivery within mammalian cells. *Nat Commun*. 2021;12(1). doi:10.1038/s41467-021-22126-y

312. Langley R, Fidler I. Tumour Cell-Organ Microenvironment Interactions in the Pathogenesis of Cancer Metastasis. *Endocr Rev*. 2007;28(3):297-321. doi:10.1210/er.2006-0027

313. Kopfstein L, Christofori G. Metastasis: cell-autonomous mechanisms versus contributions by the tumour microenvironment. *Cellular and Molecular Life Sciences*. 2006;63(4):449-468. doi:10.1007/s00018-005-5296-8

314. Chen J, Fei X, Wang J, Cai Z. Tumour-derived extracellular vesicles: Regulators of tumour microenvironment and the enlightenment in tumour therapy. *Pharmacol Res*. 2020;159:105041. doi:10.1016/j.phrs.2020.105041

315. Webber J, Yeung V, Clayton A. Extracellular vesicles as modulators of the cancer microenvironment. *Semin Cell Dev Biol*. 2015;40:27-34. doi:10.1016/j.semcdb.2015.01.013

316. Viaud S, Terme M, Flament C et al. Dendritic Cell-Derived Exosomes Promote Natural Killer Cell Activation and Proliferation: A Role for NKG2D Ligands and IL-15Rα. *PLoS One*. 2009;4(3):e4942. doi:10.1371/journal.pone.0004942

317. Lee J, Park S, Jung B et al. Exosomes Derived from Mesenchymal Stem Cells Suppress Angiogenesis by Down-Regulating VEGF Expression in Breast Cancer Cells. *PLoS One*. 2013;8(12):e84256. doi:10.1371/journal.pone.0084256

318. Meiyanto E, Hermawan A, Anindyajati A. Natural Products for Cancer-Targeted Therapy: Citrus Flavonoids as Potent Chemopreventive Agents. *Asian Pacific Journal of Cancer Prevention*. 2012;13(2):427-436. doi:10.7314/apjcp.2012.13.2.427

319. Bartel K, Pein H, Popper B et al. Connecting lysosomes and mitochondria – a novel role for lipid metabolism in cancer cell death. *Cell Communication and Signaling*. 2019;17(1). doi:10.1186/s12964-019-0399-2

320. Jong A, Wu C, Li J et al. Large-scale isolation and cytotoxicity of extracellular vesicles derived from activated human natural killer cells. *J Extracell Vesicles*. 2017;6(1):1294368. doi:10.1080/20013078.2017.1294368

321. Yuan J, Murrell G, Trickett A, Wang M. Involvement of cytochrome c release and caspase-3 activation in the oxidative stress-induced apoptosis in human tendon fibroblasts. *Biochimica et Biophysica Acta (BBA) - Molecular Cell Research*. 2003;1641(1):35-41. doi:10.1016/s0167-4889(03)00047-8

322. Garcia-Perez C, Roy S, Naghdi S, Lin X, Davies E, Hajnoczky G. Bid-induced mitochondrial membrane permeabilization waves propagated by local reactive oxygen species (ROS) signaling. *Proceedings of the National Academy of Sciences*. 2012;109(12):4497-4502. doi:10.1073/pnas.1118244109

323. Smiley S, Reers M, Mottola-Hartshorn C et al. Intracellular heterogeneity in mitochondrial membrane potentials revealed by a J-aggregate-forming lipophilic cation JC-1. *Proceedings of the National Academy of Sciences*. 1991;88(9):3671-3675. doi:10.1073/pnas.88.9.3671

324. Jeng P, Inoue-Yamauchi A, Hsieh J, Cheng E. BH3-dependent and independent activation of BAX and BAK in mitochondrial apoptosis. *Curr Opin Physiol*. 2018;3:71-81. doi:10.1016/j.cophys.2018.03.005

325. Yoon J, Ashktorab H, Smoot D, Nam S, Hur H, Park W. Uptake and tumour-suppressive pathways of exosome-associated GKN1 protein in gastric epithelial cells. *Gastric Cancer*. 2020;23(5):848-862. doi:10.1007/s10120-020-01068-2

326. Zaharie F, Muresan M, Petrushev B et al. Exosome-Carried microRNA-375 Inhibits Cell Progression and Dissemination via Bcl-2 Blocking in Colon Cancer. *Journal of Gastrointestinal and Liver Diseases*. 2015;24(4):435-443. doi:10.15403/jgld.2014.1121.244.375

327. Shi H, Li H, Zhen T, Dong Y, Pei X, Zhang X. The Potential Therapeutic Role of Exosomal MicroRNA-520b Derived from Normal Fibroblasts in Pancreatic Cancer. *Molecular Therapy - Nucleic Acids*. 2020;20:373-384. doi:10.1016/j.omtn.2019.12.029

328. Witz I. 753 Chemokines, chemokine receptors and selectin ligands expression by tumour cells: Involvement in extravasation and metastasis. *European Journal of Cancer Supplements*. 2003;1(5):S226. doi:10.1016/s1359-6349(03)90779-8

329. Joyce J, Pollard J. Microenvironmental regulation of metastasis. *Nature Reviews Cancer*. 2008;9(4):239-252. doi:10.1038/nrc2618

330. Mrschtik M, Ryan K. Lysosomal proteins in cell death and autophagy. *FEBS Journal*. 2015;282(10):1858-1870. doi:10.1111/febs.13253

331. Buraschi S, Neill T, Goyal A et al. Decorin causes autophagy in endothelial cells via Peg3. *Proceedings of the National Academy of Sciences*. 2013;110(28):E2582-E2591. doi:10.1073/pnas.1305732110

332. Goldoni S, Humphries A, Nyström A et al. Decorin is a novel antagonistic ligand of the Met receptor. *Journal of Cell Biology*. 2009;185(4):743-754. doi:10.1083/jcb.200901129